Mathematical Problems in Engineering

Safety Technologies and Fault Tolerant Methods for Engineering 2022

Lead Guest Editor: Yong Chen
Guest Editors: Fengjun Yan, Mahdi Tavakoli, Chuan Li, and Meng Li

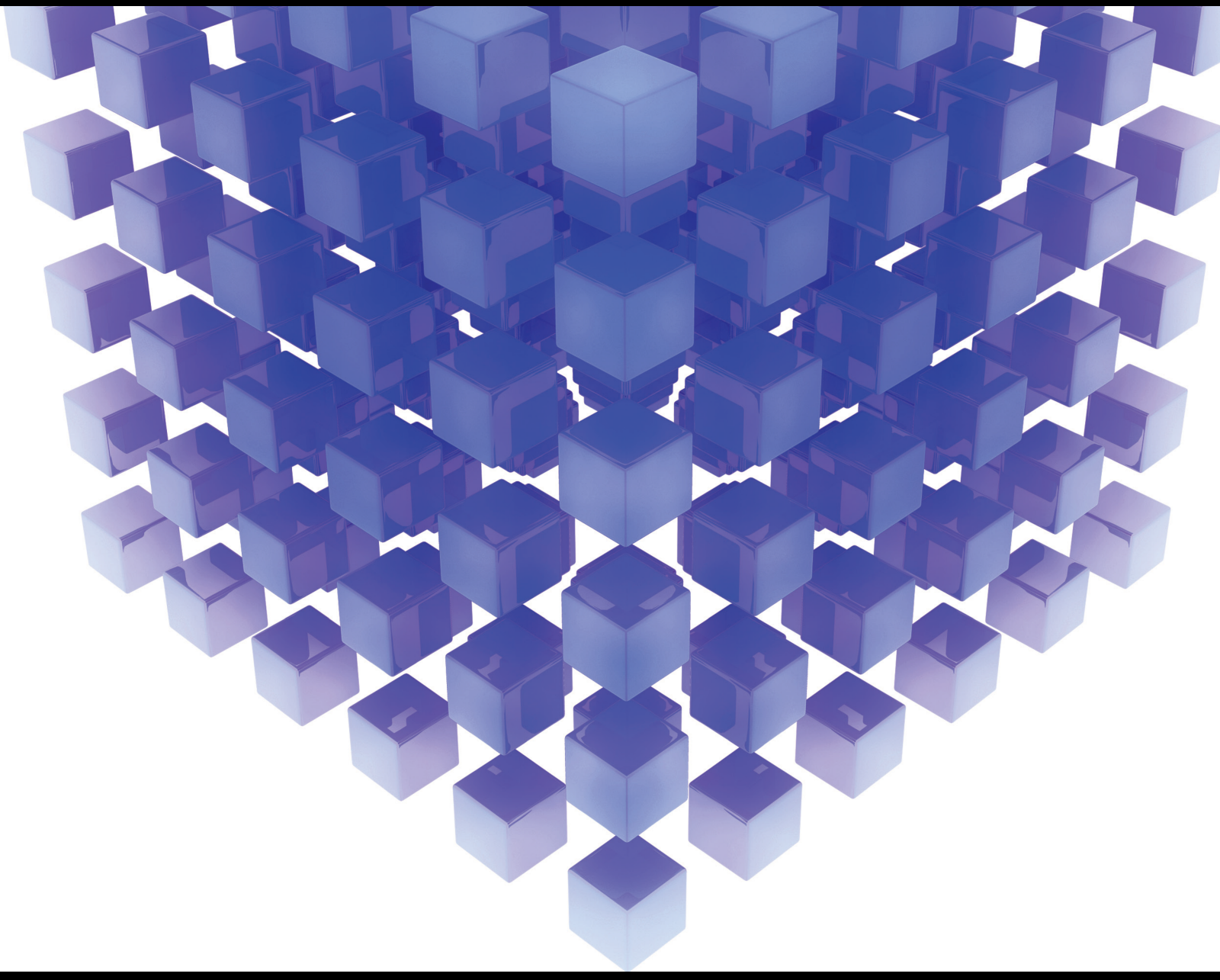

Safety Technologies and Fault Tolerant Methods for Engineering 2022

Mathematical Problems in Engineering

Safety Technologies and Fault Tolerant Methods for Engineering 2022

Lead Guest Editor: Yong Chen
Guest Editors: Fengjun Yan, Mahdi Tavakoli, Chuan Li, and Meng Li

Chief Editor

Academic Editors

Contents

Hindawi
Mathematical Problems in Engineering
Volume 2023, Article ID 6902272, 19 pages
https://doi.org/10.1155/2023/6902272

Research Article

Simultaneous Multiplicative and Additive Actuator Faults Estimation-Based Sliding Mode FTC for a Class of Uncertain Nonlinear System

Nabila Mabrouk, Ali Ben Brahim, and Fayçal Ben Hmida

Laboratory of Engineering of Industrial Systems and Renewable Energy (LISIER), National Higher Engineering School of Tunis (ENSIT), University of Tunis, 5 Avenue Taha Hussein, BP 56-1008, Tunis, Tunisia

Correspondence should be addressed to Nabila Mabrouk; mabrouk_nabila@yahoo.fr

Received 19 August 2022; Revised 19 November 2022; Accepted 5 May 2023; Published 3 July 2023

Academic Editor: Yong Chen

In this article, an adaptive sliding mode fault tolerant control (FTC) is improved in the case of uncertain nonlinear system which is affected by both multiplicative and additive faults in actuator. Especially, when the nonlinear system is modeled by Takagi–Sugeno (T-S) fuzzy system with local nonlinear model. The main contribution of this paper is developing a model of multiplicative faults, which offers a more realistic dynamic evolution of the actuator degradation. The degradation process is modeled by Wiener process and estimated by the maximum likelihood estimation (MLE). Sliding mode observer (SMO) is conceived to realize the additive actuator faults using convex multiobjective optimization. On these bases, the estimated multiplicative and additive actuator faults are used to design the adaptive sliding mode controller (SMC). Finally, the proposed fault-tolerant control scheme is demonstrated by the results of inverted pendulum system simulation.

1. Introduction

During the past few decades, the fields of fault estimation (FE) technique and fault tolerant control (FTC) have been the result drawing an intensive research interests due to the increasing demands for system's performance, safety, and reliability. Active FTC and FE to a category of nonlinear systems particularly T-S fuzzy models [1–3] have a significant position in recent control implementation, as well as in supervision and reliability of actuators. In recent decades, a variety of methods have been developed, using adaptive observer [4–6] or SMO [7–9]. The sliding mode scheme has an excellent application prospect in fault estimation and fault tolerant control due to its simple structure, strong applicability, and good robustness. Several publications have appeared in recent years regarding this issue. In [10], the authors studied Takagi–Sugeno fuzzy systems with uncertainties and multiplicative and additive actuator faults and then developed an adaptive sliding mode FTC design. However, in [11], a FTC design predicated using SMO for T-S fuzzy systems is developed. In [12], the authors used a nonquadratic Lyapunov function to estimate simultaneously actuator and sensor faults for T-S fuzzy systems. In a recent paper [13], the authors developed the FE and FTC for the T-S fuzzy systems subject to actuator and sensor faults. For nonlinear systems, popular fault detection methods have been elaborated in an effective and precise manner. In [14, 15], the authors modelled fault as an additive occurring in sensors or actuators. The main disadvantage of the previous techniques is that they regard sensor and actuator faults as additive. Nevertheless, some actuator and sensor errors, in addition to component faults, are frequently found in the multiplicative form. As a result, multiplicative faults and the system's inputs and outputs are mixed. Estimating the magnitude and characteristics of multiplicative faults has become an increasing attract in control theory due to the practical importance of decoupling their structure effects or parameter in the model or system

and improving fault tolerant control concept for nonlinear systems. We can use stochastic process to model the actuator degradation [16–19]. The actuator environment can influence the deterioration process and strongly depends on several factors [20] (shock, temperature, and load variation) of the monitored system. Degradation process for industrial systems is influenced by both external and internal factors including operating conditions and dynamic environment [21]. Stochastic dynamics are the common characteristics involved in actuator increasing degradation process in actuator. This results in system uncertainties and measurements errors. For the past few decades, extensive research studies have been conducted in the area of stochastic degradation modelling [22–24]. Degradation models can be divided into shock-based degradation model [25], progressive degradation model [26, 27], and combined degradation model [28]. The degradation such as the wear out of engineering devices, the fatigue, and the corrosion of metals can be caused by multiple degradation processes and induces total failures of actuator.

In the following, the authors point out the main focus of the present study on developing effective and robust active FTC for a class of uncertain nonlinear system. This study offers a FE-based sliding mode FTC technique for nonlinear uncertain system affected by both multiplicative and additive faults. The major contributions of this article are as follows:

(i) In this study, for more simplicity and to find a model for the description of the interactions between the control system behavior and the actuator stochastic degradation process, the deterioration of the entire control system would be supposed to lie in the actuator loss of efficiency. In practice, when an actuator operates dynamically in a random environment, its capacity decreases overtime which is related to degradation process. Therefore, the multiplicative faults model was conceived based on not only the degradation process but also the capacity of actuator. Actually, it is straight forward to think multiplicative faults should be estimated in order to conceive a fault tolerant control design for dynamic systems. To describe the actuator degradation behavior, we use stochastic Wiener process model which offers a more realistic evolution of the deterioration. In order to estimate the degradation process, the maximum likelihood method is used.

(ii) We propose to conceive an adaptive SMO for T-S systems with the existence of uncertainties to estimate additive actuator faults. To study the stability of the proposed SMO, we use a linear matrix inequality (LMI) and the theories of Lyapunov. To improve the actuator faults estimation accuracy, we use an adaptive update term.

(iii) Using FE, we study an adaptive SMC for the T-S fuzzy system having models local nonlinear that complies with the condition of Lipschitz with additive and multiplicative faults. Particularly, it is demonstrated that the suggested sliding mode FTC is used for the parameters setting of the controller in order to obtain the desired performances of actuator even in the presence of both additive and multiplicative faults.

Compared to previous works, many studies have used only actuator or senor faults in system [29]. Then, most of the previous studies do not take into account multiplicative faults. Furthermore, we use adaptive law to design the SMO which gives more freedom in comparison with [30]; the model used incorporates output disturbance and Itô stochastic noise; and they introduced time delay in the state. However, in our case study, we suppose that the degradation of the total control system lies in the actuator loss of efficiency. Therefore, the multiplicative fault model was conceived based on not only the degradation process but the capacity of the actuator. To describe the actuator degradation behaviour, we use the stochastic Wiener process model (continuous models) which offers a more realistic deterioration. Compared to [31], the authors use only additive faults in both actuator and sensor in the system. They transform sensor faults into "pseudoactuator" faults by using an augmented T-S fuzzy system that causes many constraints in the application of the hypotheses; in fact, the total number of actuator faults must not exceed the number of outputs. This model may not be practical and conventional in all situations of stochastic degradation process in actuator. Moreover, it cannot adequately capture the dynamics of the actuator's degradation process. Indeed, the model of faults must describe the interaction between the actuator stochastic degradation process and the control system behaviour. This includes the dynamics of the actuator's performance, the control system's response to changes in the actuator's performance, and the uncertainty associated with the actuator's stochastic degradation process. The model must also take into account the physical characteristics of the actuator and the system environment, as well as the impact of external factors such as maintenance and other system parameters. In our study, we develop a model of multiplicative faults, which offers a more realistic dynamic evolution of the actuator degradation. The SMO is designed according to adaptive law which offers less conservative results and gives more liberty in comparison with [32]. Yang et al. in [33] have developed simultaneous multiplicative and additive faults in jump systems, which may be considered as a special class of stochastic systems. They use the adaptive backstepping technique to construct the fuzzy logic system based an online adaptive fault-tolerant compensation controller. However, in our study, we use continuous degradation models and we propose to conceive an adaptive SMO for Takagi–Sugeno fuzzy systems having local nonlinear models.

The outline of the article is organized as follows. Section 2 describes a nonlinear system with local nonlinear models, uncertainties, additive, and multiplicative (loss of efficiency) actuator faults. In Section 3, we use Wiener process to model the degradation process in the actuator and the maximum likelihood method to estimate the stochastic model for

multiplicative fault. In Section 4, the proposed adaptive SMO is designed to estimate the additive faults of actuator. Section 5 presents the sliding mode FTC design in order to redress the impact of additive and multiplicative faults for the stabilization of the system. A simulation of the inverted pendulum and cart system is used in Section 6 in order to validate and illustrate the efficiency of the approach. Finally, Section 7 draws some conclusions.

2. Problem Formulation

In this study, we refer to a class of nonlinear uncertain systems affected both the additive and multiplicative actuator faults. Consider a nonlinear uncertain system represented by the following equations:

$$\begin{aligned}\dot{x}_t &= \varphi_{x_1}(x_t) + \varphi_{x_2}(x_t)u_t + \varphi_{x_3}(x_t)\xi(x,t)\\ &\quad + \varphi_{x_4}(x_t)\Gamma(x,t),\end{aligned} \tag{1}$$

$$y_t = \varphi(x_t), \tag{2}$$

$$y_{Lt} = \varphi_{L}(x_t). \tag{3}$$

$u_t \in R^m$ is the control input, $x_t \in R^n$ represents the state vector, $y_{Lt} \in R^{p1}$ stands for the controlled output, and $y_t \in R^p$ represents the measurement vector of output. The functions $\varphi_L(x_t), \varphi(x_t), \varphi_{x_i}(x_t)$, and $\Gamma(x,t)$ are always nonlinear for $i = 1,2,3,4$. $\xi(x,t) \in \mathrm{R}^l$ denotes the unknown uncertainties vector.

In feedback control system, the actuator is a significant part in the evaluation of the performance level. That is because, considering a degradation process in an electrical or mechanical element of the controlled system, the controlled action is affected as well, which eventually causes a poor performance of the control system.

Let us consider an actuator undergoing a progressive degradation process. It is subjected to both electrical and mechanical degradation that occurs stochastically over time, particularly in the case of the electrical actuator degradation where a rub impact between the rotor and the stator or a bend shaft can occur. It should be noted that rotor faults as well as stator faults are recognized electrical faults. Besides, there are other types of faults that depend on the failure mode. During its functioning, the actuator can be affected by several types of faults. Our study will focus on two types of faults: additive faults and multiplicative faults (loss of efficiency). In practice, the actuator operates dynamically in a random environment. Furthermore, its capacity decreases overtime which is related to degradation and depends on environmental factors as well as operational conditions of the feedback control system. Moreover, the wear or natural ageing of the electrical and/or mechanical components of the actuator due to the nondesired impacts of the working condition decreases the effectiveness of actuator in time. The actuator degradation process is a cause of the physical system performance deterioration. During the initial period of operation, the actuators function flawlessly.

The actual capacity of actuator $K_a(t) = K_{a_{\text{int}}}$ where $K_{a_{\text{int}}}$ is the initial nominal capacity. If $d(t)$ outlined the actuator degradation, the capacity of actuator (see Figure 1) can be represented by the following equation:

$$K_a(t) = K_{a_{\text{int}}} - d(t). \tag{4}$$

The efficiency factor (see Figure 2) can be written as follows:

$$\beta = \frac{K_a(t)}{K_{a_{\text{int}}}}. \tag{5}$$

The minimum efficiency is reached when $K_a(t) = K_{\min}$, and we define the minimum efficiency factor $\varepsilon = (K_{\min}/K_{a_{\text{int}}}) > 0$ such as $0 < \varepsilon \le \beta \le 1, \forall t \ge t_f$ and t_f is the time occurrence of multiplicative defect.

The loss of actuator effectiveness is examined to consequence from the dynamic progression of the degradation process $\beta = (K_{a_{\text{int}}} - d(t))/K_{a_{\text{int}}}$.

In this way, the following three cases are defined:

(i) $K_a(t) = K_{a_{\text{int}}}$: the actuator operates without degradation ($d(t) = 0$), and the efficiency factor is $\beta = 1$

(ii) $K_a(t) = K_{a_{\text{int}}} - d(t)$: the actuator deteriorates, its capacity $K_{a_{\min}} < K_a(t) < K_{a_{\text{int}}}$, and the efficiency factor is $\beta = (K_{a_{\text{int}}} - d(t))/K_{a_{\text{int}}}$

(iii) $K_a(t) = K_{a_{\min}}$: the actuator operates with its minimum capacity, and then the efficiency factor is $\beta = \varepsilon = (K_{a_{\min}}/K_{a_{\text{int}}})$

The nonlinear system (1)–(3) affected by additive and multiplicative faults at the same time can be described by the following uncertain structure and local nonlinearities as follows:

$$\begin{aligned}\dot{x}_t &= \varphi_{x_1}(x_t) + \varphi_{x_2}(x_t)\beta u_t + \varphi_{x_3}(x_t)f_a(t)\\ &\quad + \varphi_{x_4}(x_t)\Gamma(x,t) + \varphi_{x_5}(x_t)\xi(x,t),\end{aligned} \tag{6}$$

$$y_t = \varphi(x_t), \tag{7}$$

$$y_{Lt} = \varphi_{L}(x_t), \tag{8}$$

where $f_a(t) \in \mathrm{R}^q$ is the additive actuator faults.

Multiplicative fault may be rearranged as follows:

$$\begin{aligned}\varphi_{x_2}(x_t)\beta u_t &= \varphi_{x_2}(x_t)\beta u_t + \varphi_{x_2}(x_t)u_t - \varphi_{x_2}(x_t)u_t\\ &= \varphi_{x_2}(x_t)u_t + \varphi_{x_2}(x_t)(\beta - 1)u_t\\ &= \varphi_{x_2}(x_t)u_t + F(u_t,t),\end{aligned} \tag{9}$$

where $F(u_t,t)$ are the multiplicative faults.

Then, the nonlinear system (1)–(3) affected by additive and multiplicative faults at the same time can be expressed in terms of uncertain structures and local nonlinearities as follows:

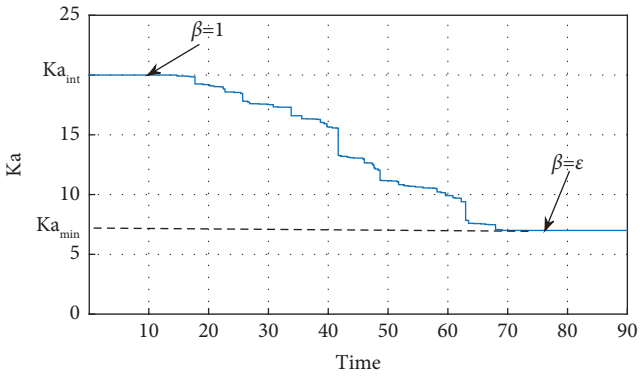

Figure 1: The actuator capacity $K_a(t)$.

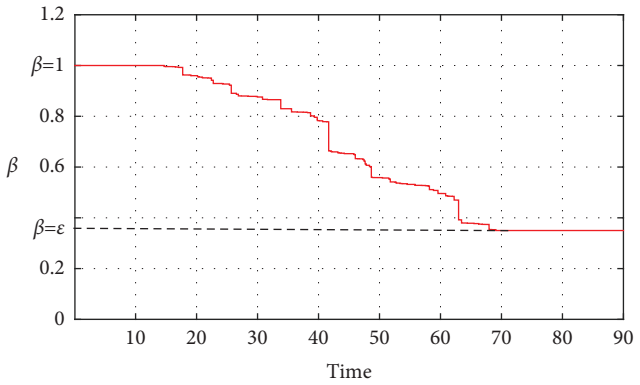

Figure 2: The efficiency factor β.

$$\dot{x}_t = \varphi_{x_1}(x_t) + \varphi_{x_2}(x_t)u_t + F(u,t) + \varphi_{x_3}(x_t)f_a(t) + \varphi_{x_4}(x_t)\Gamma(x,t) + \varphi_{x_5}(x_t)\xi(x,t), \tag{10}$$

$$y_t = \varphi(x_t), \tag{11}$$

$$y_{Lt} = \varphi_L(x_t). \tag{12}$$

The multiplicative faults are $F(u,t) = \varphi_{x_2}(x_t)(\beta - 1)u_t = \varphi_{x_2}(x_t)((K_{a_{\text{int}}} - d(t)/K_{a_{\text{int}}}) - 1)u_t$, and the following three case are defined:

(i) $d(t) = 0$: the actuator operates without degradation, the multiplicative faults are neglected $F(u,t) = 0$, so we have only the additive faults

(ii) $0 < d(t) < L$ (L is a maximum degradation process): the actuator operates with degradation process, and the multiplicative faults are

$$F(u,t) = \varphi_{x_2}(x_t)\left(\frac{K_{a_{\text{int}}} - d(t)}{K_{a_{\text{int}}}} - 1\right)u_t. \tag{13}$$

(iii) $d(t)$ reached L: the multiplicative faults are $F(u,t) = \varphi_{x_2}(x_t)((K_{a_{\min}}/K_{a_{\text{int}}}) - 1)u_t$

Given the nonlinear system (10)–(12) affected by both the additive and multiplicative actuator faults, respectively, $f_a(t)$, $F(u,t)$, and the uncertainties $\xi(x,t)$, our objective to achieve an adaptive sliding mode FTC resides principally on solving the following three problems:

(1) First problem: develop and estimate the degradation process to conceive a multiplicative faults model which offers a more realistic evolution of the deterioration in the actuator. It is very important to be able to estimate the faults before the performance systems degradation.

(2) Second problem: estimate T-S fuzzy system states and additive actuator faults, with the adaptive SMO.

(3) Third problem: we need to stabilize the closed loop of nonlinear systems, with the simultaneous occurrence of additive and multiplicative faults, using the robust adaptive sliding mode controller (10)–(12).

3. Actuator Degradation Models Estimation

In this study, we suppose that the system (10)–(12) is subject to Wiener process. The actuator degradation is denoted by a random variable d_t at time t. In this paper, we suppose that degradation is an increasing Lévy process [34] supported by the following assumptions:

(i) The initial degradation is denoted $d_0 = 0$

(ii) The degradation process is described with one-dimensional stochastic process $\{d\}_{t\geq 0}$

(iii) The increments $\{d\}_{t\geq 0}$ are independent and stationary

In this way, Wiener process has been frequently used to conceive a degradation model, particularly, when it was successfully applied to describe the increasing degradation in an actuator. The Wiener process is one of the most classic processes used in many progressive degradation modeling area; the basic idea is to model the cumulative increasing degradation $d_{W,t}$ by the stochastic Wiener process such that

$$d_{W,t} = d_{W,t_0} + W_t(\mu,\sigma), \forall t \geq 0, \tag{14}$$

where μ is a linear drift parameter and σ is a diffusion coefficient parameter and $W_t(\mu,\sigma) = \mu t + \sigma B_t$.

We consider that the Wiener process [24] is used such that the increment $W_{t_2} - W_{t_1}$ follows a Gaussian distribution with mean $E(W_{t_2} - W_{t_1}) = \mu(t_2 - t_1)$ and variance $\text{Var}(W_{t_2} - W_{t_1}) = \sigma^2(t_2 - t_1)$. If we consider the initial condition d_{W,t_0}, we can approximate the degradation measure $d_{W,t}$ with the following equation:

$$d_{W,t} = d_{W,t_0} + W(t - t_0), \forall t \geq 0. \tag{15}$$

Here in, we can deduce that

$$d_{W,t} = d_{W,t_0} + \mu(t - t_0) + \sigma B(t - t_0). \tag{16}$$

In particular, if $d_{W,t_0} = 0$, the degradation process $d_{W,t} = W_t(\mu,\sigma)$

The objective is to estimate the linear drift μ and diffusion parameter σ. We apply the maximum likelihood estimation (MLE) method.

Considering the degradation increment $\Delta d_{i,j} = (d_{i,j+1} - d_{i,j})$ of ith items at time j where $\rho = (\mu, \sigma)$, $j = 1, 2, \ldots m$ and $i = 1, 2, \ldots n$. The degradation measurements for item i, $\Delta d_i = (\Delta d_{i,1}, \Delta d_{i,2}, \ldots, \Delta d_{i,m})$. The density function is given by the following equation:

$$f_{(\mu\Delta t_{i,j}, \sigma^2 \Delta t_{i,j})}(\Delta d_{i,j}) = \frac{1}{\sqrt{2\pi\sigma^2 \Delta t_{i,j}}} * e^{a}, \tag{17}$$

where $a = -((\Delta d_{i,j} - \mu\Delta t_{i,j})^2 / 2\sigma^2 \Delta t_{i,j})$.

The likelihood function of the ith path $L_i(\rho) = f_i(\Delta d_i) = f_i(\Delta d_{i,1}, \ldots, \Delta d_{i,m}/\mu, \sigma)$ is given by the following equation:

$$\mathrm{Li}(\rho) = \prod_{j=1}^{m} \frac{1}{\sqrt{2\pi\sigma^2 \Delta t_{i,j}}} \mathrm{e}^{(a)}. \tag{18}$$

The log-likelihood function for the ith item can be expressed by the following equation:

$$\mathrm{li}(\rho) = \ln\left[\prod_{j=1}^{m} \frac{1}{\sqrt{2\pi\sigma^2 \Delta \mathrm{t_{i,j}}}} e^{(a)}\right]. \tag{19}$$

Since the measurements $d_{i,j}$ are independents, we can express $\mathrm{l}(\rho) = \ln(\Delta d_1, \Delta d_2, \Delta d_3, \ldots \Delta d_n)$ as

$$\mathrm{l}(\rho) \sum_{i=1}^{n} \ln\left(\prod_{j=1}^{m} \frac{1}{\sqrt{2\pi\sigma^2 \Delta \mathrm{t_{i,j}}}} e^{\left(-\left(\Delta d_{i,j} - \mu\Delta t_{i,j}\right)^2 / 2\sigma^2 \Delta t_{i,j}\right)}\right). \tag{20}$$

We find the MLE $\widehat{\rho} = [\widehat{\sigma}, \widehat{\mu}]$ by maximizing with respect to σ and μ, the partial derivatives of the log-likelihood function.

As a result, we write the partial derivative of log-likelihood function compared to μ as

$$\frac{\partial \mathrm{l}(\rho)}{\partial \mu} = \sum_{i=1}^{n} \sum_{j=1}^{m} \frac{\Delta d_{i,j} - \mu \Delta t_{i,j}}{\sigma^2} = 0, \tag{21}$$

and compared to σ as

$$\frac{\partial \mathrm{l}(\rho)}{\partial \sigma} = \frac{-\mathrm{mn}}{\sigma^2} + \sum_{i=1}^{n} \sum_{j=1}^{m} \frac{\Delta \mathrm{d_{i,j}} - \mu \Delta \mathrm{t}_{i,j}}{\sigma^3 \Delta \mathrm{t_{i,j}}} = 0. \tag{22}$$

Then, we obtain the expression as follows:

$$\widehat{\mu} = \frac{\sum_{i=1}^{n} \sum_{j=1}^{m} \Delta d_{i,j}}{\sum_{i=1}^{n} \sum_{j=1}^{m} \Delta t_{i,j}}, \tag{23}$$

$$\widehat{\sigma}^2 = \frac{1}{mn} \sum_{i=1}^{n} \sum_{j=1}^{m} \frac{\Delta d_{i,j} - \widehat{\mu} \Delta t_{i,j}}{\sigma^3 \Delta t_{i,j}}. \tag{24}$$

The measurements data $\Delta_{i,j}$ are generated by MATLAB with the parameters $\mu = 0.4$, $\sigma = 0.2$. We compute equations (23) and (24), and the estimated parameters are obtained as follows: $\mu = 0.398$ and $\sigma = 0.213$.

A design procedure for multiplicative fault development and estimation is described as follows:

(i) Step 1: we define the expression of the efficiency factor using the degradation process and the actuator capacity to conceive the multiplicative faults model.

(ii) Step 2: we use the Wiener process to model the stochastic degradation in actuator.

(iii) Step 3: the maximum likelihood method is used to estimate the linear drift and diffusion parameter.

4. Additive Actuator Faults Estimation

It was shown that using T-S fuzzy system with local nonlinear models concept was well suited to the study of a several class of systems. The nonlinear system (10)–(12) affected by additive and multiplicative faults at the same time is written by the T-S fuzzy system with uncertainty and models local nonlinear

$$\dot{x}(t) = \sum_{i=1}^{k} \mu_i(\zeta_t)\{A_i x(t) + B_i u(t) + F(u,t) + M_i f_a(t) + D_i \xi(x,t) + \Gamma(x,t)\}, \tag{25}$$

$$y(t) = \sum_{i=1}^{k} \mu_i(\zeta_t)\{C_i x(t)\}, \tag{26}$$

$$y_L(t) = \sum_{i=1}^{k} \mu_i(\zeta_t)\left\{C_{(L,i)} x(t)\right\}, \tag{27}$$

where M_i, D_i, C_i, B_i, and A_i are matrices with known real values. $F(u,t)$ is the multiplicative fault. We suppose that (A_i, B_i) and (A_i, C_i) are, respectively, controllable and observable. $f_a(t)$ and $F(u,t)$ represent the additive and multiplicative fault in control channel.

The functions $\mu_i(\zeta_t)$ (fuzzy normalized membership) must satisfy the properties of sum convex

$$\forall i \in [1, 2, \ldots, k], \sum_{i=1}^{k} \mu_i(\zeta_t) = 1, 1 \geq \mu_i(\zeta_t) \geq 0. \tag{28}$$

We will use the following assumptions in this paper.

Assumption 1. We assume that the uncertainties and faults are unknown and bounded. For the faults $f_a(t), F(u,t)$ and the uncertainties $\xi(x,t)$, there exist known positive

constants ξ_0, ρ_F and ρ_a such that $\|f_a(t)\| \le \rho_a, \|F(u,t)\| \le \rho_F$ and $\|\xi(x,t)\| \le \xi_0$.

Assumption 2. (A_i, M_i, C_i) is minimum phase and relative degree one, and we verify that for all complex numbers s when $\mathrm{Re}(s) \ge 0$ that

$$\mathrm{rank}\begin{bmatrix} sI_n - A_i & -M_i \\ C_i & 0 \end{bmatrix} = n + q, \tag{29}$$

Ensures that the nonasymptotically stable modes are observable which means it is detectable.

Assumption 3. The distribution matrix M_i of the additive fault in equation (24) satisfies

$$\mathrm{rank}(C_i M_i) = q. \tag{30}$$

Assumption 4. $\Gamma(x,t)$ the known nonlinear function satisfies the local condition of Lipschitz on $\mathbb{M} \subset \mathrm{R}^n$ with

$$\left\|\left(\Gamma\left(x_{a_1}, t\right) - \Gamma\left(x_{a_2}, t\right)\right)\right\| \le \left\|\left(x_{a_1} - x_{a_2}\right)\right\|\gamma, \forall\left(x_{a_2}, x_{a_1}\right) \in \mathbb{M}. \tag{31}$$

The constant of Lipschitz $\gamma > 0$ is unknown and $\Gamma(x,t)$ is globally Lipschitz if $\mathbb{M} = \mathrm{R}^n$. Edwards and Spurgeon [35] have studied an SMO to estimate faults and stats taking into account the following required assumptions.

The following lemma and definition are utilized to achieving the principal results.

4.1. Definition and Notation. Let $Z \in \mathrm{R}^{n\times m}$ a random matrix; if $Z^+ \in \mathrm{R}^{m\times n}$ satisfies $Z^+Z = I_m$, then $Z^+ = (Z^TZ)^{-1}Z^T$ is a left-inverse of Z.

Lemma 5. *For the two matrix Y and Z, the next condition carries*

$$Z^TY + Y^TZ \le \varepsilon^{-1}Z^TZ + \varepsilon Y^TY, \tag{32}$$

$\varepsilon > 0$.

We develop a novel adaptive SMO defined as

$$\dot{\hat{x}}(t) = \sum_{i=1}^{k} \mu_i(\zeta_t)\left\{A_i\hat{x}(t) + B_iu(t) + \hat{F}(u,t) + \Gamma(\hat{x},t) + G_{l,i}e_y(t) + G_{n,i}v(t)\right\}, \tag{33}$$

$$\hat{y}(t) = \sum_{i=1}^{k} \mu_i(\zeta_t)\{C_i\hat{x}(t)\}, \tag{34}$$

where $\hat{y}(t)$ and $e_y(t)$ denote, respectively, the output of the observer and estimation error, $\hat{x}(t)$ represents the observer state. $G_{n,i}$ and $G_{l,i}$ are suitable gain matrices. In this way, the signal $v(t)$ of the robust adaptive sliding mode is written as follows:

$$v(t) \coloneqq \begin{cases} \eta(t)\dfrac{P_e}{\|P_e\|}, & \text{if } e_y(t) \ne 0, \\ 0, & \text{otherwise,} \end{cases} \tag{35}$$

where $P_e = P_2e_y(t)$, $\eta(t) = \hat{\rho} + \varrho$ with ϱ is a scalar positive, $P_2 \in \mathbb{R}^{p\times p}$ is positive definite and symmetric and $\hat{\rho}$ is the adaptive term can be updated given by the following equation:

$$\dot{\hat{\rho}} = \alpha\|P_e\|, \hat{\rho}(0) \ge 0, \tag{36}$$

$\alpha > 0$ is a gain.

Under condition in equation (30), we can use a change of coordinates as follows:

$$\begin{bmatrix} x_1(t) \\ x_2(t) \end{bmatrix} = T_ix(t). \tag{37}$$

The matrices $A_i, B_i, D_i, M_i, C_i, G_{l,i}$, and $G_{n,i}$ become

$$\begin{aligned} A_i &= \begin{bmatrix} A_{11,i} & A_{12,i} \\ A_{21,i} & A_{22,i} \end{bmatrix}, \\ B_i &= \begin{bmatrix} B_{1,i} \\ B_{2,i} \end{bmatrix}, \\ D_i &= \begin{bmatrix} D_{1,i} \\ D_{2,i} \end{bmatrix}, \\ M_i &= \begin{bmatrix} 0 \\ M_{2,i} \end{bmatrix}, \\ C_i &= \begin{bmatrix} 0 & C_{2,i} \end{bmatrix}, \\ G_{l,i} &= \begin{bmatrix} G_{l1,i} \\ G_{l2,i} \end{bmatrix}, \\ G_{n,i} &= \begin{bmatrix} G_{n1,i} \\ G_{n2,i} \end{bmatrix}, \end{aligned} \tag{38}$$

where $A_{11,i} \in \mathbb{R}^{n_p\times n_p}, n_p = (n-p), D_{1,i} \in \mathbb{R}^{n_p\times l}, M_{2,i} \in \mathbb{R}^{p\times(q)}$ and $C_{2,i} \in \mathbb{R}^{p\times p}$ is nonsingular.

$e(t) = x(t) - \hat{x}(t)$ is the estimated error of the state.

$$\dot{e}_1(t) = \sum_{i=1}^{k} \mu_i(\zeta_t)\left\{A_{11,i}e_1(t) + \left(A_{12,i} - G_{l1,i}\right)e_y(t) - \Gamma_1(\hat{x},t) + \Gamma_1(x,t) + D_{1,i}\xi(x,t) - G_{n1,i}v(t) + e_{F_{a1}}(t)\right\} \tag{39}$$

$$\begin{aligned}\dot{e}_2(t) = \sum_{i=1}^{k} \mu_i(\zeta_t)\Big\{&A_{21,i}e_1(t) + \left(A_{22,i} - G_{l2,i}\right)e_y(t) - \Gamma_2(\hat{x},t) + \Gamma_2(x,t) \\ &+ D_{2,i}\xi(x,t) + M_{2,i}f_a(t) - G_{n2,i}v(t) + e_{F_{a2}}(t)\Big\}\end{aligned} \tag{40}$$

where $T_i\Gamma(x,t) = \left[\Gamma_1^T(x,t) \;\; \Gamma_2^T(x,t)\right]^T$ and $\left[e_{F_{a1}}(t) \;\; e_{F_{a2}}(t)\right]^T = T_i e_{F_a}(t) = T_i[F_a(t) - \hat{F}_a(t)]$

According to equation (37), the nonlinear gain is described by the following equation:

$$\begin{bmatrix} G_{n1,i} \\ G_{n2,i} \end{bmatrix} = \begin{bmatrix} -L_i\overline{C}_{2,i}^{-1} \\ C_{2,i}^{-1} \end{bmatrix}, \qquad L_i = \begin{bmatrix} L_{1,i} & 0 \end{bmatrix}. \tag{41}$$

4.2. Sliding Motion Stability. In addition, another change of coordinates is expressed by the following equation:

$$T_{L,i} = \begin{bmatrix} I_{n-p} & L_i \\ 0_{p\times(n-p)} & C_{2,i} \end{bmatrix}, \tag{42}$$

where L_i is discussed later. In the new coordinates system, we obtain

$$\begin{aligned} \widetilde{A}_i &= \begin{bmatrix} \widetilde{A}_{11,i} & \widetilde{A}_{12,i} \\ \widetilde{A}_{21,i} & \widetilde{A}_{22,i} \end{bmatrix}, \\ \widetilde{D}_i &= \begin{bmatrix} \widetilde{D}_{1,i} \\ \widetilde{D}_{2,i} \end{bmatrix}, \\ \widetilde{M}_i &= \begin{bmatrix} 0 \\ \widetilde{M}_{2,i} \end{bmatrix}, \\ \widetilde{C}_i &= \begin{bmatrix} 0 & I_p \end{bmatrix}. \end{aligned} \tag{43}$$

If $\widetilde{A}_{11,i} = A_{11,i} + L_iA_{21,i}$ should be stable, $\widetilde{D}_{1,i} = D_{1,i} + L_iD_{2,i}$, $\widetilde{D}_{2,i} = C_{2,i}D_{2,i}$ and $\widetilde{M}_{2,i} = C_{2,i}M_{2,i}$.

The observer gain matrices are

$$\begin{aligned} \begin{bmatrix} \widetilde{G}_{n1,i} \\ \widetilde{G}_{n2,i} \end{bmatrix} &= T_{L,i}\begin{bmatrix} G_{n1,i} \\ G_{n2,i} \end{bmatrix} = \begin{bmatrix} 0 \\ I_p \end{bmatrix}, \\ \begin{bmatrix} \widetilde{G}_{l1,i} \\ \widetilde{G}_{l2,i} \end{bmatrix} &= T_{L,i}\begin{bmatrix} G_{l1,i} \\ G_{l2,i} \end{bmatrix} = \begin{bmatrix} \widetilde{A}_{12,i} \\ \widetilde{A}_{22,i} - \widetilde{A}_{22}^s \end{bmatrix}, \end{aligned} \tag{44}$$

where $\widetilde{A}_{22}^s$ is the stable design matrix.

By referring to equation (42), the error system from equations (39)–(40) can be handled as follows:

$$\dot{\widetilde{e}}_1(t) = \sum_{i=1}^{k} \mu_i(\zeta_t)\left\{\widetilde{A}_{11,i}\widetilde{e}_1(t) + \widetilde{D}_{1,i}\xi(x,u,t) + T_{L_{1,i}}\widetilde{\Gamma}_1(x,t) + T_{L_{1,i}}e_{F_{a1}}(t)\right\}, \tag{45}$$

$$\dot{e}_y(t) = \sum_{i=1}^{k} \mu_i(\zeta_t)\left\{\widetilde{A}_{21,i}\widetilde{e}_1(t) + \widetilde{A}_{22}^s e_y(t) + \widetilde{D}_{2,i}\xi(x,t) + T_{L_{2,i}}\widetilde{\Gamma}_2(x,t) + \widetilde{M}_{2,i}f_a(t) - v(t) + T_{L_{2,i}}e_{F_{a2}}(t)\right\}, \tag{46}$$

where $\widetilde{\Gamma}_1(x,t) = \Gamma_1(x,t) - \Gamma_1(\hat{x},t)$ and $\widetilde{\Gamma}_2(x,t) = \Gamma_2(x,t) - \Gamma_2(\hat{x},t)$.

Our aim is to estimate the actuator faults and the states variables in the presence of multiplicative faults. Define

$$\begin{aligned} r(t) &= H\begin{bmatrix} \widetilde{e}_1(t) \\ e_y(t) \end{bmatrix} \\ &= H\widetilde{e}(t), \end{aligned} \tag{47}$$

where H is the weight matrix and it is supposed that $H = \mathrm{diag}(H_1, H_2)$.

We define the measure of performance in worst case as follows:

$$\|H\|_\infty := \sup_{\|\xi\|_2\neq 0} \frac{\|r(t)\|_2^2}{\|\xi(x,u,t)\|_2^2}. \tag{48}$$

Theorem 6. *Consider the T-S fuzzy system (25)–(27) and suppose that Assumptions 3 and 2 are checked. The asymptotically stability is archived for the state estimation errors (45)–(46) with both minimisation gain ς^* for $\xi(x,t)$ and maximisation admissible of γ^* for $\Gamma(x,t)$, if $\exists \varsigma, \alpha, \varepsilon$, $1 \geq \lambda \geq 0$ and matrices $P_1 > 0, P_2 > 0, W_i$ as*

$$\begin{bmatrix} \Xi_{1,i} + H_1^T H_1 & C_{2,i}^T A_{3,i}^T P_2 & P_1 D_{1,i} + W_i D_{2,i} & P_1 & 0 & I_{n-p} & 0 \\ (*) & \Xi_{2,i} + H_2^T H_2 & P_2 D_{2,i} & 0 & P_2 & 0 & I_p \\ (*) & (*) & -\varsigma I & 0 & 0 & 0 & 0 \\ (*) & (*) & (*) & -\varepsilon I & 0 & 0 & 0 \\ (*) & (*) & (*) & (*) & -\varepsilon I & 0 & 0 \\ (*) & (*) & (*) & (*) & (*) & -\alpha I_{n-p} & 0 \\ (*) & (*) & (*) & (*) & (*) & (*) & -\alpha I_p \end{bmatrix} < 0, \tag{49}$$

where

$$\begin{aligned} \Xi_{1,i} &= A_{11,i}^T P_1 + P_1 \overline{A}_{11,i} + W_i \overline{A}_{21,i} + A_{21,i}^T W_i^T + P_{F_1}, \\ \Xi_{2,i} &= \widetilde{A}_{22}^{sT} P_2 + P_2 \widetilde{A}_{22}^{s} + P_{F_2}. \end{aligned} \tag{50}$$

Proof. (see Appendix A)

Our aim is estimate the additive actuator faults in nonlinear system (25)–(27). The adaptive SMO donated by equations (33)–(34) has been developed and satisfies the condition of reachability, and then $e_y(t) = 0$ and $\dot{e}_y(t) = 0$. Then, equation (47) is then expressed as follows:

$$0 = \sum_{i=1}^{k} \mu_i(\zeta_t)\left\{\widetilde{A}_{21,i}\widetilde{e}_1(t) + T_{L2,i}\widetilde{\Gamma}_2(N,t) + \widetilde{D}_{2,i}\xi(N,t) + \widetilde{M}_{2,i} f_a(t) + T_{L2,i} e_{F_{a2}}(t) - \upsilon(t)\right\}, \tag{51}$$

where $N = T_{L,i}^{-1} x$.

The approximate equivalent of the output error injection signal $\upsilon_{eq}(t)$ is

$$\upsilon_{eq}(t) = \eta(t)\frac{P_e}{\|P_e\| + \sigma}, \tag{52}$$

where $\sigma > 0$ is a scalar to decrease the impact of chattering.

We define the next relation

$$\phi(\widetilde{e}_1, x, t) = \sum_{i=1}^{k} \mu_i(\zeta_t)\left\{T_{L2,i}\widetilde{\Gamma}_2(N,t) + \widetilde{A}_{21,i}\widetilde{e}_1(t) + \widetilde{D}_{2,i}\xi(N,t) + T_{L2,i} e_{F_{a2}}(t)\right\}. \tag{53}$$

It is clear that

$$\left\|\phi(\widetilde{e}_1, x, u)\right\|_2 \leq \sum_{i=1}^{k} \mu_i(\zeta_t)\varsigma_{\max,i}, \tag{54}$$

where $\varsigma_{\max,i} = \|\widetilde{D}_{2,i}\|_2 \xi_0 + (\|\widetilde{A}_{21,i}\|_2 + \gamma)\varpi$.

It remains to conclude from equation (54) that

$$\left\|\phi(\widetilde{e}_1, x, u)\right\| \leq \varsigma_{\max}. \tag{55}$$

Then, approximately, for a small $\varsigma_{\max}$, it seems that

$$0 = \sum_{i=1}^{k} \mu_i(\zeta_t)\left\{-\upsilon(t) + \widetilde{M}_{2,i} f_a(t)\right\}. \tag{56}$$

Therefore, the additive actuator faults estimation is given by

$$f_a(t) \approx \left(\sum_{i=1}^{k} \mu_i(\zeta_t)\widetilde{M}_{2,i}\right)^{+} \upsilon(t). \tag{57}$$

The method for FE with an adaptive SMO is outlined as

(i) Step 1: pick out the weight matrix in equation (47).

(ii) Step 2: pick out the suitable scalar "$0 \leq \lambda \leq 1$" and resolve the equation (49) (LMI optimization problem). So, we can obtain $P_1; W; P_2$ and ε, ς and γ.

(iii) Step 3: design the adaptive SMO (32)-(33); then, according to equations (51) and (57), the estimation of additive actuator faults can be accomplished. □

5. Sliding Mode FTC Design

5.1. Structure of Adaptive Sliding Mode Controller. This part of the article is devoted to explore an adaptive sliding mode FTC design founded on estimated state variables as well as actuator faults information (magnitude, type, and occurrence time). To stabilize the nonlinear system and compensate additive and multiplicative actuator faults effects, the proposed SMC with adaptive law was used to envisage a corrective action. Therefore, we assume that the nonlinear system with uncertainties (6)–(8) can be modeled by T-S fuzzy representation with both local nonlinearities and uncertainties as follows:

$$\dot{x}(t) = \sum_{i=1}^{k} \mu_i(\zeta_t)\{A_i x(t) + F(u,t) + B_i u(t) + D_i \xi(x,t) + \Gamma(x,t) + M_i f_a(t)\}, \tag{58}$$

$$y(t) = \sum_{i=1}^{k} \mu_i(\zeta_t)\{C_i x(t)\}, \tag{59}$$

$$y_L(t) = \sum_{i=1}^{k} \mu_i(\zeta_t)\{C_{(L,i)} x(t)\}. \tag{60}$$

First, the sliding motion takes place on a sliding surface denoted as $\mathbb{S}$ which is defined as follows:

$$\mathbb{S} = \{ S_c(t) = 0 :\ y_c(t) \in \mathbb{R}^p \}. \tag{61}$$

We describe the linear switching function $S_c(t) \in \mathbb{R}^m$ using the feedback information of the output

$$S_c(t) = \sum_{i=1}^{k} \mu_i(\zeta_t)\{ N_{c,i} y_c(t) \}, \tag{62}$$

$N_{c,i} = -h(-C_i B_i (C_i B_i)^{+}(+I_p)) + (C_i B_i)^{+}$ and $((C_i B_i)^{+} C_i B_i)^{-1} (C_i B_i)^{T} = (C_i B_i)^{+}$ where $h \in \mathbb{R}^{m \times p}$ is an arbitrary matrix.

The control input may be described as follows:

$$u(t) = u_l(t) + u_n(t). \tag{63}$$

The linear part denoted as $u_l(t)$ and depending on system states as well as both additive and multiplicative actuator faults estimation is expressed as follows:

$$u_l(t) = \sum_{j=1}^{k} \mu_j(\zeta_t)\left\{ -K_j \hat{x}(t) - q_a \hat{f}_a(t) - q_F \hat{F}(u,t) \right\}, \tag{64}$$

where $-q_a(\hat{f}_a(t) + \hat{F}(u,t))$ is created to compensate the additive and multiplicative faults influence. Assume that $q_a = B_i^{+} M_i, q_F = B_i^{+}$ and $K_j \in \mathbb{R}^{m \times n}$.

The adaptive nonlinear control input part $u_n(t)$ is proposed as follows:

$$u_n(t) \coloneqq \begin{cases} \eta_c(t) \dfrac{S_c(t)}{\|S_c(t)\|}, & \text{if } S_c(t) \neq 0, \\ 0, & \text{otherwise,} \end{cases} \tag{65}$$

$\eta_c(t) = \hat{\rho}_c + \varepsilon_c + \varrho_c$ where ε_c and ϱ_c are small and positive constants. $\eta_c(t)$ is determined by using $\hat{\rho}_c$.

$$\dot{\hat{\rho}}_{S_c} = \|S_c(t)\| \epsilon_c, \hat{\rho}_c(0) \geq 0, \epsilon_c > 0. \tag{66}$$

5.2. FTC Design. Using the part $u_n(t)$ of control input, we need to prove the sliding and the reaching of $\mathbb{S}$ in a finite time. Construct the function of Lyapunov as follows:

$$V_c(t) = \frac{1}{2\epsilon_c} \tilde{\rho}_c^2 + \frac{1}{2} S_c^T(t) S_c(t), \tag{67}$$

$\tilde{\rho}_c = \rho_c - \hat{\rho}_c$.

Referring to equation (58), the derivative of (67) is given by the following equation:

$$\begin{aligned} \dot{V}_c(t) &= \sum_{i=1}^{k}\sum_{j=1}^{k} \mu_i \mu_j(\zeta_t)\left\{-\rho_c - K_j \|x(t)\| - \eta_c(t)\right\}\|S_c(t)\| - \|S_c(t)\|\tilde{\rho}_c \\ &= \sum_{i=1}^{k}\sum_{j=1}^{k} \mu_i \mu_j(\zeta_t)\left\{\left(-K_j\right)\|x(t)\| - \rho_c - \varepsilon_c\right\}\|S_c(t)\|. \end{aligned} \tag{68}$$

Define Ω_c as

$$\Omega_c \coloneqq \{x :\ \|x(t)\| \leq \kappa_c\}. \tag{69}$$

If the sliding surface S is reached, the condition of reachability is satisfied. Then, ϱ_c is select to fulfill $\varrho_c > \kappa_c(C_i A_i - K_j)$ as

$$-\|S_c(t)\|\varepsilon_c \geq S_c^T(t) S_c(t). \tag{70}$$

An perfect sliding motion is guaranteed to occur in finite time by the suggested SMC with adaptive law, $\forall t \geq t_c\ S_c(t) = \dot{S}_c(t) = 0$. When the SM is required, we

examine the stability. We suppose that $u_{eq}(t)$ such that $\dot{S}_c(t) = 0$, as

$$u_{eq}(t) = \sum_{i=1}^{k} \mu_i(\zeta_t)\{-[\Gamma(x,t) + A_i x(t)] + u_l(t) - D_i \xi(x,t)\}. \tag{71}$$

The closed-loop dynamic system with equation (71) is

$$\dot{x}(t) = \sum_{i=1}^{k}\sum_{j=1}^{k} \mu_i\mu_j(\zeta_t)\left\{\left(\left(-B_iK_j\right) + \left(\theta_i A_i\right)\right)x(t) + \overline{B}_{i,j}\phi(t) + \theta_i\Gamma(x,t)\right\}, \tag{72}$$

$$y_c(t) = \sum_{i=1}^{k} \mu_i(\zeta_t)\{\, y(t)\,\}, \tag{73}$$

$$y_L(t) = \sum_{i=1}^{k} \mu_i(\zeta_t)\left\{C_{(L,i)}x(t)\right\}, \tag{74}$$

where $\theta_i = I_n, \overline{B}_{i,j} = [B_iK_jM_iI_n\theta_iD_i]$ and $\phi(t) = \begin{bmatrix} e^T(t) \\ e_{f_a}^T(t) \\ e_F^T(t) \\ \xi^T(x,t) \end{bmatrix}$.

Assumption 8. The condition of Lipschitz is satisfied by

$$\|\Gamma(x,t)\| \le \|x(t)\|, \tag{75}$$

γ denotes the constant of Lipschitz.

Theorem 9. *The T-S fuzzy system with local nonlinear models (72)–(74) is stable robustly with a maximization of the Lipschitz constant γ, positive scalars $\lambda_c, \alpha_c, \delta_c$, and the minimization of attenuation level ς_c, if there exist the matrices $Y = Y^T, Q_j$ and $\overline{P}_x = \overline{P}_x^T > 0$ where the optimization problem of multiobjective linear matrix inequality has a resolution.*

$$\text{Minimize } [(1-\lambda_c)\varsigma_c + \lambda_c(\delta_c + \alpha_c)], \text{ subject to}$$

$$\Delta_{\text{control},ij} := \begin{bmatrix} \Upsilon i,j & B_iQ_j & M_i & \theta_iD_i & \overline{P}_xC_{L,i}^T & \overline{P}_x & I_n \\ (*) & -2Y + \varsigma_cI_n & 0 & 0 & 0 & 0 & 0 \\ (*) & (*) & -\varsigma_cI_q & 0 & 0 & 0 & 0 \\ (*) & (*) & (*) & -\varsigma_cI_l & 0 & 0 & 0 \\ (*) & (*) & (*) & (*) & -I_{p1} & 0 & 0 \\ (*) & (*) & (*) & (*) & (*) & -\delta_cI_n & 0 \\ (*) & (*) & (*) & (*) & (*) & (*) & -\alpha_cI_n \end{bmatrix} < 0, \tag{76}$$

where

$$\begin{aligned} \Upsilon i,j &= \theta_iA_i\overline{P}_x + \overline{P}_xA_i^T\theta_i^T - Q_j^TB_i^T - B_iQ_j, \\ Y &= \mu_c\overline{P}_x. \end{aligned} \tag{77}$$

According to the results, it is possible to obtain the adaptive SMC from $K_j = Q_j\overline{P}_x^{-1}$.

Proof. (see Appendix B)

A design method for adaptive FTC with an adaptive SMO is outlined as follows:

(i) Step 1: select "$0 \le \lambda_c \le 1$", resolve the LMI optimization problem (76); so we get the matrices Q_j and the scalars δ_c, ς_c and γ_c

(ii) Step 2: calculate $K_j = Q_j\overline{P}_x^{-1}$

(ii) Step 3: concept the Adaptive SMC (65), then the stability of (51), (57) is accomplished. □

6. Case Study

The sliding mode FTC design according to the sliding mode observer is accomplished by considering the inverted pendulum and cart system. The objective is to conceive an adaptive stabilization controller that the considered inverted pendulum benchmark system [36, 37] consists of a moveable carriage having one degree (see Figure 3). The carriage is freely rotatable in driving direction on which a pendulum is mounted and actuated by a motor.

6.1. The Nonlinear System Modelling. We start by examining the model inverted pendulum and cart system

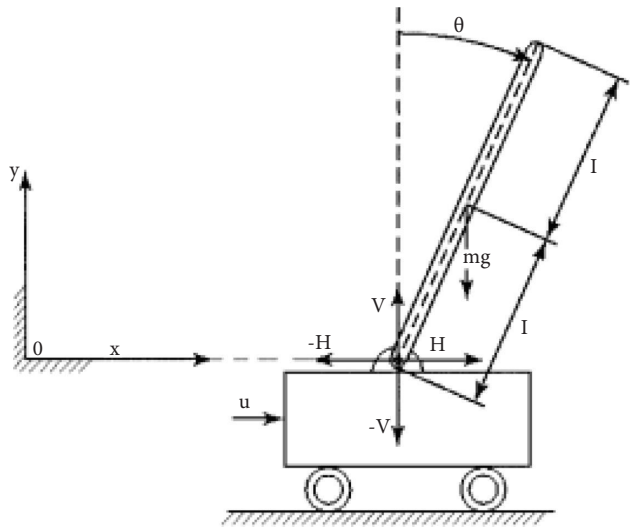

Figure 3: Inverted pendulum.

$$\begin{cases} \dot{x}_1(t) = x_2(t), \\ \dot{x}_2(t) = \dfrac{g\sin\left(x_1(t)\right) - m\,l\,a\,x_2^2(t)\,\left(\sin\left(2x_1(t)\right)/2\right) - ba\cos\left(x_1(t)\right)x_4(t)}{(4l/3) - m\,l\,a\cos\left(x_1(t)\right)^2}, \\ -\dfrac{a\cos\left(x_1(t)\right)\left(\beta u(t) - f_c\right)}{(4l/3) - m\,l\,a\cos\left(x_1(t)\right)^2}, \\ \dot{x}_3(t) = x_4(t), \\ \dot{x}_4(t) = \dfrac{-m\,g\,a\left(\sin\left(2x_1(t)\right)/2\right) + (4\,m\,l\,a/3)\,x_2^2(t)\sin\left(x_1(t)\right) - b\,a\,x_4(t)}{(4/3) - m\,a\cos\left(x_1(t)\right)^2}, \\ -\dfrac{(4a/3)\left(u(t) - f_c\right)}{(4/3) - m\,a\cos\left(x_1(t)\right)^2}, \end{cases} \tag{78}$$

where β is the efficiency factor. $x_4(t), x_3(t), x_2(t)$, and $x_1(t)$ represent, respectively, speed of cart, angular velocity of pendulum, cart position, and angle position of pendulum. Let us consider $f_c = \text{csign}(x_4(t))$ and $a = 1/(M+m)$.

The parameters of the system are shown in Table 1.

The approximation of the nonlinear faulty system may be obtained by T-S fuzzy system. We use in this study the models with local nonlinearity as follows:

$$\begin{aligned} \dot{x}(t) &= \sum_{i=1}^{k} \mu_i(\zeta_t)\{A_i x(t) + B_i u(t) + F(u,t) + M_i f_a(t) + D_i \xi(x,t) + \Gamma(x,t)\}, \\ y(t) &= \sum_{i=1}^{k} \mu_i(\zeta_t)\{C_i x(t)\}, \\ y_L(t) &= \sum_{i=1}^{k} \mu_i(\zeta_t)\left\{C_{(L,i)} x(t)\right\}. \end{aligned} \tag{79}$$

Table 1: System parameters.

Symbol	Description	Value	Unit
m	Pendulum point mass	0.2	kg
M	Cart mass	0.8	kg
l	From mass point to joint distance	0.5	m
g	Gravitational constant	9.81	ms^{-2}
L	Rail length	2	m

In this case, $\Gamma(x,t) = x_2^2(t)\text{lmsin}(x_1(t)) - f_c$, the fuzzy weights, are defined by the following equations:

$$\mu_1(t) = \frac{1 - (1/1 + \exp(-14(x_1(t) - (\Pi/8))))}{1 + \exp(-14(x_1(t) - (\Pi/8)))},$$
$$\mu_2(t) = 1 - \mu_1(t). \tag{80}$$

We assume that the actuator faults as well as the control input are in the same direction $B_i = M_i$. The matrices of the local nonlinear models are

$$A_1 = \begin{bmatrix} 0 & 1 & 0 & 0 \\ 17.3118 & 0 & 0 & 0.0106 \\ 0 & 0 & 0 & 1 \\ -1.7312 & 0 & 0 & -0.0053 \end{bmatrix},$$
$$B_1 = \begin{bmatrix} 0 \\ -0.1765 \\ 0 \\ 0.1176 \end{bmatrix},$$
$$A_2 = \begin{bmatrix} 0 & 1 & 0 & 0 \\ 14.3223 & 0 & 0 & 0.0069 \\ 0 & 0 & 0 & 1 \\ -1.0127 & 0 & 0 & -0.049 \end{bmatrix},$$
$$B_2 = \begin{bmatrix} 0 \\ -0.1147 \\ 0 \\ 0.1081 \end{bmatrix}, \tag{81}$$
$$D_1 = D_2 = \begin{bmatrix} -1 \\ -1 \\ 0 \\ -1 \end{bmatrix},$$
$$C_1 = C_2 = \begin{bmatrix} 1 & 0 & 0 & 0 \\ 0 & 1 & 0 & 0 \\ 0 & 0 & 1 & 1 \end{bmatrix},$$
$$C_{L1} = C_{L2} = \begin{bmatrix} 1 & 0 & 0 & 0 \\ 0 & 1 & 0 & 0 \\ 0 & 0 & 1 & 1 \end{bmatrix}.$$

6.2. Adaptive Sliding Mode Observer and Controller Design. We will design an adaptive SMC based on the requirements of the observer information to stabilize the system.

6.3. SMO Design. The parameters are $\tilde{A}_{22}^s = \text{diag}(-3, -5, -7), \lambda = 0.5, H_1 = I_{1\times 1}, H_2 = 10 * I_{3\times 3}$.

We obtain using Theorem 6

$$\begin{bmatrix} \varepsilon^* & \alpha^* & \tilde{\gamma}^* \end{bmatrix} = \begin{bmatrix} 1.4913 & 09233 & 0.8522 \end{bmatrix},$$
$$L_1 = \begin{bmatrix} 1.8794 & 0 & 0 \end{bmatrix},$$
$$L_2 = \begin{bmatrix} 2.0548 & 0 & 0 \end{bmatrix},$$
$$P_1 = 3.6952, \tag{82}$$
$$P_2 = \begin{bmatrix} 1.4048 & 0 & -0.23 \\ 0 & 5.3765 & 0 \\ -0.2300 & 0 & 2.6683 \end{bmatrix},$$

The adaptive sliding mode observer (33) and (34) design is as follows:

$$G_{l,1} = \begin{bmatrix} 31.8794 & 0 & -1.5 \\ 73.6923 & -0.0106 & -104.9894 \\ 0 & 49 & 1 \\ -1.7318 & -49.9947 & 69.9947 \end{bmatrix},$$
$$G_{l,2} = \begin{bmatrix} 3.5548 & 0 & -1.0607 \\ 17.4045 & -0.0069 & -3.7054 \\ 0 & 1.5 & 1 \\ -1.0127 & -2.4951 & 3.4951 \end{bmatrix},$$
$$G_{n,1} = \begin{bmatrix} 1 & 0 & 0 \\ 1.8794 & 0 & -1.5 \\ 0 & 1 & 0 \\ 0 & -1 & 1 \end{bmatrix}, \tag{83}$$
$$G_{n,2} = \begin{bmatrix} 1 & 0 & 0 \\ 2.548 & 0 & -1.0607 \\ 0 & 1 & 0 \\ 1 & -1 & 1 \end{bmatrix}.$$

6.4. SMC Design. By using Theorem 9 for $\lambda_c = 0.95$, we find that

$$\varsigma_c^* = 0.3465,$$
$$\delta_c^* = 6.0749,$$
$$\alpha^* = 17.5312,$$
$$\gamma^* = 0.0969, \tag{84}$$
$$P_x = \begin{bmatrix} 0.4532 & -1.3951 & 0.2459 & -0.6225 \\ -1.3951 & 7.1217 & -0.0516 & -1.6025 \\ 0.2459 & -0.0516 & 5.6132 & -4.8928 \\ -0.6225 & -1.6025 & -4.8928 & 8.0061 \end{bmatrix}.$$

The sliding mode controller gains are expressed by the following equation:

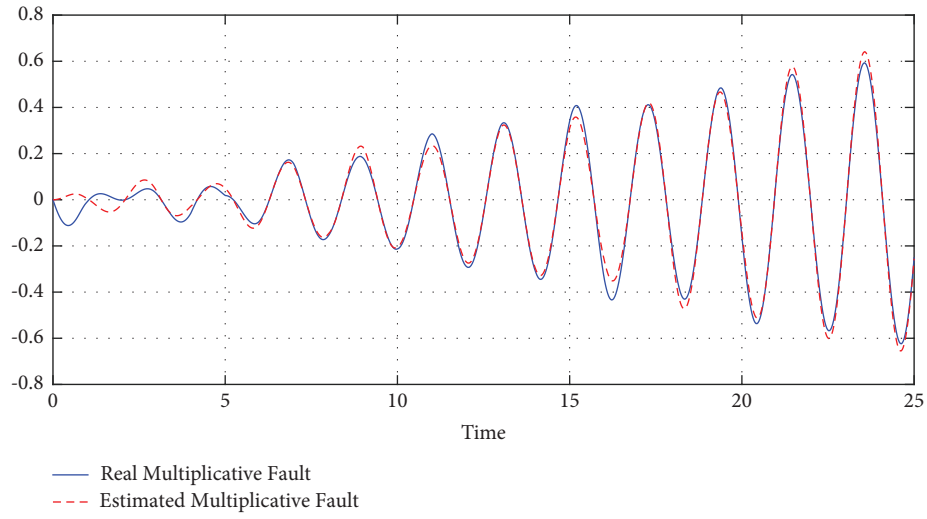

Figure 4: Multiplicative actuator FE.

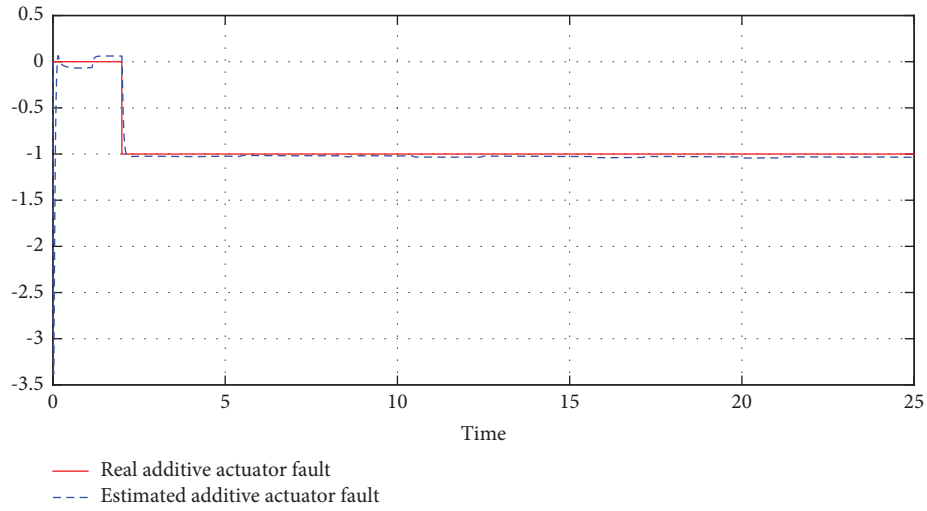

Figure 5: Additive actuator FE.

$$K_1 = K_2 = \begin{bmatrix} -1898 & -486.4 & -238.3 & -370 \end{bmatrix}. \quad (85)$$

6.5. Simulation Results. It is worth mentioning that the results are obtained using online simultaneous additive and multiplicative faults estimation.

Figure 4 illustrates multiplicative actuator fault estimation. In our example, we consider an additive linear time varying actuator fault. The developed adaptive sliding mode observer (33) and (34) can reject the effects of system uncertainties and make an estimation of actuator fault with satisfactory accuracy. Meanwhile, at $t = 2$, the additive actuator fault (Figure 5) has been introduced, in order to demonstrate the capacity of the developed estimation method to additive faults.

As shown in Figure 5, it is worth noting that in spite of the existence of uncertainties, the SMO can still track the additive faults $f_a(t)$. Hence, the simulation results outline that the suggested fault estimation with the adaptive law for the inverted pendulum and cart system described by T-S fuzzy representation with local nonlinear models accomplishes the first objective of this article (actuator faults estimation) with an excellent performance in terms of robustness and precision despite the presence of the uncertainties.

Figures 6–8 compare nonlinear output referring to three cases: output without faults, output without sliding mode FTC, and output responses with the conceived FTC design.

As can be seen from the comparison with the output responses without faults, the conceived adaptive sliding mode controller (63) is capable of the stabilization of the system.

Zoomed versions of the nonlinear inverted pendulum and cart system output responses illustrated in Figures 6–8 highlight a good satisfactory precision of the proposed adaptive FTC, which ensures the stability of the system subject to both additive and multiplicative faults. More precisely, it can be seen clearly that the integrated adaptive law is an effective way to improve both faults estimation and compensation.

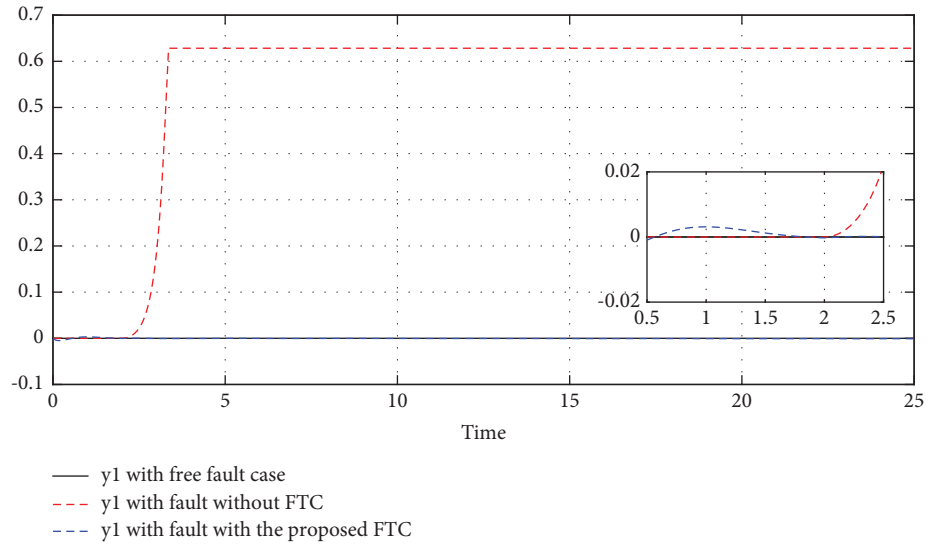

Figure 6: y_1 (black line) with free faults, y_1 (red line) without FTC, and y_1 (blue line) with FTC.

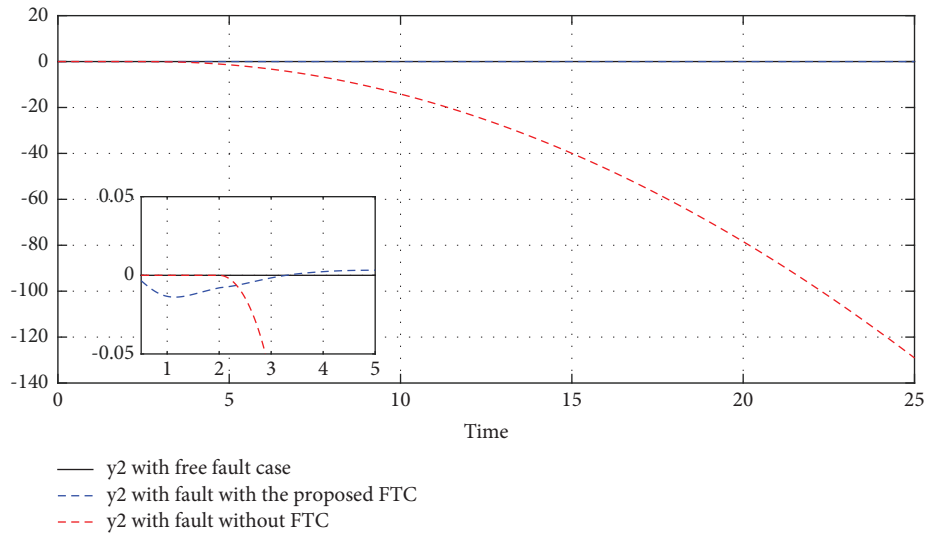

Figure 7: y_2 (black line) with free faults, y_2 (red line) without FTC, and y_2 (blue line) with FTC.

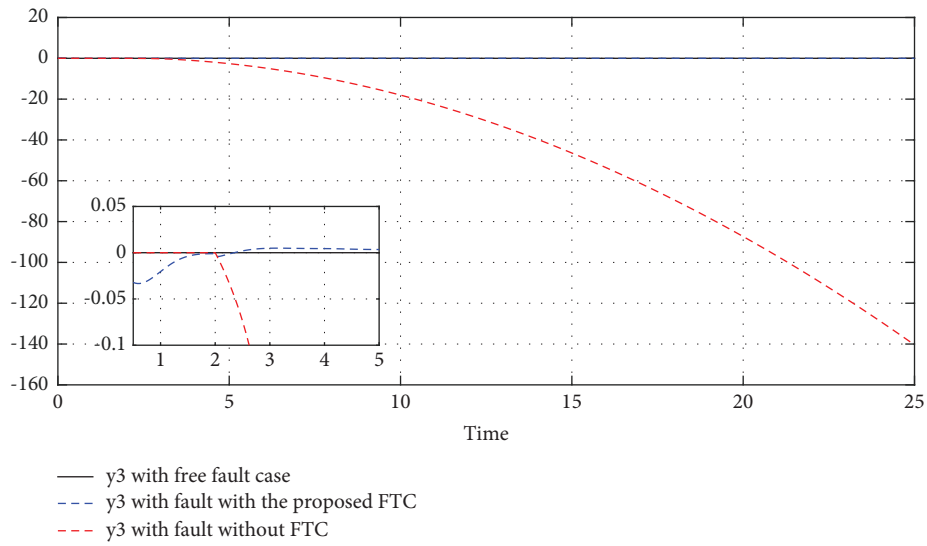

Figure 8: y_3 (black line) with free faults, y_3 (red line) without FTC, and y_3 (blue line) with FTC.

7. Conclusions

This paper addresses two powerful problems: the SMO scheme and the FE-based sliding mode FTC, concerning system described by T-S fuzzy representation and local nonlinear models. We start by the study of the multiplicative faults, and the actuator degradation process is considered as a source of performance deterioration. The degradation process in the actuator is modeled by Wiener process. The additive actuator faults are estimated using robust adaptive SMO in the existence of uncertainties so that the proposed observer's stability has been derived using H_∞ performances in order to minimize the uncertainties' effect on the dynamics of estimation error and solved within the linear matrix inequalities (LMI's) optimization design. To compensate the effects of both additive and multiplicative actuator faults and guarantee the system stability, an adaptive FTC with sliding mode control is studied. The existence conditions are expressed via Lyapunov approach in terms of LMI. Convex multiobjective optimization is employed to simultaneously maximize the nonlinear term Lipschitz constant in the T-S fuzzy modeling in addition to the uncertainties attenuation level, in order to obtain satisfactory gain of the adaptive SMO and controller. The results of the simulation on the application clearly display the efficiency of the proposed additive actuator FE and the adaptive FTC design with uncertainties in system. In our future work, we can use shock models (Poisson process) or combined models to characterize the stochastic deterioration process in an actuator. Indeed, the actuator is a device that operates dynamically in a random environment; its capacity may decrease in an accelerated way. So, we can integrate covariates in the degradation model with accelerated mode deterioration. The derivative of the output in the designer of observers could be taken into account to increase the performance of the estimation.

Appendix

Construct Lyapunov function as follows:

$$V(t) = V_{e_1}(t) + V_{e_y}(t), \tag{A.1}$$

$V_{e_y}(t) = (1/\beta)\tilde{\rho}^2 + e_y^T(t)P_e, V_{e_1}(t) = \tilde{e}_1^T(t)P_1\tilde{e}_1(t), P_1 \in \mathbb{R}^{(n_p)\times(n_p)}$. Taking $\dot{V}(t)$ along a trajectory of the taken system error,

$$\begin{aligned}\dot{V}_{e_1}(t) = \sum_{i=1}^{k}\mu_i(\zeta_t)\Big\{&\tilde{e}_1^T(t)\Big(\tilde{A}_{11,i}^T P_1 + P_1\tilde{A}_{11,i}\Big)\tilde{e}_1(t) + 2\tilde{e}_1^T(t)P_1\tilde{D}_{(1,i)}\xi(x,t)\\ &+ 2\tilde{e}_1^T(t)P_1T_{L_1,i}\tilde{\Gamma}_1(x,t) + 2\tilde{e}_1^T(t)P_1T_{L_1,i}e_{F_{a1}}(t)\Big\},\end{aligned} \tag{A.2}$$

$$\begin{aligned}\dot{V}_{e_y}(t) = \sum_{i=1}^{k}\mu_i(\zeta_t)\Big\{&e_y^T(t)\Big(\tilde{A}_{22}^{sT}P_2 + P_2\tilde{A}_{22}^{s}\Big)e_y(t) + 2e_y^T(t)P_2\tilde{A}_{21,i}\tilde{e}_1(t)\\ &+ 2e_y^T(t)P_2\tilde{D}_{2,i}\xi(x,t) + 2e_y^T(t)P_2T_{L_2,i}\tilde{\Gamma}_2(x,t) + 2e_y^T(t)P_2T_{L_2,i}e_{F_{a2}}(t)\\ &+ 2e_y^T(t)P_2\left[\tilde{M}_{2,i}f_a(t) - \upsilon(t)\right] - \frac{1}{\beta}\tilde{\rho}\dot{\tilde{\rho}}\},\end{aligned} \tag{A.3}$$

where $\tilde{\rho} = \rho - \hat{\rho}$.

By applying Lemma 5 and Assumption 4, it could be proving that

$$\begin{aligned}2\tilde{e}_1^T(t)P_1T_{L1,i}\tilde{\Gamma}_1(x,t) &\le \varepsilon\tilde{\gamma}^2\left\|\tilde{e}_1(t)\right\|^2 + \frac{1}{\varepsilon}\tilde{e}_1^T(t)P_1^2\tilde{e}_1(t),\\ 2\tilde{e}_y^T(t)P_2T_{L_2,i}\tilde{\Gamma}_2(x,t) &\le \varepsilon\tilde{\gamma}^2\left\|e_y(t)\right\|^2 + \frac{1}{\varepsilon}e_y^T(t)P_2^2\tilde{e}_y(t),\end{aligned} \tag{A.4}$$

$\widetilde{\gamma} = \gamma\|T_{L1,i}\|$, where γ is the constant of Lipschitz of $\Gamma(x,t)$

From the expression of $v(t)$ in equation (34), we deduce that

$$\begin{aligned} e_y^T(t)P_2M_{2,i}\left(-v(t)+f_a(t)\right) - \frac{1}{\beta}\widetilde{\rho}\dot{\widetilde{\rho}} &\le e_y^T(t)M_{2,i}^TP_2\left\|f_a(t)\right\| - \eta(t)e_y^T(t)P_2\frac{P_e}{\left\|P_e\right\|} - \widetilde{\rho}\left\|P_e\right\| \\ &\le e_y^T(t)M_{2,i}^TP_2\left\|f_a(t)\right\| - (\widehat{\rho}+\varrho)\left\|P_e\right\| - \widetilde{\rho}\left\|P_e\right\| \\ &\le \kappa_{i,\max}\left\|P_e\right\| - \varrho\left\|P_e\right\| \\ &< 0, \end{aligned} \tag{A.5}$$

where $\rho\|M_{2,i}\|_{\max} = \kappa_{i,\max}, \rho \ge \kappa_{i,\max}$.

For the multiplicative fault, we can write the inequality as follows:

$$\begin{aligned} 2\widetilde{e}_1^T(t)\left[P_1T_{L1,i}\right]e_{F_{a1}}(t) &\le \widetilde{e}_1^T(t)P_1\widetilde{e}_1(t) + \delta_{F_1}, \\ 2e_y^T(t)\left[P_2T_{L2,i}\right]e_{F_{a2}}(t) &\le e_y^T(t)P_2e_y(t) + \delta_{F_2}, \end{aligned} \tag{A.6}$$

where $\delta_{F_2} = \|e_{F_{a2}}(t)\|^2\lambda_{\max}(X_2^TP_2^{-1}X_2)$ and $\delta_{F_1} = \|e_{F_{a_1}}(t)\|^2\lambda_{\max}(X_1^TP_1^{-1}X_1)$.

The time derivative of $V_e(t)$ and $V_{e_y}(t)$

$$\begin{aligned} \dot{V}_e(t) \le \sum_{i=1}^{k}\mu_i(\zeta_t)\Big\{&\widetilde{e}_1^T(t)\Big[\widetilde{A}_{11,i}^TP_1 + P_1\widetilde{A}_{11,i} + \frac{1}{\varepsilon}P_1^2 + \varepsilon\widetilde{\gamma}^2I_{n-p} + P_1\Big]\widetilde{e}_1(t) \\ &+ 2\widetilde{e}_1^T(t)P_1\widetilde{D}_{1,i}\xi(x,t)\Big\}, \end{aligned} \tag{A.7}$$

and

$$\begin{aligned} \dot{V}_{e_y}(t) \le \sum_{i=1}^{k}\mu_i(\zeta_t)e_y^T(t)\Big[&P_2\widetilde{A}_{22}^s + \widetilde{A}_{22}^{sT}P_2 + \frac{1}{\varepsilon}P_2^2 + \varepsilon\widetilde{\gamma}^2I_p + P_2\Big]e_y(t) \\ &+ 2e_y^T(t)P_2\widetilde{D}_{2,i}\xi(x,t) + 2e_y^T(t)P_2\widetilde{A}_{21,i}\widetilde{e}_1(t)\Big\}. \end{aligned} \tag{A.8}$$

To obtain the robustness of the proposed adaptive SMO (33)-(34), let $V_0(t)$ be defined as

$$V_0(t) \coloneqq \dot{V}(t) - \varsigma\xi^T(x,t)\xi(x,t) + r^T(t)r(t). \tag{A.9}$$

We define the following variable α as

$$\alpha \coloneqq \frac{1}{\varepsilon\widetilde{\gamma}^2} \longrightarrow \widetilde{\gamma} = \frac{1}{\sqrt{\alpha\varepsilon}}. \tag{A.10}$$

To maximize $\widetilde{\gamma}$ for $\Gamma(x,t)$, we simultaneously minimize both ε and α. Referring to equation (A.10), we shall write the abovementioned expression (A.9) as follows:

$$V_0(t) \le \sum_{i=1}^{k}\mu_i(\zeta_t)\left\{\begin{bmatrix}\widetilde{e}_1(t)\\ e_y(t)\\ \xi(x,t)\end{bmatrix}\Delta_{\text{est},i}\begin{bmatrix}\widetilde{e}_1(t)\\ e_y(t)\\ \xi(x,t)\end{bmatrix}\right\}, \tag{A.11}$$

where

$$\Delta_{est,i} = \begin{bmatrix} \Pi_{1,i} & \widetilde{A}_{21,i}^TP_2 & P_1\widetilde{D}_{1,i} \\ P_2\widetilde{A}_{21,i} & \Pi_{2,i} & P_2\widetilde{D}_{2,i} \\ \widetilde{D}_{1,i}^TP_1 & \widetilde{D}_{2,i}P_2 & -\varsigma I_l \end{bmatrix}, \tag{A.12}$$

$$\Pi_{1,i} = \widetilde{A}_{11,i}^TP_1 + P_1\widetilde{A}_{11,i} + \frac{1}{\varepsilon}P_1^2 + \alpha^{-1}I_{n-p} + P_{F_1},$$

$$\Pi_{2,i} = \widetilde{A}_{22}^{sT}P_2 + P_2\widetilde{A}_{22}^s + \frac{1}{\varepsilon}P_2^2 + \alpha^{-1}I_p + P_{F_2}.$$

Thus, we conclude that $V_0(t)$ is negative, if

$$\sum_{i=1}^{k} \mu_i(\zeta_t)\Delta_{\text{est},i} < 0. \tag{A.13}$$

From the Schur complement, we deduce that the relation (A.13) and the relation (49) are equivalent. If equation (49) is satisfied, $V_0(t)$ is negative.

For proving that the error system of equation (45)–(47) is stable asymptotically with ς such that

$$\|r(t)\|_2^2 \le \|\xi(x,t)\|_2^2 \varsigma, \tag{A.14}$$

where ς is the attenuation level.

This completes the proof.

B

To guarantee the stability of system, we should investigate the next Lyapunov function

$$V_x(t) = x^T(t) P_x x(t), \tag{B.1}$$

$P_x \in \mathbb{R}^{n\times n}$ is definite positive symmetric.

According to (72)–(74),

$$\begin{aligned}\dot{V}_x(t) = \sum_{i=1}^{k}\sum_{j=1}^{k} \mu_i\mu_j(\zeta_t)\Big\{ & x^T(t)\Big(\left(-B_iK_j + \theta_iA_i\right)^T P_x + P_x\left(-B_iK_j + \theta_iA_i\right)\Big)x(t) \\ & + 2x^T(t)P_x\left[\overline{B}_{i,j}\phi(t) + \theta_i\Gamma(x,t)\right]\Big\}.\end{aligned} \tag{B.2}$$

Using Assumption 8 and Lemma 5, we obtain

$$\begin{aligned}2x^T(t)P_x\theta_i\Gamma(x,t) &\le \delta_c\Gamma^T(x,t)\theta_i^T\theta_i\Gamma(x,t) + \frac{1}{\delta_c}x^T(t)P_xP_xx(t) \\ &\le x^T(t)\left[\delta_c\left(\gamma\|\theta_i\|\right)^2 + \frac{1}{\delta_c}P_x^2\right]x(t).\end{aligned} \tag{B.3}$$

Let us define $J(t)$

$$J(t) = y_L^T(t)y_L(t) + \dot{V}_x(t) - \varsigma_c\phi^T(t)\phi(t). \tag{B.4}$$

We write equation (B.4) as follows:

$$\begin{aligned}J(t) = \sum_{i=1}^{k}\sum_{j=1}^{k} \mu_i\mu_j(\zeta_t)\Big\{ & x^T(t)\Big[+P_x\left(-B_iK_j + \theta_iA_i\right) + \left(-B_iK_j + \theta_iA_i\right)^T P_x + C_L^TC_L \\ & + \delta_c\tilde{\gamma}_c^2 + \frac{1}{\delta_c}P_x^2\Big]x(t) - \varsigma_c\phi^T(t)\phi(t) + 2x^T(t)P_x\overline{B}_{i,j}\phi(t)\Big\},\end{aligned} \tag{B.5}$$

where $(\|\theta_i\|\gamma) = \tilde{\gamma}_c$.

A novel variable is defined as

$$\alpha_c := \frac{1}{\delta_c\tilde{\gamma}_c{}^2} \Longleftrightarrow \tilde{\gamma}_c = \frac{1}{\sqrt{\alpha_c\delta_c}}. \tag{B.6}$$

The simultaneous minimization of α_c and δ_c, i.e., minimization of $\alpha_c + \delta_c$, can maximize $\tilde{\gamma}_c$ according to the nonlinear function of Lipschitz

Therefore, it must be proved that $J(t)$ are negative, if

$$\begin{bmatrix} \psi_{i,j} & P_x\overline{B}_{i,j} \\ \overline{B}_{i,j}^T P_x & -I\varsigma_c \end{bmatrix} < 0, \tag{B.7}$$

$$\psi_{i,j} = \left(-B_iK_j + \theta_iA_i\right)^T P_x + P_x\left(-B_iK_j + \theta_iA_i\right) + C_{L,i}^TC_{L,i} + \frac{1}{\delta_c}P_x^2 + \alpha_c^{-1}I_n.$$

Using the Shur complement, the following relation is easily obtained as follows:

$$\begin{bmatrix} \Theta_{i,j} & P_x B_i K_j & P_x M_i & P_x \theta_i D_i & C_{L,i}^T & P_x & I_n \\ (*) & -\varsigma_c I_n & 0 & 0 & 0 & 0 & 0 \\ (*) & (*) & -\varsigma_c I_q & 0 & 0 & 0 & 0 \\ (*) & (*) & (*) & -\varsigma_c I_l & 0 & 0 & 0 \\ (*) & (*) & (*) & (*) & -I_{p1} & 0 & 0 \\ (*) & (*) & (*) & (*) & (*) & -\delta_c I_n & 0 \\ (*) & (*) & (*) & (*) & (*) & (*) & -\alpha_c I_n \end{bmatrix} < 0, \tag{B.8}$$

where $\Theta_{i,j} = P_x \theta_i A_i + \theta_i^T A_i^T P_x - P_x B_i K_j - K_j^T B_i^T P_x$.

The following matrix X will be made as $X = \mathrm{diag}\left\{(P_x)^{-1}, (P_x)^{-1}, I_q, I_l, I_{p_1}, I_n, I_n\right\}$ post, pre-multiplying by X^T, X in (B.8), we obtain

$$\begin{bmatrix} \Upsilon i,j & B_i Q_j & M_i & \theta_i D_i & \overline{P}_x C_{L,i}^T & \overline{P}_x & I_n \\ (*) & -\varsigma_c \overline{P}_x \overline{P}_x & 0 & 0 & 0 & 0 & 0 \\ (*) & (*) & -\varsigma_c I_q & 0 & 0 & 0 & 0 \\ (*) & (*) & (*) & -\varsigma_c I_l & 0 & 0 & 0 \\ (*) & (*) & (*) & (*) & -I_{p1} & 0 & 0 \\ (*) & (*) & (*) & (*) & (*) & -\delta_c I_n & 0 \\ (*) & (*) & (*) & (*) & (*) & (*) & -\alpha_c I_n \end{bmatrix} < 0 \tag{B.9}$$

where

$$\Upsilon_{i,j} = \theta_i A_i \overline{P}_x + \overline{P}_x A_i^T \theta_i^T - Q_i^T B_i^T - B_i Q_j, P_x^{-1} = \overline{P}_x$$
$$K_j P_x^{-1} = Q_j. \tag{B.10}$$

Using Lemma 5, we obtain

$$-\overline{P}_x \overline{P}_x \varsigma_c \leq -2\overline{P}_x \varsigma_c + I_n \varsigma_c. \tag{B.11}$$

We can deduce that (B.11) holds, if

$$\sum_{i=1}^{k} \sum_{j=1}^{k} \mu_i \mu_j (\zeta_t) \Delta_{\mathrm{control},ij} < 0 \tag{B.12}$$

where $\Delta_{\mathrm{control},ij}$ has a similar structure as (76). Moreover, whether (B.12) is fulfilled, then $J(t)$ are negative, the T-S fuzzy system (72)–(74) is robustly stable in regard to γ and ς_c.

The proof is completed.

Data Availability

The data used to support the findings of this study are available from the corresponding author upon request.

Additional Points

The authors use Matlab simulink for simulation results, and they will improve it for other publication.

Conflicts of Interest

The authors declare that they have no conflicts of interest.

Acknowledgments

This study was funded by Laboratory of Engineering of Industrial Systems and Renewable Energy.

References

[1] Y. Wang, T. Li, and Y. Wu, "L∞ Fault Estimation and Faultfault-tolerant control for nonlinear systems by T–S fuzzy model method with local nonlinear models," *International Journal of Fuzzy Systems*, vol. 23, no. 1, pp. 1–14, 2021.

[2] X. Liu, Z. Gao, and A. Zhang, "Observer-based fault estimation and tolerant control for stochastic Takagi–Sugeno fuzzy systems with Brownian parameter perturbations," *Automatica*, vol. 102, pp. 137–149, 2019.

[3] R. Tayari, A. Ben Brahim, F. Ben Hmida, and A. Sallami, "Active fault tolerant control design for lpv systems with simultaneous actuator and sensor faults," *Mathematical Problems in Engineering*, vol. 2019, Article ID 5820394, 14 pages, 2019.

[4] A. Xu and Q. Zhang, "Nonlinear system fault diagnosis based on adaptive estimation," *Automatica*, vol. 40, no. 7, pp. 1181–1193, 2004.

[5] I. Jmel, H. Dimassi, S. Hadj-Said, and F. M'Sahli, "Adaptive observer-based sliding mode control for a two-wheeled self-balancing robot under terrain inclination and disturbances," *Mathematical Problems in Engineering*, vol. 2021, Article ID 8853441, 15 pages, 2021.

[6] P. Jin, W. Xue, and K. Li, "Actuator fault estimation for vehicle active suspensions based on adaptive observer and genetic algorithm," *Shock and Vibration*, Article ID 1783850, 12 pages, 2019.

[7] Y. Gao and H. Lu, "Sliding mode control of flexible articulated manipulator based on robust observer," *Computational Intelligence and Neuroscience*, vol. 2022, Article ID 2440770, 10 pages, 2022.

[8] A. B. Brahim, S. Dhahri, F. B. Hmida, and A. Sellami, "Simultaneous actuator and sensor faults estimation design for LPV systems using adaptive sliding mode observers," *International Journal of Automation and Control*, vol. 15, no. 1, pp. 1–27, 2021.

[9] H. L. Gao, H. C. Zhang, and X. L. Li, "Sliding mode control of the vehicle speed system based on LMIs," *Complexity*, vol. 2021, Article ID 5535213, 8 pages, 2021.

[10] A. Ben Brahim, S. Dhahri, F. Ben Hmida, and A. Sellami, "Multiplicative fault estimation-based adaptive sliding mode fault-tolerant control design for nonlinear systems," *Complexity*, vol. 2018, Article ID 1462594, 15 pages, 2018.

[11] A. Ben Brahim, S. Dhahri, F. Ben Hmida, and A. Sellami, "Simultaneous actuator and sensor faults reconstruction based on robust sliding mode observer for a class of nonlinear systems," *Asian Journal of Control*, vol. 19, no. 1, pp. 362–371, 2017.

[12] S. Asadi, A. Khayatian, M. Dehghani, N. Vafamand, and M. H. Khooban, "Robust sliding mode observer design for simultaneous fault reconstruction in perturbed Takagi-Sugeno fuzzy systems using non-quadratic stability analysis," *Journal of Vibration and Control*, vol. 26, no. 11-12, pp. 1092–1105, 2020.

[13] S. Dhahri, E. B. Alaïa, and F. B. Hmida, "Fault Estimation and Faultfault-tolerant control for TS fuzzy systems with actuator

and sensor faults using sliding mode observer," *Mathematical Problems in Engineering*, vol. 2022, Article ID 3647171, 14 pages, 2022.

[14] R. Raoufi, H. J. Marquez, and A. S. I. Zinober, "$\mathscr{H}_\infty$ sliding mode observers for uncertain nonlinear Lipschitz systems with fault estimation synthesis: $\mathscr{H}_\infty$ slidingmodeobservers," *International Journal of Robust and Nonlinear Control*, vol. 20, no. 16, pp. 1785–1801, 2010.

[15] A. Valibeygi, A. Toudeshki, and K. Vijayaraghavan, "Observer-based sensor fault estimation in nonlinear systems," vol. 230, no. 8, pp. 759–777, 2016.

[16] K. Le Son, M. Fouladirad, and A. Barros, "Remaining useful lifetime estimation and noisy gamma deterioration process," *Reliability Engineering & System Safety*, vol. 149, pp. 76–87, 2016.

[17] J. Riascos-Ochoa, M. Sánchez-Silva, and G. A. Klutke, "Modeling and reliability analysis of systems subject to multiple sources of degradation based on lévy processes," *Probabilistic Engineering Mechanics*, vol. 45, pp. 164–176, 2016.

[18] Q. Zhai and Z. S. Ye, "Rul prediction of deteriorating products using an adaptive wiener process model," *IEEE Transactions on Industrial Informatics*, vol. 13, no. 6, pp. 2911–2921, 2017.

[19] N. Mabrouk, M. H. Moulahi, and F. B. Hmida, "Combined degradation process and remaining useful life improvement in an actuator," in *Proceedings of the International Conference on Signal, Control and Communication (SCC)*, pp. 207–212, Hammamet, Tunisia, December 2021.

[20] L. Sun, X. Gu, and P. Song, "Accelerated degradation process analysis based on the nonlinear Wiener process with covariates and random effects," *Mathematical Problems in Engineering*, vol. 201613 pages, Article ID 5246108, 2016.

[21] A. F. Shahraki, O. P. Yadav, and H. Liao, "A review on degradation modelling and its engineering applications," *International Journal of Performability Engineering*, vol. 13, no. 3, pp. 299–314, 2017.

[22] Z. S. Ye, N. Chen, and Y. Shen, "A new class of Wiener process models for degradation analysis," *Reliability Engineering & System Safety*, vol. 139, pp. 58–67, 2015.

[23] M. Nabila, M. M. Hedi, and B. H. Fayçal, "Gamma process with covariets and remaining useful life improvement in an actuator," in *Proceedings of the 19th International Conference on Sciences and Techniques of Automatic Control and Computer Engineering (STA)*, pp. 208–213, Sousse, Tunisia, June 2019.

[24] H. Hove and F. Mlambo, "On wiener process degradation model for product reliability assessment: a simulation study," *Modelling and Simulation in Engineering*, vol. 2022, Article ID 7079532, 14 pages, 2022.

[25] T. Nakagawa, *Shock and Damage Models in Reliability Theory*, Springer Science and Business Media, Berlin, Germany, 2007.

[26] Z. Zhang, X. Si, C. Hu, and X. Kong, "Degradation modeling–based remaining useful life estimation: a review on approaches for systems with heterogeneity," vol. 229, no. 4, pp. 343–355, 2015.

[27] I. El-Thalji and E. Jantunen, "A descriptive model of wear evolution in rolling bearings," *Engineering Failure Analysis*, vol. 45, pp. 204–224, 2014.

[28] Y. Cao, S. Liu, Z. Fang, and W. Dong, "Modeling ageing effects in the context of continuous degradation and random shock," *Computers & Industrial Engineering*, vol. 145, Article ID 106539, 2020.

[29] A. Zemzemi, M. Kamel, A. Toumi, and M. Farza, "Robust integral-observer-based fault estimation for Lipschitz nonlinear systems with time-varying uncertainties," *Transactions of the Institute of Measurement and Control*, vol. 41, no. 7, pp. 1965–1974, 2019.

[30] H. Yang, Y. Jiang, and S. Yin, "Fault-tolerant control of time-delay Markov jump systems with Itô stochastic process and output disturbance based on sliding mode observer," *IEEE Transactions on Industrial Informatics*, vol. 14, no. 12, pp. 5299–5307, 2018.

[31] R. Hmidi, A. Ben Brahim, S. Dhahri, F. Ben Hmida, and A. Sellami, "Sliding mode fault-tolerant control for Takagi-Sugeno fuzzy systems with local nonlinear models: application to inverted pendulum and cart system," *Transactions of the Institute of Measurement and Control*, vol. 43, no. 4, pp. 975–990, 2021.

[32] X. G. Yan and C. Edwards, "Nonlinear robust fault reconstruction and estimation using a sliding mode observer," *Automatica*, vol. 43, no. 9, pp. 1605–1614, 2007.

[33] H. Yang, Y. Jiang, and S. Yin, "Adaptive fuzzy fault-tolerant control for Markov jump systems with additive and multiplicative actuator faults," *IEEE Transactions on Fuzzy Systems*, vol. 29, no. 4, pp. 772–785, 2021.

[34] D. Vališ and D. Mazurkiewicz, "Application of selected Levy processes for degradation modelling of long range mine belt using real-time data," *Archives of Civil and Mechanical Engineering*, vol. 18, no. 4, pp. 1430–1440, 2018.

[35] C. Edwards and S. K. Spurgeon, "On the development of discontinuous observers," *International Journal of Control*, vol. 59, no. 5, pp. 1211–1229, 1994.

[36] J. Han, H. Zhang, Y. Wang, and X. Liu, "Robust fault estimation and accommodation for a class of T–S fuzzy systems with local nonlinear models," *Circuits, Systems, and Signal Processing*, vol. 35, no. 10, pp. 3506–3530, 2016.

[37] M. Sami and R. J. Patton, "Active fault tolerant control for nonlinear systems with simultaneous actuator and sensor faults," *International Journal of Control, Automation and Systems*, vol. 11, no. 6, pp. 1149–1161, 2013.

Hindawi
Mathematical Problems in Engineering
Volume 2023, Article ID 6064024, 12 pages
https://doi.org/10.1155/2023/6064024

Research Article

H_∞ Control for the Nonlinear Markov Networked Control System in the Presence of Data Packet Loss and DoS Attacks via Observer

Yanfeng Wang,[1,2] **Xiaoyue Sun**,[2] **Youliang Tang**,[1] **Yuqin Hou**,[2] **Fanjun Lin**,[2] **Peiliang Wang**,[2] **and Linfeng Chen**[3]

[1]*School of Mechanical and Electrical Engineering, Suqian University, Suqian 223800, Jiangsu, China*
[2]*School of Engineering, Huzhou University, Huzhou 313000, Zhejiang, China*
[3]*Huzhou Jiuding Electronics Company Limited, Huzhou, Zhejiang, China*

Correspondence should be addressed to Fanjun Lin; lfj17860561716@163.com

Received 8 August 2022; Revised 5 December 2022; Accepted 4 May 2023; Published 2 June 2023

Academic Editor: Meng Li

The H_∞ control issue for nonlinear Markov networked control systems in the presence of data packet loss and periodic denial-of-service (DoS) attacks is researched in this paper. First, two Bernoulli random variables are used to describe the packet loss between sensor to controller and controller to actuator. Considering the impact of DoS attacks, the probability of packet loss is set to be different during the attack sleeping interval and the attack active interval. Secondly, an observer is constructed on the controller side, and a comprehensive mathematical model including packet loss and DoS attacks is established. The sufficient conditions for the stochastic stability of the system are derived by the Lyapunov theory, and the design method of the controller and the minimum disturbance suppression performance index are also provided. Finally, a numerical example is utilized to reveal the applicability of the approach.

1. Introduction

Over the years, owing to the continuous development of network technology and the widespread application of computer networks, the structure of the control system is undergoing changes. The traditional point-to-point control method gradually loses its dominant position as the system becomes more complex and geographically dispersed. The network control system (NCS) formed by introducing a network into a control system and connecting sensors, controllers, and actuators has appeared [1–5]. NCS has far-going application backgrounds in different fields such as aerospace, national defense, transportation, wireless communications, and industrial automation, which makes networked control one of the research hot spots in academia [6–10].

NCS integrates various infrastructures through the network, thereby making human-computer interaction and physical processes more convenient. However, the introduction of communication networks impacts the stability of the system and also makes the system face the threat of network attacks. Generally speaking, typical network attacks are mainly divided into two types. The first type is the deception attack, which destroys the system by inserting incorrect data or processing raw data. The second type is the denial of service (DoS) attack, whose intent is to prevent intercourse between different system components, thereby degrading system functionality or destroying system stability [11–13]. DoS attacks are easy to implement. For this reason, they have been extensively researched [14–17]. For example, for a NCS under stochastic disturbances and DoS attacks, a distributed predictive controller was designed [18]. By using random perturbation information and explicitly considering packet loss due to DoS attacks, an observer was designed to reconstruct the state. For a class of NCS with DoS attacks, a resilient state feedback controller was

designed [19]. The closed-loop system was modeled as an aperiodic sample data system that was related to the bound of the DoS attack duration. A state-error-dependent switched system model for NCS under resilient event-triggered communication schemes and periodic DoS attacks was proposed [20].

Data packet loss affects system performance as well as destabilizes the system, which has attracted a lot of attention and many research results have appeared. For instance, for the discrete NCSs subject to data packet loss in sensor-to-controller (S-C) and controller-to-actuator (C-A) channels, the range of successful packet transmission rates that made closed-loop NCSs stable was obtained with the asynchronous dynamical system theory [21]. For NCS suffering from S-C and C-A packet loss, an observer-based feedback control method was proposed. Considering the unmeasurable state of the controlled object, an observer was constructed to realize feedback control by describing the packet missing in S-C and C-A channels as stochastic Bernoulli variables [22]. The issue of predictive tracking control of NCSs subject to S-C data packet loss was investigated. The analysis of the packet miss impact on the performance of NCSs was carried out by taking input and output constraints into account [23]. Modeling the packet loss in the two channels as two independent Markov chains, the quantified dynamic output feedback control considering packet loss in the S-C and C-A channels was considered [24]. The above-mentioned results considered the problem of data packet loss without taking DoS attacks into account.

Currently, there are few results on the control problem for NCS in the presence of data packet loss and DoS attacks. The control issue for NCS with data packet dropout and DoS attacks was investigated [25]. However, the controlled plant in [25] was linear invariant system, and only the data packet loss in the S-C channel was considered. Moreover, resulted from the impacts such as component failures and environment changes, some control systems cannot be described by a definite model. The Markov jump system can be exploited to express the changes in the system parameters [26–29]. Therefore, the research for a networked Markov jump system subject to DoS attacks and data packet dropout has important theoretical and practical significance. The control problem of nonlinear Markov jump system subject to DoS attacks and data packet in both the S-C channel and C-A channel has not been researched, which motivates the current research. The contributions of this paper can be mainly exhibited as follows:

(1) Two independent Bernoulli variables are used to represent data packet loss in the S-C channel and C-A channel, respectively. Considering the fact that there is data packet transmission during the attack active interval, the probability of successful data packet transmission is set to be nonzero, which is much smaller than that during the attack sleeping interval.

(2) The closed-loop system is modeled as a class of control system with two variables. Under the designed controller, the closed-loop system is still stochastically stable and attains the H_∞ performance. And the connection between the disturbance suppression capability and DoS attacks is revealed.

The following content is divided into four sections. Section 2 establishes the mathematical model for nonlinear Markov NCS. Section 3 provides sufficient conditions on stochastic stability and the design method of the controller. In Section 4, numerical simulation example shows the effectiveness of the designed controller. Section 5 gives conclusions of this paper.

Notations: R^n represents the-dimensional Euclidean space. $*$ represents the transpose of the corresponding matrix block. A^{T} represents the transpose of the matrix A. If the matrix A is invertible, A^{-1} represents the inverse of A. The real positive definite matrix X is represented as $X > 0$. I represents the unit matrix of appropriate dimensions, and $\mathrm{diag}\{a, b \ldots\}$ represents the diagonal matrix with a, b as the main diagonal. $\Pr\{\cdot\}$ means mathematical probability. $E\{\cdot\}$ stands for mathematical expectation and $\mathrm{Var}\{\cdot\}$ denotes variance.

2. Problem Formulation

The structure of nonlinear NCS subject to data packet loss and DoS attacks is exhibited in Figure 1, and the state equation of the plant is as follows:

$$\begin{cases} x(l+1) = A_{\delta(l)}x(l) + B_{\delta(l)}u(l) + D_{\delta(l)}\omega(l) \\ +f_{\delta(l)}(l, x(l)), \\ y(l) = C_{\delta(l)}x(l), \end{cases} \tag{1}$$

where $x(l) \in R^n$ represents the state, $u(l) \in R^m$ denotes the control input, $\omega(l) \in R^s$ stands for the disturbance, $y(l) \in R^r$ is the output, and $A_{\delta(l)}$, $B_{\delta(l)}$, $C_{\delta(l)}$, and $D_{\delta(l)}$ are known matrices with suitable dimensions. $\delta(l)$ takes value from $\ell = \{1, 2, \ldots, g\}$, and the transition possibility matrix of ℓ is $\Pi = [\pi_{ij}]$, $\pi_{ij} = \Pr\{\delta(l+1) = j \mid \delta(l) = i\}$, $\sum_{j=1}^{g} \pi_{ij} = 1$, and $\pi_{ij} \geq 0, i, j \in \ell$. $f_{\delta(l)}(l, x(l))$ is a nonlinear vector function and satisfies the following global Lipschitz condition [22]:

$$\left\| f_{\delta(l)}(l, x(l)) \right\| \leq \left\| G_{\delta(l)}x(l) \right\|, \tag{2}$$

$$\left\| f_{\delta(l)}(l, x(l)) - f_{\delta(l)}(l, y(l)) \right\| \leq \left\| G_{\delta(l)}(x(l) - y(l)) \right\|, \tag{3}$$

where $G_{\delta(l)}$ is a known real constant matrix.

Communication between NCS components usually suffers damage from malicious attackers. We suppose that the DoS attacks occur in the S-C channel. For the intent to describe the DoS attacks more conveniently, a power-constrained periodic jamming signal is illustrated as follows:

$$\lambda = \begin{cases} 1, l \in [(d-1)T, (d-1)T + T_{\mathrm{off}}), \\ 2, l \in [(d-1)T + T_{\mathrm{off}}, \mathrm{d}T), \end{cases} \tag{4}$$

where d indicates the period number, T indicates the attack period, T_{off} indicates attack sleeping interval, $\lambda = 1$ indicates it is in the sleeping interval of attack in the dth attack cycle, and $\lambda = 2$ indicates it is in the active interval of attack in the dth attack cycle.

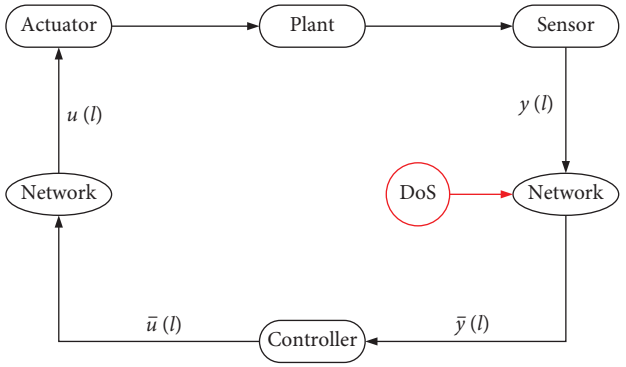

FIGURE 1: Nonlinear networked control system with data packet loss and DoS attacks.

Owing to the nature of the network, such as bandwidth limitations and network overcrowding, packets are unavoidably lost during transference. We suppose that the packet loss scenarios also exist during the sleeping interval. A random variable $\alpha(l) \in \{0, 1\}$ is defined to describe the data packet transmission in the S-C channel. If $\alpha(l) = 0$, the data packet in the S-C channel is lost; if $\alpha(l) = 1$, the packet is successfully transmitted.

The random variable $\alpha(l)$ follows a Bernoulli distribution. For the sleeping interval, we suppose that the probability of successful data packet transference is $\Pr\{\alpha(l) = 1\} = \alpha_1$, and the probability of data packet transference failure is $\Pr\{\alpha(l) = 0\} = 1 - \alpha_1$. For the active period, the probability of successful data packet transmission is $\Pr\{\alpha(l) = 1\} = \alpha_2$, and the probability of data packet transference failure is $\Pr\{\alpha(l) = 0\} = 1 - \alpha_2$.

Therefore, the following equation can be obtained:

$$\begin{cases} \Pr\{\alpha(l) = 1\} = \alpha_\lambda, \\ \Pr\{\alpha(l) = 0\} = 1 - \alpha_\lambda, \end{cases} \tag{5}$$

where $\lambda = \begin{cases} 1, l \in [(d-1)T, (d-1)T + T_{\text{off}}) \\ 2, l \in [(d-1)T + T_{\text{off}}, \mathrm{d}T) \end{cases}$ and $\mathrm{Var}\{\alpha(l)\} = E\{(\alpha_\lambda(l) - \alpha_\lambda)^2\} = (1 - \alpha_\lambda)\alpha_\lambda = \overline{\alpha}_\lambda^2$.

Remark 1. In the attack active interval, the data packet loss phenomenon is more severe than that in the sleeping period, therefore, $\alpha_2 < \alpha_1$.

Similarly, we define a random variable $\beta(l) \in \{0, 1\}$ to describe the data packet transmission in the C-A channel. When $\beta(l) = 0$, the data packets transmitted in the C-A channel are lost; when $\beta(l) = 1$, the data packets are successfully transmitted, and the Bernoulli distribution white sequence of random variable $\beta(l)$ is as follows:

$$\begin{aligned} &\Pr\{\beta(l) = 1\} = \beta, \\ &\Pr\{\beta(l) = 0\} = 1 - \beta, \\ &\mathrm{Var}\{\beta(l)\} = E\{(\beta(l) - \beta)^2\} = (1 - \beta)\beta = \overline{\beta}^2. \end{aligned} \tag{6}$$

The state equation of the observer is as follows:

$$\begin{cases} \hat{x}(l+1) = A_{\delta(l)}\hat{x}(l) + B_{\delta(l)}\overline{u}(l) + f_{\delta(l)}(l, \hat{x}(l)) \\ + L\left(\overline{y}(l) - \alpha_\lambda C_{\delta(l)}\hat{x}(l)\right), \\ u(l) = \beta(l)\overline{u}(l), \end{cases} \tag{7}$$

where $\overline{y}(l) = \alpha_\lambda(l)y(l)$, $\hat{x}(l) \in R^n$ means the state of the observer, and $\overline{u}(l) \in R^m$ means the control input of the observer.

Due to the possible data packet loss in C-A channel, the control input of the controlled plant is as follows:

$$\overline{u}(l) = K\hat{x}(l). \tag{8}$$

Define the state estimation error $e(l) = x(l) - \hat{x}(l)$. Substituting (7) into (1) and (8), the closed-loop system model can be written as follows:

$$\begin{cases} x(l+1) = \left(A_{\delta(l)} + \beta B_{\delta(l)}K\right)x(l) - \beta B_{\delta(l)}Ke(l) \\ + (\beta(l) - \beta)B_{\delta(l)}Kx(l) + D_{\delta(l)}\omega(l) \\ - (\beta(l) - \beta)B_{\delta(l)}Ke(l) + f_{\delta(l)}(l, x(l)), \\ e(l+1) = (\beta - 1)B_{\delta(l)}Kx(l) - (\beta(l) - \beta)B_{\delta(l)}Ke(l) \\ + \left(A_{\delta(l)} - (\beta - 1)B_{\delta(l)}K - \alpha_\lambda LC_{\delta(l)}\right)e(l) \\ + (\beta(l) - \beta)B_{\delta(l)}Kx(l) + D_{\delta(l)}\omega(l) \\ - (\alpha_\lambda(l) - \alpha_\lambda)LC_{\delta(l)}e(l) + F_{\delta(l)}(l), \end{cases} \tag{9}$$

where $F_{\delta(l)}(l) = f_{\delta(l)}(l, x(l)) - f_{\delta(l)}(l, \hat{x}(l))$.

Define $\eta(l) = \left[x^T(l) \;\; e^T(l)\right]^T$; then the closed-loop system (9) can be expressed as follows:

$$\begin{aligned} \eta(l+1) = \overline{A}\eta(l) + (\beta(l) - \beta)\overline{B}\eta(l) + \overline{D}\omega(l) \\ + (\alpha_\lambda(l) - \alpha_\lambda)\overline{C}\eta(l) + \overline{F}(l), \end{aligned} \tag{10}$$

where

$$\begin{aligned} \overline{A} &= \begin{bmatrix} A_{\delta(l)} + \beta B_{\delta(l)}K & -\beta B_{\delta(l)}K \\ (\beta - 1)B_{\delta(l)}K & A_{\delta(l)} - (\beta - 1)B_{\delta(l)}K - \alpha_\lambda LC_{\delta(l)} \end{bmatrix}, \\ \overline{B} &= \begin{bmatrix} B_{\delta(l)}K & -B_{\delta(l)}K \\ B_{\delta(l)}K & -B_{\delta(l)}K \end{bmatrix}, \overline{C} = \begin{bmatrix} 0 & 0 \\ 0 & -LC_{\delta(l)} \end{bmatrix}, \\ \overline{D} &= \begin{bmatrix} D_{\delta(l)} \\ D_{\delta(l)} \end{bmatrix}, \overline{F}(l) = \begin{bmatrix} f_{\delta(l)}(l, x(l)) \\ F_{\delta(l)}(l) \end{bmatrix}. \end{aligned} \tag{11}$$

Definition 2. (see [30]) When $\omega(l) = 0$, if for whichever initial mode $\delta(0)$ and state $\eta(0)$, such that

$$E\left\{\sum_{l=0}^{\infty} \|\eta(l)\|^2 \mid \eta(0), \delta(0)\right\} < \infty, \tag{12}$$

then system (10) is stochastically stable.

System (10) under random data packet loss and DoS attacks is stochastically stable and attains the H_∞ performance requirement, if the following two requirements are satisfied:

(1) System (10) under consideration is stochastically stable

(2) Under the zero initial condition, for all $\omega(l) \neq 0$, the controlled output $y(l)$ satisfies

$$E\left\{\sum_{l=0}^{\infty} y^{\mathrm{T}}(l)y(l)\right\} < \gamma^2 E\left\{\sum_{l=0}^{\infty} \omega^{\mathrm{T}}(l)\omega(l)\right\}, \tag{13}$$

where $\gamma > 0$ is a prescribed scalar.

Remark 3. Only the DoS attacks in the S-C channel is considered in this paper. The obtained results can be extended to the case where the DoS attacks exist in both the S-C and C-A channel, and the probability of packet loss in the C-A channel can be considered for both attack active interval and attack sleeping interval.

Lemma 4. *(see [31]) (S-procedure) Letting $T_i \in R^{n\times n}(i = 0, 1, \ldots, p)$ be symmetric matrices, $T_i(i = 0, 1, \ldots, p)$, $\varsigma^{\mathrm{T}}T_0\varsigma > 0$, $\forall \varsigma \neq 0, s.t.\ \varsigma^{\mathrm{T}}T_i\varsigma \geq 0\,(i = 0, 1, \ldots, p)$ holds if there exist $\tau_i \geq 0\,(i = 1, 2, \ldots, p)$ such that $T_0 - \sum_{i=1}^{p}\tau_i T_i > 0$.*

3. Main Results

The following theorem presents a sufficient condition on the stochastic stability of system (10).

Theorem 5. *For the communication channel parameters $0 \leq \alpha_\lambda \leq 1$ and $0 \leq \beta \leq 1$, if there exist positive definite matrices $P_i > 0$, $Y_i > 0$, controller gain matrix K, observer gain matrix L, and nonnegative scalars $\tau_1 \geq 0$, $\tau_2 \geq 0$, such that*

$$\begin{bmatrix} \Gamma_{11} & * \\ \Gamma_{21} & \Gamma_{22} \end{bmatrix} < 0, \qquad P_i Y_i = I, \tag{14}$$

where

$$\Gamma_{11} = \begin{bmatrix} -P_i + \tau_1 G_i^{\mathrm{T}} G_i & * & * & * \\ 0 & -P_i + \tau_2 G_i^{\mathrm{T}} G_i & * & * \\ 0 & 0 & -\tau_1 I & * \\ 0 & 0 & 0 & -\tau_2 I \end{bmatrix},$$

$$\Gamma_{21} = \begin{bmatrix} \Xi_{11} & \Xi_{12} & \Xi_{13} & 0 \\ \Xi_{21} & \Xi_{22} & 0 & \Xi_{24} \\ \Xi_{31} & \Xi_{32} & 0 & 0 \\ \Xi_{31} & \Xi_{32} & 0 & 0 \\ \Xi_{41} & 0 & 0 & 0 \end{bmatrix},$$

$$\Gamma_{22} = \begin{bmatrix} \Xi & * & * & * & * \\ 0 & \Xi & * & * & * \\ 0 & 0 & \Xi & * & * \\ 0 & 0 & 0 & \Xi & * \\ 0 & 0 & 0 & 0 & \Xi \end{bmatrix},$$

$$\Xi_{11} = \left[\sqrt{\pi_{i1}}\left(A_i + \beta B_i K\right)^{\mathrm{T}}, \ldots, \sqrt{\pi_{ig}}\left(A_i + \beta B_i K\right)^{\mathrm{T}}\right]^{\mathrm{T}},$$

$$\Xi_{12} = \left[\sqrt{\pi_{i1}}\left(-\beta B_i K\right)^{\mathrm{T}}, \ldots, \sqrt{\pi_{ig}}\left(-\beta B_i K\right)^{\mathrm{T}}\right]^{\mathrm{T}},$$

$$\Xi_{13} = \left[\sqrt{\pi_{i1}}\, I, \ldots, \sqrt{\pi_{ig}}\, I\right]^{\mathrm{T}},$$

$$\Xi_{21} = \left[\sqrt{\pi_{i1}}\left((\beta - 1)B_i K\right)^{\mathrm{T}}, \ldots, \sqrt{\pi_{ig}}\left((\beta - 1)B_i K\right)^{\mathrm{T}}\right]^{\mathrm{T}},$$

$$\Xi_{22} = \left[\sqrt{\pi_{i1}}\left(\left(A_i - (\beta - 1)B_i K - \alpha_\lambda L C_i\right)\right)^{\mathrm{T}}, \ldots, \sqrt{\pi_{ig}}\left(\left(A_i - (\beta - 1)B_i K - \alpha_\lambda L C_i\right)\right)^{\mathrm{T}}\right]^{\mathrm{T}},$$

$$\Xi_{24} = \left[\sqrt{\pi_{i1}}\, I, \ldots, \sqrt{\pi_{ig}}\, I\right]^{\mathrm{T}},$$

$$\Xi_{31} = \left[\sqrt{\pi_{i1}}\left(\overline{\beta} B_i K\right)^{\mathrm{T}}, \ldots, \sqrt{\pi_{ig}}\left(\overline{\beta} B_i K\right)^{\mathrm{T}}\right]^{\mathrm{T}},$$

$$\Xi_{32} = \left[\sqrt{\pi_{i1}}\left(-\overline{\beta} B_i K\right)^{\mathrm{T}}, \ldots, \sqrt{\pi_{ig}}\left(-\overline{\beta} B_i K\right)^{\mathrm{T}}\right]^{\mathrm{T}},$$

$$\Xi_{41} = \left[\sqrt{\pi_{i1}}\left(\overline{\alpha}_\lambda \mathrm{LC}_i\right)^{\mathrm{T}}, \ldots, \sqrt{\pi_{ig}}\left(\overline{\alpha}_\lambda \mathrm{LC}_i\right)^{\mathrm{T}}\right]^{\mathrm{T}},$$

$$\Xi = \mathrm{Diag}\left\{-Y_1, \ldots, -Y_g\right\},$$

$$\overline{\alpha} = \left[(1 - \alpha_\lambda)\alpha_\lambda\right]^{\frac{1}{2}}, \overline{\beta} = \left[(1 - \beta)\beta\right]^{\frac{1}{2}}. \tag{15}$$

then system (10) is stochastically stable.

Proof. Define Lyapunov function for system (12) as follows:

$$V(l) = x^{\mathrm{T}}(l)P_{\delta(l)}x(l) + e^{\mathrm{T}}(l)P_{\delta(l)}e(l), \tag{16}$$

where $P_{\delta(l)} > 0$. From (9) with $\omega(l) = 0$, we can get

$$\begin{aligned}
&\Delta V(l) \\
&\quad = E\{V(l+1) \mid x(l), \ldots, x(0), e(l), \ldots, e(0), \delta(l) = i\} \\
&\qquad - V(l), \\
&\quad = E\left\{x^{\mathrm{T}}(l+1)\sum_{j\in\ell}\pi_{ij}P_j x(l+1) - x^{\mathrm{T}}(l)P_i x(l)\right. \\
&\qquad \left. + e^{\mathrm{T}}(l+1)\sum_{j\in\ell}\pi_{ij}P_j e(l+1)\right\} - e^{\mathrm{T}}(l)P_i e(l), \\
&\quad = E\{\left[\left(A_i + \beta B_i K\right)x(l) - \beta B_i K e(l) + f_i(l, x(l))\right. \\
&\qquad \left. + (\beta(l) - \beta)B_i K x(l) - (\beta(l) - \beta)B_i K e(l)\right]^{\mathrm{T}}
\end{aligned}$$

$$
\begin{aligned}
&\sum_{j\in\ell}\pi_{ij}P_j\big[\big(A_i+\beta B_iK\big)x(l)-\beta B_iKe(l)+f_i(l,x(l))\\
&+(\beta(l)-\beta)B_iKx(l)-(\beta(l)-\beta)B_iKe(l)\big]\\
&+\big[(\beta-1)B_iKx(l)+F_i(l)+(\beta(l)-\beta)B_iKx(l)\\
&+\big(A_i-(\beta-1)B_iK-\alpha_\lambda LC\big)e(l)-(\beta(l)-\beta)B_iKe(l)\\
&-\big(\alpha_\lambda(l)-\alpha_\lambda\big)LC_ix(l)\big]^{\mathrm{T}}\sum_{j\in\ell}\pi_{ij}P_j\big[(\beta-1)B_iKx(l)\\
&+F_i(l)+\big(A_i-(\beta-1)B_iK-\alpha_\lambda LC\big)e(l)\\
&+(\beta(l)-\beta)B_iKx(l)-(\beta(l)-\beta)B_iKe(l)\\
&-\big(\alpha_\lambda(l)-\alpha_\lambda\big)LC_ix(l)\big]\big\}-x^{\mathrm{T}}(l)P_ix(l)-e^{\mathrm{T}}(l)P_ie(l).
\end{aligned}
\tag{17}
$$

Owing to $E\{(\beta(l)-\beta)^2\}=\overline{\beta}^2$, $E\{(\alpha_\lambda(l)-\alpha_\lambda)^2\}=\overline{\alpha}_\lambda^2$, thus we can get

$$
\begin{aligned}
&\Delta V(l)\\
&=\big[\big(A_i+\beta B_iK\big)x(l)-\beta B_iKe(l)+f_i(l,x(l))\big]^{\mathrm{T}}\\
&\quad\sum_{j\in\ell}\pi_{ij}P_j\big[\big(A_i+\beta B_iK\big)x(l)-\beta B_iKe(l)+f_i(l,x(l))\big]\\
&\quad+\big[\big(A_i-(\beta-1)B_iK-\alpha_\lambda LC\big)e(l)\\
&\quad+(\beta-1)B_iKx(l)+F_i(l)\big]^{\mathrm{T}}\\
&\quad\sum_{j\in\ell}\pi_{ij}P_j\big[\big(A_i-(\beta-1)B_iK-\alpha_\lambda LC\big)e(l)\\
&\quad+(\beta-1)B_iKx(l)+F_i(l)\big]\\
&\quad+\overline{\beta}^2\big[B_iKx(l)-B_iKe(l)\big]^{\mathrm{T}}\sum_{j\in\ell}\pi_{ij}P_j\\
&\quad\big[B_iKx(l)-B_iKe(l)\big]\\
&\quad+\overline{\beta}^2\big[B_iKx(l)-B_iKe(l)\big]^{\mathrm{T}}\sum_{j\in\ell}\pi_{ij}P_j\\
&\quad\big[B_iKx(l)-B_iKe(l)\big]\\
&\quad+\overline{\alpha}_\lambda^2x^{\mathrm{T}}(l)C_i^{\mathrm{T}}L^{\mathrm{T}}\sum_{j\in\ell}\pi_{ij}P_jLC_ix(l)\\
&\quad-x^{\mathrm{T}}(l)P_ix(l)-e^{\mathrm{T}}(l)P_ie(l)\\
&=\begin{bmatrix}x(l)\\e(l)\\f_i(l,x(l))\\F_i(l)\end{bmatrix}^{\mathrm{T}}\Lambda\begin{bmatrix}x(l)\\e(l)\\f_i(l,x(l))\\F_i(l)\end{bmatrix}\\
&\triangleq=\xi^{\mathrm{T}}(l)\Lambda\xi(l),
\end{aligned}
\tag{18}
$$

where

$$
\Lambda=\begin{bmatrix}\Lambda_{11}&*&*&*\\\Lambda_{21}&\Lambda_{22}&*&*\\\Lambda_{31}&\Lambda_{32}&\sum_{j\in\ell}\pi_{ij}P_j&*\\\Lambda_{41}&\Lambda_{42}&0&\sum_{j\in\ell}\pi_{ij}P_j\end{bmatrix},
$$

$$
\begin{aligned}
\Lambda_{11}&=\big(A_i+\beta B_iK\big)^{\mathrm{T}}\sum_{j\in\ell}\pi_{ij}P_j\big(A_i+\beta B_iK\big)\\
&\quad+\overline{\beta}^2K^{\mathrm{T}}B_i^{\mathrm{T}}\sum_{j\in\ell}\pi_{ij}P_jB_iK\\
&\quad+\overline{\beta}^2K^{\mathrm{T}}B_i^{\mathrm{T}}\sum_{j\in\ell}\pi_{ij}P_jB_iK\\
&\quad+\overline{\alpha}_\lambda^2C_i^{\mathrm{T}}L^{\mathrm{T}}\sum_{j\in\ell}\pi_{ij}P_jLC_i-P_i\\
&\quad+\big((\beta-1)B_iK\big)^{\mathrm{T}}\sum_{j\in\ell}\pi_{ij}P_j\big((\beta-1)B_iK\big),\\
\Lambda_{21}&=-\beta K^{\mathrm{T}}B_i^{\mathrm{T}}\sum_{j\in\ell}\pi_{ij}P_j\big(A_i+\beta B_iK\big)\\
&\quad-\overline{\beta}^2K^{\mathrm{T}}B_i^{\mathrm{T}}\sum_{j\in\ell}\pi_{ij}P_jB_iK\\
&\quad-\overline{\beta}^2K^{\mathrm{T}}B_i^{\mathrm{T}}\sum_{j\in\ell}\pi_{ij}P_jB_iK\\
&\quad+\big(A_i-(\beta-1)B_iK-\alpha_\lambda LC_i\big)^{\mathrm{T}}\\
&\quad\sum_{j\in\ell}\pi_{ij}P_j(\beta-1)B_iK,\\
\Lambda_{22}&=\beta^2K^{\mathrm{T}}B_i^{\mathrm{T}}\sum_{j\in\ell}\pi_{ij}P_jB_iK-P_i\\
&\quad+\overline{\beta}^2K^{\mathrm{T}}B_i^{\mathrm{T}}\sum_{j\in\ell}\pi_{ij}P_jB_iK\\
&\quad+\overline{\beta}^2K^{\mathrm{T}}B_i^{\mathrm{T}}\sum_{j\in\ell}\pi_{ij}P_jB_iK\\
&\quad+\big(A_i-(\beta-1)B_iK-\alpha_\lambda LC_i\big)^{\mathrm{T}}\\
&\quad\sum_{j\in\ell}\pi_{ij}P_j\big(A_i-(\beta-1)B_iK-\alpha_\lambda LC_i\big),\\
\Lambda_{31}&=\sum_{j\in\ell}\pi_{ij}P_j\big(A_i+\beta B_iK\big),\\
\Lambda_{32}&=\sum_{j\in\ell}\pi_{ij}P_j\big(-\beta B_iK\big),\\
\Lambda_{41}&=(\beta-1)\sum_{j\in\ell}\pi_{ij}P_jB_iK,\\
\Lambda_{42}&=\sum_{j\in\ell}\pi_{ij}P_j\big(A_i-(\beta-1)B_iK-\alpha_\lambda LC_i\big).
\end{aligned}
\tag{19}
$$

It follows from (2)-(3) that

$$\begin{aligned} & f_i^{\mathrm{T}}(l,x(l))f_i(l,x(l)) \\ &\quad = \left\|f_i(l,x(l))\right\|^2 \\ &\quad \le \left\|G_i x(l)\right\|^2 \\ &\quad = x^{\mathrm{T}}(l)G_i^{\mathrm{T}}G_i x(l), \end{aligned} \tag{20}$$

$$\begin{aligned} & F_i^{\mathrm{T}}(l)F_i(l) \\ &\quad = \left\|F_i(l)\right\|^2 \\ &\quad \le \left\|G_i e(l)\right\|^2 \\ &\quad = e^{\mathrm{T}}(l)G_i^{\mathrm{T}}G_i e(l), \end{aligned} \tag{21}$$

which indicates that

$$\begin{aligned} & f_i^{\mathrm{T}}(l,x(l))f_i(l,x(l)) - x^{\mathrm{T}}(l)G_i^{\mathrm{T}}G_i x(l) \\ &\quad = \xi^{\mathrm{T}}(l)\begin{bmatrix} -G_i^{\mathrm{T}}G_i & 0 & 0 & 0 \\ 0 & 0 & 0 & 0 \\ 0 & 0 & I & 0 \\ 0 & 0 & 0 & 0 \end{bmatrix}\xi(l) \\ &\quad \triangleq = \xi^{\mathrm{T}}(l)\Lambda_1\xi(l) \\ &\quad \le 0, \end{aligned} \tag{22}$$

$$\begin{aligned} & F_i^{\mathrm{T}}(l)F_i(l) - e^{\mathrm{T}}(l)G_i^{\mathrm{T}}G_i e(l) \\ &\quad = \xi^{\mathrm{T}}(l)\begin{bmatrix} 0 & 0 & 0 & 0 \\ 0 & -G_i^{\mathrm{T}}G_i & 0 & 0 \\ 0 & 0 & 0 & 0 \\ 0 & 0 & 0 & I \end{bmatrix}\xi(l) \\ &\quad \triangleq = \xi^{\mathrm{T}}(l)\Lambda_2\xi(l) \\ &\quad \le 0. \end{aligned} \tag{23}$$

By the well-known S-procedure, that is, Lemma 4, we can get $\Delta V(l) = \xi^{\mathrm{T}}(l)\Lambda\xi(l) < 0$ with constrains (22) and (23) holding, if there exist non-negative real scalars $\tau_1 \ge 0$, $\tau_2 \ge 0$ such that

$$\Lambda - \tau_1\Lambda_1 - \tau_2\Lambda_2 < 0. \tag{24}$$

From (24), we have

$$\begin{aligned} & \Delta V(l) \\ &\quad = \xi^{\mathrm{T}}(l)\Lambda\xi(l) \\ &\quad \le -\lambda_{\min}(-\Lambda)\xi^{\mathrm{T}}(l)\xi(l) \\ &\quad = -\lambda_{\min}(-\Lambda)\Big(\eta^{\mathrm{T}}(l)\eta(l) + F_i^{\mathrm{T}}(l)F_i(l) \\ &\qquad + f_i^{\mathrm{T}}(l,x(l))f_i(l,x(l))\Big) \\ &\quad = -\lambda_{\min}(-\Lambda)\Big(\left\|\eta(l)\right\|^2 + \left\|F_i(l)\right\|^2 + \left\|f_i(l,x(l))\right\|^2\Big) \\ &\quad \le -\lambda_{\min}(-\Lambda)\left\|\eta(l)\right\|^2. \end{aligned} \tag{25}$$

From (25), for any $N \ge 0$, we have

$$\begin{aligned} & E\left\{\sum_{l=0}^{N}\left\|\eta(l)\right\|^2\right\} \\ &\quad \le \frac{E\{V(0)\} - E\{V(N+1)\}}{\lambda_{\min}(-\Lambda)} \\ &\quad \le \frac{E\{V(0)\}}{\lambda_{\min}(-\Lambda)} \\ &\quad \le \infty. \end{aligned} \tag{26}$$

Therefore, in accordance with Definition 2, that system (10) under consideration is stochastically stable. □

Remark 7. Theorem 5 provides sufficient conditions, which makes sure system (12) is stochastically stable. The following Theorem 8 will provide the proof that system (12) under consideration is stochastically stable and attain the H_∞ performance requirement (13).

Theorem 8. *When $\omega(l) \ne 0$, take as given the communication channel parameters $0 \le \alpha_\lambda \le 1$, $0 \le \beta \le 1$ and a scalar $\gamma > 0$, if there exist positive definite matrices $P_i > 0$, $Y_i > 0$, matrices K, L, and scalars $\tau_1 \ge 0$, $\tau_2 \ge 0$, such that*

$$\begin{bmatrix} \Upsilon_{11} & 0 \\ \Upsilon_{21} & \Upsilon_{22} \end{bmatrix} < 0, \tag{27}$$

$$P_i Y_i = I, \tag{28}$$

where

$$\Upsilon_{11} = \begin{bmatrix} \chi_{11} & * & * & * & * \\ 0 & \chi_{22} & * & * & * \\ 0 & 0 & -\gamma^2 I & * & * \\ 0 & 0 & 0 & -\tau_1 I & * \\ 0 & 0 & 0 & 0 & -\tau_2 I \end{bmatrix},$$

$$\Upsilon_{21} = \begin{bmatrix} \Theta_{11} & \Theta_{12} & \Theta_{13} & \Theta_{14} & 0 \\ \Theta_{21} & \Theta_{22} & \Theta_{13} & 0 & \Theta_{14} \\ C_i & 0 & 0 & 0 & 0 \\ \Theta_{31} & \Theta_{32} & 0 & 0 & 0 \\ \Theta_{31} & \Theta_{32} & 0 & 0 & 0 \\ \Theta_{41} & 0 & 0 & 0 & 0 \end{bmatrix},$$

$$\Upsilon_{22} = \begin{bmatrix} \Theta & * & * & * & * & * \\ 0 & \Theta & * & * & * & * \\ 0 & 0 & -I & * & * & * \\ 0 & 0 & 0 & \Theta & * & * \\ 0 & 0 & 0 & 0 & \Theta & * \\ 0 & 0 & 0 & 0 & 0 & \Theta \end{bmatrix},$$

$$
\begin{aligned}
&\chi_{11} = -P_i + \tau_1 G_i^{\mathrm{T}} G_i, \chi_{22}\\
&\Theta_{11} = \left[\sqrt{\pi_{i1}}\left(A_i + \beta B_i K\right)^{\mathrm{T}}, \ldots, \sqrt{\pi_{ig}}\left(A_i + \beta B_i K\right)^{\mathrm{T}}\right]^{\mathrm{T}},\\
&\Theta_{12} = \left[\sqrt{\pi_{i1}}\left(-\beta B_i K\right)^{\mathrm{T}}, \ldots, \sqrt{\pi_{ig}}\left(-\beta B_i K\right)^{\mathrm{T}}\right]^{\mathrm{T}},\\
&\Theta_{13} = \left[\sqrt{\pi_{i1}}\, D_i^{\mathrm{T}}, \ldots, \sqrt{\pi_{ig}}\, D_i^{\mathrm{T}}\right]^{\mathrm{T}},\\
&\Theta_{14} = \left[\sqrt{\pi_{i1}}\, I, \ldots, \sqrt{\pi_{ig}}\, I\right]^{\mathrm{T}},\\
&\Theta_{21} = \left[\sqrt{\pi_{i1}}\left((\beta-1)B_i K\right)^{\mathrm{T}}, \ldots, \sqrt{\pi_{ig}}\left((\beta-1)B_i K\right)^{\mathrm{T}}\right]^{\mathrm{T}},\\
&\Theta_{31} = \left[\sqrt{\pi_{i1}}\left(\overline{\beta} B_i K\right)^{\mathrm{T}}, \ldots, \sqrt{\pi_{ig}}\left(\overline{\beta} B_i K\right)^{\mathrm{T}}\right]^{\mathrm{T}},\\
&\Theta_{22} = \left[\sqrt{\pi_{i1}}\left(\left(A_i - (\beta-1)B_i K - \alpha_\lambda L C_i\right)\right)^{\mathrm{T}}, \ldots,\right.\\
&\qquad \left.\sqrt{\pi_{ig}}\left(\left(A_i - (\beta-1)B_i K - \alpha_\lambda L C_i\right)\right)^{\mathrm{T}}\right]^{\mathrm{T}},\\
&\Theta_{32} = \left[\sqrt{\pi_{i1}}\left(-\overline{\beta} B_i K\right)^{\mathrm{T}}, \ldots, \sqrt{\pi_{ig}}\left(-\overline{\beta} B_i K\right)^{\mathrm{T}}\right]^{\mathrm{T}},\\
&\Theta_{41} = \left[\sqrt{\pi_{i1}}\left(\overline{\alpha}_\lambda L C_i\right)^{\mathrm{T}}, \ldots, \sqrt{\pi_{ig}}\left(\overline{\alpha}_\lambda L C_i\right)^{\mathrm{T}}\right]^{\mathrm{T}},\\
&\Theta = \mathrm{Diag}\left\{-Y_1, \ldots, -Y_g\right\},\\
&\overline{\alpha} = \left[(1-\alpha_\lambda)\alpha_\lambda\right]\frac{1}{2}, \overline{\beta}
\end{aligned}
\tag{29}
$$

then system (10) attains the H_∞ performance requirement (13).

Proof. When $\omega(l) \neq 0$, from (11) we can get

$$
\begin{aligned}
&E\left\{\Delta V(l) + y^{\mathrm{T}}(l) y(l) - \gamma^2 \omega^{\mathrm{T}}(l)\omega(l)\right\}\\
&\quad = E\left\{\left[\left(A_i + \beta B_i K\right)x(l) - \beta B_i K e(l) + D_i \omega(l)\right.\right.\\
&\qquad + (\beta(l) - \beta)B_i K x(l) - (\beta(l) - \beta)B_i K e(l)\\
&\qquad \left.+ f_i(l, x(l))\right]^{\mathrm{T}} \sum_{j\in\ell} \pi_{ij} P_j \left[\left(A_i + \beta B_i K\right)x(l)\right.\\
&\qquad - \beta B_i K e(l) + D_i \omega(l) + f_i(l, x(l))\\
&\qquad \left.+ (\beta(l) - \beta)B_i K x(l) - (\beta(l) - \beta)B_i K e(l)\right]\\
&\qquad + \left[(\beta-1)B_i K x(l) + (\beta(l) - \beta)B_i K x(l) + F_i(l)\right.\\
&\qquad + D_i \omega(l) + \left(A_i - (\beta-1)B_i K - \alpha_\lambda L C\right)e(l)\\
&\qquad \left.-(\beta(l) - \beta)B_i K e(l) - \left(\alpha_\lambda(l) - \alpha_\lambda\right)L C_i x(l)\right]^{\mathrm{T}}\\
&\qquad \sum_{j\in\ell} \pi_{ij} P_j \left[(\beta-1)B_i K x(l) + D_i \omega(l)\right.\\
&\qquad + F_i(l) + \left(A_i - (\beta-1)B_i K - \alpha_\lambda L C\right)e(l)\\
&\qquad \left.+ (\beta(l) - \beta)B_i K x(l) - (\beta(l) - \beta)B_i K e(l)\right.\\
&\qquad \left.- \left(\alpha_\lambda(l) - \alpha_\lambda\right)L C_i x(l)\right]\Big\} - x^{\mathrm{T}}(l) P_i x(l)\\
&\qquad - e^{\mathrm{T}}(l) P_i e(l) + x^{\mathrm{T}}(l) C_i^{\mathrm{T}} C_i x(l) - \gamma^2 \omega^{\mathrm{T}}(l)\omega(l)\\
&\quad = \zeta^{\mathrm{T}}(l)\Omega\zeta(l),
\end{aligned}
\tag{30}
$$

where

$$
\begin{aligned}
&\zeta^{\mathrm{T}} = \left[x^{\mathrm{T}}(l)\ \ e^{\mathrm{T}}(l)\ \ \omega^{\mathrm{T}}(l)\ \ f_i^{\mathrm{T}}(l, x(l))\ \ F_i^{\mathrm{T}}(l)\right],\\
&\Omega = \begin{bmatrix}
\varphi_{11} & * & * & * & *\\
\varphi_{21} & \varphi_{22} & * & * & *\\
\varphi_{31} & \varphi_{32} & \varphi_{33} & * & *\\
\varphi_{41} & -\beta P_i B_i K & P D_i & P_i & *\\
\varphi_{51} & \varphi_{52} & P D_i & 0 & P_i
\end{bmatrix},\\
&\varphi_{11} = \left(A_i + \beta B_i K\right)^{\mathrm{T}} \sum_{j\in\ell} \pi_{ij} P_j \left(A_i + \beta B_i K\right)\\
&\qquad + \overline{\beta}^2 K^{\mathrm{T}} B_i^{\mathrm{T}} \sum_{j\in\ell} \pi_{ij} P_j B_i K + \overline{\beta}^2 K^{\mathrm{T}} B_i^{\mathrm{T}} \sum_{j\in\ell} \pi_{ij} P_j B_i K\\
&\qquad + \overline{\alpha}_\lambda^2 C_i^{\mathrm{T}} L^{\mathrm{T}} \sum_{j\in\ell} \pi_{ij} P_j L C_i - P_i\\
&\qquad + \left((\beta-1)B_i K\right)^{\mathrm{T}} \sum_{j\in\ell} \pi_{ij} P_j (\beta-1) B_i K + C^{\mathrm{T}} C,\\
&\varphi_{21} = -\beta K^{\mathrm{T}} B_i^{\mathrm{T}} \sum_{j\in\ell} \pi_{ij} P_j \left(A_i + \beta B_i K\right)\\
&\qquad - \overline{\beta}^2 K^{\mathrm{T}} B_i^{\mathrm{T}} \sum_{j\in\ell} \pi_{ij} P_j B_i K - \overline{\beta}^2 K^{\mathrm{T}} B_i^{\mathrm{T}} \sum_{j\in\ell} \pi_{ij} P_j B_i K\\
&\qquad + \left(A_i - (\beta-1)B_i K - \alpha_\lambda L C_i\right)^{\mathrm{T}} \sum_{j\in\ell} \pi_{ij} P_j (\beta-1) B_i K,\\
&\varphi_{22} = \beta^2 K^{\mathrm{T}} B_i^{\mathrm{T}} \sum_{j\in\ell} \pi_{ij} P_j B_i K + \overline{\beta}^2 K^{\mathrm{T}} B_i^{\mathrm{T}} \sum_{j\in\ell} \pi_{ij} P_j B_i K\\
&\qquad + \overline{\beta}^2 K^{\mathrm{T}} B_i^{\mathrm{T}} \sum_{j\in\ell} \pi_{ij} Q_j B_i K - P_i\\
&\qquad + \left(A_i - (\beta-1)B_i K - \alpha_\lambda L C_i\right)^{\mathrm{T}} \sum_{j\in\ell} \pi_{ij} P_j\\
&\qquad \left(A_i - (\beta-1)B_i K - \alpha_\lambda L C_i\right),\\
&\varphi_{31} = D_i^{\mathrm{T}} \sum_{j\in\ell} \pi_{ij} P_j \left(A_i + \beta B_i K\right)\\
&\qquad + D_i^{\mathrm{T}} \sum_{j\in\ell} \pi_{ij} P_j (\beta-1) B_i K,\\
&\varphi_{32} = -\beta D_i^{\mathrm{T}} \sum_{j\in\ell} \pi_{ij} P_j B_i K\\
&\qquad + D_i^{\mathrm{T}} \sum_{j\in\ell} \pi_{ij} P_j \left(A_i - (\beta-1)B_i K - \alpha_\lambda L C_i\right),\\
&\varphi_{33} = D_i^{\mathrm{T}} \sum_{j\in\ell} \pi_{ij} P_j D_i + D_i^{\mathrm{T}} \sum_{j\in\ell} \pi_{ij} P_j D_i - \gamma^2 I,\\
&\varphi_{41} = P_i A_i + \beta P_i B_i K,\\
&\varphi_{51} = (\beta-1) P_i B_i K,\\
&\varphi_{52} = P_i \left(A_i - (\beta-1)B_i K - \alpha_\lambda L C_i\right).
\end{aligned}
\tag{31}
$$

From (18)-(19), we can obtain

$$
\begin{aligned}
&f_i^{\mathrm{T}}(l,x(l))f_i(l,x(l)) - x^{\mathrm{T}}(l)G_i^{\mathrm{T}}G_i x(l) \\
&= \zeta^{\mathrm{T}}(l)\begin{bmatrix} -G_i^{\mathrm{T}}G_i & 0 & 0 & 0 & 0 \\ 0 & 0 & 0 & 0 & 0 \\ 0 & 0 & 0 & 0 & 0 \\ 0 & 0 & 0 & I & 0 \\ 0 & 0 & 0 & 0 & 0 \end{bmatrix}\zeta(l) \\
&\triangleq = \zeta^{\mathrm{T}}(l)\Omega_1\zeta(l) \\
&\le 0,
\end{aligned} \tag{32}
$$

$$
\begin{aligned}
&F_i^{\mathrm{T}}(l)F_i(l) - e^{\mathrm{T}}(l)G_i^{\mathrm{T}}G_i e(l) \\
&= \zeta^{\mathrm{T}}(l)\begin{bmatrix} 0 & 0 & 0 & 0 & 0 \\ 0 & -G_i^{\mathrm{T}}G_i & 0 & 0 & 0 \\ 0 & 0 & 0 & 0 & 0 \\ 0 & 0 & 0 & 0 & 0 \\ 0 & 0 & 0 & 0 & I \end{bmatrix}\zeta(l) \\
&\triangleq = \zeta^{\mathrm{T}}(l)\Omega_2\zeta(l) \\
&\le 0.
\end{aligned} \tag{33}
$$

By the well-known S-procedure, that is, Lemma 4, we can get

$$\zeta^{\mathrm{T}}(l)\Omega\zeta(l) < 0, \tag{34}$$

with constrains (32) and (33) holding. If there exist non-negative real scalars $\tau_1 \ge 0$, $\tau_2 \ge 0$ such that

$$\Omega - \tau_1\Omega_1 - \tau_2\Omega_2 < 0. \tag{35}$$

From (26)–(30), we can conclude that

$$E\left\{\Delta V(l) + y^{\mathrm{T}}(l)y(l) - \gamma^2\omega^{\mathrm{T}}(l)\omega(l)\right\} < 0. \tag{36}$$

Adding up (39) from $l = 0$ to $l = \infty$:

$$
\begin{aligned}
&\sum_{l=0}^{\infty} E\left\{y^{\mathrm{T}}(l)y(l)\right\} \\
&< \gamma^2\sum_{l=0}^{\infty} E\left\{\omega^{\mathrm{T}}(l)\omega(l)\right\} + E\{V(0)\} - E\{V(\infty)\}.
\end{aligned} \tag{37}
$$

Duo to the condition that system (10) is stochastically stable, we can get

$$\sum_{l=0}^{\infty} E\left\{y^{\mathrm{T}}(l)y(l)\right\} < \gamma^2\sum_{l=0}^{\infty} E\left\{\omega^{\mathrm{T}}(l)\omega(l)\right\}. \tag{38}$$

which implies the H_∞ performance index (12) is achieved. This ends the proof. □

Remark 10. The prerequisites in Theorem 8 are a series of matrix inequalities under matrix inverse constraints, which can be settled by the cone complementary linearization method as follows:

$$\text{Mintr}\left(\sum_{i=1}^{g} P_i Y_i\right), \text{s.t. (24) and (32)}, \tag{39}$$

$$\begin{bmatrix} P_i & I \\ I & Y_i \end{bmatrix} > 0, i \in \ell. \tag{40}$$

The computing steps are illustrated in Algorithm 1, where μ is a suitable scalar.

4. Numerical Example

In this section, an example is presented to illustrate the effectiveness of the obtained method.

The parameter of the controlled plant is as follows:

$$
\begin{cases} x(l+1) = A_{\delta(l)}x(l) + B_{\delta(l)}u(l) + D_{\delta(l)}\omega(l) \\ +f_{\delta(l)}(l,x(l)), \\ y(l) = C_{\delta(l)}x(l), \end{cases} \tag{41}
$$

where

$$
\begin{aligned}
&A_1 = \begin{bmatrix} 0.8266 & -0.6330 & 0 \\ 0.5 & 0 & 0 \\ 0 & 1.0 & 0 \end{bmatrix}, B_1 = \begin{bmatrix} 1 \\ 0 \\ 0 \end{bmatrix}, D_1 = \begin{bmatrix} 0.5 \\ 0 \\ 0.2 \end{bmatrix}, \\
&A_2 = \begin{bmatrix} 0.9226 & -0.6330 & 0 \\ 1.0 & 0 & 0 \\ 0 & 1.0 & 0 \end{bmatrix}, B_2 = \begin{bmatrix} 0.5 \\ 0 \\ 0.2 \end{bmatrix}, D_2 = \begin{bmatrix} 1 \\ 0 \\ 0 \end{bmatrix}, \\
&C_1 = \begin{bmatrix} 0.1 & 0 & 0 \end{bmatrix}, C_2 = \begin{bmatrix} 0.1 & 0 & 0 \end{bmatrix}, \delta(l) \in \{1,2\}, \\
&f_1(l,x(l)) = \begin{bmatrix} 0.01\sin x_1(l) \\ 0.01\sin x_2(l) \\ 0.01\sin x_3(l) \end{bmatrix}, x(l) = \begin{bmatrix} x_1(l) \\ x_2(l) \\ x_3(l) \end{bmatrix}, \\
&f_2(l,x(l)) = \begin{bmatrix} 0.02\sin x_1(l) \\ 0.02\sin x_2(l) \\ 0.02\sin x_3(l) \end{bmatrix}, \tau_1 = 0.5, \tau_2 = 0.3, \\
&G_1 = \begin{bmatrix} 0.01 & 0 & 0 \\ 0 & 0.01 & 0 \\ 0 & 0 & 0.01 \end{bmatrix}, G_2 = \begin{bmatrix} 0.02 & 0 & 0 \\ 0 & 0.02 & 0 \\ 0 & 0 & 0.02 \end{bmatrix}.
\end{aligned} \tag{42}
$$

Suppose the attack period is $T = 10$, the sleeping period is set as $T_{\text{off}} = 6$, and the total operating time is $l = 60$, which is $d = \{1, 2, \ldots, 6\}$. The transition possibility matrices of $\delta(l)$ is $Q = \begin{bmatrix} 0.8 & 0.2 \\ 0.3 & 0.7 \end{bmatrix}$. To analyze the impact caused by the DoS attacks, the probabilities of success to transmission data packet in the sleeping period are fixed, that is $\alpha_1 = 0.9$ and $\beta = 0.8$. Table 1 lists the allowable minimum value of γ. It is clear that when α_2 gets bigger, $\gamma_{\min}$ gets smaller. The impact of DoS attacks is clear, demonstrating the importance of investigating security issues.

According to Theorem 8, when $\alpha_1 = 0.9$, $\alpha_2 = 0.3$, and $\beta = 0.8$, K, L, and $\gamma_{\min}$ can be obtained as follows:

(1) Set $R_{\max}$ as the maximal iteration number, and let $\gamma = \gamma_0$
(2) Obtain a feasible solution (P_i^0, Y_i^0, K^0, L^0) satisfying (23) and (31), and let $l = 0$
(3) Settle the optimization issue bellow: Min $\mathrm{tr}(\sum_{i=1}^{g} P_i^l Y_i + Y_i^l P_i)$ such that (27) and (40)
(4) Set $P_i^l = P_i, Y_i^l = Y_i, K^l = K, L^l = L$
(5) **while** iterations number $< R_{\max}$ **do**
(6) **if** (27) and (28) hold, **then**
(7) $\gamma = \gamma - \mu$, $l = l + 1$, go to step 3
(8) **else**
(9) $l = l + 1$, go to step 3
(10) **end if**
(11) **end while**
(12) **if** $\gamma < \gamma_0$, **then**
(13) $\gamma_{\min} = \gamma + \mu$
(14) **else**
(15) No solution can be obtained within $R_{\max}$
(16) **end if**

Algorithm 1: Computing steps of (24) and (25).

Table 1: The minimum value of γ for different α_2.

α_2	$\gamma_{\min}$
0.3	0.4164
0.4	0.4157
0.5	0.4150
0.6	0.4141
0.7	0.4133
0.8	0.4124
0.9	0.4111

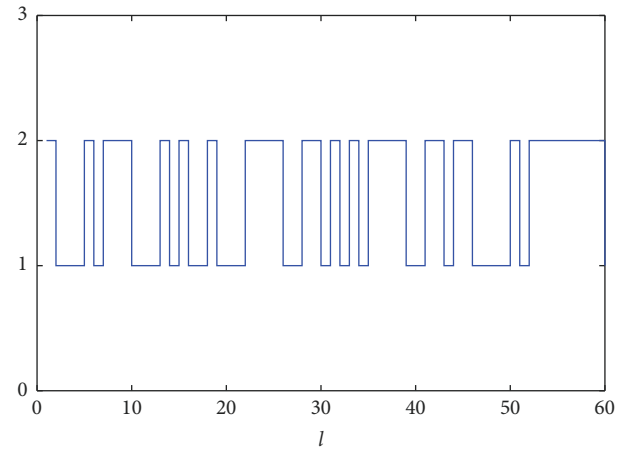

Figure 2: The mode of the closed-loop system $\delta(l)$.

$$K = \begin{bmatrix} -0.1339 & -0.0274 & -0.0026 \end{bmatrix}, L = \begin{bmatrix} 1.0868 \\ 0.1465 \\ -0.7119 \end{bmatrix},$$

$$\gamma_{\min} = 0.417. \tag{43}$$

The initial conditions of the nonlinear NCS are supposed as $x_0 = \begin{bmatrix} 0.2 & 0.3 & 0.1 \end{bmatrix}^{\mathrm{T}}$, $\hat{x}_0 = \begin{bmatrix} 0 & 0 & 0 \end{bmatrix}^{\mathrm{T}}$, and the disturbance input is assumed to be $\omega(l) = 1/l^2$. The mode of the system under consideration is shown in Figure 2. The data packet dropout in the S-C channel is shown in Figure 3, and the data packet dropout in the C-A channel is exhibited in

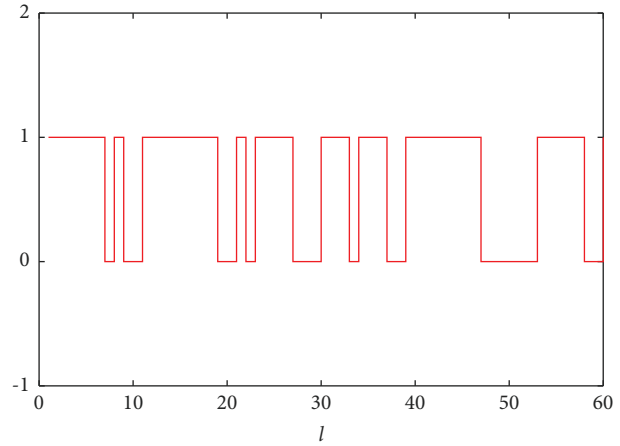

Figure 3: The data packet dropout in the S-C channel $\alpha(l)$.

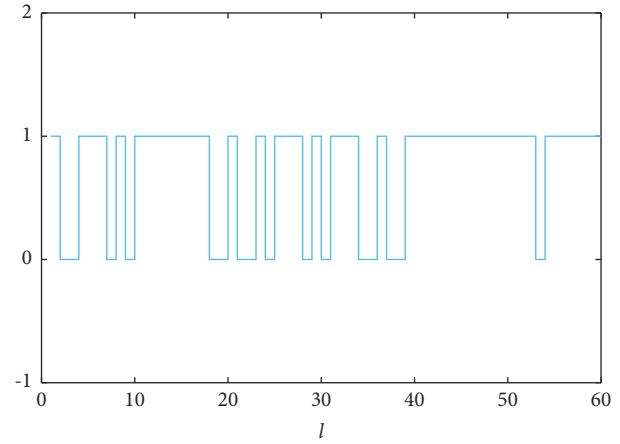

Figure 4: The data packet dropout in the C-A channel $\beta(l)$.

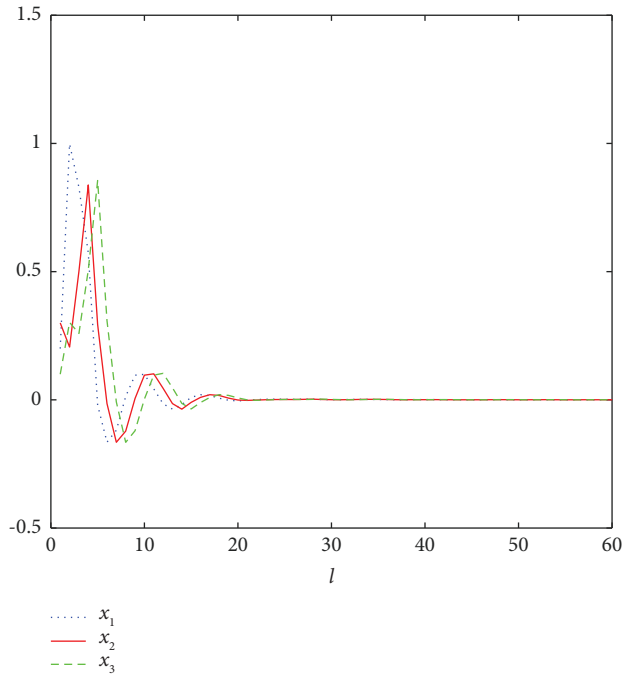

Figure 5: The state responses of the open-loop system.

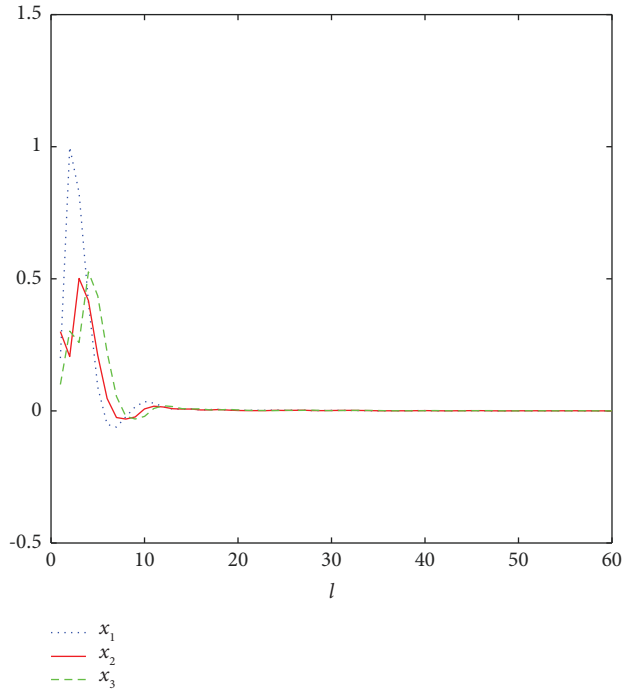

Figure 6: The state responses of the closed-loop system.

Figure 4. As can be seen from Figure 3, the probability of data packet loss during the active attack period is significantly greater than that during the attack sleep period. In the total running time, the number of successful packet transfers is 34. The number of packet transmission failures is 26, which is much higher than the average packet transmission failure probability of 0.1 when there is no network attack. In Figure 4, the number of successful data packet transmission in the total running time is 51. The number of packet transmission failures is 6, which is very close to the average data packet loss failure probability of 0.2 when there is no network attack.

We give the response curve of the open-loop system, as shown in Figure 5. Since both subsystems of the controlled object are stable, the system state converges to zero in the

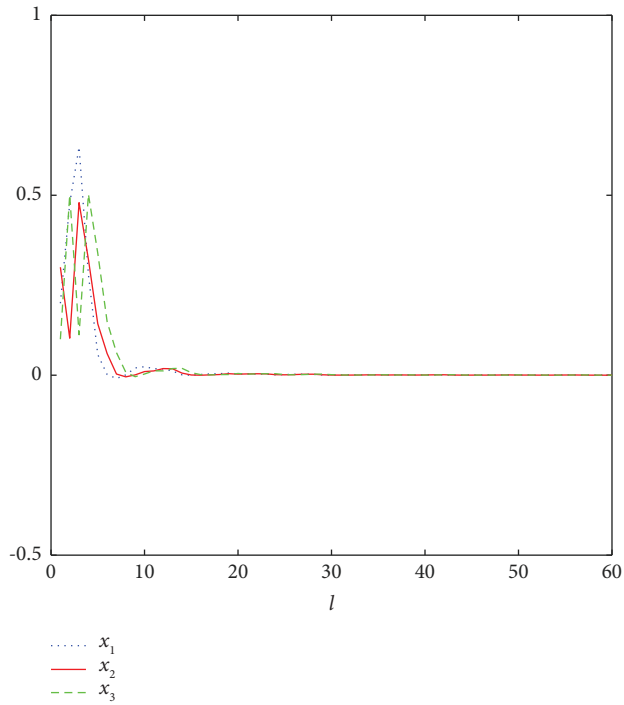

Figure 7: The state responses of the closed-loop system without data packet dropout.

open-loop case. As can be seen from Figure 6, under the action of the designed controller, the system performance such as convergence time and overshoot is better than that of the open-loop system.

If there is no packet loss in S-C and C-A channels, the system state curve is shown in Figure 7. Compared with Figure 6, the system performance is better than that in the case of packet loss. Hence, data packet loss will reduce system performance.

5. Conclusions

This paper researches the H_∞ control problem for a nonlinear Markov NCS with random data packet loss and periodic DoS attacks via observer. Premeditating the data packet loss in the S-C channel and C-A channel, sufficient conditions for the stochastic stability of the system are derived, and the controller design method is also proposed. Simulation results demonstrate the effectiveness of the proposed method. Under the event-triggered mechanism, the controller design for NCS subject to data packet dropout and DoS attacks in both the S-C channel and C-A channel will be researched in the future.

Data Availability

The data used in this study are available upon reasonable request to the corresponding author.

Conflicts of Interest

The authors declare that there are no conflicts of interest regarding the publication of this paper.

Acknowledgments

This work was supported by Suqian Basic Research Program Natural Science Foundation Project (grant no. K202224), Zhejiang Provincial Leader Innovation Team Project (grant no. 2020R01013).

References

[1] S. A. Pasha and A. Ayub, "Zero-dynamics attacks on networked control systems," *Journal of Process Control*, vol. 105, pp. 99–107, 2021.

[2] Y. Mao, H. Jafarnejadsani, P. Zhao, E. Akyol, and N. Hovakimyan, "Novel stealthy attack and defense strategies for networked control systems," *IEEE Transactions on Automatic Control*, vol. 65, no. 9, pp. 3847–3862, 2020.

[3] D. Tolić, "Stabilizing transmission intervals and delays in nonlinear networked control systems through hybrid-system-with-memory modeling and Lyapunov–Krasovskii arguments," *Nonlinear Analysis Hybrid Systems*, vol. 36, no. 5, Article ID 100834, 2020.

[4] A. Borri, G. Pola, and M. Benedetto, "Design of symbolic controllers for networked control systems," *IEEE Transactions on Automatic Control*, vol. 64, no. 3, pp. 1034–1046, 2019.

[5] E. Mousavinejad, X. Ge, Q. L. Han, F. Yang, and L. Vlacic, "Resilient tracking control of networked control systems under cyber attacks," *IEEE Transactions on Cybernetics*, vol. 51, no. 4, pp. 2107–2119, 2021.

[6] C. Wu, X. Zhao, W. Xia, J. Liu, and T. Basar, "L2-gain analysis for dynamic event-triggered networked control systems with packet losses and quantization," *Automatica*, vol. 129, no. 12, Article ID 109587, 2021.

[7] V. Lechappe, E. Moulay, F. Plestan, and Q. Han, "Discrete predictor-based event-triggered control of networked control systems," *Automatica*, vol. 107, pp. 281–288, 2019.

[8] C. Chen, W. Gui, L. Wu, Z. Liu, and H. Yan, "Tracking performance limitations of mimo networked control systems with multiple communication constraints," *IEEE Transactions on Cybernetics*, vol. 50, no. 7, pp. 2982–2995, 2020.

[9] X. Xie, S. Li, and B. Xu, "Stabilisation of networked control systems under a novel stochastic-sampling-based adaptive event-triggered scheme," *IET Control Theory & Applications*, vol. 14, no. 9, pp. 1158–1169, 2020.

[10] J. W. Hu, X. S. Zhan, J. Wu, and H. C. Yan, "Analysis of optimal performance of mimo networked control systems with encoding and packet dropout constraints," *IET Control Theory & Applications*, vol. 14, no. 13, pp. 1762–1768, 2020.

[11] A. Reis de Souza, D. Efimov, A. Polyakov, and J. Gouze, "Robust stabilization of competing species in the chemostat," *Journal of Process Control*, vol. 87, pp. 138–146, 2020.

[12] L. Zhao, Y. Li, Y. C. Yuan, and H. Yuan, "Optimal power allocation for multiple DoS attackers in wireless networked control systems," *ISA Transactions*, vol. 104, pp. 204–211, 2020.

[13] C. De Persis and P. Tesi, "Input-to-state stabilizing control under denial-of-service," *IEEE Transactions on Automatic Control*, vol. 60, no. 11, pp. 2930–2944, 2015.

[14] C. Peng and H. Sun, "Switching-like event-triggered control for networked control systems under malicious denial of service attacks," *IEEE Transactions on Automatic Control*, vol. 65, no. 9, pp. 3943–3949, 2020.

[15] T. Li, B. Chen, L. Yu, and W. A. Zhang, "Active security control approach against dos attacks in cyber-physical systems," *IEEE Transactions on Automatic Control*, vol. 66, no. 9, pp. 4303–4310, 2021.

[16] H. Zhang, P. Cheng, L. Shi, and J. Chen, "Optimal DoS attack scheduling in wireless networked control system," *IEEE Transactions on Control Systems Technology*, vol. 24, no. 3, pp. 843–852, 2016.

[17] N. Zhao, P. Shi, W. Xing, and J. Chambers, "Observer-based event-triggered approach for stochastic networked control systems under denial of service attacks," *IEEE Transactions on Control of Network Systems*, vol. 8, no. 1, pp. 158–167, 2021.

[18] H. Yang, Y. Li, L. Dai, and Y. Xia, "Mpc-based defense strategy for distributed networked control systems under dos attacks," *Systems & Control Letters*, vol. 128, pp. 9–18, 2019.

[19] X. M. Zhang, Q. L. Han, X. Ge, and L. Ding, "Resilient control design based on a sampled-data model for a class of networked control systems under denial-of-service attacks," *IEEE Transactions on Cybernetics*, vol. 50, no. 8, pp. 3616–3626, 2020.

[20] S. Hu, D. Yue, X. Xie, X. Chen, and X. Yin, "Resilient event-triggered controller synthesis of networked control systems under periodic dos jamming attacks," *IEEE Transactions on Cybernetics*, vol. 49, no. 12, pp. 4271–4281, 2019.

[21] H.-Y. Sun and C.-Z. Hou, "Stability of networked control systems with data packet dropout and multiple-packet transmission," *Control and Decision*, vol. 20, no. 5, pp. 511–515, 2005.

[22] J. G. Li, J. Q. Yuan, and J.-G. Lu, "Observer-based control for networked nonlinear systems with random packet lossesH∞control for networked nonlinear systems with random packet losses," *ISA Transactions*, vol. 49, no. 1, pp. 39–46, 2010.

[23] J.-M. Yu, C.-H. Kuang, and X.-M. Tang, "Model predictive tracking control for networked control systems subject to Markovian packet dropout," in *Proceedings of the 36th Chinese Control Conference*, pp. 301–305, Dalian, China, July 2017.

[24] M. Yu, S. Bai, T. Yang, and J. Zhang, "Quantized output feedback control of networked control systems with packet dropout," *International Journal of Control, Automation and Systems*, vol. 16, no. 5, pp. 2559–2568, 2018.

[25] L. Su and D. Ye, "Observer-based output feedback h control for cybercphysical systems under randomly occurring packet dropout and periodic dos attacks," *ISA Transactions*, vol. 95, pp. 58–67, 2019.

[26] A. U. Udom, "Almost surely exponential stability of impulsive stochastic delay dynamical system with semi-markov jump structure," *Journal of Information and Optimization Sciences*, vol. 39, no. 5, pp. 1029–1045, 2018.

[27] Y. Hong and M. Wu, "Markov model-based energy storage system planning in power systems," *IEEE Systems Journal*, vol. 13, no. 4, pp. 4313–4323, 2019.

[28] L. Liu, A. Chen, and Y.-J. Liu, "Adaptive fuzzy output-feedback control for switched uncertain nonlinear systems with full-state constraints," *IEEE Transactions on Cybernetics*, vol. 52, no. 8, pp. 7340–7351, 2022.

[29] W. Mei and M. Ogura, "Kronecker weights for instability analysis of Markov jump linear systems," *IET Control Theory & Applications*, vol. 13, no. 3, pp. 360–366, 2019.

[30] X. Song, Y. Men, J. Zhou, J. Zhao, and H. Shen, "Event-triggered H∞control for networked discrete-time Markov jump systems with repeated scalar nonlinearities," *Applied Mathematics and Computation*, vol. 298, pp. 123–132, 2017.

[31] E. Last, "Linear matrix inequalities in system and control theory," *Proceedings of the IEEE*, vol. 86, no. 12, pp. 2473-2474, 1994.

Hindawi
Mathematical Problems in Engineering
Volume 2022, Article ID 3938051, 12 pages
https://doi.org/10.1155/2022/3938051

Research Article

Unsafe Behavior Analysis and Risk Measurement of Traffic Accidents in Mountainous Highway Tunnel

Xiaoxiang Zhou[1,2], **Chengfeng Huang**[1,3] and **Yixiang Zhou**[1]

[1]*School of Economics and Management, Chongqing Jiaotong University, Chongqing 400074, China*
[2]*Transportation-Economic-Society Development Study Center, Chongqing Jiaotong University, Chongqing 400074, China*
[3]*European Research Center, Chongqing Jiaotong University, Chongqing 400074, China*

Correspondence should be addressed to Xiaoxiang Zhou; zhouxxjs@126.com

Received 19 August 2022; Accepted 3 October 2022; Published 13 October 2022

Academic Editor: Chuan Li

Traffic accidents in mountainous highway tunnels have resulted in significant negative effects and losses. Among the potential hazards that can lead to fatal injuries, human-related hazards have been recognized as the leading cause. Determining the risk management effectively and prioritizing unsafe human behavior are the basis for preventing and controlling traffic accidents in mountainous highway tunnels. Therefore, hazards that could potentially cause highway tunnel traffic accidents were identified by using a tail-biting fish diagram combined with the fault tree method. A risk assessment model was constructed based on probability, degree of importance, and loss. Furthermore, the probability can be calculated by assessing the degree of unreliability, which can be obtained by assessing the degree of importance of unsafe behavior in the fault tree, and the loss can be acquired from the authority. The case of 8–10 traffic accidents that occurred in the Qinling No. 1 Tunnel of the Ankang section of the Beijing-Kunming expressway was studied, and the values of the unsafe behaviors were assessed. According to the risk values, the priority for controlling unsafe behaviors can be acquired and tailored measures can be taken to prevent and control the risks, which provides a theoretical basis and new method for the effective control of mountainous highway tunnel traffic accidents.

1. Introduction

The highway is not only an important symbol of traffic modernization but also a symbol of national modernization [1]. By 2021, China's highway mileage is 169,000 km, accounting for 3.2% of the world's total highway mileage, ranking first worldwide.

With the fast construction of highways and extending to mountainous areas, tunnels, as a direct traffic facility crossing mountains, have been increased greatly, as the tunnels have the functions of improving alignment standards, ameliorating technical status, shortening operation distance, enhancing transport capacity, and protecting the ecological environment. According to statistics, the number of highway tunnels in China has exceeded 20,000, reaching 21316, and the total length has exceeded 20 million meters (21.999 million meters actually) by 2020, far more than the other countries in the world (Figure 1). Moreover, the number of long freeway tunnels in China increased rapidly from 2010 to 2020 (Figure 2). By 2020, the number of long freeway tunnels in China had reached 5541, with a total length of 9.633 million meters. Among them, the number of extra-long highway tunnels has reached up to 1394, with a total length exceeding 6.23 million meters.

Serious road traffic accidents often occur in tunnels worldwide. The earliest recorded tunnel traffic accident occurred in 1949 at the Holland Tunnel in New York City, where a dangerous chemical vehicle caught fire and generated a large amount of toxic gas, causing 66 people to be poisoned and 23 vehicles damaged. In 1982, a serious tunnel traffic accident occurred at the Salang Tunnel in Afghanistan, where a truck collided with a tanker, resulting in an explosion; more than 200 people were killed, and hundreds of vehicles were damaged. In 1999, a truck fire accident

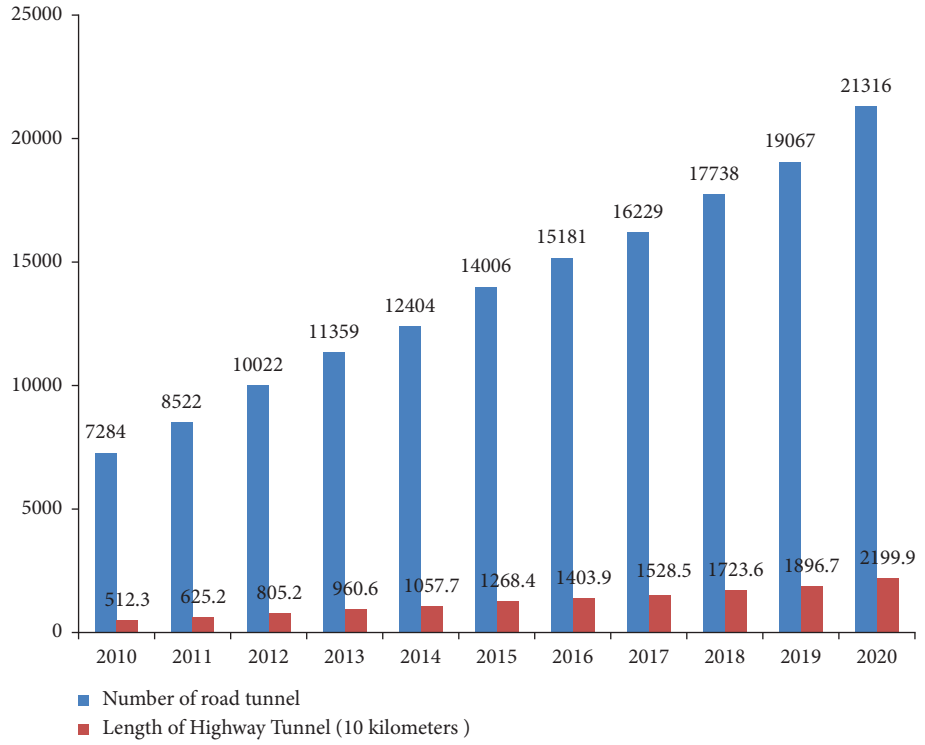

Figure 1: Statistics on the number and length of highway tunnels in China (2010–2020). Source: Transportation Knowledge Service System of China (2021).

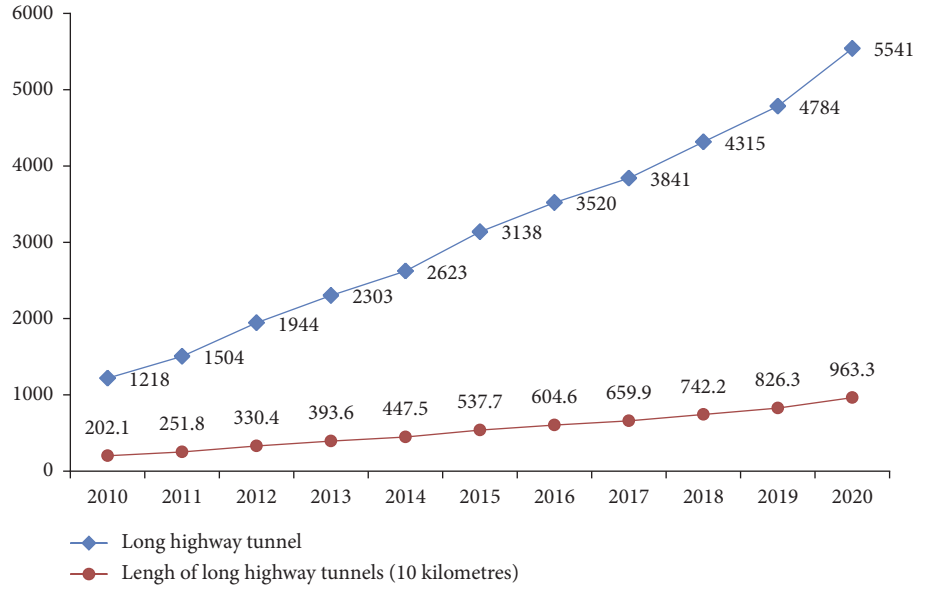

Figure 2: Statistics on the number and length of long highway tunnels in China (2010–2020). Source: Transportation Knowledge Service System of China (2021).

occurred at the French/Italian Mont Blanc tunnel, which led to fierce burning, the temperature exceeding 1000°C, and the asphalt pavement had been burned as the bus contained flour and cream. A total of 39 people were killed, 40 vehicles were damaged, and most of the casualties were caused by suffocation as a result of fire smoke and toxic gas [2]. In 2001, a truck fire accident occurred in the St. Gotthard Tunnel in Switzerland. The accident was caused by a collision between two trucks, which led to a heavy fire and smoke, resulting in 11 deaths, mainly due to smoke, gas suffocation, and high temperature. The high temperature also caused the collapse of the tunnel vault. In 2004, a series of rear-end collision fire accidents occurred in Japan's Takayama Tunnel [3], causing four-vehicle rear-end collisions and fires when a large truck

hit a car parked near the road. Five people were killed, and 23 others, including the firefighters, were hospitalized after smoking. In recent years, a large number of highway tunnel traffic accidents have occurred in China (Table 1), resulting in serious economic losses and significant negative social impacts.

Owing to the particularity of traffic environments, tunnels have become the main spatial distribution points of accident-prone traffic sections, which seriously affects highway safety [4]. Compared with general roads, the death rate of highway accidents is twice higher [5], especially with the increasing frequency of traffic accidents in highway tunnels, which has affected traffic safety dramatically and caused significant social and economic losses. It shows that nearly 93% of accidents are caused by human internal risk factors [6], according to an analysis of 2258 traffic accidents by the National Highway Traffic Safety Administration (NHTSA). Statistical data from China also verified the conclusion that human factors are the main cause of traffic accidents. Moreover, road tunnel traffic accidents are dominated by rear ends and collisions [7], and tracing collisions account for 57.46% of total accidents [8]. A strong positive correlation exists between traffic accidents and driving speeds [9–11].

Currently, relevant theoretical research and technical measures are more interested in reducing the risk factors of vehicles and road environments, and less attention has been paid to reducing human risk factors. It has been verified that human factors are the primary and key factors in accidents, and research has also shown that accidents caused by unsafe behaviors are much higher than other unsafe hazards, such as machines, environments, and management [12]. Humans are the main body of multinomial collaborative systems. Therefore, unsafe behavior control has become a key factor in highway tunnel traffic safety management. The measurement of human factors in human-machine-environment systems is the focus of management [13]. However, few studies have focused on the measurement of the specific and single hazard of unsafe human behavior and rarely quantitative research on human unsafe behavior in highway tunnel traffic accidents. Therefore, to address the gaps in research knowledge, we conducted a study on the risk assessment of the unsafe behavior of humans in highway tunnel traffic accidents using a tail-biting fish diagram combined with the fault tree method. A risk assessment model was constructed to obtain the risk ranking of unsafe behaviors, which was intended to provide a theoretical basis for the effective control of unsafe behavior in highway tunnel traffic accidents.

The remainder of this paper is organized as follows: In Section 2, unsafe human behaviors that can potentially cause highway tunnel traffic accidents are identified. In Section 3, a risk assessment model composed of probability, importance degree, and loss is constructed and the method for assessing the probability and importance degree is proposed. In Section 4, we apply this model to the "8.10 traffic accident" that occurred in the Qinling No. 1 Tunnel of the Ankang Section of the Beijing-Kunming Expressway. Finally, we discuss and conclude the study in Section 4.

2. Identification and Analysis of Human Unsafe Behavior in Highway Tunnel Traffic Accidents

tThe mechanisms underlying traffic accidents in highway tunnels are complex. According to the accident causation theory, the highway tunnel traffic system can be expressed as a complex system composed of people, vehicles, roads, environment, and management. These five factors were coordinated and interacted with each other. If any factor has potential hazards, it will affect the safety status of the system and can lead to accidents. Therefore, tunnel traffic accidents can be expressed as a process in which people, vehicles, roads, the environment, and other dynamic and static factors are out of balance [14]. Among these factors, human factors account for approximately 80% of accidents [15], mainly manifesting as unsafe human behaviors. Human unsafe behaviors refer to the behavior characteristics when the man's ability is lower than the system's requirements in a specific space-time environment, which shows that human behavior does not meet the requirements of the system.

The adverse source of the accident was the quality of the man. Specifically, people are the dominant factors in accidents. The main cause of traffic accidents is the interaction between internal and external risk factors. Various external environmental risk factors affect the driver, stimulate individual internal risk factors, and ultimately lead to traffic accidents. When drivers experience severe traffic violations, such as distraction, fatigue, overspeed, mental workload, and drunk driving, traffic accidents are likely to take place during the driving process. In the causes of highway tunnel safety accidents, human unsafe behaviors are caused by a variety of factors, mainly including psychological causes, physiological factors, skills, working environment, and the influence of management. The first three aspects are subjective reasons (internal causes), and the latter two are objective reasons (external causes) [16]. Furthermore, the primary causative factors in highway traffic environments include drivers and passengers. According to the statistics, driver-induced factors are 8–9 times more than those of passengers. Therefore, in this study, we focused on the unsafe behavior of drivers.

2.1. Driver-Induced Factors. Drivers are the main participants in traffic behavior [17], and their psychological and physiological reactions directly affect traffic safety, with factors including physiology, psychology, technical experience, and traffic behavior. Simultaneously, the driver is affected by the driving environment, road conditions, weather conditions, and other factors:

(1) Some highway tunnels are located at high altitudes with low air pressure and low oxygen, which can easily lead to physiological discomforts such as plateau reactions, dizziness, heartbeat, acceleration, and other symptoms, thus affecting the driver's attention and reducing their ability to respond to emergencies.

Table 1: Major tunnel traffic accidents in China (2002–2022).

Serial number	Accident location	Time (years)	Type of accident	Consequence	Cause of accident
1	Gansu Tangjiafengtai Tunnel	2002	Rear-end collision	8 dead, 8 wounded	Miss operation
2	Zhejiang Shangsan Expressway Tunnel	2002	Rear-end collision	7 dead, many injured	Dim lights in the tunnel
3	Sichuan Fengdian Tunnel	2004	Rollover	5 dead, 27 injured	Over speed
4	Chongqing Jinyunshan Tunnel	2005	Collision	1 dead, 11 injured	Too fast
5	Chongqing Huangshi Tunnel	2006	Crashed into tunnel	4 dead, 3 wounded	Vehicle out of control
6	Guangdong Tianluyuan Tunnel	2007	Crashes into tunnel	2 dead, 3 wounded	Collision
7	Guangdong Dabaoshan Tunnel	2008	Rear-end fire	Tunnel collapse partially	Chemical explosion
8	Shaanxi Fengbaozhai Tunnel	2008	Vehicle collision	4 dead, 1 seriously injured	Over speed
9	Shandong Panlong Tunnel	2009	Tailgating fire	3 dead, 5 wounded	Fatigue driving
10	Zhejiang Daxiling Tunnel	2010	Spontaneous ignition	Facilities damaged, great economic loss	Semitrailer burning
11	Jiangsu huishan tunnel	2010	Fire	24 dead, 19 injured	Arson
12	Gansu xinqidaoliang tunnel	2011	Fire	4 deed, 1 injured, 3 vehicles burned, tunnel damaged	Rear-end fire and explosion
13	Sichuan longquanshan tunnel	2011	Vehicle collision	7 dead, 4 wounded	Brake failure
14	Shanghai Bund Tunnel	2012	Crashes into tunnel	3 dead, 1 injured	Disoperation
15	Shanxi Yanhou Tunnel	2013	Fire	40 dead, 12 injured, 43 vehicles burned	Illegal operation
16	Guangdong Kaoyishan tunnel	2014	Rear-end collision	5 dead, 13 injured	Fatigue driving
17	Shanxi Jincheng section Yanhou Tunnel	2014	Hazardous chemical explosion	40 killed, 12 injured, and 42 vehicles burned	Articulated train crash
18	Shaanxi Baojiashan Tunnel	2015	Vehicle collision	1 dead, 1 injured	Miss operation
19	Shaanxi Qinling No. 2 Tunnel	2016	Rear-end collision	2 dead, 2 wounded	Over speed
20	Yunnan Maanshan Tunnel	2017	Bus rollover	10 dead, 38 injured	Miss operation
21	Shandong Taojiakuang Tunnel	2017	Fire	13 dead (11 children)	Fire
22	Shaanxi Qinling No. 1 Tunnel	2017	Bus collision	36 dead, 13 injured	Collision
23	Zhejiang Wangzhai Tunnel	2018	Collision	1 dead, many injured	Over speed
24	Hubei Liziping Tunnel	2018	Collision	2 dead, many injured	Over speed
25	Zhejiang Maoliling Tunnel	2019	Fire	5 dead, 36 injured	Tires triggered fire
26	Guangxi Hezuo village Tunnel	2019	Collision	4 dead, 4 seriously injured	Out of control, collision
27	Sichuan Xudianzi Tunnel	2020	Bus collision	6 dead, 29 injured	Vehicle rollover
28	Jielong Tunnel	2021	Chain collision	4 dead, many injured	Over speed
29	Shanxi Yagou Tunnel	2022	Collision	5 dead, many injured	Lose control

(2) When driving in the tunnel, especially in freeway tunnel groups, the light changes frequently and the driver experiences a black hole and white hole effect in a very short time, which seriously affects the driver's visual perception [18]. Moreover, the high spirit concentration in tunnels causes fatigue, which can easily lead to accidents.

(3) Owing to the different usages of materials at the entrance and exit of the tunnel, there is a transition area that leads to a significant difference in the adhesion coefficient of the pavement inside and outside the tunnel. Under the stress of bad weather, such as rain and snow, the road adhesion coefficient changes dramatically and vehicles are easy to ski.

(4) In a depressed driving environment in a tunnel, drivers tend to leave the tunnel quickly and engage in illegal driving behaviors, such as speeding and overtaking. When the traffic flow in the tunnel is large or the road surface is wet, overspeed and overtaking are often prone to collisions or rear-end collisions and sometimes even lead to a series of rear-end accidents.

(5) In bad weather, drivers are prone to anxiety, irritability, misjudgment, missed operations, and other behaviors, coupled with the impact of wet and slippery roads on vehicle performance, which increases the possibility of traffic accidents.

(6) When driving at night, drivers can easily relax their vigilance and drive quickly. In addition, when driving in an external environment of dawn, dusk, and dim light, the driver's vision decreases significantly. Therefore, the accident rates at dawn and dusk are much higher.

Generally, when driving in the complex environment of a tunnel, the driver is likely to experience speed, fatigue, driving, overload, negligence, and other illegal driving behaviors owing to weak safety consciousness. Tunnel environment driving is prone to traffic accidents, particularly for drivers of dangerous chemical transport vehicles and trucks [19]. Therefore, driver factors include driver safety awareness, illegal traffic behaviors, improper operation, psychological changes, emergencies, and environmental impact.

2.2. Passenger-Related Factors. Passenger-related factors mainly refer to the factors that directly or indirectly lead to tunnel traffic accidents owing to passengers' unsafe behavior, such as carrying contraband goods (which may lead to fire and explosions), talking with the driver (which may affect safe driving), or even encouraging the driver to violate regulations and speed. Although passengers cannot control the vehicle directly as drivers, improper behavior increases the risk rate. In addition, passengers should fasten their seatbelts and escape abilities along with their self-rescue capabilities.

Owing to its closed distribution in space [20], a tunnel is the bottleneck of a freeway. Once a tunnel traffic safety accident occurs, it has serious impacts, including traffic congestion, vehicle damage, tunnel damage, and casualties [21]. Meanwhile, the limitations of the tunnel environment aggravate the consequences of accidents [22]. According to Table 1, once a traffic accident occurs in a freeway tunnel, it will seriously affect the traffic situation, leading to traffic jams. Personnel rescue, and vehicle dragging, which are very inconvenient, and the evacuation and rescue processing will be prolonged, further aggravating the situation and causing chain reactions and large seepage accidents in the surrounding environment. Moreover, tunnel traffic accidents, often prone to chain accidents or secondary damage such as chain tails, may also cause casualties [23]. If a vehicle fires in a tunnel, it can easily cause the pavement asphalt material to melt or even be on fire. Once a fire or explosion occurs, particularly when a truck or hazardous chemical vehicle explodes in a tunnel, an extremely high-temperature flame front or shock wave will be generated, which is accompanied by a large number of toxic and harmful gases. Owing to the relatively closed tunnel, people trapped in it are easily suffocated by smoke and the rescue work is extremely difficult, resulting in significant casualties and property losses [24]. Based on this, we drew a tail-biting fishbone figure: a chart with two fishbones, one biting another, to describe and analyse the accident risk factors, risk events, and risk loss based on Ishikawa Char (Fish Bone chart) (Figure 3, the diagram looks like two fishbones with one biting another); from the aspect of car insecurity, road and environmental defects, security management deficiencies and human unsafe behaviors, we acquired all the potential hazards and their impacts and losses systematically.

Simultaneously, the fault tree can be applied to the systematic analysis and quantitative evaluation of the special causes of system accidents, such as human factors. Combined with the results of the tail-biting fishbone figure, a fault tree model of traffic accidents in mountainous highway tunnels was established (Figure 4 and Table 2).

As shown in Figure 4 and Table 2, unsafe behaviors that cause traffic accidents in mountainous freeway tunnels include speeding (X_1), overload (X_2), irregular overtaking (X_3), drowsy driving (X_4), drunk driving (X_5), sudden illnesses (X_6), negative emotions (X_7), psychological shadows (X_8), and weak awareness of safety (X_9).

3. Risk Assessment of Human Unsafe Behaviors of Traffic Accidents in the Highway Tunnel

3.1. Risk Evaluation Model of Human Unsafe Behavior. To evaluate specific unsafe human behaviors and rank these activities, the risk values of each unsafe behavior should be assessed. Subsequently, tailored measures can be taken according to the risk values. The risk values can be calculated using possibility (P) and loss (L).

$$R_i = \cdot P_i \cdot L_i. \tag{1}$$

The possibility of unsafe human behavior risk is mainly measured by the human unreliability degree (HUD) and its degree of importance (I). Therefore, the risk evaluation model for unsafe human behavior can be revised as follows:

$$RH_i = HUD_i \cdot I_i \cdot L_i, \tag{2}$$

where RH_i is the risk value of unsafe behavior at time t; HUD_i is the unreliability of unsafe behavior i at time t; I_i is the importance of unsafe behavior i in the accident system; and L_i is the possible loss of the accident caused by the unsafe behavior i。

3.2. Assessment Model of Human Unreliability. In a system, human behavior is usually measured by reliability, that is, the probability of a person completing a specified task (or function) without an error within the specified time and under a given condition. Corresponding to human reliability is unreliability, which can be used to scientifically measure unsafe behavior.

Reliability is a function of time and can be expressed as a reliability function $R(t)$, which represents the probability of continuous operation during the period of $(0, t)$. The corresponding reliability is unreliable, which indicates the probability that people cannot complete a specified action

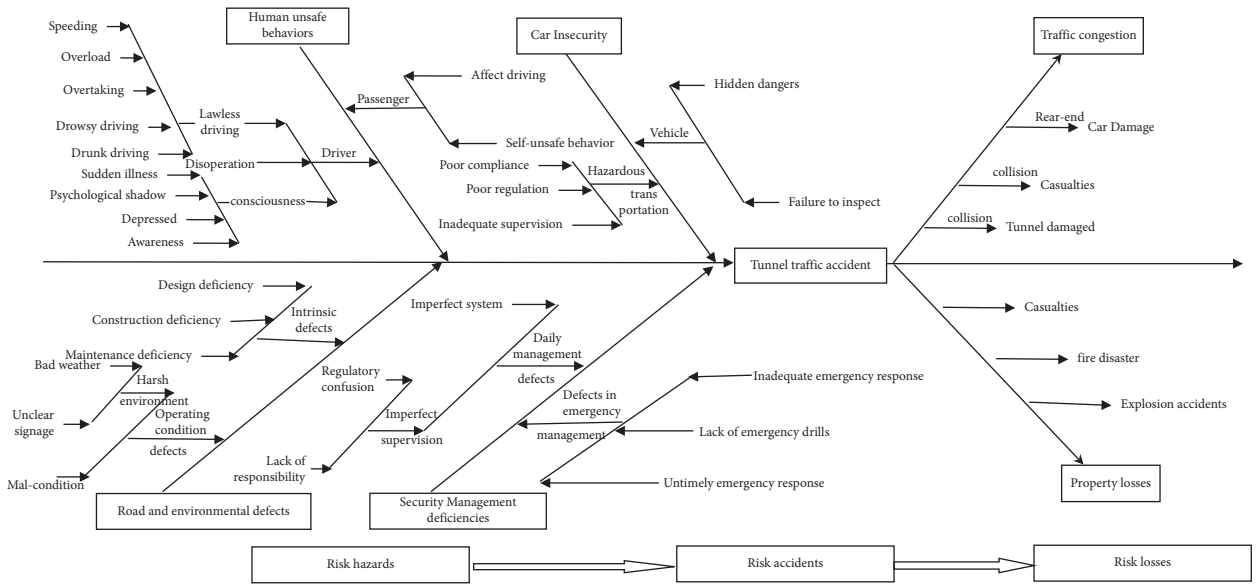

Figure 3: Tail-biting fishbone figure of a traffic accident in a mountainous highway tunnel.

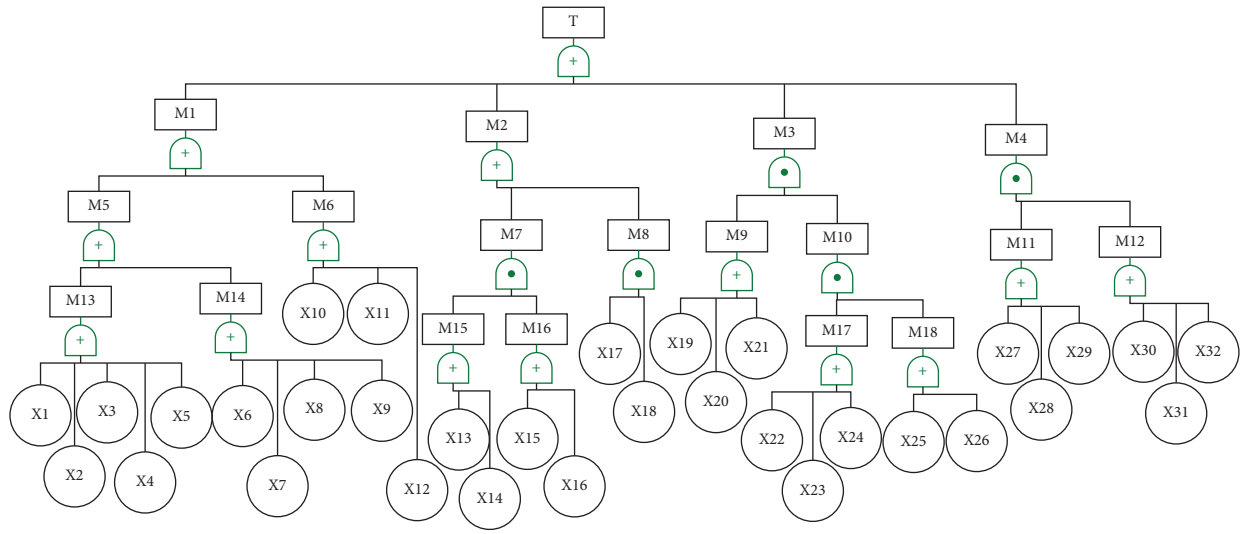

Figure 4: Fault tree of highway tunnel traffic accidents.

under a given condition and within a specified time. It is also known as the failure probability or failure rate and can be expressed as the available $F(t)$. It is apparent that $R(t) + F(t) = 1$.

Let ξ represent the time from unit to failure, which is a random variable. According to the definition of reliability, the probability of an event being $\{\xi > t\}$ is the reliability of the unit at time. In other words, there is a probability that no failure will occur within the $(0, t)$ unit. If $R(t)$ is a reliability function, then

$$R(t) = P\{\xi > t\}. \tag{3}$$

Here, P represents probability and event $\{\xi \le t\}$ is the complement set of events $\{\xi > t\}$. Its probability is often referred to as the cumulative distribution function $(F(t))$.

$$F(t) = P\{\xi \le t\} = 1 - R(t). \tag{4}$$

Its physical meaning is the failure probability of the unit in the time interval $(0, t)$, that is, the degree of unreliability.

For a limited sample, the total number of products operated under the specified conditions is N_0 and $(0, t)$, and the cumulative number of failures for a product during its operating hours is $r(t)$. Reliability and unreliability were estimated as follows:

$$R(t) = \frac{N_0 - r(t)}{N_0},$$
$$F(t) = \frac{r(t)}{N_0}. \tag{5}$$

Table 2: Accident tree event description for mountain highway tunnel accidents.

Number	Meaning
T	Tunnel traffic accident
M_1	Human unsafe behaviors
M_2	Car insecurity
M_3	Road and environmental defects
M_4	Security management deficiencies
M_5	Driver-induced factors
M_6	Passenger-related factors
M_7	Vehicle factors
M_8	Hazardous material transportation
M_9	Tunnel defect
M_{10}	Defects conditions
M_{11}	Management defects
M_{12}	Defects in emergency management
M_{13}	Miss operation
M_{14}	Physical and mental deficiency
M_{15}	Vehicle safety hazards
M_{16}	Daily check not in place
M_{17}	Harsh environment
M_{18}	Emergency disposal defects
X_1	Speeding
X_2	Overload
X_3	Illegal overtaking
X_4	Drowsy driving
X_5	Drunk driving
X_6	Sudden illness
X_7	Psychological shadow
X_8	Being depressed
X_9	Weak awareness
X_{10}	Affect driving
X_{11}	No seat belts
X_{12}	Carrying flammable and explosive articles
X_{13}	On-the-road crash
X_{14}	Brake failure
X_{15}	Distraction
X_{16}	Inadequate daily maintenance
X_{17}	Poor compliance
X_{18}	Poor regulation
X_{19}	Complex lines
X_{20}	Low road adhesion coefficient
X_{21}	Design defect
X_{22}	Ventilation and lighting defects
X_{23}	Unclear traffic signs
X_{24}	Inclement weather
X_{25}	Slow emergency response
X_{26}	Roadblock
X_{27}	Inadequate management system
X_{28}	Inadequate on-site supervision
X_{29}	Insufficient safety education and training
X_{30}	Inadequate emergency response system
X_{31}	Lack of emergency drills
X_{32}	Untimely emergency response

Similarly, the degree of unreliability of unsafe behaviors may be defined as

$$HU\ D = 1 - \frac{N_r}{N_t}, \tag{6}$$

where N_r is the number of error-free operations completed and N_t means the total number of times the operational task was executed.

Therefore, the SOR model was used to assess the unreliability of unsafe behaviors. SOR is a theoretical model of "stimulus-organism-response," which was proposed by Mehrabian and Russel in 1974 in the field of environmental psychology [25]. The model considers that environmental factors can stimulate human emotions and cognition and elicit close or escape responses. The model primarily involved three variables: stimulation, organism, and response. The theory holds that the relationship between external stimuli and individual responses is neither direct nor mechanical, as the individual is an organism with rich thought and emotional activity and has a certain subjective initiative. When facing a stimulus, it is not a passive response but an active selection. The face of some external stimulation may have a certain psychological activity, which may affect the individual state; this also means that the internal state of the organism plays an essential role in it. According to the SOR model, a calculation method for determining the operational reliability of human beings was proposed by Professor Yachi Ichi Michizui of Tokyo University in Japan. He believes that the basic reliability of the operator is

$$\gamma = \gamma_1\gamma_2\gamma_3, \tag{7}$$

where γ_1 represents the basic reliability of the information input process, γ_2 refers to the basic reliability of the decision process, and γ_3 refers to the basic reliability of the operation output process [26]. The values for γ_1, γ_2, and γ_3 are presented in Table 3.

In this study, the reliability degree model was revised by considering operating time, operating frequency, physical and psychological conditions, degree of danger, and environmental conditions. After obtaining the basic reliability of the operator γ, it can be modified more precisely according to the operating conditions, operating time, operating frequency, risk, and psychological and physiological effects; the operation reliability R can be obtained as follows:

$$R = 1 - bc\mathrm{def}\,(1 - \gamma). \tag{8}$$

R is the revised reliability degree, b is the correction factor for the operation time, c is the correction factor for the operating frequency, d is the correction factor for the degree of danger, e is the correction factor for the physical and psychological conditions, f is the correction factor for the environmental conditions, and $1 - \gamma$ is the basic unreliability, with each correction factor covering a certain range (Table 4).

Based on the reliability R value, we can also get the corresponding unreliability U value as follows:

$$\begin{aligned} U &= 1 - R \\ &= 1 - [1 - bc\mathrm{def}\,(1 - \gamma)] \\ &= bc\mathrm{def}\,(1 - \gamma). \end{aligned} \tag{9}$$

The rolling quantitative fusion method is adapted to calculate the reliability degree, as in the method, the closer it is to the mean, the greater the data weight and there is no relationship with the data itself.

Table 3: Values of parameters in basic reliability.

Category	Content	γ_1, γ_3	γ_2
Simple	Few variables, ergonomic principles considered	0.9995–0.9999	0.999
General	Variables below 10	0.9990–0.9995	0.995
Complex	Variables over 10, inadequate consideration of ergonomic principles	0.990–0.999	0.990

Table 4: Value of the correction coefficient.

Coefficient	b	c	d	e	f
1.0	Sufficient slack time	Low	Safe	Good	Good
1.0–3.0	Insufficient slack time	Appropriate	Risky	Bad	Bad
3.0–10.0	No slack time	High	Fatal	Very bad	Very bad

Suppose that for the same behavior or operations, different experts' judgement according to the SOR model of an unreliability series is $U_{(1)}, U_{(2)}, \ldots, U_{(j)} \ldots, U_{(n)}$, which is arranged in order from small to large.

$$U = (u_1, u_2, \ldots, u_i, \ldots, u_n), \quad u_i \le u_{i+1},\ i = 1, 2, \ldots, m-1. \tag{10}$$

This is calculated as

$$\xi_j = \frac{1}{m-j+1} \sum_{i=1}^{m-j+1} \sum_{k=i}^{i+j-1} \frac{u_k}{j}, \quad j = 1, 2, \ldots, m. \tag{11}$$

The unreliability quantitative fusion results can be obtained:

$$HU\ D = \frac{1}{m} \sum_{j=1}^{m} \xi_j. \tag{12}$$

3.3. Importance Degree Analysis Based on Fault Tree. As shown in Figure 4, Boolean algebra is used to solve the minimum cut set. The minimum cut set is a set of necessary and sufficient bottom events that leads to the occurrence of a fault tree. Using the fault tree analysis software FreeFta, 44 minimum cut sets of traffic accidents in highway tunnels were obtained as follows:

$$\left\{ \begin{array}{c} X_1, X_{10}, X_{11}, X_{12}, X_{13}X_{15}, X_{13}X_{16}, X_{14}X_{15}, X_{14}X_{16}, X_{17}X_{18}, X_{19}X_{22}X_{26}, X_{19}X_{23}X_{25}, X_{19}X_{23}X_{26}, \\ X_{19}X_{24}X_{25}, X_{19}X_{24}X_{26}, X_2, X_{20}X_{22}X_{25}, X_{20}X_{22}X_{26}, X_{20}X_{23}X_{25}, X_{20}X_{24}X_{26}, X_{27}X_{30}, X_{27}X_{31}, \\ X_{28}X_{30}, X_{28}X_{31}, X_{28}X_{32}, X_{29}X_{30}, X_{27}X_{31}, X_{27}X_{32}, X_3, X_4, X_5, X_6, X_7, X_8, X_9 \end{array} \right\}. \tag{13}$$

This shows that 44 possible routes can lead to traffic accidents in mountain highway tunnels and that there is at least one basic event in the minimum cut set, indicating that accidents can easily occur.

When the minimal cut set is determined, the importance of each basic event in the structure of the accident can be approximately calculated according to (14), which is used to analyse the impact of each basic event on the top event [27, 28].

$$I_\phi(i) = 1 - \prod_{x_i \in k_j} \left(1 - \frac{1}{2^{n_j - 1}}\right), \tag{14}$$

where $I_\phi(i)$ represents the structural importance of the underlying event i and n_j is the minimum cut set in which the base events are located for each event i.

For example, event X_4 has only one event in a minimal cut set and its structural importance.

$$I_\phi(4) = 1. \tag{15}$$

The event X_{13} exists in two minimal cut sets, and each cut set has two basic events: its structural importance as

$$I_\phi(13) = 1 - \left(1 - \frac{1}{2^{2-1}}\right)\left(1 - \frac{1}{2^{2-1}}\right) = 0.75. \tag{16}$$

The structural importance of each event is calculated as follows:

$$\begin{aligned} I(X_1) = I(X_{11}) = I(X_{10}) = I(X_9) = I(X_8) = I(X_7) = I(X_6) = I(X_5) = I(X_4) = I(X_3) = I(X_2) = I(X_1) > I(X_{32}) \\ = I(X_{31}) = I(X_{30}) = I(X_{29}) = I(X_{28}) = I(X_{27}) = I(X_{26}) = I(X_{25}) = I(X_{18}) = I(X_{17}) = I(X_{16}) = I(X_{15}) \\ = I(X_{14}) = I(X_{13}) > I(X_{24}) \\ = I(X_{23}) = I(X_{22}) = I(X_{21}) = I(X_{20}) = I(X_{19}). \end{aligned} \tag{17}$$

3.4. Loss Measurement Standard. According to the Road Traffic Accident Treatment Law in China (the NPC Standing Committee, 2003), the classification criteria for road traffic accidents are as follows.

3.4.1. Minor Accidents. This denotes a minor injury to one to two people or property loss of less than 1000 CNY.

3.4.2. General Accidents. This denotes serious injury in one to two people, mild injury in more than three people, or property loss of less than 30,000 CNY.

3.4.3. Major Traffic Accidents. It refers to an accident that causes one to two deaths, serious injury to more than three people and less than ten people, or property losses between CNY 30,000 and 60,000.

3.4.4. Extraordinarily Serious Traffic Accidents. It refers to an accident that causes more than three deaths, eleven serious injuries, one death, eight serious injuries, two deaths, five serious injuries, or loss of more than 60,000 CNY.

4. Case Studies

On August 10, 2017, at 23 : 34, a bus (number Yu C88858) travelled from Chengdu to Luoyang. When it passed through the south entrance of the Qinling No. 1 Tunnel (1164 km + 930 m) in the Ankang section of the Beijing-Kunming Expressway, a traffic accident occurred at the tunnel entrance, resulting in serious deformation and damage to the bus; 36 people were killed, and 13 people were injured in the accident.

The investigation found that the direct cause of the accident was that Baiming Wang, the driver, drove over the speed and fatigued when he passed the tunnel and did not take any safety measures such as steering and braking before the collision, which caused the vehicle to deviate from the right side of the road and collide frontally with the wall of the Qinling No. 1 Tunnel entrance. Furthermore, the fact that passengers are unattached to seat belts is another important cause of extremely serious secondary injuries.

In "8·10" traffic accidents, people's unsafe behaviors include driver's fatigue, driving at night and speeding passengers in a sleeping state, and not wearing seat belts; both the passenger and the driver become victims. The driver's driving speed was identified at speeds ranging from 80 to 86 km/h when entering the tunnel, which is higher than the speed limit (60 km/h for the bus), with 33% to 43% above the limit, and he drove continuously for 2.5 hours deep in the night with a severe fatigue state. Passengers did not tie any safety belts. Owing to the large inertia when the accident occurred, the loss of necessary protection caused a serious secondary injury. Night and fatigued driving are derived from human cognitive defects, which are often caused by the social environment, weak security awareness, and insufficient management of relevant departments [29–32].

According to the above assessment model of the probability and importance degree model, the "8·10" Special Major Road Traffic Accident on the Ankang Jingkun Expressway in Shanxi Province was studied and its unsafe behaviors were measured.

As shown in Figure 4 and Table 2, we consider overspeed (X_1) as an example. According to Table 5, the gradual cumulative results of the rolling average ξ_i and final fusion results of the reliability degrees are obtained as follows:

$$\begin{aligned}
\xi_1 &= 0.903096;\\
\xi_2 &= 0.898916;\\
\xi_3 &= 0.898916;\\
\xi_4 &= 0.903096,\\
\overline{HFP}_1 &= \frac{1}{m}\sum_{j=1}^{m}\xi_j,\\
&= \frac{1}{4}(0.903096 + 0.898916 + 0.898916 + 0.903096)\\
&= 0.901006.
\end{aligned} \tag{18}$$

Furthermore, the degree of importance of overspeed (X_1), as described in Section 3.3, is

$$I_\phi(1) = 1. \tag{19}$$

Therefore, the risk value of overspeed (X_1) is obtained as follows:

$$\begin{aligned}
RH_1 &= HFP_1 \cdot P_1 \cdot D_1\\
&= 0.901006 * 1 * L\\
&= 0.901006L.
\end{aligned} \tag{20}$$

L is the consequence of tunnel traffic accidents, and in this case, its quantitative value was 40 in this study, according to Table 6. Similarly, the risk value for drowsy driving (X_4) was obtained according to (11) and Table 7.

$$\begin{aligned}
\overline{HFP}_4 &= \frac{1}{m}\sum_{j=1}^{m}\xi_j,\\
&= \frac{1}{4}(0.938935 + 0.996555 + 0.996555 + 0.938935)\\
&= 0.967745.
\end{aligned} \tag{21}$$

And its importance degree refers to (12).

$$I_\phi(4) = 1. \tag{22}$$

Therefore, the risk value of drowsy driving (X_4) is obtained as follows:

$$\begin{aligned}
RH_4 &= HFP_4 \cdot P_4 \cdot D_4\\
&= 0.967745 * 1 * L\\
&= 0.967745L.
\end{aligned} \tag{23}$$

Table 5: Analysis table of overspeed driving.

Category	Expert1	Expert2	Expert3	Expert4
Stimulus reliability (γ_1)	0.992	0.993	0.9991	0.9996
Organism reliability (γ_2)	0.99	0.995	0.99	0.99
Response reliability (γ_3)	0.994	0.992	0.9995	0.99
Basic reliability (γ)	0.976188	0.980131	0.988614	0.979708
Correction factor of the operation time (b)	1.5	1.8	3	2
Correction factor of the operating frequency (c)	2	1	1	2
Correction factor of the degree of danger (d)	6	6	4	3
Correction factor of the physical and psychological conditions (e)	1	1.6	2	2
Correction factor of the environmental conditions (f)	2	2.8	3	2
Reliability $R_{(j)}$	0.14275072	0.038645	0.237882	0.025982

Table 6: Consequence and its value of traffic accidents.

Values	Extent of injuries	Losses caused by accidents (CNY)
10	1 to 2 people with minor injuries	Less than 1000
20	Serious injury of 1 to 2 people/more than 3 people with slight injuries	Less than 30,000
30	1 to 2 deaths/more than 3 people with grievous injuries	Between 30,000 and 60,000
40	More than 3 deaths/11 serious injuries/1 death, 8 serious injuries/2 deaths, 5 serious injuries	More than 60,000

Table 7: Analysis table of drowsy driving.

Category	Expert1	Expert2	Expert3	Expert4
Stimulus reliability (γ_1)	0.991	0.991	0.9991	0.993
Organism reliability (γ_2)	0.992	0.995	0.991	0.991
Response reliability (γ_3)	0.992	0.993	0.9993	0.992
Basic reliability (γ)	0.975207	0.979143	0.989415	0.97619
Correction factor of the operation time (b)	1.2	2	3	1
Correction factor of the operating frequency (c)	1.8	1.3	1	2
Correction factor of the degree of danger (d)	3.9	4.9	4	3
Correction factor of the physical and psychological conditions (e)	2.3	2.2	2	2
Correction factor of the environmental conditions (f)	2	2.5	3	2
Reliability $R_{(j)}$	0.039277763	−0.46147	0.237882	0.428572

According to the above risk values, the risk value for drowsy driving (X_4) was higher than that for high-speed driving (X_1). Accordingly, the priority level of X_4 is superior to that of X_1 when taking precontrol measures.

In view of the fact that the single risk value of drowsy driving is higher than that of speeding, drowsy driving should be given higher management authority and more resources when formulating management standards or taking management measures and unsafe behaviors that reach a specific risk value should be included in key supervision. For drowsy driving, the penalty standard (fine or deduction of driver's license points) should be formulated and its penalty standard should be higher than that of speeding. But, the reality is that we lack penalties standard for drowsy driving as it is difficult to identify fatigue driving. However, drowsy driving can be controlled through some technical means. For example, biological recognition technology and AI intelligence can be carried out for early warning and identification of drowsy driving before the vehicle is launched, the location information can be used to monitor continuous driving for a certain period of time (4 hours), and the black box video monitoring system can be used to record the driver's behavior. AI identification smart technology can be applied to early warning of unsafe behavior to achieve intelligent control and effective prevention of unsafe behavior.

Similarly, the risk values of other specific unsafe human behaviors can be obtained using this model and method. Finally, the risk ranking of a specific unsafe human behavior in highway tunnel traffic accidents can be obtained according to the risk values, and tailored measures can be taken to prevent and control hazards.

5. Discussion and Conclusions

The occurrence of an accident is a complex process, and most accidents have multiple causes. Hazard control is the main objective of safety management. Therefore, hazard identification and assessment are the base of risk management, which aims to establish a proactive safety strategy by investigating potential risks. This process is used to determine risk management priorities by evaluating the value of the hazards.

In this study, a tail-biting fishbone and fault tree model was used to establish a causal model for traffic accidents in mountainous highway tunnels. Based on the characteristics of unsafe human behaviors and their consequences, a human unsafe behavior risk measurement model for traffic accidents in highway tunnels was established, which was derived from the degree of human unreliability, the importance of the accident system, and possible loss after the accident. Moreover, a risk assessment model for unsafe human behavior was introduced to obtain the risk ranking. Methods for assessing the probability and degree of importance were proposed. Furthermore, the probability was obtained by assessing the unreliability degree of the unsafe behaviors, and the degree of importance was obtained by analysing the degree of influence in the fault tree using the Boolean algebra algorithm. Finally, the risk value was calculated, and the priorities for controlling the unsafe behaviors of humans were obtained, which provided a theoretical basis for the scientific, reasonable, and effective control of tunnel traffic accidents. This model may also be applied to other tunnel traffic accidents; however, some induced factors may change, so the model needs to be revised slightly. For other accidents, they may be assessed from unreliability, degree of importance, and loss and the model needs to adjust according to the actual situation. In the future, the process of unsafe human behavior and its mechanism can be analysed systematically, and its value can be assessed quantitatively. With the determined value, then the formulation of management standards and the optimization of management processes can be carried out to achieve fine and effective safety control.

The management standards of human unsafe behavior can be established, and tailored management measures can be taken, for example, classification/hierarchical control for drowsy driving, speeding, illegal overtaking, AI identification, and early warning of unsafe behavior with smart technology, to achieve intelligent control and effective prevention of unsafe behavior.

Data Availability

The data used to support the study conclusions were from some open-access articles that have been properly cited, and the assessment data are available from the corresponding author upon request.

Conflicts of Interest

The authors declare that they have no conflicts of interest.

Acknowledgments

The authors gratefully acknowledge the Humanities and Social Sciences Research Program of the Chongqing Municipal Education Commission, China (22SKGH183), and the Technological Research Program of Chongqing Municipal Education Commission, China (KJ1705150).

References

[1] B. Yang, J. Xu, and X. Y. Ni, "Highway tunnel traffic safety analysis," *Safety and Environmental Engineering*, vol. 3, no. 3, pp. 59–63, 2011.

[2] Y. D. Zhou, Y. F. Xin, and S. Z. Zhang, "Review of tunnel safety facilities by major international highway long tunnel accidents in recent years," *Journal of Rock Mechanics and Engineering*, vol. 23, no. 2, pp. 4882–4887, 2004.

[3] L. Zeng, S. F. Wang, Z. Lin, and G. Q. Liu, "Highway tunnel fire accident investigation and analysis," *Modern Tunnel Technology*, vol. 49, no. 3, pp. 41–48, 2022.

[4] T. Zhu, C. Wang, C. Yang, and R. Zhao, "Evaluation of effectiveness of speed reduction markings on driving speed in highway tunnel entrance and exit areas," *Promet - Traffic & Transportation*, vol. 32, no. 1, pp. 141–152, 2020.

[5] B. Kohl, K. Botched, and R. Horan, "Austrian Risk Analysis for Road Tunnels," in *Proceedings of the 3rd International conference, tunnel safety and ventilation*, Graz, Austria, January 2007.

[6] J. R. Treat, N. S. Tumbes, S. T. McDonald, D. Shinar, and R. D. Hume, "Tri-level study of the causes of traffic accidents: final report," *Executive Summary*, Institute for Research in Public Safety Indiana University, Bloomington, Indiana, 1979.

[7] Q. Hou, X. Hou, and J. Lang, "A correlated random parameters tobit model to analyze the safety effects and temporal instability of factors affecting crash rates," *Accident Analysis & Prevention*, vol. 134, Article ID 105326, 2020.

[8] S. R. Zhang, Z. J. Ma, and J. C. Xu, "Highway tunnel traffic accident distribution," *Journal of Chang ' a university (Natural Science Edition)*, vol. 13, no. 4, pp. 74–78, 2008.

[9] X. F. Wang, Q. Yang, and Y. Yan, "Analysis of distribution of freeway accidents under various conditions in China," *Advances in Mechanical Engineering*, vol. 20, no. 8, pp. 1–10, 2016.

[10] C. Caliendo, M. L. De Guglielmo, and M. Guida, "Comparison and analysis of road tunnel traffic accident frequencies and rates using random-parameter models," *Journal of Transportation Safety & Security*, vol. 8, no. 2, pp. 177–195, 2016.

[11] S. Chen, Y. Chen, and Y. Xing, "Comparison and analysis of crash frequency and rate in cross-river tunnels using random-parameter models," *Journal of Transportation Safety & Security*, vol. 14, no. 2, pp. 280–304, 2020.

[12] Z. M. Li, J. N. Kang, J. N. Miao, and J. F. Zhu, "Cause analysis of driver 's unsafe behavior in highway secondary accident," *Ergonomics*, vol. 6, no. 25, pp. 63–68, 2019.

[13] D. Meister, "Empirical measurement of human factors research themes," *Proceedings of the Human Factors and Ergonomics Society - Annual Meeting*, vol. 47, no. 18, pp. 1977–1981, 2003.

[14] E. P. Hu and L. Lei, "Research on highway tunnel traffic safety strategy from the perspective of driving psychology," *Engineering Technology Research*, vol. 26, no. 8, pp. 243–246, 2016.

[15] C. Caliendo and M. L. De Guglielmo, "Accident rates in road tunnels and social cost evaluation," *Procedia-Social and Behavioral Sciences*, vol. 53, no. 1, pp. 166–177, 2012.

[16] X. F. Meng, Q. L. Liu, X. X. Luo, and X. X. Zhou, "Risk assessment of the unsafe behaviours of humans in fatal gas explosion accidents in China's underground coal mines," *Journal of Cleaner Production*, vol. 210, pp. 970–976, 2019.

[17] C. Zond, S. Jimson, and F. Lai, "Investigating unsafe behaviors in traffic conflict situations: an observational study in

Nigeria," *Journal of Traffic and Transportation Engineering*, vol. 6, pp. 11–16, 2019.
[18] Z. Zheng, Z. G. Du, Q. X. Yan, Q. Xiang, and G. Chen, "The impact of rhythm-based visual reference system in long highway tunnels," *Safety Science*, vol. 95, pp. 75–82, Mar.2017.
[19] C. Caliendo and G. Genovese, "Quantitative risk assessment on the transport of dangerous goods vehicles through unidirectional road tunnels: an evaluation of the risk of transporting hydrogen," *Risk Analysis*, vol. 41, no. 9, pp. 1522–1539, 2020.
[20] K. Guo and L. Zhang, "Multi-source information fusion for safety risk assessment in underground tunnels," *Knowledge-Based Systems*, vol. 227, Article ID 107210, 2021.
[21] M. T. Keenan, K. G. Pittman, P. J. Stephens, and N. Ketchell, "Passenger detrainment and tunnel evacuation detrain modeling and experience," *Proceedings of the Institution of Mechanical Engineers Part F Journal of Rail & Rapid Transit*, vol. 208, no. 2, pp. 115–122, 1994.
[22] J. Y. Lee, K. Kirytopoulos, A. Pervez, and H. Huang, "Understanding drivers' awareness, habits and intentions inside road tunnels for effective safety policies," *Accident Analysis & Prevention*, vol. 172, Article ID 106690, 2022.
[23] C. Caliendo, M. Guide, F. Postilion, I. Russo, and T. Poretti, "A Bayesian bivariate hierarchical model with correlated parameters for the analysis of road crashes in Italian tunnels," *Statistical Methods and Applications*, vol. 436, pp. 1–23, 2021.
[24] C. Caliendo, P. Ciambelli, M. L. D. Guglielmo, M. G. Meo, P. Russo, and A. Amy, "Computational analysis of fire and people evacuation for different positions of burning vehicles in a road tunnel with emergency exits," *Cogent Engineering*, vol. 5, no. 1, Article ID 1530834, 2018.
[25] T. Zhou and K. X. Chen, "Research on the behavior mechanism of social commerce users based on SOR model," *Modern intelligence*, vol. 38, no. 3, pp. 7–12, 2018.
[26] E. Sherman, A. Mathur, and R. B. Smith, "Store environment and consumer purchase behavior: mediating role of consumer emotions," *Psychology and Marketing*, vol. 14, no. 4, pp. 361–378, 1997.
[27] Y. X. Li, J. H. Sun, C. R. Wei, and T. W. Jiang, "Study on solution method of structural importance of accident tree," *Chinese Science and Technology of Safety Production*, vol. 8, no. 5, pp. 107–110, 2021.
[28] G. N. Xu, Y. P. Xin, and F. Y. Lu, "A structure safety assessment method for overhead traveling crane based on accident tree analysis," *Advanced Materials Research*, vol. 230-232, pp. 16–20, 2011.
[29] F. Wen, Z. Yin, and Y. Zhou, "Research on tunnel risk control and evaluation index based on Fuzzy Theory," *IOP Conference Series: Earth and Environmental Science*, vol. 295, no. 4, Article ID 042052, 2019.
[30] J. C. Wang and D. P. Wang, "Risk evaluation of mountainous expressway sections based on cloud model and D-S evidence theory," *Science Technology and Engineering*, vol. 23, no. 19, pp. 286–291, 2019.
[31] X. D. Zhang, C. W. Huang, and Y. S. Chen, "Highway risk prediction and factor evaluation using convolutional neural networks," *International Journal of Computer Science*, vol. 49, no. 1, 2022.
[32] G. Z. Cheng, R. Cheng, S. L. Zhang, and X. Sun, "Risk evaluation method for highway roadside accidents," *Advances in Mechanical Engineering*, vol. 11, no. 1, pp. 168781401882174–1687814018821743, 2019.

Hindawi
Mathematical Problems in Engineering
Volume 2022, Article ID 6728062, 15 pages
https://doi.org/10.1155/2022/6728062

Research Article

Robust Fault-Tolerant Control of Continuous Lurie Networked Control Systems Based on the Observer with the Event-Triggered Mechanism

Yanfeng Wang,[1,2] **Yuqin Hou**,[2] **Guoyou Shao**,[1] **Youliang Tang**,[1] **and Peiliang Wang**[2]

[1]*School of Mechanical and Electrical Engineering, Suqian University, Suqian 223800, Jiangsu, China*
[2]*School of Engineering, Huzhou University, Huzhou 313000, Zhejiang, China*

Correspondence should be addressed to Peiliang Wang; wpl@zjhu.edu.cn

Received 8 August 2022; Revised 30 August 2022; Accepted 5 September 2022; Published 28 September 2022

Academic Editor: Yong Chen

For a class of uncertain continuously networked Lurie control systems with both sensor-to-controller time-delay and controller-to-actuator time-delay, the problem of codesigning its observer and fault-tolerant controller based on an event-triggered mechanism under actuator failure is investigated. Firstly, considering that the state of the system cannot be measured directly, an observer is constructed on the controller node. Secondly, to reduce the waste of network bandwidth resources and improve the performance of the network control system, a network control system approach based on event-triggered mechanism is proposed. By introducing the event-triggered mechanism and the actuator fault indication matrix, the Lurie networked control system is modeled as a Lurie system with time-delay using the state augmentation technique to obtain a model of the closed-loop system. Finally, based on Lyapunov stability theory, sufficient condition for the stability of the closed-loop system is obtained, and the design method of the fault-tolerant controller and the observer is given. The obtained results are given in the form of linear matrix inequalities, which are easy to be solved by using the linear matrix inequality toolbox. Finally, the feasibility and effectiveness of the method are illustrated by a simulation example.

1. Introduction

With the rapid development and wide application of computer, communication and control technologies, networked control systems (NCSs), and control systems, in which nodes (sensors, controllers, actuators, and controlled objects) transmit data through a shared communication network, have attracted much attention [1]. Compared with the traditional point-to-point control system, the NCS has the advantages of low installation cost, easy maintenance, high flexibility, information resource sharing, and easy remote operation. It has been widely used in intelligent medical, intelligent transportation, and intelligent manufacturing fields [2–5]. However, due to the problems of time-delay, packet loss, and wasted communication resources derived from the application of NCS, the actual production process will be affected by many uncertain factors, such as equipment wear and tear and production line aging, and the system will inevitably fail [6]. Once the system fails, it may cause catastrophic losses or even damage to personal safety, so it is of great economic and social significance to improve the reliability and stability of NCS operation with the help of fault-tolerant control.

Fault-tolerant control is the most common and effective control method [7, 8], which has received a lot of attention from academics and has achieved some results. The existing research literature on fault-tolerant control of NCS with time-delay can be divided into two categories. The first category of literature focuses on fault-tolerant control of NCS with time-delay between the sensor and the controller. In Ref. [9], a fault-tolerant controller design method based on observer estimation is proposed for the time-delay

between the sensor and the controller, and a closed-loop NCS is made asymptotically stable and satisfies the given control performance by combining Lyapunov stability theory and the linear matrix inequality method. The literature [10] models the time-delay from the sensor to the controller as a Markov chain with incomplete transfer probability and uses the state augmentation technique to transform the closed-loop system into a Markov jump system, gives sufficient conditions to guarantee the stability of the NCS, and designs fault-tolerant controllers. The second type of literature focuses on fault-tolerant control of NCS with time-delay between both sensors to controllers and controllers to actuators. The literature [11] combined the time-delay in the sensor-to-controller network and the time-delay in the controller-to-actuator network into a total time-delay, established a robust fault-tolerant control method for discrete NCS with time-delay, and combined Lyapunov stability theory and switching system theory, for the design of fault-tolerant controllers. The literature [12] describes the sum of the time-delay from the sensor to the controller and from the controller to the actuator in terms of random variables conforming to the Bernoulli distribution. A stability criterion for systems with stochastic time-varying time-delay is proposed to ensure that the designed fault-tolerant controller can satisfy the asymptotic stability conditions and operability requirements when the state trajectory enters the slip surface.

With the development and integration of control science and computer technology, the demand for data and information transmission is also increasing. Due to the limitation of network communication bandwidth, communication resources are limited, and if the amount of data transmitted by the system exceeds the threshold value that can be carried, it will lead to network congestion or even system collapse. To address this problem, some scholars have conducted research. The traditional time-triggered mechanism is simple and easy to implement, but the selected sampling period is small, and frequent data transmission and update will lead to the waste of communication resources and easily cause network congestion [13, 14]. In order to overcome the shortcomings of the time-triggered mechanism, many scholars have successively adopted the event-triggered mechanism to save network resources. The implementation method is to let the sampled signal reach an event generator, then the event generator decides whether the signal is transmitted to the network according to the triggering conditions. This mechanism of transmitting only necessary signals and reducing unnecessary signal transmission determined by the triggering conditions effectively reduces the occupation of limited communication resources and improves the efficiency of information transmission [15–17]. With the continuous development of NCS, many innovative results have been achieved for event-triggered mechanisms. For example, the adaptive event-triggered mechanism proposed in the literature [18, 19] has attracted much attention. Compared with the traditional event-triggered mechanism, its triggering threshold is a time-variable related to the system state, so it can flexibly adjust the triggering conditions according to the system state to further reduce the data transmission and maintain a better system performance, which is significant for NCS. Scholars have introduced different kinds of event-triggered mechanisms into NCS to replace the traditional time-based periodic transmission method, which has become an important research element in NCS.

In recent years, some results have been achieved in the research about fault-tolerant control of NCS with time-delay under the event-triggered mechanism. For example, an event-triggered mechanism with the fault-tolerant control strategy is proposed for continuous uncertain NCS with time-delay from the sensor to thecontroller, which enables the system to remain stable in case of actuator failure [20]. The literature [21] investigated the asynchronous H_∞ fault-tolerant control of discrete Markov jump systems with actuator failure and time-delay, proposed a pattern-dependent event-triggered mechanism method based on the pattern-dependent Lyapunov–Krasovskii function, and obtained the performance of the closed-loop system with stochastic mean-square stability under actuator failure and the joint design method of the asynchronous fault-tolerant controller and event-triggered mechanism. However, all the above-mentioned literatures are studies done based on state feedback in the case of measurable system states. For the case where the system state is not measurable, literature [22] proposes a delay-based event-triggered fault estimation observer for a class of continuous NCSs with time-delay and faults, gives a fault-tolerant control method based on fault estimation to compensate the effects generated by system faults, and designs fault-tolerant controller gains and event-triggered parameters to ensure the required performance of the faulty system and to reduce the communication resources wastage. However, only the time-delay in the sensor-to-controller network is considered in the paper. In the literature [23], a fault-tolerant control model for linear NCS with time-delay under the dynamic event-triggered mechanism is developed, an observer design method for simultaneously estimating the state vector and unknown actuator faults is proposed, and an observer-based fault-tolerant controller is designed, but the time-delay from sensor-to-controller and controller-to-actuator is combined in the paper to deal with them.

Lurie systems are a class of nonlinear systems with typical structural features that can be more accurately modeled to reflect objective reality, and they represent many essential features of nonlinear systems. The absolute stability of Lurie systems has received much attention. However, few literature have been devoted to the problem of fault-tolerant control under actuator failure as an object of study.

It is well known that time-delay is the main cause of system instability in NCS. Most of the existing techniques have only studied the controller-to-actuator time-delay or have combined the sensor-to-controller and controller-to-actuator time-delay into one treatment. Based on the above discussion, the following questions naturally arise: Is it possible to build a unified model of NCS with bilateral delays based on event-triggered mechanisms? How can the joint design of event-triggered mechanism, observer, and fault-tolerant controller

under this unified model make the closed-loop system with time-delay, uncertainty, and actuator failure stable?

In this paper, we address the codesign of its event-triggered mechanism and fault-tolerant controller under actuator failure for a continuously networked Lurie control system with time-delay and uncertainties, with the following main contributions:

(1) The influence of the time-delay from the sensor to the controller and from the controller to the actuator on the control system is taken into account, which is more interpretable and mechanistic

(2) Also considering the time-delay, uncertainty of system parameters, and actuator failure, an observer is constructed on the controller node to establish the Lurie NCS model under the event-triggered mechanism, which enables the impact of time-delay, uncertainty, event-triggered mechanism, and actuator failure on system performance to be analyzed in the same framework

(3) According to Lyapunov stability theory, the stability conditions of the closed-loop system are obtained, and the design methods for solving the event-triggered weight matrix, robust fault-tolerant controller, and observer are given

The remainder of this paper is organized as follows. The modeling of a continuous Lurie NCS with actuator failures under an event-triggered mechanism is shown in Section 2. In Section 3, the system stability analysis and the codesign of the observer, fault-tolerant controller, and event-triggered mechanism are provided. Section 4 exhibits the construction of the simulation model and the verification of the algorithm. Section 5 summarizes the contents of the full paper.

Notations are as follows: R^n represents the n-dimensional Euclidean space; $*$ represents the transpose of the corresponding matrix block; if the matrix A is invertible, A^{-1} represents the inverse of A; A^{T} and A^{+} represent the transpose and Moore–Penrose inverse of the matrix, respectively, and the real positive definite matrix X is represented as $X > 0$; I represents the unit matrix of appropriate dimensions; and diag$\{a, b \ldots\}$ represents the diagonal matrix with a, b as the main diagonal.

2. Problem Description

Consider the following Lurie system with uncertainty and actuator failure:

$$\begin{cases} \dot{x}(t) = (A + \Delta A)x(t) + (B + \Delta B)Fu(t) + (D + \Delta\ D)\omega(t), \\ y(t) = Cx(t), \\ \omega(t) = -\psi(y(t)). \end{cases} \tag{1}$$

where $x(t) \in R^n, u(t) \in R^m, y(t) \in R^q$ are the system state vector, input vector, and output vector, respectively; A, B, C, D are real constant matrices of appropriate dimensions; $\Delta A, \Delta B, \Delta\ D$ are uncertainty matrices with bounded parametrization and satisfy $[\Delta A\ \ \Delta B\ \ \Delta\ D] = U\Xi(t)[H_1\ \ H_2\ \ H_3]$, where U, H_1, H_2, H_3 are known matrices with appropriate dimensions, and $\Xi(t)$ is an unknown matrix satisfying $\Xi(t)^T\Xi(t) < I$; F is the fault indication matrix which we define under actuator failure and satisfies $F = \mathrm{diag}\{f_1, f_2, \ldots f_m\}, f_j \in [0, 1], \quad j = 1, 2, \ldots m$, where $f_j = 0$ means the jth actuator is completely failed, $f_j = 1$ indicates normal operation of the j th actuator, and $f_j \in (0, 1)$ indicates partial failure of the j th actuator. $\psi(\cdot)$: $R^q \longrightarrow R^q$ is a memoryless nonlinear function, satisfying the local Lipschitz condition, $\psi(0) = 0$, and for any $y(t) \in R^q$ satisfies, the sector condition is

$$\psi^T(y(t))[\psi(y(t)) - \Theta y(t)] \le 0, \tag{2}$$

where Θ is the real diagonal matrix. Such a nonlinear function $\psi(\cdot)$ is usually said to belong to the sector $[0, \Theta]$, denoted as $\psi(\cdot) \in \ell[0, \Theta]$.

Remark 1. For the more general case $\psi(\cdot) \in \ell[\Theta_1, \Theta_2]$, it can always be transformed into the case of $\psi(\cdot) \in \ell[0, \Theta]$ by loop transformation, so only the case of $\psi(\cdot) \in \ell[0, \Theta]$ is considered in this paper.

The NCS structure diagram shown in Figure 1 consists of an actuator, a controlled object, a sensor, a sampler, a zero-order retainer, an observer, an event generator, and a controller. The sampler acquires the output signal of the system with a fixed period h. The signal collected by the sampler is directly transmitted to the event generator connected to it. Then, whether the event generator can send the sampled data $y(t_k h + jh)$ to the controller needs to be determined according to the following conditions:

$$\begin{aligned} &[y(t_k h + jh) - y(t_k h)]^T V [y(t_k h + jh) - y(t_k h)] \\ &\quad > \sigma y^T(t_k h + jh) V y(t_k h + jh), \end{aligned} \tag{3}$$

where V is a positive definite matrix and $j \in Z^+, \sigma \in [0, 1]$.

Remark 2. Only the output sampled data $y(t_k h + jh)$ satisfying equation (3) will be transmitted, and obviously this event-triggered mechanism will reduce the communication load in the network and reduce the computation of the controller. There is a special case that if $\sigma = 0$ in Eq. (3) holds for all sampled output data $y(t_k h + jh)$, then the event-triggered mechanism will degrade to a time-triggered mechanism. In addition, the triggering instant of the event-triggered mechanism used in this paper is based on the system sampling period h, which can be triggered only at the sampling instant, ensuring that the minimum event interval time is positive and avoiding Zeno behavior.

After the event generator has released the current sample signal, the sample signal is transmitted directly to the zero-order keeper via the network and then to the actuator via the observer. In this process, the time-delay from the sensor to the controller is denoted by $\tau_{i_k}^{sc}$, and the time-delay from the controller to the actuator is denoted by $\tau_{i_k}^{ca}$.

To facilitate the following analysis, the following hypotheses are proposed:

(a) The matrix C is a row-full rank matrix

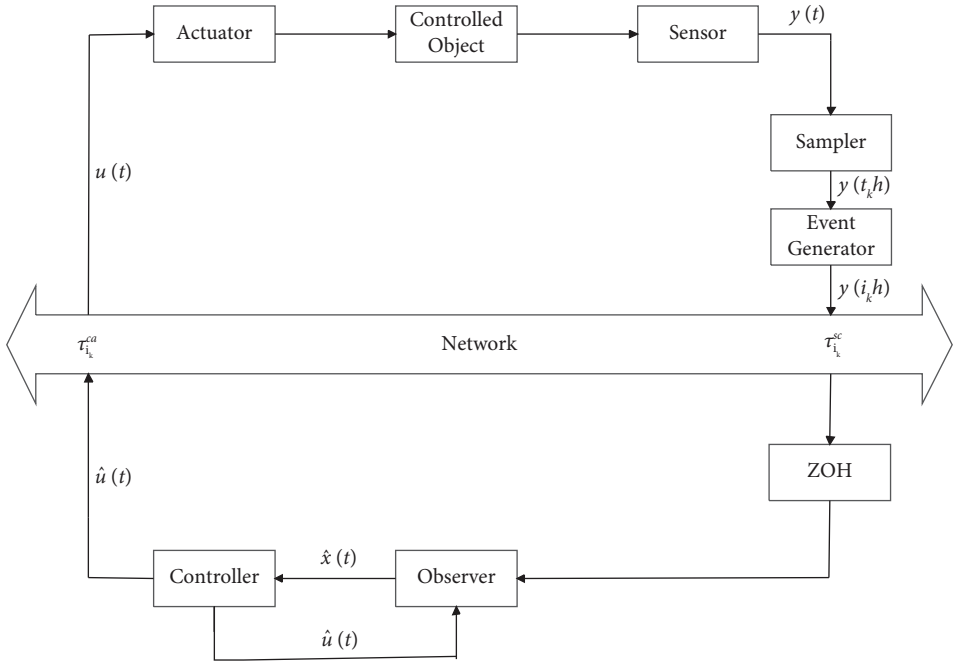

Figure 1: Structure of observer-based NCS under the event-triggered mechanism.

(b) The sensor is time-driven, the controller and actuator are event-driven, and the data is single packet transmission

(c) Time-delay $\tau^{sc}_{i_k}$ and $\tau^{ca}_{i_k}$ are both bounded for any $t \geq 0$, $0 < \tau^{sc}_m \leq \tau^{sc}_{i_k} \leq \tau^{sc}_M$, $0 < \tau^{ca}_m \leq \tau^{ca}_{i_k} \leq \tau^{ca}_M$

The instants when the event generator sends data are noted as $i_0 h, i_1 h, i_2 h, \ldots$, where $i_0 h = 0$ is the initial triggering instant. Due to the network time-delay, the instants when those released signals reach the observer are $i_0 h + \tau^{sc}_{i_0}, i_1 h + \tau^{sc}_{i_1}, i_2 h + \tau^{sc}_{i_2}, \ldots$. In addition, the period of the event generator sending data can be expressed as $\lambda_k h = i_{k+1} h - i_k h$.

Based on the above analysis of the system output received at the observer side, we get

$$\tilde{y}(t) = y(i_k h), \quad t \in \left[i_k h + \tau^{sc}_{i_k}, i_{k+1} h + \tau^{sc}_{i_{k+1}} \right). \tag{4}$$

For $t \in [i_k h + \tau^{sc}_{i_k}, i_{k+1} h + \tau^{sc}_{i_{k+1}})$ and $\lambda_k h = i_{k+1} h - i_k h$, two cases are discussed:

(a) If $\lambda_k h \leq h + \tau^{sc}_M - \tau^{sc}_{i_{k+1}}$, we define

$$\rho(t) = t - i_k h, \quad t \in \left[i_k h + \tau^{sc}_{i_k}, i_{k+1} h + \tau^{sc}_{i_{k+1}} \right). \tag{5}$$

We can obtain

$$\tau^{sc}_{i_k} \leq \rho(t) \leq i_{k+1} h - i_k h + \tau^{sc}_{i_{k+1}} \leq h + \tau^{sc}_M. \tag{6}$$

Accordingly, define an error vector as

$$\vartheta_k(t) = 0. \tag{7}$$

(b) If $\lambda_k h > h + \tau^{sc}_M - \tau^{sc}_{i_{k+1}}$, since $0 \leq \tau^{sc}_{i_k} \leq \tau^{sc}_M$, it is easy to prove the existence of a positive integer $\varepsilon \geq 1$ such that

$$\varepsilon h + \tau^{sc}_M - \tau^{sc}_{i_{k+1}} < \lambda_k h \leq (\varepsilon + 1) h + \tau^{sc}_M - \tau^{sc}_{i_{k+1}}. \tag{8}$$

To simplify the expression, let

$$\begin{cases} \Theta_0 = \left[i_k h + \tau^{sc}_{i_k}, i_k h + h + \tau^{sc}_M \right), \\ \Theta_\delta = \left[i_k h + \delta h + \tau^{sc}_M, i_k h + (\delta + 1) h + \tau^{sc}_M \right), \\ \Theta_n = \left[i_k h + \varepsilon h + \tau^{sc}_M, i_{k+1} h + \tau^{sc}_{i_{k+1}} \right). \end{cases} \tag{9}$$

Then the interval $[i_k h + \tau^{sc}_{i_k}, i_{k+1} h + \tau^{sc}_{i_{k+1}})$ can be divided into the following $\varepsilon + 1$ subintervals

$$\left[i_k h + \tau^{sc}_{i_k}, i_{k+1} h + \tau^{sc}_{i_{k+1}} \right) = \Theta_0 \cup \left\{ \cup_{\delta=1}^{\varepsilon-1} \Theta_\delta \right\} \cup \Theta_n. \tag{10}$$

Define the segmentation function as

$$\rho(t) = \begin{cases} t - i_k h, & t \in \Theta_0, \\ t - i_k h - \delta h, & t \in \Theta_\delta, \quad \delta = 1, 2, \ldots, \varepsilon - 1, \\ t - i_k h - \varepsilon h, & t \in \Theta_n. \end{cases} \tag{11}$$

From (9) and (11), we can obtain

$$\tau^{sc}_m \leq \rho(t) \leq h + \tau^{sc}_M. \tag{12}$$

At this point, define the error vector

$$\vartheta_k(t) = \begin{cases} 0, & t \in \Theta_0, \\ y(i_k h) - y(i_k h + \delta h), & t \in \Theta_\delta, \\ y(i_k h) - y(i_k h + \varepsilon h), & t \in \Theta_n. \end{cases} \tag{13}$$

From the definition of $\vartheta_k(t)$, the following equation holds for $t \in [i_k h + \tau^{sc}_{i_k}, i_{k+1} h + \tau^{sc}_{i_{k+1}})$

$$y(i_k h) = \vartheta_k(t) + y(t-\rho(t)), \tag{14}$$

$$\vartheta_k^T(t) V \vartheta_k(t) \le \sigma y^T(t-\rho(t)) V y(t-\rho(t)). \tag{15}$$

Construct an observer of the following form on the controller side as

$$\begin{cases} \dot{\hat{x}}(t) = A\hat{x}(t) + B\hat{u}(t) + L\left[y(t-\rho(t)) + \vartheta_k(t) - \hat{y}(t-\rho(t))\right], \\ \hat{y}(t) = C\hat{x}(t), \end{cases} \tag{16}$$

where $\hat{x}(t)$ represents the state of the observer, $\hat{y}(t)$ represents the output of the observer, and L is the gain matrix of the observer to be designed.

The following observer-based feedback control law is used as

$$\hat{u}(t) = K\hat{x}(t), \tag{17}$$

where K is the controller gain matrix.

Remark 3. Due to the time-delay $\tau_{i_k}^{ca}$ in the controller-to-actuator network, the input of the control object is different from the input of the observer, and the following equation holds true:

$$u(t) = \hat{u}\left(t - \tau_{i_k}^{ca}\right) = K\hat{x}\left(t - \tau_{i_k}^{ca}\right). \tag{18}$$

Define $e(t) = x(t) - \hat{x}(t)$, the augmentation vector $z(t) = \left[\, x^T(t) \;\; e^T(t) \,\right]^T$, $h_1 = \tau_m^{sc}, h_2 = \tau_M^{sc} + h$, and $h_3 = \tau_m^{ca}$, $h_4 = \tau_M^{ca}$. Based on the above analysis, the closed-loop network control system can be written in the following form:

$$\begin{cases} \dot{z}(t) = \left(A_1 + \overline{U\Xi}(t)\overline{H}_1 + B_1K_1\right)z(t) - \left(B_2 + \overline{U\Xi}(t)\overline{H}_2\right)\mathrm{FK}_1 z\left(t - \tau_{i_k}^{ca}\right) + L_1C_1 z(t-\rho(t)) + \left(D_1 + \overline{U\Xi}(t)\overline{H}_3\right)\omega(t) + L_1\vartheta_k(t), \\ z(t) = \phi(t), \quad \forall t \in \left[t_0 - \max\left(h_4, h_3, h_2, h_1\right), t_0 - h_1\right). \end{cases} \tag{19}$$

where

$$\begin{aligned} A_1 &= \begin{bmatrix} A & 0 \\ 0 & A \end{bmatrix}, B_1 = \begin{bmatrix} 0 \\ B \end{bmatrix}, B_2 = \begin{bmatrix} B \\ B \end{bmatrix}, C_1 = \begin{bmatrix} 0 & C \end{bmatrix}, D_1 = \begin{bmatrix} D \\ D \end{bmatrix}, K_1 = \begin{bmatrix} -K & K \end{bmatrix}, L_1 = \begin{bmatrix} 0 \\ -L \end{bmatrix}, \overline{U} = \begin{bmatrix} U & 0 \\ 0 & U \end{bmatrix}, \\ \overline{\Xi}(t) &= \begin{bmatrix} \Xi(t) & 0 \\ 0 & \Xi(t) \end{bmatrix}, \overline{H}_1 = \begin{bmatrix} H_1 & 0 \\ H_1 & 0 \end{bmatrix}, \overline{H}_2 = \begin{bmatrix} H_2 \\ H_2 \end{bmatrix}, \overline{H}_3 = \begin{bmatrix} H_3 \\ H_3 \end{bmatrix}. \end{aligned} \tag{20}$$

At this point, condition (2) becomes

$$\omega^T(t)\omega(t) + \omega^T(t)\overline{\Theta}z(t) \le 0, \tag{21}$$

where $\overline{\Theta} = \Theta C\left[\, I \;\; 0 \,\right]$.

Remark 4. In a real industrial system, the actuator failure indication matrix $F = \mathrm{diag}\{0, 0\}$ means the actuator is completely failed and the controller will not be able to realize the control of the controlled object. Therefore, this paper only considers the case of partial actuator failure, and the actuator can still work normally within a certain range even though it has failed.

3. Main Results

3.1. System Stability Analysis. The following lemmas will be used in the derivation of the expected result.

Lemma 1. *(Jensen's inequality) [24] For any constant matrix $Q \in R^{n\times n}$, $Q = Q^T \ge 0$, scalar $0 \le d_1 \le d_2$, the vector-valued function $\dot{x}$: $[-d_2 - d_1] \longrightarrow R^n$, the following inequality holds true:*

$$-(d_2 - d_1)\int_{t-d_2}^{t-d_1} \dot{x}^T(\alpha) Q \dot{x}(\alpha) d\alpha \le -\begin{bmatrix} x(t-d_1) \\ x(t-d_2) \end{bmatrix}^T \begin{bmatrix} Q & -Q \\ * & Q \end{bmatrix} \begin{bmatrix} x(t-d_1) \\ x(t-d_2) \end{bmatrix}. \tag{22}$$

Lemma 2. *[25] Suppose that $l_1, l_2, \ldots l_N$: $R^m \longrightarrow R$ has positive values in a subset of the open set D, $D \in R^m$, then the mutually inverse convex combination of l_i in the set D satisfies*

$$\min_{\left\{\gamma_i|\gamma_i>0,\sum_i\gamma_i=1\right\}}\sum_i\frac{1}{\gamma_i}l_i(t)=\sum_i l_i(t)+\max_{f_{i,j}(t)}\sum_{i\neq j}f_{i,j}(t), \tag{23}$$

where

$$\left\{f_{i,j}\colon R^m\longrightarrow R, f_{j,i}(t)=f_{i,j}(t),\ \begin{bmatrix} l_i(t) & f_{i,j}(t)\\ f_{j,i}(t) & l_i(t)\end{bmatrix}\geq 0\right\}. \tag{24}$$

Lemma 3. *[26] Given a symmetric matrix Λ_1 and real matrices of any proper dimensions Λ_2 and Λ_3, for all $\Delta\in\Omega$, there is $\Lambda_1+\Lambda_2\Delta\Lambda_3+\Lambda_3^T\Delta\Lambda_2^T<0$, where $\Omega=\{\Delta=diag\{\Delta_1,\ldots,\Delta_k,p_1I,\ldots,p_lI\}\colon\|\Delta\|\leq 1,\ \Delta_i\in R^{n_i\times n_i},\ i=1,\ldots,k,\ p_j\in R,\ j=1,\ldots,g,k,g\in Z^+\}$, when and only when there exists $\Gamma\in\chi$ satisfying*

$$\begin{bmatrix}\Lambda_1+\Lambda_3^T\Gamma\Lambda_3 & \Lambda_2\\ * & -\Gamma\end{bmatrix}<0, \tag{25}$$

where $\chi=\{diag\{s_1I,\ldots,s_kI,S_1,\ldots S_g\}\colon 0<s_i\in R,0<S_j\in R^{n_j\times n_j},k,g\in Z^+\}$, *in particular, when* $k=1,g=0$, *and this inequality* $\Lambda_1+\Lambda_2\Delta_1\Lambda_3+\Lambda_3^T\Delta_1^T\Lambda_2^T<0$ *is equivalent to* $\Lambda_1+s_1\Lambda_3^T\Lambda_3+s_1^{-1}\Lambda_2\Lambda_2^T<0$.

Definition 1. [27] If it is globally asymptotically stable for all $\psi(\cdot)\in\ell[0,\Theta]$, then the Lurie system (18) is absolutely stable within $\ell[0,\Theta]$.

Theorem 1. *Consider the system shown in Figure 1, for given scalars h_1,h_2,h_3,h_4,σ, actuator failure indication matrix F, and gain matrices K and L, if there exists matrices of proper dimensions M,N and positive definite matrices $W>0,V>0,S_i>0,P_i>0$, where $i=1,2,3,4$, then we have*

$$\begin{bmatrix}\aleph_{11} & \aleph_{12}\\ * & \aleph_{22}\end{bmatrix}<0,\quad \begin{bmatrix}P_2 & M\\ * & P_2\end{bmatrix}>0,\quad \begin{bmatrix}P_4 & N\\ * & P_4\end{bmatrix}>0, \tag{26}$$

where

$$\aleph_{11}=\begin{bmatrix}\phi_{11} & P_1 & \mathrm{WL}_1C_1 & 0 & \phi_{15} & P_3 & 0 & \mathrm{WL}_1 & \phi_{19}\\ * & \phi_{22} & \phi_{23} & M & 0 & 0 & 0 & 0 & 0\\ * & * & \phi_{33} & \phi_{34} & 0 & 0 & 0 & 0 & 0\\ * & * & * & \phi_{44} & 0 & 0 & 0 & 0 & 0\\ * & * & * & * & \phi_{55} & \phi_{56} & \phi_{57} & 0 & 0\\ * & * & * & * & * & \phi_{66} & N & 0 & 0\\ * & * & * & * & * & * & \phi_{77} & 0 & 0\\ * & * & * & * & * & * & * & -V & 0\\ * & * & * & * & * & * & * & * & -2I\end{bmatrix}, \tag{27}$$

$$\aleph_{12}=\left[h_1\zeta_1^TP_1(h_2-h_1)\zeta_1^TP_2h_3\zeta_1^TP_3(h_4-h_3)\zeta_1^TP_4\right],\aleph_{22}=\mathrm{diag}\{-P_1,-P_2,-P_3,-P_4\},$$

$$\zeta_1=\left[(A_1+\overline{U\Xi}(t)\overline{H}_1+B_1K_1)\,0\ \ L_1C_1\ \ 0\ -(B_2+\overline{U\Xi}(t)\overline{H}_2)\mathrm{FK}_1\,0\ \ 0\ \ L_1\ (D_1+\overline{U\Xi}(t)\overline{H}_3)\right],$$

$$\phi_{11}=W(A_1+\overline{U\Xi}(t)\overline{H}_1+B_1K_1)+(A_1+\overline{U\Xi}(t)\overline{H}_1+B_1K_1)^TW+\mathrm{WB}_1K_1+K_1^TB_1^TW+S_1+S_2+S_3+S_4-P_1-P_3,$$

$$\phi_{15}=-W(B_2+\overline{U\Xi}(t)\overline{H}_2)\mathrm{FK}_1,\phi_{19}=W(D_1+\overline{U\Xi}(t)\overline{H}_3)-\overline{\Theta}^T,\phi_{22}=-S_1-P_1-P_2,\phi_{23}=-M+P_2,\overline{C}=\left[C\ \ 0\right],$$

$$\phi_{33}=-2P_2+M+M^T+\sigma\overline{C}^TV\overline{C},\phi_{34}=-M+P_2,\phi_{44}=-S_2-P_2,\ \phi_{55}=-2P_4+N+N^T,\phi_{56}=P_4^T-N^T,$$

$$\phi_{57}=P_4-N,\phi_{66}=-S_3-P_3-P_4,\phi_{77}=-S_4-P_4.$$

Then the Lurie system (19) is robust and absolutely stable within $\ell[0,\Theta]$.

Proof. Construct a Lyapunov–Krasovskii function

$$V(t,z(t)) = V_1(t,z(t)) + V_2(t,z(t)) + V_3(t,z(t)), \tag{28}$$

where

$$\begin{aligned}
V_1(t,z(t)) &= z^T(t)Wz(t),\\
V_2(t,z(t)) &= \int_{t-h_1}^{t} z^T(\alpha)S_1z(\alpha)\mathrm{d}\alpha + \int_{t-h_2}^{t} z^T(\alpha)S_2z(\alpha)\mathrm{d}\alpha + \int_{t-h_3}^{t} z^T(\alpha)S_3z(\alpha)\mathrm{d}\alpha + \int_{t-h_4}^{t} z^T(\alpha)S_4z(\alpha)\mathrm{d}\alpha,\\
V_3(t,z(t)) &= h_1\int_{-h_1}^{0}\int_{t+\theta}^{t}\dot{z}^T(\alpha)P_1\dot{z}(\alpha)\mathrm{d}\alpha\mathrm{d}\theta + (h_2-h_1)\int_{-h_2}^{-h_1}\int_{t+\theta}^{t}\dot{z}^T(\alpha)P_2\dot{z}(\alpha)\mathrm{d}\alpha\mathrm{d}\theta + h_3\int_{-h_3}^{0}\int_{t+\theta}^{t}\dot{z}^T(\alpha)P_3\dot{z}(\alpha)\mathrm{d}\alpha\mathrm{d}\theta\\
&\quad + (h_4-h_3)\int_{-h_4}^{-h_3}\int_{t+\theta}^{t}\dot{z}^T(\alpha)P_4\dot{z}(\alpha)\mathrm{d}\alpha\mathrm{d}\theta.
\end{aligned} \tag{29}$$

By taking derivation of $V(t,z(t))$ for t along the system (19), it can be obtained that

$$\dot{V}(t,z(t)) = \dot{V}_1(t,z(t)) + \dot{V}_2(t,z(t)) + \dot{V}_3(t,z(t)), \tag{30}$$

where

$$\begin{aligned}
\dot{V}_1(t,z(t)) &= \dot{z}^T(t)Wz(t) + z^T(t)W\dot{z}(t) = 2z^T(t)W\dot{z}(t),\\
\dot{V}_2(t,z(t)) &= z^T(t)S_1z(t) - z^T(t-h_1)S_1z(t-h_1) + z^T(t)S_2z(t) - z^T(t-h_2)S_2z(t-h_2) + z^T(t)S_3z(t)\\
&\quad - z^T(t-h_3)S_3z(t-h_3) + z^T(t)S_4z(t) - z^T(t-h_4)S_4z(t-h_4),\\
\dot{V}_3(t,z(t)) &= h_1^2\dot{z}^T(t)P_1\dot{z}(t) - h_1\int_{t-h_1}^{t}\dot{z}^T(\alpha)P_1\dot{z}(\alpha)\mathrm{d}\alpha + (h_2-h_1)^2\dot{z}^T(t)P_2\dot{z}(t) - (h_2-h_1)\int_{t-h_2}^{t-h_1}\dot{z}^T(\alpha)P_2\dot{z}(\alpha)\mathrm{d}\alpha\\
&\quad + h_3^2\dot{z}^T(t)P_3\dot{z}(t) - h_3\int_{t-h_3}^{t}\dot{z}^T(\alpha)P_3\dot{z}(\alpha)\mathrm{d}\alpha + (h_4-h_3)^2\dot{z}^T(t)P_4\dot{z}(t) - (h_4-h_3)\int_{t-h_4}^{t-h_3}\dot{z}^T(\alpha)P_4\dot{z}(\alpha)\mathrm{d}\alpha.
\end{aligned} \tag{31}$$

Applying Lemma 1 and Lemma 2 to the integral term in (29), the following equations hold true:

$$-h_1\int_{t-h_1}^{t}\dot{z}^T(\alpha)P_1\dot{z}(\alpha)\mathrm{d}\alpha \le -\varphi_1^T(t)\Pi_1\varphi_1(t), \tag{32}$$

$$\begin{aligned}
-(h_2-h_1)\int_{t-h_2}^{t-h_1}\dot{z}^T(\alpha)P_2\dot{z}(\alpha)\mathrm{d}\alpha &= -(h_2-h_1)\int_{t-\tau(t)}^{t-h_1}\dot{z}^T(\alpha)P_2\dot{z}(\alpha)\mathrm{d}\alpha - (h_2-h_1)\int_{t-h_2}^{t-\tau(t)}\dot{z}^T(\alpha)P_2\dot{z}(\alpha)\mathrm{d}\alpha\\
&\le -\varphi_2^T(t)\Pi_2\varphi_2(t),
\end{aligned} \tag{33}$$

$$-h_3\int_{t-h_3}^{t}\dot{z}^T(\alpha)P_3\dot{z}(\alpha)\mathrm{d}\alpha \le -\varphi_3^T(t)\Pi_3\varphi_3(t), \tag{34}$$

$$\begin{aligned}
-(h_4-h_3)\int_{t-h_4}^{t-h_3}\dot{z}^T(\alpha)P_4\dot{z}(\alpha)\mathrm{d}\alpha &= -(h_4-h_3)\int_{t-\tau(t)}^{t-h_3}\dot{z}^T(\alpha)P_4\dot{z}(\alpha)\mathrm{d}\alpha - (h_4-h_3)\int_{t-h_4}^{t-\tau(t)}\dot{z}^T(\alpha)P_4\dot{z}(\alpha)\mathrm{d}\alpha\\
&\le -\varphi_4^T(t)\Pi_4\varphi_4(t),
\end{aligned} \tag{35}$$

where

$$\varphi_1^T(t)=\begin{bmatrix} z(t) \\ z(t-h_1)\end{bmatrix}^T,\varphi_2^T=\begin{bmatrix} z(t-h_1) \\ z(t-\rho(t))\\ z(t-h_2)\end{bmatrix}^T,\varphi_3^T(t)=\begin{bmatrix} z(t) \\ z(t-h_3)\end{bmatrix}^T,\varphi_4^T=\begin{bmatrix} z(t-h_3) \\ z\left(t-\tau_{i_k}^{ca}\right)\\ z(t-h_4)\end{bmatrix}^T,\Pi_1=\begin{bmatrix} P_1 & -P_1 \\ * & P_1\end{bmatrix},$$
$$\Pi_2=\begin{bmatrix} P_2 & M-P_2 & -M \\ * & 2P_2-M-M^T & M-P_2 \\ * & * & P_2\end{bmatrix},\Pi_3=\begin{bmatrix} P_3 & -P_3 \\ * & P_3\end{bmatrix},\Pi_4=\begin{bmatrix} P_4 & N-P_4 & -N \\ * & 2P_4-N-N^T & N-P_4 \\ * & * & P_4\end{bmatrix}. \tag{36}$$

Substituting (32), (33), (34), (35) into (29) and combining (15) and (21), we can obtain

$$\begin{aligned}\dot{V}(t,z(t))\le{}& 2z^T(t)W\dot{z}(t)+z^T(t)S_1z(t)-z^T(t-h_1)S_1z(t-h_1)+z^T(t)S_2z(t)-z^T(t-h_2)S_2z(t-h_2)\\ &+z^T(t)S_3z(t)-z^T(t-h_3)S_3z(t-h_3)+z^T(t)S_4z(t)-z^T(t-h_4)S_4z(t-h_4)\\ &+h_1^2\dot{z}^T(t)P_1\dot{z}(t)+(h_2-h_1)^2\dot{z}^T(t)P_2\dot{z}(t)+h_3^2\dot{z}^T(t)P_3\dot{z}(t)+(h_4-h_3)^2\dot{z}^T(t)P_4\dot{z}(t)\\ &+\sigma y^T(t-\rho(t))Vy(t-\rho(t))-\vartheta_k^T(t)V\vartheta_k(t)-2\omega^T(t)\omega(t)-2\omega^T(t)\overline{\Theta}z(t)\\ \le{}&\eta^T(t)\left(\aleph_{11}-\aleph_{12}\aleph_{22}^{-1}\aleph_{12}^T\right)\eta(t),\end{aligned} \tag{37}$$

where $\eta^T(t)=\left[z^T(t)\,z^T(t-h_1)z^T(t-\rho(t))z^T(t-h_2)z^T(t-\tau_{i_k}^{ca})z^T(t-h_3)z^T(t-h_4)\vartheta_k^T(t)\omega^T(t)\right]$.

From Schur's complement lemma and Definition 1, if (36) is less than 0, it is known that the Lurie system (19) is globally asymptotically stable for any $\ell[0,\Theta]$ and therefore is absolutely stable. □

3.2. Joint Design of the Observer and the Controller under the Event-Triggering Mechanism

Theorem 2. *Consider the system shown in Figure 1, for given scalars h_1,h_2,h_3,h_4,σ, actuator fault indication matrix F, and gain matrices K and L, if there exist matrices of suitable dimensions $\overline{M},\overline{N},Y_1,Y_2$ and positive definite matrices $X>0,V>0,Y>0,\overline{S}_i>0,\overline{P}_i>0,\quad i=1,2,3,4$, then we have*

$$\begin{bmatrix}\widetilde{\Lambda}_{11} & \widetilde{\Lambda}_{12}\\ * & \widetilde{\Lambda}_{22}\end{bmatrix}<0, \tag{38}$$

$$\begin{bmatrix}P_2 & M\\ * & P_2\end{bmatrix}>0,\begin{bmatrix}P_4 & N\\ * & P_4\end{bmatrix}>0, \tag{39}$$

where

$$\widetilde{\Lambda}_{11}=\begin{bmatrix}\widetilde{\phi}_{11} & \overline{P}_1 & -I_2\overline{Y}_2I_2 & 0 & \widetilde{\phi}_{15} & \overline{P}_3 & 0 & -I_2\overline{Y}_2C & \widetilde{\phi}_{19}\\ * & \widetilde{\phi}_{22} & \widetilde{\phi}_{23} & \overline{M} & 0 & 0 & 0 & 0 & 0\\ * & * & \widetilde{\phi}_{33} & \widetilde{\phi}_{34} & 0 & 0 & 0 & 0 & 0\\ * & * & * & \widetilde{\phi}_{44} & 0 & 0 & 0 & 0 & 0\\ * & * & * & * & \widetilde{\phi}_{55} & \widetilde{\phi}_{56} & \widetilde{\phi}_{57} & 0 & 0\\ * & * & * & * & * & \widetilde{\phi}_{66} & \overline{N} & 0 & 0\\ * & * & * & * & * & * & \widetilde{\phi}_{77} & 0 & 0\\ * & * & * & * & * & * & * & -\mathrm{CYC}^T & 0\\ * & * & * & * & * & * & * & * & -2I\end{bmatrix},$$

$$\widetilde{\Lambda}_{12}=\left[h_1\widetilde{\zeta}^T\ (h_2-h_1)\widetilde{\zeta}^T\ h_3\widetilde{\zeta}^T\ (h_4-h_3)\widetilde{\zeta}^T\widetilde{\xi}_1^T\widetilde{\xi}_2^T\right],\widetilde{\Lambda}_{22}=\mathrm{diag}\left\{\overline{P}_1-2\overline{X},\overline{P}_2-2\overline{X},\overline{P}_3-2\overline{X},\overline{P}_4-2\overline{X},-sI,-s^{-1}I\right\},$$

$$\widetilde{\zeta}=\left[\ A_1\overline{X}+B_1\overline{Y}_1I_1\ \ 0\ \ -I_2^T\overline{Y}_2I_2\ \ 0\ \ -B_2F\overline{Y}_1I_1\ \ 0\ \ 0\ \ -I_2^T\overline{Y}_2C^T\ \ D_1\ \right],\widetilde{\xi}_1=\left[\ \overline{U}^T\ \ 0\ 0\ 0\ 0\ 0\ 0\ 0\ 0\ \overline{U}^T\ \ \overline{U}^T\ \ \overline{U}^T\ \ \overline{U}^T\ \right],$$

$$\widetilde{\xi}_2=\left[\ \overline{XH}_1\ \ 0\ \ 0\ \ 0\ \ -\overline{H}_2F\overline{Y}_1I_1\ \ 0\ \ 0\ \ 0\ \ \overline{H}_3\ \ 0\ \ 0\ \ 0\ \ 0\ \right],\widetilde{\phi}_{11}=A_1\overline{X}+B_1\overline{Y}_1I_1+\overline{X}A_1^T+I_1^T\overline{Y}_1^TB_1^T+\overline{S}_1+\overline{S}_2+\overline{S}_3+\overline{S}_4$$
$$-\overline{P}_1-\overline{P}_3,$$

$$\widetilde{\phi}_{15}=-B_2F\overline{Y}_1I_1,\widetilde{\phi}_{19}=D_1-\overline{X\Theta}^T,\widetilde{\phi}_{22}=-\overline{S}_1-\overline{P}_1-\overline{P}_2,\widetilde{\phi}_{23}=-\overline{M}+\overline{P}_2,\widetilde{\phi}_{33}=-2\overline{P}_2+\overline{M}+\overline{M}^T+\sigma I_3^TYI_3,\widetilde{\phi}_{34}=-\overline{M}+\overline{P}_2,$$

$$\widetilde{\phi}_{44}=-\overline{S}_2-\overline{P}_2,\widetilde{\phi}_{55}=-2\overline{P}_4+\overline{N}+\overline{N}^T,\widetilde{\phi}_{56}=\overline{P}_4^T-\overline{N}^T,\widetilde{\phi}_{57}=\overline{P}_4-\overline{N},\widetilde{\phi}_{66}=-\overline{S}_3-\overline{P}_3-\overline{P}_4,\widetilde{\phi}_{77}=-\overline{S}_4-\overline{P}_4,I_1=\left[\ -I\ \ I\ \right],$$
$$I_2=\left[\ 0\ \ I\ \right],$$

(40)

then the Lurie system (19) is robust and absolutely stable within $\ell[0,\Theta]$, controller gain matrix K, observer gain matrix L, then the event-triggered weight matrix V can be obtained from the following equation

$$K=Y_1X^{-1},L=Y_2X^{-1}C^+,V=C^{+T}X^{-1}\mathrm{YX}^{-1}C^+. \tag{41}$$

Proof. : From Schur's complement lemma and Lemma 3, $\aleph_{11}-\aleph_{12}\aleph_{22}^{-1}\aleph_{12}^T$ can be transformed into

$$\aleph_{11}-\aleph_{12}\aleph_{22}^{-1}\aleph_{12}^T\le\Lambda_{11}-\Lambda_{12}\Lambda_{22}^{-1}\Lambda_{12}^T, \tag{42}$$

where

Table 1: τ_M^{sc} or τ_M^{ca} under different event-triggering thresholds σ.

σ	0.4	0.3	0.2	0.1	0.05
Given $\tau_M^{sc} = 0.1$, the upper bound of τ_M^{ca}	1.532	1.541	1.557	1.586	1.611
Given $\tau_M^{ca} = 0.1$, the upper bound of τ_M^{sc}	1.546	1.548	1.552	1.561	1.569

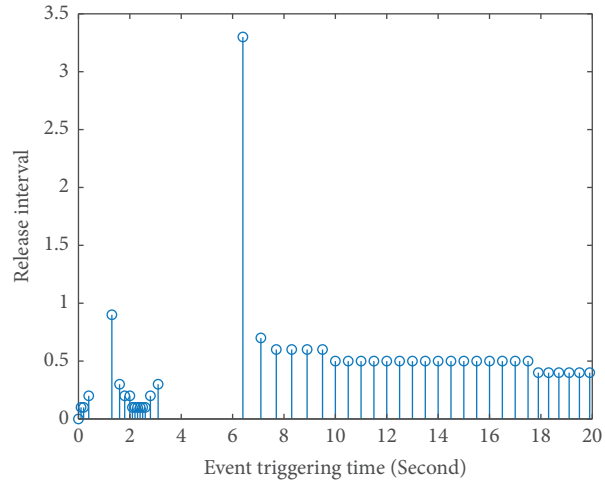

Figure 2: Event-triggering time and intervals when the actuator is normal.

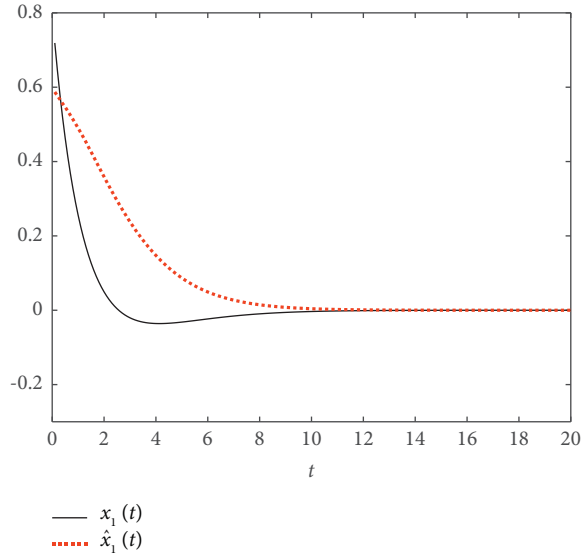

Figure 3: System state when the actuator is normal $x_1(t)$ and its estimated value $\hat{x}_1(t)$.

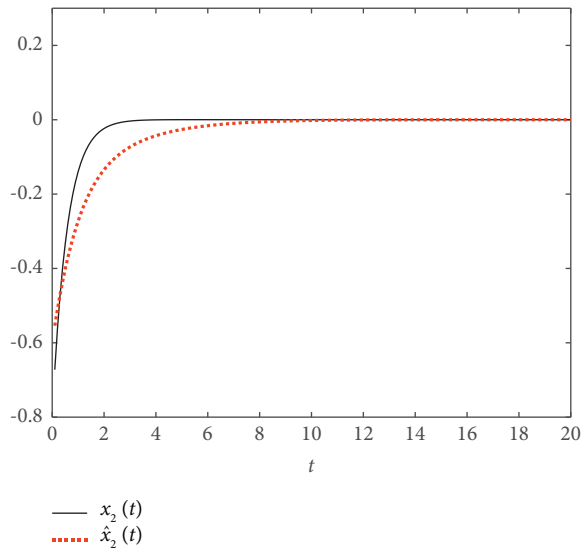

FIGURE 4: System state when the actuator is normal $x_2(t)$ and its estimated value $\hat{x}_2(t)$.

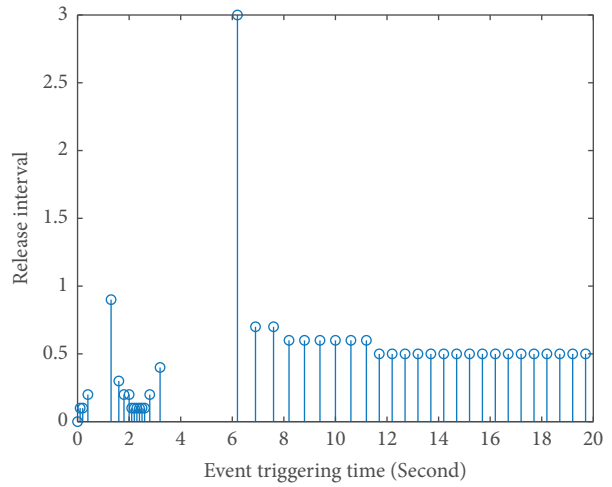

FIGURE 5: Event-triggering time and intervals in case of $F = \text{diag}\{1, 0\}$.

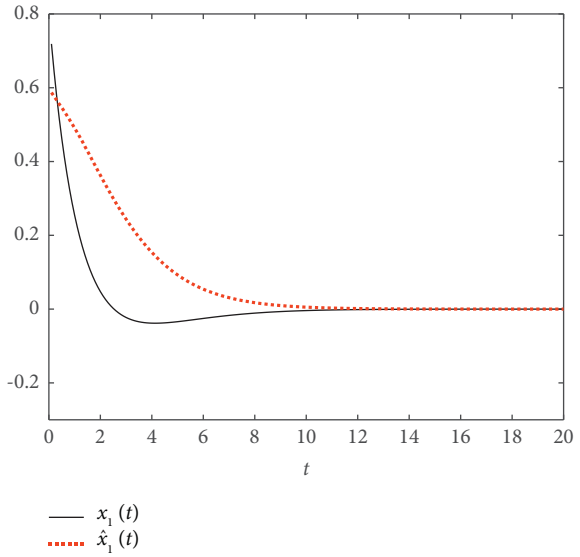

FIGURE 6: System state $x_1(t)$ and its estimated value $\hat{x}_1(t)$ in case of $F = \text{diag}\{1, 0\}$.

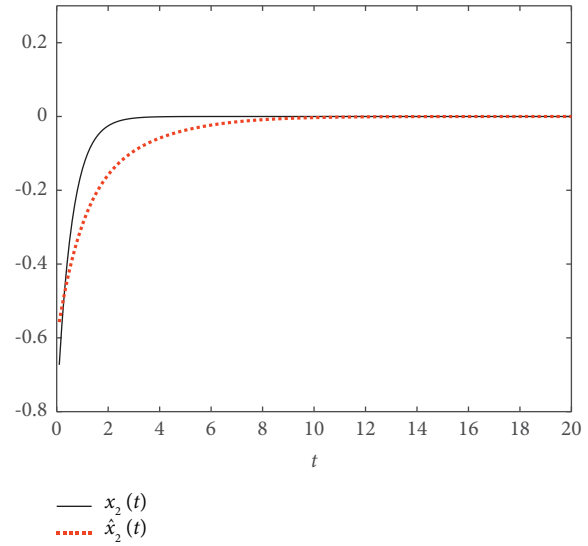

FIGURE 7: System state $x_2(t)$ and its estimated value $\hat{x}_2(t)$ in case of $F = \text{diag}\{1, 0\}$.

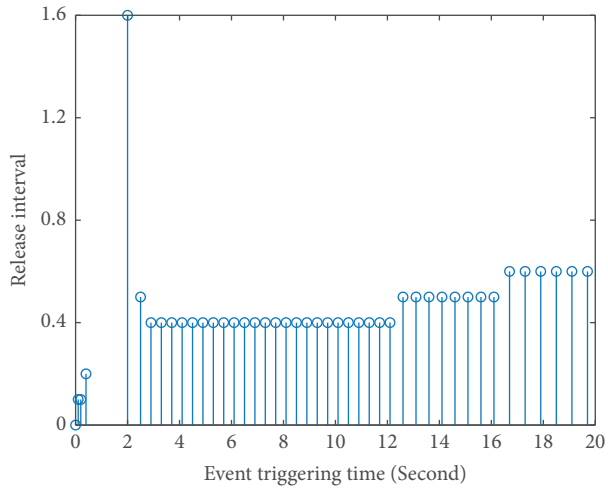

Figure 8: Event-triggering time and intervals in case of $F = \text{diag}\{0, 1\}$.

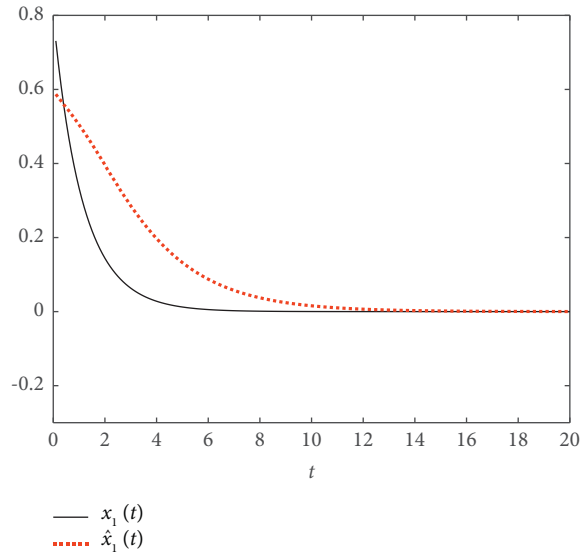

Figure 9: System state $x_1(t)$ and its estimated value $\hat{x}_1(t)$ in case of $F = \text{diag}\{0, 1\}$.

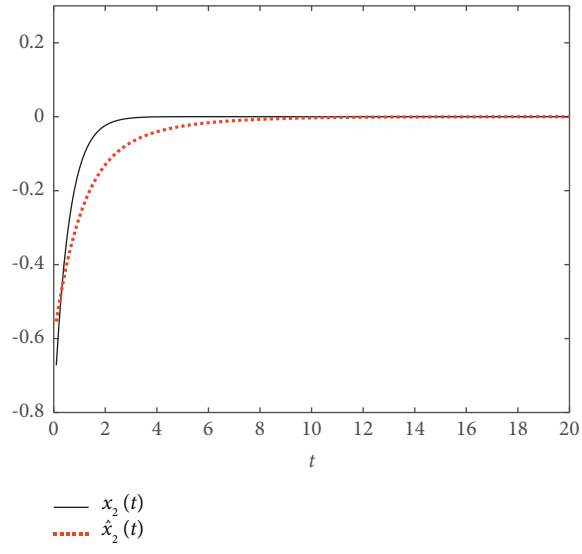

Figure 10: System state $x_2(t)$ and its estimated value $\hat{x}_2(t)$ in case of $F = \text{diag}\{0, 1\}$.

$$\Lambda_{11}=\begin{bmatrix}\overline{\phi}_{11} & P_1 & \mathrm{WL}_1C_1 & 0 & \overline{\phi}_{15} & P_3 & 0 & \mathrm{WL}_1 & \overline{\phi}_{19}\\ * & \phi_{22} & \phi_{23} & M & 0 & 0 & 0 & 0 & 0\\ * & * & \phi_{33} & \phi_{34} & 0 & 0 & 0 & 0 & 0\\ * & * & * & \phi_{44} & 0 & 0 & 0 & 0 & 0\\ * & * & * & * & \phi_{55} & \phi_{56} & \phi_{57} & 0 & 0\\ * & * & * & * & * & \phi_{66} & n & 0 & 0\\ * & * & * & * & * & * & \phi_{77} & 0 & 0\\ * & * & * & * & * & * & * & -V & 0\\ * & * & * & * & * & * & * & * & -2I\end{bmatrix}$$

$$\Lambda_{12}=\left[h_1\overline{\zeta}^TP_1\ (h_2-h_1)\overline{\zeta}^TP_2\ h_3\overline{\zeta}^TP_3\,(h_4-h_3)\overline{\zeta}^TP_4\xi_1^T\xi_2^T\right],\Lambda_{22}=\mathrm{diag}\left\{-P_1,-P_2,-P_3,-P_4,-sI,-s^{-1}I\right\},$$

$$\xi_1^T=\left[\ (\mathrm{W}\overline{U})^T\ \ 0\ 0\ 0\ 0\ 0\ 0\ 0\ 0\ \ (P_1\overline{U})^T\ \ (P_2\overline{U})^T\ \ (R_3\overline{U})^T\ \ (P_4\overline{U})^T\ \right]^T,$$

$$\xi_2^T=\left[\ \overline{H}_1\ \ 0\ 0\ 0\ \ -\overline{H}_2FK_1\ \ 0\ 0\ 0\ \ \overline{H}_3\ \ 0\ 0\ 0\ \ 0\ \right]^T,$$

$$\overline{\zeta}=\left[\ A_1+B_1K_1\ \ 0\ \ L_1C_1\ \ 0\ \ -B_2\mathrm{FK}_1\ \ 0\ \ 0\ \ L_1\ \ D_1\ \right],\overline{\phi}_{11}=\mathrm{WA}_1+\mathrm{WB}_1K_1+A_1^TW+K_1^TB_1^TW+S_1+S_2+S_3+S_4-P_1-P_3,$$

$$\overline{\phi}_{15}=-\mathrm{WB}_2\mathrm{FK}_1,\overline{\phi}_{19}=\mathrm{WD}_1-\overline{\Theta}^T,\phi_{22}=-S_1-P_1-P_2,\phi_{23}=-M+P_2,\phi_{33}=-2P_2+M+M^T+\sigma\overline{C}^TV\overline{C},\phi_{34}=-M+P_2,$$

$$\phi_{44}=-S_2-P_2,\phi_{55}=-2P_4+N+N^T,\phi_{56}=P_4^T-N^T,\phi_{57}=P_4-N,\phi_{66}=-S_3-P_3-P_4,\phi_{77}=-S_4-P_4,\overline{C}=\left[\ C\ \ 0\ \right].\tag{43}$$

Due to the presence of nonlinear terms in $\Lambda_{11}-\Lambda_{12}\Lambda_{22}^{-1}\Lambda_{12}^T$, it is inconvenient to solve the controller, so take $W=\mathrm{diag}\{\overline{W},\overline{W}\}$, and define $X=\overline{W}^{-1},\overline{X}=W^{-1}=\mathrm{diag}\{X,X\},Y_1=\mathrm{KX},Y_2=\mathrm{LCX},Y=\mathrm{XC}^T\mathrm{VCX},\overline{Y}_1=\left[\ Y_1\ \ -Y_1\ \right]$, $\overline{Y}_2=\begin{bmatrix}0 & 0\\ 0 & -Y_2\end{bmatrix},\overline{M}=\overline{X}M\overline{X},\overline{N}=\overline{X}N\overline{X},\overline{P}_i=\overline{X}P_i\overline{X},\overline{S}_i=\overline{X}S_i\overline{X},\quad i=1,2,3,4$. Pre and postmultiply $\mathrm{diag}\{\overline{X},\overline{X},\overline{X},\overline{X},\overline{X},\overline{X},\overline{X},\mathrm{CXC}^T,I,P_1^{-1},P_2^{-1},P_3^{-1},P_4^{-1},I,I\}$ on both sides of the matrix $\begin{bmatrix}\Lambda_{11} & \Lambda_{12}\\ * & \Lambda_{22}\end{bmatrix}$, noting that since $\overline{P}_1>0,\overline{P}_2>0,\overline{P}_3>0,\overline{P}_4>0$, there must be

$$\begin{cases}(\overline{P}_1-\overline{X})\overline{P}_1^{-1}(\overline{P}_1-\overline{X})\ge 0,\\ (\overline{P}_2-\overline{X})\overline{P}_2^{-1}(\overline{P}_2-\overline{X})\ge 0,\\ (\overline{P}_3-\overline{X})\overline{P}_3^{-1}(\overline{P}_3-\overline{X})\ge 0,\\ (\overline{P}_4-\overline{X})\overline{P}_4^{-1}(\overline{P}_4-\overline{X})\ge 0.\end{cases}\tag{44}$$

Equation (43) is equivalent to

$$\begin{cases}-\overline{X}\overline{P}_1^{-1}\overline{X}\le\overline{P}_1-2\overline{X},\\ -\overline{X}\overline{P}_2^{-1}\overline{X}\le\overline{P}_2-2\overline{X},\\ -\overline{X}\overline{P}_3^{-1}\overline{X}\le\overline{P}_3-2\overline{X},\\ -\overline{X}\overline{P}_4^{-1}\overline{X}\le\overline{P}_4-2\overline{X}.\end{cases}\tag{45}$$

That is, we can get the linear matrix inequality (38), where $K=Y_1X^{-1},L=Y_2X^{-1}C^+$ and $V=C^{+\mathrm{T}}X^{-1}\mathrm{YX}^{-1}C^+$. □

Remark 5. Since the matrix C is a row full rank matrix of $m\times n$, the matrix C^+ of $n\times m$ exists such that $CC^+=I$, C^+ is called the right inverse of C, and the observer gain matrix $L=Y_2X^{-1}C^+$ is obtained from $Y_2=\mathrm{LCX}$.

Remark 6. Since $X>0,V>0,\mathrm{CX}\ne 0,C$ is a row full rank matrix, there must exist $(\mathrm{CX})^TV(\mathrm{CX})>0$; $Y=XC^TVCX$ is a nonsingular matrix, which yields the event-triggered weight matrix $V=C^{+\mathrm{T}}X^{-1}\mathrm{YX}^{-1}C^+$.

Remark 7. The upper and lower bounds of time-delay are introduced in the proof, which makes the conclusion less conservative. In addition to the decision variables required for constructing Lyapunov function, no other free-weighting-matrix is introduced, which avoids the computational burden caused by too many decision variables and the possible conservatism caused by the optimization of too many decision variables. A modified Jensen's inequality is used in the paper. This inequality has a tighter integration bound, which reduces the computational complexity while reducing the conservatism of the conclusion.

4. Simulation Example

To verify the effectiveness and usability of the method, consider the following Lurie system, where

$$A=\begin{bmatrix}0.1 & 0.1\\ 0 & -0.9\end{bmatrix}, B=\begin{bmatrix}1.2 & 0\\ 0 & 0.1\end{bmatrix}, C=\begin{bmatrix}0.1 & 0.1\end{bmatrix}, D=\begin{bmatrix}0.1\\ 0.1\end{bmatrix}, U=\begin{bmatrix}0.2 & 0\\ 0 & 0\end{bmatrix}, H_1=\begin{bmatrix}0 & 0.1\\ 0 & 0\end{bmatrix}, H_2=\begin{bmatrix}0 & 0.1\\ 0 & 0\end{bmatrix},$$
$$H_3=\begin{bmatrix}0\\ 0.1\end{bmatrix}, \Xi(t)=\begin{bmatrix}\sin t & 0\\ 0 & \cos t\end{bmatrix}, \psi(\cdot)\in \ell[0,1]. \tag{46}$$

Obviously this system is not stable.

According to Theorem 2, when the other parameters are chosen constant, the upper bound of the allowed time-delay of the system varies with the event-triggered threshold σ as shown in Table 1.

As can be seen from Table 1, the smaller the event-triggered threshold σ is, the larger the upper bound of the allowed time-delay is. Therefore, in order to mitigate the impact of time-delay of the system performance, the event threshold σ can be appropriately decreased.

Assume that an event-triggering threshold is set as $\sigma = 0.1$, a system sampling period is given as $h = 0.01s$, and the upper and lower bounds of the time-delay are $h_1 = 0.01, h_2 = 0.11, h_3 = 0.01, h_4 = 0.11$. The nonlinear function $\psi(\cdot)$ is taken as the saturation function $\mathrm{sat}(\cdot)$, and the initial state of the system $x(0) = \begin{bmatrix}-0.8 & 0.8\end{bmatrix}^T$, $\hat{x}(0) = \begin{bmatrix}-0.6 & 0.6\end{bmatrix}^T$.

According to Theorem 2, given the fault indication matrix $F=\begin{bmatrix}1 & 0\\ 0 & 1\end{bmatrix}$, the controller gain matrix, observer gain matrix, and event-triggered weight matrix for normal operation of the system are as follows:

$$K=\begin{bmatrix}-0.1945 & -0.0245\\ -0.0431 & -0.1645\end{bmatrix}, L=\begin{bmatrix}4.1849\\ 0.8596\end{bmatrix}, V=4.6857. \tag{47}$$

The triggering instants are shown in Figure 2, the state and its estimated value curves of the system are shown in Figures 3–4.

Given the fault indication matrix $F=\begin{bmatrix}1 & 0\\ 0 & 0\end{bmatrix}\begin{bmatrix}1 & 0\\ 0 & 0\end{bmatrix}$, the controller gain matrix, observer gain matrix, and event-triggered weight matrix for a system actuator failure are as follows:

$$K=\begin{bmatrix}-0.1973 & -0.0185\\ 0.1882 & -0.7919\end{bmatrix}, L=\begin{bmatrix}4.1656\\ 0.8093\end{bmatrix}, V=4.6690. \tag{48}$$

The triggering instants are shown in Figure 5, the state and its estimated value curves of the system are shown in Figures 6–7.

Given the fault indication matrix $F=\begin{bmatrix}0 & 0\\ 0 & 1\end{bmatrix}$, the controller gain matrix, observer gain matrix, and event-triggered weight matrix for a system actuator failure are as follows:

$$K=\begin{bmatrix}-0.1942 & -0.0246\\ -0.0426 & -0.1639\end{bmatrix}, L=\begin{bmatrix}4.1673\\ 0.8359\end{bmatrix}, V=4.5781. \tag{49}$$

The triggering instants are shown in Figure 8, and the state and its estimated value curves of the system are shown in Figures 9–10.

As can be seen from Figures 2, 5, and 8, the system requires much less data to be transmitted near the equilibrium point than during the transient process, which is exactly in line with the expectation of transmitting data according to the control demand and can effectively save network communication resources, reduce waste, and save resources compared to the time-triggered mechanism. As can be seen from Figures 6, 7, 9, and 10, the system remains stable with effective fault-tolerant control in the event of an actuator failure.

5. Conclusion

In this paper, a robust fault-tolerant controller is designed for the Lurie NCS with time-delay and uncertainty from the sensor to the controller and from the controller to the actuator, which makes the system fault-tolerant effective and keeps the system stable in case of an actuator failure. By constructing an observer on the controller node, a mathematical model of the observer-based event-triggered mechanism is established to ensure the stability of the closed-loop system while also reducing the amount of data transmission in the network, which in turn saves network bandwidth resources. According to Lyapunov stability theory, sufficient conditions for the stability of the closed-loop system are derived, and the collaborative design of the event-triggered mechanism, fault-tolerant controller, and the observer is realized. In future research, the focus will be on more complex systems based on event-triggered mechanisms, such as T-S fuzzy systems that simultaneously consider the effects of packet loss and external disturbances.

Data Availability

The data used to support the findings of this study are available from the corresponding author upon request.

Conflicts of Interest

The authors declare that there are no conflicts of interest regarding the publication of this paper.

Acknowledgments

This work is supported by National Natural Science Foundation of China (61573137) and Research Foundation for Advanced Talents of Suqian University (2022XRC048).

References

[1] X. Yan, J. Li, and B. Mei, "Collaborative optimization design for centralized networked control system," *IEEE Access*, vol. 9, pp. 19479–19487, 2021.

[2] X. M. Zhang, Q. L. Han, X. Ge et al., "Networked control systems: a survey of trends and techniques," *IEEE/CAA Journal of Automatica Sinica*, vol. 7, no. 1, pp. 1–17, 2019.

[3] H. A. Shah, L. Zhao, and I. M. Kim, "Joint network control and resource allocation for space-terrestrial integrated network through hdacrl," *IEEE Transactions on Vehicular Technology*, vol. 70, no. 5, pp. 4943–4954, 2021.

[4] M. Fetanat, M. Stevens, C. Hayward, and N. H. Lovell, "A s control system for an implantable heart pump using a real-time deep convolutional neural network," *IEEE Transactions on Biomedical Engineering*, vol. 68, no. 10, pp. 3029–3038, 2021.

[5] S. Hou, J. Fei, C. Chen, and Y. Chu, "Finite-time adaptive fuzzy-neural-network control of active power filter," *IEEE Transactions on Power Electronics*, vol. 34, no. 10, pp. 10298–10313, 2019.

[6] Y. Wang, P. He, P. Shi, and H. Zhang, "Fault detection for systems with model uncertainty and disturbance via cfgm," *IEEE Transactions on Cybernetics*, vol. 52, no. 8, pp. 7765–7775, 2022.

[7] X. Gao, J. X. Zhang, and L. Hao, "fault-tolerant control of pneumatic continuum manipulators under actuator faults," *IEEE Transactions on Industrial Informatics*, vol. 17, no. 12, pp. 8299–8307, 2021.

[8] H. Kang, B. Xiao, Y. Ni et al., "Sensor fault diagnosis and fault tolerant control for automated guided forklift," *IEEE Access*, vol. 9, pp. 56191–56200, 2021.

[9] X. Fu and X. Pang, "Robust fault estimation and fault-tolerant control for nonlinear Markov jump systems with time-delays," *Automatika*, vol. 62, no. 1, pp. 21–31, 2021.

[10] M. Bahreini and J. Zarei, "Robust fault-tolerant control for networked control systems subject to random delays via static-output feedback," *ISA Transactions*, vol. 86, pp. 153–162, 2019.

[11] K. Telbissi and A. Benzaouia, "Robust fault-tolerant control for discrete-time switched systems with time delays," *International Journal of Adaptive Control and Signal Processing*, vol. 34, no. 3, pp. 389–406, 2020.

[12] H. Zhang, J. Hu, and X. Yu, "Adaptive sliding mode fault-tolerant control for a class of uncertain systems with probabilistic random delays," *IEEE Access*, vol. 7, pp. 64234–64246, 2019.

[13] L. Ding, Q. L. Han, X. Ge, and X. M. Zhang, "An overview of recent advances in event-triggered consensus of m systems," *IEEE Transactions on Cybernetics*, vol. 48, no. 4, pp. 1110–1123, 2018.

[14] S. Zhu, J. Lu, L. Lin, and Y. Liu, "Minimum-time and minimum-triggering o of stochastic boolean networks," *IEEE Transactions on Automatic Control*, vol. 67, no. 3, pp. 1558–1565, 2022.

[15] C. Wang, X. Su, Y. Yang, and W. Lian, "Sliding mode control of Markovian jump system via an event-triggered mechanism," in *Proceedings of the 2019 Chinese Automation Congress (CAC)*, pp. 4345–4348, IEEE, Hangzhou, China,, November 2019.

[16] Y. Xu, J. Sun, G. Wang, and Z. G. Wu, "Dynamic triggering mechanisms for distributed adaptive synchronization control and its application to circuit systems," *IEEE Transactions on Circuits and Systems I: Regular Papers*, vol. 68, no. 5, pp. 2246–2256, 2021.

[17] X. Ge, Q. L. Han, L. Ding, Y. L. Wang, and X. M. Zhang, "Dynamic event-triggered distributed coordination control and its applications: a survey of trends and techniques," *IEEE Transactions on Systems, Man, and Cybernetics: Systems*, vol. 50, no. 9, pp. 3112–3125, 2020.

[18] J. Liu, T. Yin, J. Cao, D. Yue, and H. R. Karimi, "Security control for T–S fuzzy systems with adaptive event-triggered mechanism and multiple cyber-attacks," *IEEE Transactions on Systems, Man, and Cybernetics: Systems*, vol. 51, no. 10, pp. 6544–6554, 2021.

[19] Z. Gu, P. Shi, D. Yue, S. Yan, and X. Xie, "fault estimation and fault-tolerant control for networked systems based on an adaptive memory-based event-triggered mechanism," *IEEE Transactions on Network Science and Engineering*, vol. 8, no. 4, pp. 3233–3241, 2021.

[20] A. M. Wang and J. N. Li, "Event-triggered asynchronous H_∞ fault-tolerant control for discrete-time Markov jump system with actuator faults," *Proceedings of the Institution of Mechanical Engineers - Part I: Journal of Systems & Control Engineering*, vol. 235, no. 6, pp. 781–794, 2021.

[21] J. Qiu, M. Ma, and T. Wang, "Event-triggered adaptive fuzzy fault-tolerant control for stochastic nonlinear systems via command filtering," *IEEE Transactions on Systems, Man, and Cybernetics: Systems*, vol. 52, no. 2, pp. 1145–1155, 2022.

[22] X. Wang, Z. Fei, Z. Wang, and X. Liu, "Event-triggered fault estimation and fault-tolerant control for networked control systems," *Journal of the Franklin Institute*, vol. 356, no. 8, pp. 4420–4441, 2019.

[23] M. S. Qian and X. G. Yan, "Integrated fault-tolerant control approach for linear time-delay systems using a dynamic event-triggered mechanism," *International Journal of Systems Science*, vol. 51, no. 16, pp. 3471–3490, 2020.

[24] X. Jiang, Q. L. Han, S. Liu, and A. Xue, "A New H_∞ stabilization criterion for networked control systems," *IEEE Transactions on Automatic Control*, vol. 53, no. 4, pp. 1025–1032, 2008.

[25] F. Yang, H. Zhang, and Y. Wang, "An enhanced input-delay approach to sampled-data stabilization of T–S fuzzy systems via mixed convex combination," *Nonlinear Dynamics*, vol. 75, no. 3, pp. 501–512, 2014.

[26] F. Hao, "New conditions on absolute stability of uncertain Lur'e systems and the maximum admissible perturbed bound," *IMA Journal of Mathematical Control and Information*, vol. 24, no. 3, pp. 425–433, 2006.

[27] B. Liu and X. C. Jia, "New absolute stability criteria for uncertain Lur'e systems with time-varying delays," *Journal of the Franklin Institute*, vol. 355, no. 9, pp. 4015–4031, 2018.

Hindawi
Mathematical Problems in Engineering
Volume 2022, Article ID 7891232, 14 pages
https://doi.org/10.1155/2022/7891232

Research Article

Analysis of Vehicle-Pedestrian Accident Risk Based on Simulation Experiments

Rui Cheng,[1] **Ye Pan**,[1] **and Lian Xie**[1,2]

[1]*Key Laboratory of ITS (Guilin University of Electronic Technology), Education Department of Guangxi Zhuang Autonomous Region, Guilin 541004, China*
[2]*Intelligent Transportation Systems Research Center, Wuhan University of Technology, Wuhan 430063, China*

Correspondence should be addressed to Lian Xie; xielian@whut.edu.cn

Received 16 May 2022; Revised 16 July 2022; Accepted 4 August 2022; Published 29 August 2022

Academic Editor: Meng Li

Vehicle-pedestrian accidents are one of the main types of road traffic accidents in China because of their mixed traffic features. By analyzing the characteristics of vehicle-pedestrian accidents, the head injury criterion (HIC) was selected as a quantitative index of pedestrian head injury risk, and vehicle-pedestrian collision simulation tests were carried out using PC-Crash. From the collected test data, the multivariate relationship models between the HIC, vehicle speed, and collision angle were fitted for different vehicle types. A risk assessment method for vehicle-pedestrian accidents based on the HIC was proposed by the Fisher optimal segmentation algorithm. Finally, a new index for evaluating the accuracy of accident risk classification, the degree of error classification, was proposed to verify the validity of the accident risk assessment method. The results show that vehicle speed, collision angle, and vehicle type play a key role in pedestrian injury. Flat-headed vehicles are more likely to cause head injuries to pedestrians than high-headed and low-headed vehicles. Rear-end collisions cause more injuries to pedestrians than side collisions. The research results can provide guidance and a basis for accident liability determination, speed limit management, vehicle safety design, and human injury mechanism analysis.

1. Introduction

With the rapid growth of the social economy and the continuous innovation of science and technology, automobile manufacturers are increasingly pursuing comfort, safety, and environmental protection, as well as the protection of passengers in vehicles, while their awareness of the protection of pedestrians outside vehicles is relatively weak. Among all road traffic participants, pedestrians are one of the most vulnerable groups. In recent years, the lack of safety awareness of drivers and pedestrians in observing traffic rules and poor traffic management has caused frequent pedestrian traffic accidents, and the resulting losses are difficult to estimate. According to statistics in China's annual statistical report of road traffic accidents (2021), pedestrian traffic accidents accounted for approximately 21% of all accidents in the whole year but lead to approximately 27% mortality [1]. The reason is that road traffic in China is mainly typical plane cross-mixed traffic. Although most urban roads are divided into nonlane isolation facilities, collision accidents between cars and pedestrians cannot be eliminated.

The USA and the European Union began to pay attention to pedestrian safety in the mid-1970s. Since then, biological samples and mechanical dummies have been used to carry out real vehicle test studies instead of pedestrians, including human injury evaluation, the impact of overall vehicle structure design on pedestrian injury, and human injury prevention measures and safety countermeasures [2–5]. For example, Severy et al. used mechanical dummies to study vehicle-pedestrian collision accidents successively in 1963 and 1966, which was the first experiment in this field [6]. On this basis, other relevant scholars used dummies or corpses to conduct a series of experiments under different collision conditions. The data obtained from a test are fitted using mathematical regression with different methods to obtain a corresponding empirical formula [7].

Due to the high cost of real vehicle tests and considering the feasibility of computer technology simulation, some scholars have developed mature accident reconstruction software (SMAC, AUTOSMAC, PC-Crash, etc.) by building digital dummy models, providing another way to analyze and study vehicle-pedestrian collision accidents [8]. A dummy model should not only adapt to human body dynamics analysis but also be able to carry out human body damage analysis [9, 10]. Therefore, a digital dummy should have high computational efficiency, be able to adapt to different environments, conform to various biomechanical characteristics of the human body, and output corresponding parameter information for the calculation of a damage index.

For example, Xu et al. proposed a personalized customization method to divide the pedestrian structure into independent modules according to obvious bone markers and establish a multibody model and a finite element (FE) model for each independent module to form a hybrid pedestrian model [11]. To characterize the complex vehicle-pedestrian interaction process, Grindle et al. developed and validated a detailed pedestrian FE model corresponding to 50% male to predict injuries caused by pedestrian accidents. Compared with a simplified pedestrian model, the constructed model shows higher biofidelity [12]. In addition, to explore the damage prediction ability of the Total Human Body Model for Safety (THUMS) finite element human model (FE-HBM) in real-world vehicle-pedestrian collisions, Panday et al. used sequences of multibody tools and finite element tools to reconstruct 10 vehicle-pedestrian crashes with lower limb injuries. The conclusion shows that the THUMS FE-HBM can better predict pedestrian injuries in real traffic accidents [13]. Lalwala et al. also reconstructed a THUMS pedestrian model using pedestrian accident cases. It can be observed from the reconstruction study that the kinematic response and damage response of their THUMS lower limb model are in good agreement with the actual collision data [14].

With the continuous improvement of accident databases by traffic research institutions in various countries, in recent years, some scholars have relied on cases in a database to explore the significant cause factors affecting the frequency and severity of vehicle-pedestrian accidents. For example, in terms of road control, based on three years of traffic accident data in Hong Kong, Zhu selected the best performance artificial neural network (ANN) model by comparing various data mining algorithms and determined the most significant factors causing fatal and serious accidents. The results show that in rainy weather, fatal and serious vehicle-pedestrian collisions are more likely to occur in the case of intersection signal failures [15]. Sheykhfard et al. used a structural equation model (SEM) to investigate the data of 1358 pedestrian accidents in Gilan Province, Iran, from 2012 to 2018. Factor analysis results showed that the quality defects of automobiles and poor traffic design at intersections, major urban roads, and outer ring roads are important reasons for the increase in fatal accidents [16]. With the continuous improvement of research methods, Kamboozia et al. constructed a pedestrian accident severity prediction model using ANNs and multiple logistic regression. By comparing the severity prediction results of pedestrian accidents using different methods, they put forward the best prevention and control measures to improve pedestrian safety on rural roads [17].

In terms of vehicle and pedestrian characteristics, Park et al. used a multilevel model to investigate the differences between the low-level individual characteristics and high-level community environmental characteristics of pedestrian collisions in Seoul, South Korea. The results showed that older pedestrians suffered more serious pedestrian injuries; trucks and vans were more likely to cause serious pedestrian injuries [18]. While researching the influence of alcohol, Lasota's survey found that younger victims were more likely to die at the scene of an accident, especially in rural areas [19].

To determine the high-risk and low-risk areas of pedestrian death accidents in Iran, Hasani et al. input collected pedestrian accident data into ArcGIS software to identify high-risk and low-risk areas by calculating the spatial autocorrelation of the data [20]. Jamali-dolatabad et al. collected pedestrian traffic accident data in Tabriz from 2014 to 2015, with fatal accidents as the case group and nonfatal accidents as the control group. Their results showed that the significantly related factors influencing pedestrian death were pedestrian age, type of license plate, accident season, type of driving license, gender of pedestrian, and pedestrian fault [21]. Feng et al. used a multivariate logistic regression model to analyze 111 collision accidents and found that collision with the front windshield frame usually leads to more serious damage. When the collision speed exceeds 40 km/h, the risk of serious head injury for pedestrians increases sharply [22]. While discussing the characteristics of fatal pedestrian accidents involving low-speed vehicles, Matsui, a Japanese scholar, thought the relative percentage of pedestrian deaths is significantly higher when vehicles are traveling at low speeds, except for accidents involving box trucks or SUVs [23].

At present, researchers mainly carry out vehicle-pedestrian accident research through simulation and accident case statistical analysis. In terms of simulation, most existing studies are optimized and improved for a dummy model, and few involve the risk assessment of pedestrian accidents by developed dummy models. However, an accident risk assessment based on the statistical analysis of accident cases mainly considers macro factors, such as vehicle speed, vehicle type, accident environment, and road design, but lacks in-depth discussion of the impact of micro-factors (such as pedestrian speed, collision angle, type of head, and pedestrian and vehicle lateral contact position) on human injuries. Therefore, this paper adopts computer simulation technology to carry out a risk analysis of vehicle-pedestrian accidents with a more mature multirigid body dummy model. Common computer simulation software for accident reappearance includes SMAC and AUTOSMAC, developed by the National Road Traffic Safety Administration of the USA, and PC-Crash, developed by the DSD of Austria. Since SMAC and AUTOSMAC cannot realize pedestrian collision simulation, PC-Crash has been constantly updated and

upgraded, adding pedestrian multirigid body and FE calculation models on the basis of a single rigid body model, which has been widely recognized in the field of road traffic accident reconstruction and has become the most widely used accident simulation software. In view of this, this paper chooses PC-Crash to carry out simulation tests. Through the investigation and analysis of accident cases, the typical collision patterns of vehicle-pedestrian traffic accidents are determined. Based on a rigid body dynamics method, PC-Crash is utilized to build three vehicle rigid body models (short head, high head, and flat head) and a pedestrian multirigid body model, HTC is used to measure the risk of pedestrian head injuries, a vehicle-pedestrian collision simulation test is carried out under the influence of different vehicle types, vehicle speeds, pedestrian speeds, collision angles, and relative collision positions, and the influence of multiple factors on pedestrian injury is studied. According to the collected test data, the relationship model between the HIC and vehicle speed under different collision angles is fitted using multiple regression analysis for different vehicle models. A reasonable evaluation series and corresponding HIC threshold of pedestrian injury risk in vehicle-pedestrian accidents are determined using the Fisher optimal segmentation algorithm, and the vehicle-pedestrian accident risk evaluation method based on HIC is given. Compared with risk assessment based on accident case analysis, the research results obtained by simulation in this paper are not affected by factors, such as region, time, and traffic characteristics, and have universal applicability.

2. Characteristics Analysis of Vehicle-Pedestrian Collision Accidents

2.1. Collision Form. Compared with people in a vehicle, pedestrians are completely exposed to the external environment, have strong subjective randomness when walking, and choose the road, direction, and walking speed that they think will reach their destination. The characteristics of pedestrian traffic are related to the height, age, psychology, physique, and gender of pedestrians, which leads to the diversity and complexity of vehicle-pedestrian collision accident patterns and makes them face different injury risks.

There are three common collision patterns between cars and pedestrians: front, side, and rear collisions with pedestrians. Because frontal collisions between vehicles and pedestrians occur most frequently and are most likely to lead to pedestrian deaths, this paper focuses on frontal collisions between vehicles and pedestrians. This collision process can be divided into three stages, as shown in Figure 1.

① Collision phase: The pedestrian's lower limbs first collide with the front part of the vehicle. As the vehicle continues to move forward, the pedestrian's chest and abdomen contact and collide with the engine hood of the vehicle. If the vehicle speed is high, the pedestrian's head will collide with the front windshield or A-pillar of the vehicle. Usually, at this stage, pedestrians are subjected to a large impact force, resulting in very serious pedestrian damage. ② Flight phase: After the collision, the human body continues to fly in the air. At this stage, the pedestrian does not contact any object and only receives friction resistance from the air. ③ Landing and rolling stage: After falling to the ground, pedestrians are affected by the friction resistance of the road and immediately begin to slow down. According to the different falling speeds and directions, the pedestrian experiences a composite motion state of sliding, rolling, or rotating on the road surface.

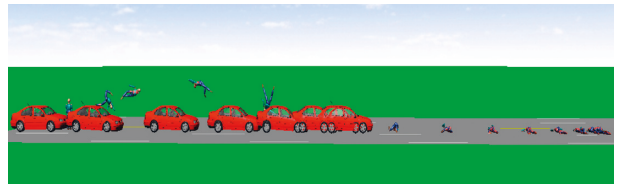

Figure 1: Diagram of the collision process.

2.2. Pedestrian Injury Mechanism. In vehicle-pedestrian collision accidents, the injuries suffered by pedestrians can be roughly divided into two categories, namely, primary injuries and secondary injuries. A primary injury refers to an injury caused by the first collision or crushing of the human body between a vehicle and a pedestrian. A secondary injury refers to an injury caused by the collision and scraping between the human body and the ground or other objects after being hit. Generally, pedestrian injury mechanisms can be divided into the following two categories according to different vehicle types:

(1) When a pedestrian collides with a high-head vehicle (such as an off-road vehicle) or a low-head vehicle (such as a car), because the front collision contact point of the vehicle is not higher than the center of gravity of the human body, the first damage to the human body is the car's front bumper, engine cover, and front windshield contact collision with the human body. The second collision is the human body in the air after the overturn of the vehicle, subsequent contact collision or landing, and road impact causing damage.

(2) When a pedestrian collides with a flat-headed vehicle (such as a van or truck), the height of the front part of the vehicle is higher than the height of the pedestrian's center of gravity, and the pedestrian's legs, torso, or even their whole body contact with the front part of the vehicle, resulting in a large contact surface and easily causing nonobvious trauma to the human body but especially serious internal injuries. After the collision, the human body experiences a flat throwing movement, which will cause obvious falling injury and then scratching or rolling.

According to the statistical analysis results of pedestrian traffic accidents in China [24], Figures 2 and 3 show the injury frequency of pedestrian body parts and the distribution frequency of fatal body parts, respectively. Figure 2 shows that the most vulnerable parts are people's legs and head, among which leg injuries account for 40%, and 32% of pedestrians suffer head injuries. Figure 3 shows that head and chest injuries are the main causes of pedestrian deaths,

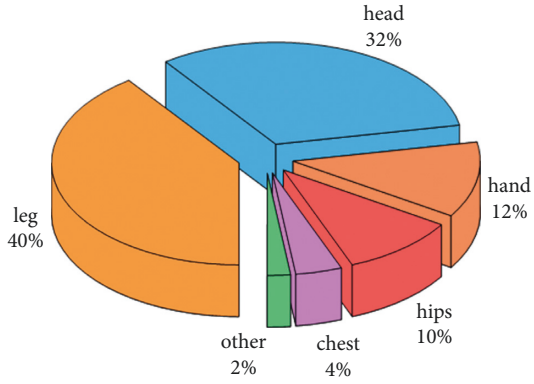

Figure 2: Distribution of pedestrian injuries.

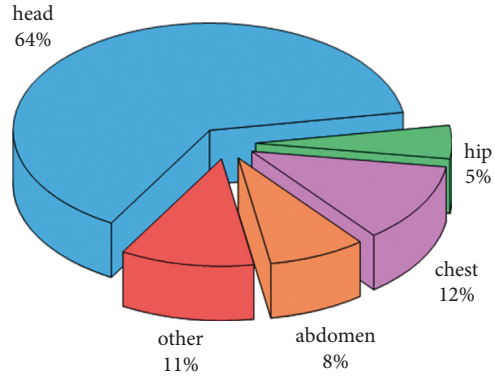

Figure 3: Distribution of fatal pedestrian parts due to injury.

accounting for 64% and 12%, respectively. Therefore, the analysis and protection of head injuries play an important role in pedestrian safety research.

3. Evaluation Standard and Method of Head Injury

3.1. Head Injury Criterion. The head injury evaluation standard is defined by physical parameters related to injury intensity or a function composed of several physical parameters, which is related to the degree of risk of a certain part of the human body being damaged and is used to measure whether the load exceeds the degree of causing a certain injury. At present, the head injury criterion (HIC) proposed by Versace in 1971 is widely adopted internationally, serves as the basis of the Federal Motor Vehicle Safety Standards (FMVSS), and is used to evaluate vehicle safety. In domestic and foreign laws and standards, the HIC has become the most extensively employed criterion for evaluating head injuries. The safety limit value for the HIC is generally 1,000. According to related statistics, when the HIC > 1,000, the probability of fatal head fracture exceeds 33%. Its calculation formula is as follows [25]:

$$\mathrm{HIC} = \left[(t_2 - t_1)\left(\frac{1}{t_2 - t_1}\int_{t_1}^{t_2} a(t)\mathrm{d}t\right)^{2.5}\right]_{\max} \quad (1)$$

where a represents the resultant acceleration at the center of gravity of the head in a collision; t_1 and t_2 are two different times during the collision, which are chosen to maximize the HIC; and $1/t_2 - t_1 \int_{t_1}^{t_2} a_t \mathrm{d}t$ represents the average resultant acceleration between t_1 and t_2. The time interval (i.e., from t_1 to t_2) of the HIC substantially affects the calculation of its value. Thus, this paper selects 15 ms, as adopted by the U-NCAP collision test.

3.2. Fisher Optimal Segmentation Method. When the HIC > 1,000, head injuries tend to be more severe, but there is no clear standard for using the HIC to measure the severity of head injuries. Therefore, this paper uses the Fisher optimal segmentation algorithm to classify the HIC data obtained from a simulation test to obtain a pedestrian accident risk classification scheme, including the optimal classification number and corresponding index thresholds of each level. The principle of Fisher optimal segmentation is to ensure the ordered sample data of each group after segmentation and minimize the sum of squares of deviations within the group. In this case, the corresponding grouping is the optimal segmentation. The specific implementation method is described below [26].

3.2.1. Define and Calculate the Class Diameter. The Fisher optimal segmentation algorithm usually uses the diameter to define the difference degree in a class. When the difference degree in the class is smaller, the class diameter is smaller, indicating that the sample attributes in the class tend to be consistent. If the data samples are divided into k categories and have C_{m-1}^{k-1} classification methods, assuming that H_{ij} is one of the classifications, then the sample data contained in the classification are denoted as $\{x_i, x_{i+1}, \ldots, x_j\}$ $(1 \le i < j)$. The sum of the squares of deviations of the samples in H_{ij} is defined as the class diameter $D(i, j)$, namely,

$$D(i, j) = \sum_{i=1}^{j} \left(x_i - \overline{x}_{ij}\right)^T \left(x_i - \overline{x}_{ij}\right), \quad (2)$$

where x_i is the standardized sample value and $\overline{x}_{ij}$ is the average value from sample i to sample j.

3.2.2. Calculate the Classification Error Function. Generally, an error function is used to define the merits and demerits of data sample classification. If m data samples are divided into k categories, the corresponding error function of this category is

$$e[p(m, k)] = \sum_{\eta=1}^{k} D\left(i_\eta, i_{\eta+1} - 1\right). \quad (3)$$

That is, the error function of any classification method is expressed as the sum of all diameters. The smaller $e[p(m, k)]$ is, the smaller the sum of diameters of all classifications is, and the better the classification effect is.

3.2.3. Determine the Optimal Solution. According to formula (3), when $k = 2$, the error function corresponding to the optimal 2 classifications is

$$e[p(m,2)] = \min_{2\le i\le m}\{D(1,i-1) + D(i,m)\}. \quad (4)$$

When $k>2$, the error function corresponding to the optimal k classification is

$$e[p(m,k)] = \min_{2\le i\le m}\{e[p(i-1,k-1)] + D(i,m)\}, \quad (5)$$

Here, it is necessary to determine the appropriate classification point i_k guarantee formula (5) to calculate the minimum value, that is, $e[p(m,k)] = e[p(i_k-1,k-1)] + D(i_k,m)$ is the minimum, so the k class $H_k = \{i_k, i_{k+1}, \ldots, m\}$ can be obtained. Then, the classification point $i_{k\text{-}1}$ is determined to make it satisfy $e[p(i_k-1,k-1)] = e[p(i_{k-1}-1,k-2)] + D(i_{k-1},i_k-1)$ so that the k–1 class $H_{k-1} = \{i_{k-1}, i_{k-1}+1, \ldots, i_k-1\}$ can be obtained, all the classifications $H_1, H_2, \ldots, H_k$ can be obtained by analogy, and finally, the optimal solution can be obtained.

3.2.4. Determine the Optimal Classification Number. Generally, the optimal classification is determined by drawing the curve of the minimum error function changing with the classification number k. When the curve curvature changes significantly, the corresponding k value is the appropriate classification number. In addition, to determine the k value more accurately, the minimum error function ratio $\beta(k)$ between adjacent classification numbers can be further calculated. The larger $\beta(k)$ is, the better the classification effect is, as shown in

$$\beta(k) = \frac{e[p(m,k)]}{e[p(m,k+1)]}. \quad (6)$$

3.3. Abbreviated Injury Scale. In addition, to standardize the evaluation of injury levels after accidents, countries around the world have put forward the abbreviated injury scale (AIS) to evaluate the risk of injury after years of accident research. The AIS is a scoring method for classifying trauma based on anatomical indexes. It defines nine anatomical ranges to determine the location of trauma, specifically including head (skull and brain), face (eyes and ears), neck, chest, abdominal and pelvic organs, spine (cervical spine, thoracic spine, and lumbar spine), upper limbs, lower limbs, pelvis and buttocks, body surface (skin) and thermal injury, and other injuries. According to the pedestrian injury report, the trauma level of the pedestrian after the accident was assessed with six grades, as shown in Table 1.

4. Data Collection

4.1. Test Scenario. First, a two-way four-lane road model with a lane width of 3.5 m, total length of 100 m, and pavement adhesion coefficient of 0.7 is constructed using PC-Crash, as shown in Figure 4. Then, the software's human body model is used. The model is a multibody dynamic system consisting of 16 independent rigid bodies and 15 hinge joints, as shown in Figure 5. Each part of the human body (head, trunk, limbs, buttocks, etc.) is regarded as an independent rigid body, and its surface shape is defined by an ellipsoid, which simplifies the joint of each part to a hinge connection. In this paper, adult males were selected as the research object, and multiple rigid body model parameters were assigned according to physical characteristics. The specific setting parameters are shown in Table 2.

Table 1: AIS classification standard.

AIS score	Description	Mortality rate (%)
1	Mild	0.6
2	Moderate	3.2
3	Heavy	9.3
4	Severe	28.3
5	Critical	78.4
6	Extreme (currently incurable)	100

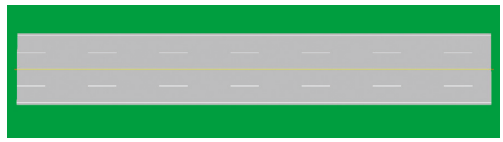

Figure 4: Road scenario.

According to the analysis in Section 2.2, a Volkswagen Bora 2.0, Audi Q5 2.0TDI, and Volkswagen T4 2.5 TDI (as shown in Figure 6) were selected from the PC-Crash database as representative models of low-head, high-head, and flat-head vehicles, respectively, to explore the impact of different head types on pedestrian injury risk.

4.2. Test Scheme. Considering that pedestrian speed may affect accident risk, this research carries out vehicle-pedestrian collision simulation tests under a pedestrian moving state. According to the statistical analysis of pedestrian motion state and collision angle in vehicle-pedestrian accidents in the literature [27], 55% of pedestrians are in a walking state, 38% are in a running state, and 4% are in a stationary state. The proportion of pedestrians in the lateral position (i.e., the walking direction of pedestrians is 90° from the driving direction of vehicles) is 68%, followed by the rear position (i.e., the walking direction of pedestrians is 0° from the driving direction of vehicles) and the facing position (i.e., the walking direction of pedestrians is 180° from the driving direction of vehicles), accounting for 21% and 7%, respectively. Therefore, this research chooses two states of walking and jogging for pedestrians (corresponding to a walking speed of adult males being approximately 5 km/h and a jogging speed being approximately 10 km/h), and the two orientations of collision angle between pedestrians and cars are 90° and 0° for experiments. In addition, to explore the impact of pedestrian collision position relative to vehicle on accident risk, this study selects the front 1/4 and 1/2 positions as research variables. Figure 7 shows the collision position of pedestrians relative to cars at different collision angles.

Considering the demands of road traffic car speed in China, at the same time to make the research more reasonable, the car speed is set to $V_S \in \{20, 30, 40, 50, 60, 70, 80, 90, 100, 110\}$ km/h. Combined with the analysis of the above

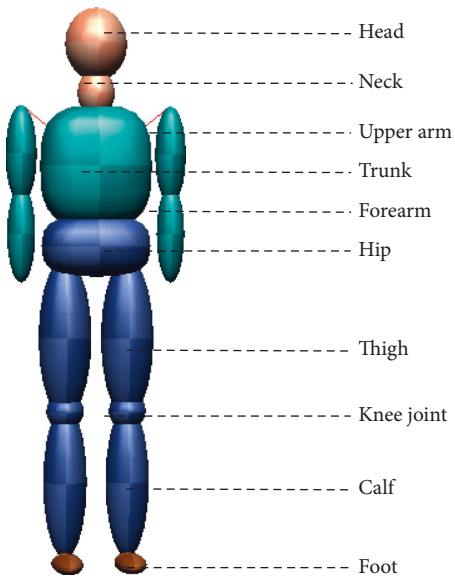

Figure 5: Pedestrian multibody model.

Table 2: Body parameters of 90th percentile adult males aged 18–60 years in China.

Height (mm)	Weight (kg)	Upper arm length (mm)	Forearm length (mm)	Thigh length (mm)	Calf length (mm)
1754	71	333	253	496	396

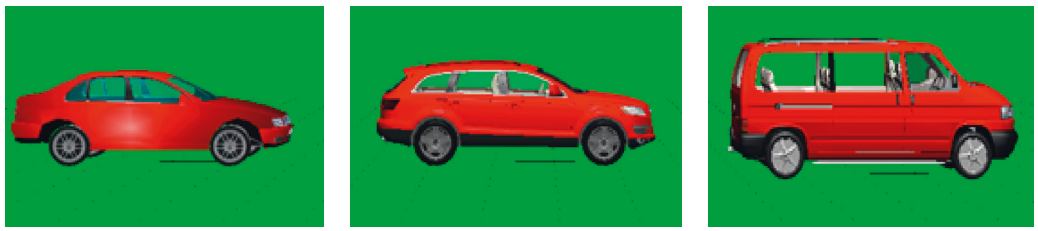

(a) (b) (c)

Figure 6: Test vehicle models. (a) VW Bora 2.0. (b) Audi Q5 2.0TDI. (c) VW T4 2.5 TDI.

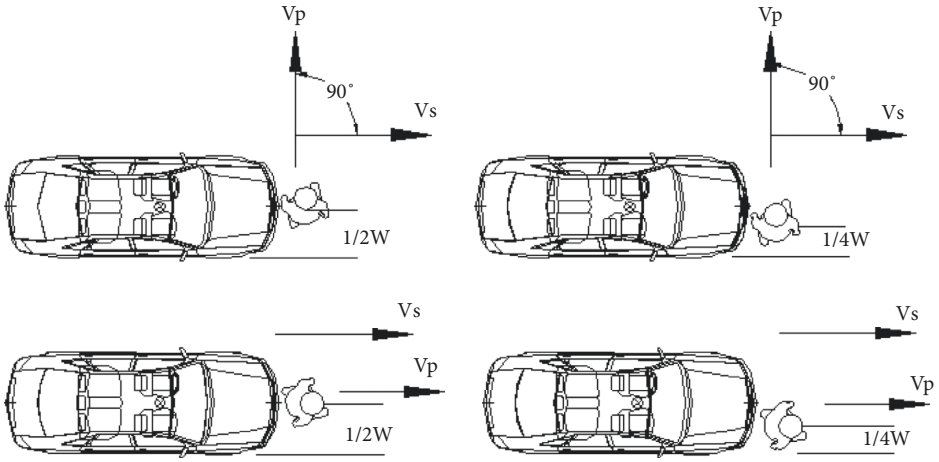

Figure 7: Diagram of the test collision location.

Table 3: Resultant head acceleration value of low-head vehicle and pedestrian collision (m/s^2).

Speed (km/h)	1/4W				1/2W			
	5 km/h		10 km/h		5 km/h		10 km/h	
	0°	90°	0°	90°	0°	90°	0°	90°
20	7325	4910	10743	5710	8893	5523	7418	5661
30	18432	8492	19722	5691	18817	7517	19366	5863
40	31446	10111	28788	12198	31143	7824	31050	9156
50	38902	16472	39020	12151	38179	17399	36127	11671
60	37538	19569	37202	20320	34151	26587	36897	17693
70	39112	29179	40570	25684	38536	32482	37900	32015
80	83079	57019	96861	46872	73810	36515	96522	30526
90	61532	70732	54079	52682	91077	58322	67637	48716
100	66272	70748	75818	58711	72905	54236	77429	35124
110	98648	73310	112221	75050	94712	55597	117232	60774

Table 4: Resultant head acceleration value of high-head vehicle and pedestrian collision (m/s^2).

Speed (km/h)	1/4W				1/2W			
	5 km/h		10 km/h		5 km/h		10 km/h	
	0°	90°	0°	90°	0°	90°	0°	90°
20	6850	6018	4975	3768	9324	4959	9367	4932
30	19676	6205	21291	5873	17794	8436	18627	5697
40	27784	10803	28913	11685	26035	11672	26990	10196
50	41633	17836	39939	14931	34615	16708	35541	13995
60	30945	22409	32566	16596	33216	24322	32900	17927
70	41164	27664	37652	24207	57948	33650	45046	23883
80	70486	32955	60383	31991	118726	37902	89432	37764
90	82572	54328	69229	38435	69090	53954	59607	45422
100	78490	57858	91205	51966	69118	54485	136390	64674
110	96015	64113	160570	84012	136823	54876	112009	54378

Table 5: Resultant head acceleration value of flat-head vehicle and pedestrian collision (m/s^2).

Speed (km/h)	1/4W				1/2W			
	5 km/h		10 km/h		5 km/h		10 km/h	
	0°	90°	0°	90°	0°	90°	0°	90°
20	72581	68028	57022	56185	102776	58738	96927	63485
30	55403	50536	65902	56045	93834	51304	77411	49532
40	63699	39733	84445	46869	76342	48448	86677	49439
50	78634	51023	103047	44617	115872	46188	102369	42441
60	115818	78840	130771	64405	152051	69207	147071	53681
70	130897	121951	168717	109352	157615	82202	171708	73181
80	154287	158591	144967	143215	207197	122008	206549	104993
90	152299	173736	147755	147764	183070	122477	177983	141675
100	282092	178430	244815	166398	264413	156806	260346	153319
110	375455	229065	418680	187684	430182	178198	448000	166874

variables, we set the model $M \in \{M_1, M_2, M_3\}$, wherein M_1, M_2, and M_3 represent the low-head, high-head, and flat-head vehicles, respectively; collision angle $\theta \in \{0°, 90°\}$; pedestrian walking speed $V_P \in \{5\,\text{km/h}, 10\,\text{km/h}\}$; collision position $R \in \{1/4\,W, 1/2\,W\}$, where W is the width of the front part of the car in meters. The simulation test involves 5 variables, namely, $\{M, \theta, V_S, V_P, R\}$. According to the values of each variable, a total of $3 \times 2 \times 10 \times 2 \times 2 = 240$ collision modes were simulated. Before the collision, the vehicle moves in a straight line, and after the collision, the vehicle is fully braked until it stops. The collision process is shown in Figure 1.

5. Results and Analysis

5.1. Model Fitting. Through each simulation test, the resultant acceleration value of the pedestrian head under different collision forms is obtained, as shown in Tables 3–5. The HIC value can be calculated using formula (1), as shown in Tables 6–8. Among them, the test data with a HIC value ≥ 1000 account for 75.8% of the total.

First, the Pearson correlation analysis between each variable and the HIC is carried out, and the results are listed in Table 9. ** in the table represents a significant

Table 6: HIC value of collision head between low-head vehicle and pedestrian.

	1/4W				1/2W			
Speed (km/h)	5 km/h		10 km/h		5 km/h		10 km/h	
	0°	90°	0°	90°	0°	90°	0°	90°
20	46	17	121	25	75	23	48	24
30	466	67	551	25	490	49	527	27
40	1770	104	1419	166	1728	55	1715	81
50	3013	352	3036	164	2875	403	2504	149
60	2756	541	2695	594	2176	1164	2640	420
70	3054	1468	3347	1067	2943	1920	2823	1851
80	20084	7837	29477	4802	14942	2572	29220	1644
90	9481	13432	6866	6431	25272	8293	12011	5288
100	11414	13440	15979	8432	14488	6916	16842	2334
110	30856	14690	42589	15577	27870	7358	47504	9192

Table 7: HIC value of collision head between high-head vehicle and pedestrian.

	1/4W				1/2W			
Speed (km/h)	5 km/h		10 km/h		5 km/h		10 km/h	
	0°	90°	0°	90°	0°	90°	0°	90°
20	39	28	18	9	85	17	86	17
30	548	31	668	27	426	66	478	25
40	1299	122	1435	149	1104	149	1208	106
50	3570	429	3218	275	2250	364	2404	234
60	1701	759	1932	358	2030	931	1982	434
70	3471	1285	2777	920	8160	2097	4348	890
80	13316	1990	9045	1848	49033	2823	24146	2798
90	19778	6945	12730	2924	12666	6826	8757	4439
100	17424	8129	25361	6215	12679	6995	69354	10738
110	28838	10507	104299	20653	69906	7122	42389	6961

Table 8: HIC value of collision head between flat-head vehicle and pedestrian.

	1/4W				1/2W			
Speed (km/h)	5 km/h		10 km/h		5 km/h		10 km/h	
	0°	90°	0°	90°	0°	90°	0°	90°
20	14327	12185	7838	7554	34185	8441	29527	10251
30	7294	5796	11255	7507	27228	6019	16832	5512
40	10338	3177	20919	4801	16256	5216	22329	5486
50	17504	5936	34412	4245	46139	4629	33848	3746
60	46085	17619	62430	10627	91011	12720	83740	6740
70	62581	52429	118035	39919	99565	19558	123337	14626
80	94393	101114	80777	78359	197276	52491	195738	36059
90	91382	127011	84717	84730	144763	52997	134915	76269
100	426669	135763	299372	114021	362929	98293	349136	92919
110	871989	253521	1145038	154059	1225307	135322	1356163	114839

Table 9: Correlation analysis.

	Vehicle speed	Collision position	Pedestrian speed	Collision angle	Vehicle type
HIC	0.333**	0.017	0.005	−0.181**	0.311**

correlation at a level of 0.01 (two-tailed test). The vehicle speed, collision angle, and vehicle type are significantly correlated with the HIC, while the collision position and pedestrian speed show a weak correlation. The analysis shows that the impact force of any part of the front of the vehicle on the pedestrian is equivalent, and the pedestrian speed relative to the vehicle speed can be ignored at the moment of collision. The above reasons lead to a change in

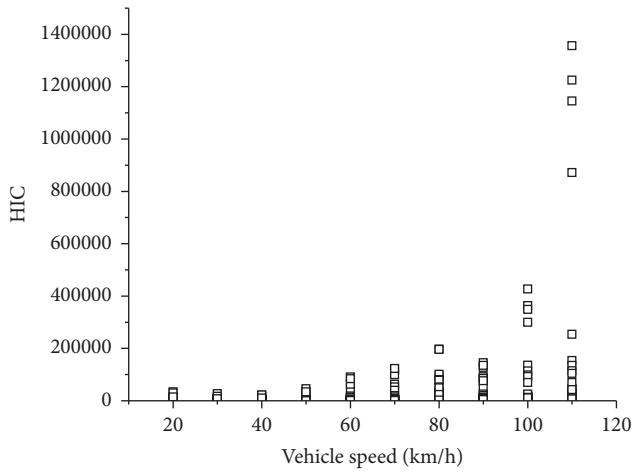

Figure 8: Relationship between vehicle speed and the HIC.

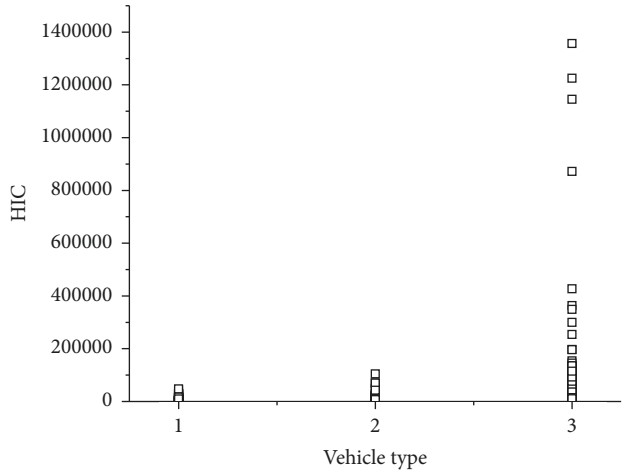

Figure 9: Relationship between vehicle model and the HIC.

collision position and pedestrian speed, which has little impact on pedestrian injury. Therefore, it will be eliminated in the later analysis.

Figures 8–10 show the relationship between significant risk factors and the HIC. Figure 8 shows that the HIC value gradually increases with increasing vehicle speed, and the increasing trend is increasingly larger. As shown in Figure 9, a flat head, high head, and short head are more likely to cause injury to the pedestrian head, while a high head and short head have the same impact on the pedestrian head. As shown in Figure 10, pedestrian injury is more serious when the collision angle is 0° than when the collision angle is 90°; that is, injury caused by a rear collision between the vehicle and the pedestrian is greater than that caused by a side collision between the vehicle and pedestrian. The analysis shows that a rear collision between cars and pedestrians easily causes pedestrians to recline, which increases the probability of a serious collision between the head and automobile engine cover, front windshield, or A-pillar.

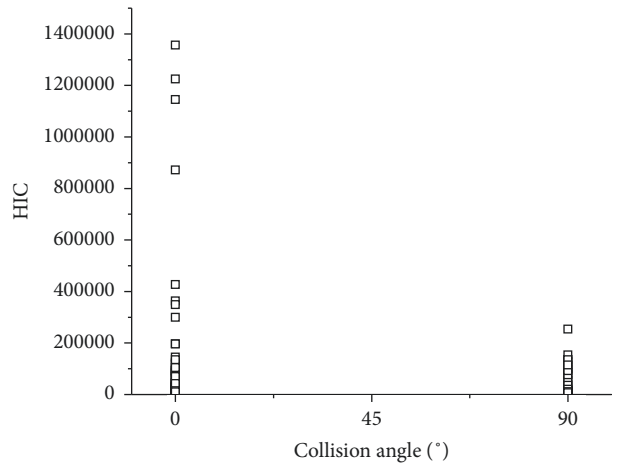

Figure 10: Relationship between impact angle and the HIC.

Table 10 shows how scholars use various methods to identify the significant risk factors based on data sources from different areas and times. Besides collision angle, the significant risk factors identified in this paper are basically consistent with those identified by other researchers, such as the vehicle speed and vehicle type. In terms of vehicle type, factors screened by other scholars, such as larger vehicles, light machinery trucks, and light passenger vehicles, all belong to the category of flat-headed vehicles identified in this paper, which indicate that the research results of this paper are not limited by region and time and have universal applicability.

With reference to the relationship between the above variables and the HIC value, the nonlinear relationship between the HIC and vehicle speed was fitted using multiple regression analysis for different vehicle types and collision angles, as shown in Table 11. According to the determination coefficient R^2 between different expressions (the greater the value is, the better the goodness of fit), the optimal relationship models of the HIC, vehicle speed, and collision angle corresponding to different models are determined as follows.

(1) Short head type:

$$\mathrm{HIC} = \frac{\theta}{90^\circ}\left(-1105.442 + 105.627V_S - 3.196V_S^2 + 0.032V_S^3\right) + \left(1 - \frac{\theta}{90^\circ}\right)\left(0.006V_S^{3.276}\right). \tag{7}$$

(2) High head type:

$$\mathrm{HIC} = \frac{\theta}{90^\circ}\left(0.0001V_S^{3.831}\right) + \left(1 - \frac{\theta}{90^\circ}\right)\left(4313.065 - 271.598V_S + 4.424V_S^2\right). \tag{8}$$

(3) Flat head type:

Table 10: Comparison of the conclusions in this paper and other research.

Literature	Method	Significant risk factor	Data source
This paper	Multiple regression analysis and correlation analysis	Vehicle speed, vehicle type (flat-headed vehicles), and collision angle (rear-end collision)	PC-Crash simulation
[18]	Multilevel model	Pedestrian age and vehicle type (larger vehicles)	Pedestrian-vehicle collision data from 2015 to 2017 in South Korea
[21]	Partial least squares discriminant analysis	Pedestrian age, pedestrian gender, vehicle type (light machinery), and accident time	Fatal pedestrian crash in Tabriz, Iran, during 2014 to 2015
[22]	Multivariate logistic regression	Vehicle speed (in excess of 40 km/h) and collision location	Pedestrian-vehicle accident cases in Chongqing, China, from 2011 to 2015
[23]	Statistical tests	Vehicle type (trucks, light passenger vehicles) and light level	Fatal pedestrian accidents of low-speed vehicles in Japan from 2005 to 2014

Table 11: Model fitting results.

Number	Model	Collision angle	Model expression	R^2
1	Short head type	$\theta = 90^\circ$	$\mathrm{HIC} = 5.195e^{0.08V_S}$	0.958
2			$\mathrm{HIC} = -1105.442 + 105.627V_S - 3.196V_S^2 + 0.032V_S^3$	0.980
3			$\mathrm{HIC} = 8.968e^{-5}V_S^{3.935}$	0.945
4		$\theta = 0^\circ$	$\mathrm{HIC} = 5.616e^{0.069V_S}$	0.941
5			$\mathrm{HIC} = e^{10.922-143.901V_S^{-1}}$	0.931
6			$\mathrm{HIC} = 0.013V_S^{3.09}$	0.905
7			$\mathrm{HIC} = 0.006V_S^{3.276}$	0.935
8			$\mathrm{HIC} = 0.002V_S^{3.552}$	0.918
9	High head type	$\theta = 90^\circ$	$\mathrm{HIC} = 7.222e^{0.071V_S}$	0.966
10			$\mathrm{HIC} = 3.344e^{0.078V_S}$	0.975
11			$\mathrm{HIC} = 0.0001V_S^{3.831}$	0.988
12		$\theta = 0^\circ$	$\mathrm{HIC} = 4.43e^{0.075V_S}$	0.969
13			$\mathrm{HIC} = 4313.065 - 271.598V_S + 4.424V_S^2$	0.934
14			$\mathrm{HIC} = -72412.624 + 5232.291V_S - 107.569V_S^20.67V_S^3$	0.920
15			$\mathrm{HIC} = 0.002V_S^{3.622}$	0.909
16			$\mathrm{HIC} = 0.002V_S^{3.608}$	0.924
17	Flat head type	$\theta = 90^\circ$	$\mathrm{HIC} = 39206.161 - 1867.829V_S + 20.139V_S^2 + 0.119V_S^3$	0.963
18			$\mathrm{HIC} = 57651.927 - 3377.693V_S + 55.218V_S^2 - 0.152V_S^3$	0.982
19			$\mathrm{HIC} = 17718.827 - 449.132V_S - 3.278V_S^2 + 0.155V_S^3$	0.984
20		$\theta = 0^\circ$	$\mathrm{HIC} = 56592.336 - 2915.804V_S + 40.36V_S^2 - 0.079V_S^3$	0.978
21			$\mathrm{HIC} = -458713.785 + 34542.659V_S - 735.559V_S^2 + 4.804V_S^3$	0.966
22			$\mathrm{HIC} = 2946.727e^{0.047V_S}$	0.910
23			$\mathrm{HIC} = -729141.994 + 54160.807V_S - 1112.044V_S^2 + 7.001V_S^3$	0.907
24			$\mathrm{HIC} = -871724.682 + 63661.079V_S - 1297.743V_S^2 + 8.087V_S^3$	0.890

$$\mathrm{HIC} = \frac{\theta}{90^\circ}\left(17718.827 - 449.132V_S - 3.278V_S^2 + 0.155V_S^3\right) + \left(1 - \frac{\theta}{90^\circ}\right)\left(-458713.785 + 34542.659V_S - 735.559V_S^2 + 4.804V_S^3\right). \tag{9}$$

5.2. Accident Risk Assessment. According to the data obtained in the tests, combined with the HIC security threshold introduced in Section 3.1, the data with $\mathrm{HIC} \le 1$ were screened out and classified as a separate group, and the risk level was determined as level I. The remaining 183 groups of data were numbered according to the HIC value from small to large, and the HIC ordered sample was generated, which was denoted as x_i ($i = 1, 2, \ldots, 183$).

According to the specific implementation steps of Fisher's optimal segmentation algorithm introduced in Section 3.2, this study uses MATLAB to write the algorithm code, calculates the class diameter and minimum error function of the HIC ordered samples, and draws the variation curve of the minimum error function with the classification number k, as shown in Figure 11.

As shown in Figure 11, when $k = 3$ and 4, the curvature of the minimum error function curve changes significantly. To further determine the optimal classification number, the minimum error function ratio $\beta(k)$ between adjacent classification numbers is calculated as shown in Table 12.

According to Table 12, $\beta(4)$ is greater than $\beta(3)$, so $k = 4$ is the optimal classification number. In addition, the classification numbers corresponding to the optimal classification of ordered samples can be obtained from Table 6, and

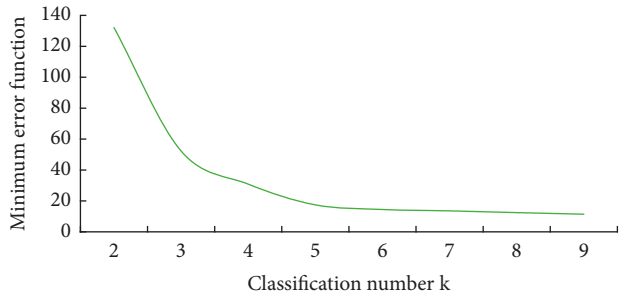

Figure 11: Relationship between the minimum error function and the classification number.

Table 12: Classification results.

k	Minimum error function	Classification	β value
2	132.125	{1~117} {118~183}	-
3	52.271	{1~117} {118~171} {172~183}	1.69
4	30.856	{1~64} {65~117} {118~171} {172~183}	1.77
5	17.451	{1~64} {65~94} {95~117} {118~171} {172~183}	-

Table 13: Risk evaluation standards for vehicle-pedestrian accidents.

Accident risk level	HTC threshold	Pedestrian injury level
Class I	≤1000	Mild or moderate
Class II	(1000, 5216]	Heavier
Class III	(5216, 20084]	Severe
Class IV	(20084, 144763]	Critical
Class V	>144763	Extreme

then the corresponding HIC index threshold can be determined. Based on the above research results in combination with the AIS injury classification standard (as shown in Table 1), the automobile and pedestrian accident risk classification evaluation method is presented, as shown in Table 13.

6. Case Analysis

To evaluate the effectiveness of the accident risk classification evaluation method proposed in this paper, 50 typical vehicle-pedestrian accidents are selected for verification (as shown in Table 14), including 20 short-head automobile accidents, 19 high-head automobile accidents, and 11 flat-head automobile accidents. First, according to the information of each accident case, combined with models (7)–(9) fitted in Section 5.1, the HIC value corresponding to each accident is calculated, and then the accident risk level is determined according to Table 13. Finally, the evaluation method of automobile pedestrian accident risk classification is verified using the actual injury level of pedestrians. Among them, the actual injury level of pedestrians is evaluated using the trauma scoring system Version 3.0 according to the injury report issued by a hospital or medical examiner.

It can be seen from the evaluation results in Table 14 that the risk level corresponding to 5 accidents calculated using the accident risk evaluation method proposed in this paper is not consistent with the actual pedestrian injury level, namely, cases 22, 30, 39, 43, and 46, with an error rate of 10%. Considering that the error rate cannot accurately measure the degree of error classification of accident risk using risk assessment methods, this paper proposes a new index to evaluate the accuracy of accident risk assessment methods, namely, the error classification degree α, as shown in formula (10). According to formula (10), the degree of error classification is 2.59%, which is within the acceptable range, thus verifying the accuracy of the risk assessment method of automobile and pedestrian accidents proposed in this paper.

$$\alpha = \frac{\sum_{i=1}^{n} \eta_{ij} \mathrm{FN}_{ij}}{\mathrm{TN} + \sum_{i=1}^{n} \eta_{ij} \mathrm{FN}_{ij}} \quad i \neq j, \tag{10}$$

where TN is the number of correctly graded cases; FN_{ij} is the number of cases of the i pedestrian injury level misclassified at the j risk level; n is the number of risk levels divided; and η_{ij} is the corresponding weight coefficient; the calculation formula is

$$\eta_{ij} = \frac{|j - i|}{n}. \tag{11}$$

The research results of this paper can not only provide a scientific judgment basis for accident analysis and treatment but also provide a reference for speed limit management. For example, in the absence of effective accident scene evidence and video surveillance, a judicial appraisal institution can determine the corresponding HIC range from Table 13 according to the pedestrian injury level in the accident. Then, combined with the car accident and collision shape, using the optimal fitting model, this research deduced the range of speed in a trouble-causing car accident, and the calculation result is helpful to a traffic police department responsible for both sides of the accident. Similarly, for sections with a high incidence of vehicle-pedestrian accidents, the maximum allowable speed that can guarantee HIC≤1000 (the accident risk is grade I) can also be deduced based on the optimal model for different models to formulate the speed management scheme.

Table 14: Case validation.

Number	Accident speed (km/h)	Collision form	Model	Actual pedestrian injury level	HIC	Accident risk level
1	75	Rear-end collision	Short head type	Severe	8334	III
2	84	Side collision	Short head type	Heavier	4183	II
3	50	Rear-end collision	Short head type	Heavier	2208	II
4	47	Side collision	Short head type	Mild	121	I
5	56	Side collision	Short head type	Moderate	407	I
6	70	Side collision	Short head type	Heavier	1604	II
7	82	Side collision	Short head type	Heavier	3710	II
8	95	Side collision	Short head type	Severe	7521	III
9	34	Rear-end collision	Short head type	Moderate	624	I
10	51	Rear-end collision	Short head type	Heavier	2356	II
11	49	Rear-end collision	Short head type	Heavier	2066	II
12	80	Rear-end collision	Short head type	Severe	10296	III
13	85	Rear-end collision	Short head type	Severe	12558	III
14	44	Side collision	Short head type	Mild	81	I
15	48	Side collision	Short head type	Mild	140	I
16	66	Side collision	Short head type	Heavier	1144	II
17	71	Rear-end collision	Short head type	Severe	6964	III
18	77	Rear-end collision	Short head type	Severe	9084	III
19	89	Side collision	Short head type	Severe	5539	III
20	40	Side collision	Short head type	Mild	54	I
21	37	Rear-end collision	High head type	Mild	320	I
22	69	Rear-end collision	High head type	Heavier	6635	III
23	76	Rear-end collision	High head type	Severe	9225	III
24	99	Rear-end collision	High head type	Critical	20784	IV
25	105	Rear-end collision	High head type	Critical	24570	IV
26	73	Rear-end collision	High head type	Severe	8062	III
27	62	Rear-end collision	High head type	Heavier	4480	II
28	55	Side collision	High head type	Moderate	465	I
29	78	Rear-end collision	High head type	Severe	10044	III
30	74	Side collision	High head type	Severe	1449	II
31	55	Side collision	High head type	Moderate	465	I
32	53	Side collision	High head type	Moderate	403	I
33	30	Side collision	High head type	Mild	46	I
34	50	Side collision	High head type	Moderate	323	I
35	47	Rear-end collision	High head type	Heavier	1321	II
36	49	Rear-end collision	High head type	Heavier	1627	II
37	51	Side collision	High head type	Moderate	348	I
38	63	Side collision	High head type	Moderate	782	I
39	65	Side collision	High head type	Heavier	882	I
40	76	Rear-end collision	Flat head type	Critical	26780	IV
41	72	Side collision	Flat head type	Extreme	186242	V
42	58	Side collision	Flat head type	Extreme	170884	V
43	48	Side collision	Flat head type	Severe	165750	V
44	69	Side collision	Flat head type	Extreme	182041	V
45	78	Side collision	Flat head type	Extreme	196299	V
46	34	Rear-end collision	Flat head type	Severe	54247	IV
47	83	Rear-end collision	Flat head type	Critical	87926	IV
48	88	Rear-end collision	Flat head type	Extreme	158663	V
49	97	Rear-end collision	Flat head type	Extreme	355531	V
50	77	Rear-end collision	Flat head type	Critical	33126	IV

In addition, because the collision between an automobile hood and pedestrians easily causes fatal injuries, the space between the hood and various parts in the engine compartment can be considered in the design of a vehicle to ensure that the hood has enough deformation space for cushioning the impact force. Of course, improving active safety technology and road design will also play a role in protecting pedestrians. For example, by capturing the movement characteristics of pedestrians and vehicles, computer vision technology can be used to predict potential accidents between pedestrians and vehicles at signalized intersections, which can be used for the development of collision warning systems in connected vehicle environments [28].

7. Conclusion

Based on accident case investigations, this research uses PC-Crash to carry out vehicle-pedestrian collision simulation tests under different accident patterns, revealing the significant risk factors (i.e., vehicle speed, collision angle, and vehicle type) affecting pedestrian injury. For different vehicle types, a multivariate relationship model between the HIC, vehicle speed, and collision angle is built, and a classification evaluation method of vehicle-person accident risk based on the HIC is proposed and verified. Research results of this paper can promote pedestrian injury reduction in accidents and provide guidance on speed limit measures.

Although this research has made some innovative achievements, there are still the following deficiencies. For example, this paper only selects Chinese 90^{th}% adult men as representatives for the crash tests, without considering adult women, children, the elderly, and other groups. As a result, the factors involved in the proposed accident risk evaluation method are not sufficiently comprehensive and ignore factors of pedestrian gender or pedestrian age that may affect the accident risk. In addition, the values of the variables were relatively low in the test process, and there was no relevant research on occupant movement. Therefore, follow-up research work can consider increasing the value range of variables and combining PC-Crash and MADYMO software to conduct in-depth research on the injury mechanisms of different pedestrian groups and the response of drivers in the car before and after the accident.

Data Availability

The data used to support the findings of this study are available from the corresponding author upon request.

Conflicts of Interest

The authors declare that they have no conflicts of interest.

Acknowledgments

This study was supported by the National Nature Science Foundation of Guangxi Province (Nos. 2022GXNSFBA035640, 2019GXNSFBA245050, and 2019JJB160047), the Guangxi University Young and Middle-aged Teachers Scientific Research Basic Ability Improvement Project (2022KY0193), the Guangxi Science and Technology Base and Talent Special Project (Nos. AD20159035 and AD22035153), and the Fund for Less-developed Regions of the National Natural Science Foundation of China (No. 71861006).

References

[1] Traffic Management Bureau of the Ministry of Public Security, *Road Traffic Accident Statistical Annual Report*, OECD, Beijing, China, 2021.

[2] H. Pritz, C. Hassler, J. Herridge, and E. Weis, "Experimental study of pedestrian injury minimization through vehicle design," in *Proceedings of the 19 Th Stapp Car Crash Conference*, pp. 725–751, SAE Warrendale PA, California, USA, November 1975.

[3] H. Cheng and A. L. Rizer, *Articulated Total Body Model Version V User's Manual*, pp. 637–648, United States Air Force Research Laboratory, USA, 1998.

[4] R. R. Mchenry, "Analysis of the dynamics of automobile passenger restraint systems," in *Proceedings of the 7th Stapp Car Crash Conference*, pp. 420–431, California, USA, 1963.

[5] H. Appel, G. Sturtz, and L. Gotzen, "Influence of impact speed and vehicle parameter on injuries of children and adults in pedestrian accidents," in *Proceedings of the 2nd IRCOBI Conference*, pp. 83–100, Hong Kong, China, September 1975.

[6] D. Severy and H. Brink, "Auto-pedestrian collision experiments," *SAE Transactions*, vol. 75, pp. 323–371, 1967.

[7] Y. Matsui, H. Ishikawa, and A. Sasaki, "Proposal of injury risk curves for evaluating pedestrian femur/pelvis injury risk using EEVC upper legform impactor based on accident reconstruction," *International Journal of Crashworthiness*, vol. 11, no. 2, pp. 97–104, 2006.

[8] R. Cheng, Y. Pan, and T. Wang, "A design method for the roadside clear zone based on accident simulation analysis," *Mathematical Problems in Engineering*, vol. 202116 pages, Article ID 2605095, 2021.

[9] G. Cheng, R. Cheng, Y. Pei, and L. Xu, "Probability of roadside accidents for curved sections on highways," *Mathematical Problems in Engineering*, vol. 2020, Article ID 9656434, 18 pages, 2020.

[10] J. Mandelík and M. Bundzel, "Application of neural network in order to recognise individuality of course of vehicle and pedestrian body contacts during accidents," *International Journal of Crashworthiness*, vol. 24, no. 2, pp. 221–234, 2019.

[11] S. Xu, X. Jin, C. Qin, and X. Chai, "Personalized customization method of hybrid human model for pedestrian-vehicle accident reconstruction," *Journal of Mechanics in Medicine and Biology*, vol. 21, no. 02, Article ID 2150009, 2021.

[12] D. Grindle, W. Pak, B. Guleyupoglu et al., "A detailed finite element model of a mid-sized male for the investigation of traffic pedestrian accidents," *Proceedings of the Institution of Mechanical Engineers - Part H: Journal of Engineering in Medicine*, vol. 235, no. 3, pp. 300–313, 2021.

[13] P. Panday, A. Vikram, A. Chawla, and S. Mukherjee, "Prediction of lower extremity injuries in car-pedestrian crashes – real-world accident study," *Traffic Injury Prevention*, vol. 22, no. 2, pp. 173–176, 2021.

[14] M. Lalwala, A. Chawla, P. Thomas, and S. Mukherjee, "Finite element reconstruction of real-world pedestrian accidents using thums pedestrian model," *International Journal of Crashworthiness*, vol. 25, no. 4, pp. 360–375, 2020.

[15] S. Zhu, "Analyse vehicle–pedestrian crash severity at intersection with data mining techniques," *International Journal of Crashworthiness*, vol. 5, no. 26, pp. 1–9, 2021.

[16] A. Sheykhfard, F. Haghighi, T. Nordfjærn, and M. Soltaninejad, "Structural equation modelling of potential risk factors for pedestrian accidents in rural and urban roads," *International Journal of Injury Control and Safety Promotion*, vol. 28, no. 1, pp. 46–57, 2021.

[17] N. Kamboozia, M. Ameri, and S. M. Hosseinian, "Statistical analysis and accident prediction models leading to pedestrian injuries and deaths on rural roads in Iran," *International Journal of Injury Control and Safety Promotion*, vol. 27, no. 4, pp. 493–509, 2020.

[18] S. Park and D. Ko, "A multilevel model approach for investigating individual accident characteristics and neighborhood environment characteristics affecting pedestrian-vehicle

crashes," *International Journal of Environmental Research and Public Health*, vol. 17, no. 9, p. 3107, 2020.

[19] D. Lasota, A. Al-Wathinani, P. Krajewski, K. Goniewicz, and W. Pawlowski, "Alcohol and road accidents involving pedestrians as unprotected road users," *International Journal of Environmental Research and Public Health*, vol. 17, no. 23, pp. 8995–95, 2020.

[20] J. Hasani, S. Erfanpoor, A. Rajabi et al., "Spatial analysis of mortality rate of pedestrian accidents in Iran during 2012–2013," *Traffic Injury Prevention*, vol. 20, no. 6, pp. 636–640, 2019.

[21] M. Jamali-Dolatabad, H. Sadeghi-Bazargani, and P. Sarbakhsh, "Predictors of fatal outcomes in pedestrian accidents in Tabriz Metropolis of Iran: application of pls-da method," *Traffic Injury Prevention*, vol. 20, no. 8, pp. 873–879, 2019.

[22] C. Feng, A. Duan, J. Qiu et al., "Investigation of head injuries suffered by pedestrians in traffic accidents via videos," *International Journal of Crashworthiness*, vol. 25, no. 6, pp. 680–688, 2020.

[23] Y. Matsui and S. Oikawa, "Situational characteristics of fatal pedestrian accidents involving vehicles traveling at low speeds in Japan," *Traffic Injury Prevention*, vol. 20, no. sup1, pp. 1–6, 2019.

[24] Editorial Department of China Journal of Highway and Transport, "Review on China's automotive engineering research process: 2017," *China Journal of Highway and Transport*, vol. 30, no. 6, pp. 1–197, 2017.

[25] G. Cheng, R. Cheng, Y. Pei, L. Xu, and W. Qi, "Severity assessment of accidents involving roadside trees based on occupant injury analysis," *PLoS One*, vol. 15, no. 4, Article ID e0231030, 2020.

[26] G. Cheng, R. Cheng, L. Xu, and W. Zhang, "Risk assessment of roadside accidents based on occupant injuries analysis," *Journal of Jilin University (Engineering and Technology Edition)*, vol. 51, no. 3, pp. 875–885, 2021.

[27] D. Liu, Y. Li, H. Zhao, and X. Zhu, "Relativity analysis of pedestrian head injuries and the headform to bonnet top test method," *Journal of Highway and Transportation Research and Development*, vol. 2004, no. 1, pp. 98–101, 2004.

[28] S. Zhang, M. Abdel-Aty, Y. Wu, and O. Zheng, "Modeling pedestrians' near-accident events at signalized intersections using gated recurrent unit (GRU)," *Accident Analysis & Prevention*, vol. 148, Article ID 105844, 2020.

Hindawi
Mathematical Problems in Engineering
Volume 2022, Article ID 5482290, 13 pages
https://doi.org/10.1155/2022/5482290

Research Article

Event-Triggered Fault-Tolerant Control for Nonlinear Networked Control Systems

Xiaoyu Zhou, Xia Liu, and Lu Wang

School of Electrical Engineering and Electronic Information, Xihua University, Chengdu 610039, China

Correspondence should be addressed to Xia Liu; xliu_uestc@yahoo.com

Received 2 July 2022; Accepted 28 July 2022; Published 25 August 2022

Academic Editor: Chuan Li

This paper addresses the communication congestion and actuator fault in a nonlinear networked control system. A weighted average event-triggered mechanism adopted the weighted average of data packets is proposed to alleviate the communication congestion and save the network communication resources. Meanwhile, based on the system state estimation and fault estimation obtained by a state-fault observer, a fault-tolerant controller is designed to compensate and reduce the influence of fault and nonlinear factors in the networked control systems. The stability of the closed-loop system is proved by the Lyapunov–Kroasovskii theory, and the gains of the observer and controller are obtained by linear matrix inequalities. The feasibility of the proposed scheme is verified by the networked motor control system. The proposed weighted average event-triggered fault-tolerant control scheme can reduce the data transmission without affecting system performance. Meanwhile, it not only has fault-tolerant control performance but also reduces the influence of nonlinear factors on the system output.

1. Introduction

In recent decades, networked control systems (NCSs) have gradually attracted considerable attentions. Compared with conventional control systems with point-to-point wired communication, NCSs have more advantages. For example, the introduction of the network can reduce the complexity and cost of the control systems and improve the reliability and scalability of the control systems. Therefore, NCSs have been widely applied in the industrial process, automatic control, robotics, aircraft, and unmanned technology [1–3]. Nevertheless, some unfavorable factors also unavoidably appear in NCSs, such as communication congestion, actuator fault, nonlinear factors, network-induced delay, and so on, which inevitably affects the control performance [4–6].

Due to limited communication bandwidth and imperfect communication link, the communication congestion may appear in NCSs [7–9]. In order to alleviate the communication congestion and save the network communication resources, the event-triggered mechanism is usually adopted in NCSs [10–13]. Different from the conventional time-triggered sampling, the event-triggered mechanism is based on data sampling. Therefore, an event-triggered mechanism can improve the efficiency of data transmission in the communication and calculation of NCSs. In [14], an adaptive event-triggered scheme was designed to alleviate the communication congestion. In [15], a self-triggered and event-triggered mixed sampling scheme was proposed to reduce the numbers of transmitted data packets in wireless NCSs. In order to get better quality of service for network communication, a hybrid method of random switching based on time-triggered and event-triggered was introduced in [16]. Nevertheless, the possible actuator fault in NCS is ignored in [14–16].

Besides communication congestion, actuator fault is inevitable in practical NCSs which decreases the system performance. Therefore, the fault-tolerant control (FTC) of NCSs as well as event-triggered mechanism is widely studied. In [17], an adaptive event-triggered mechanism was proposed and a fault-tolerant controller based on the triggered output data was designed. In [18], a sliding mode fault-tolerant controller for NCSs was proposed under a dynamic event-triggered mechanism to ensure that the trajectories of the system can reach the sliding surface. In [19], an

impulsive FTC was designed based on the estimated fault and an integral-based event-triggered mechanism was designed to alleviate communication congestion. In [20], a fault-tolerant controller based on an adaptive memory-based event-triggered mechanism was proposed to compensate for the influence of fault according to the fault estimation. In [21], based on the system state and fault estimation, a fault-tolerant controller was designed to compensate for the fault and the event-triggered mechanism was adopted to save communication resources. However, the NCSs considered in [17–21] are linear and the influence of nonlinear factors is ignored.

Along with communication congestion and possible actuator fault, the modeling of NCSs is often accompanied with some complex nonlinear factors in practice [22–24], such as the nonlinear coupling relationship among different nodes in complex dynamic networks [25] and the communication topology structure of nonlinear multiagent systems [26]. Therefore, the research of nonlinear NCSs has further significance. In [27], a resilient event-triggered mechanism was developed, and the sufficient conditions were constructed to ensure that the switched control strategy subjected to actuator fault and nonlinear factors was exponentially stable. In [28], a period event-triggered sampling scheme was designed, and an FTC was proposed for nonlinear NCSs to guarantee its stability under the actuator fault. In [29], an adaptive event-triggered communication scheme was adopted to save the network communication resources by adjusting event-triggered threshold, and a state feedback controller was designed for nonlinear NCSs under fault. In [30], an event-based adaptive FTC using a fuzzy approximation mechanism was proposed for the nonlinear system, which could also be applied to NCSs. In [31], an adaptive event-triggered mechanism with an adjustable triggering threshold was proposed, and an FTC with stochastic event-driven actuator scheduling was investigated for nonlinear NCSs. However, some unexpected triggered events can be further avoided in [27–31].

Inspired by the discussions above, in this paper, a weighted average event-triggered fault-tolerant control scheme is proposed for nonlinear NCSs subjected to communication congestion and actuator fault. The main contributions of this paper are as follows:

(1) Different from the conventional event-triggered mechanism, the weighted average event-triggered mechanism (WAETM) considers the weighted average of data packets, which can further alleviate the communication congestion and save the network communication resources.

(2) Based on the WAETM a state-fault observer is designed to obtain the system state estimation and fault estimation, which can guarantee the asymptotically stability of the observation error dynamic system.

(3) With the system state estimation and fault estimation, a fault-tolerant controller is designed, which can compensate for the influence of fault and reduce the influence of nonlinear factors in NCSs.

The remainder of this paper is structured as follows. The model of nonlinear NCSs is presented in Section 2. The design of the WAETM, state-fault observer, and fault-tolerant controller are presented, and the stability of the closed-loop system is proved in Section 3. The feasibility of the weighted average event-triggered FTC scheme for nonlinear NCSs is demonstrated by the networked motor control system in Section 4.

Notations: the following notations are adopted in this paper. I denotes the identity matrix with an appropriate dimension. For matrix B, its inverse and transpose matrices are denoted by $B^{\dagger}$ and B^{T}, respectively. 0 denotes zero matrix. $\mathbf{R}^{n}$ denotes the n-dimension Euclidean space and $\mathbf{R}^{n\times n}$ denotes the $n\times n$ matrix. $\{*\}$ denotes the symmetric term in a symmetric block matrix.

2. Problem Statement

The model of nonlinear NCSs with actuator fault is as follows:

$$\begin{cases} \dot{x}(t) = Ax(t) + Bu(t) + B_f f(t) + F\rho(x(t), t), \\ y(t) = Cx(t), \end{cases} \tag{1}$$

where $x(t) \in \mathbf{R}^{n}$ is the system state vector, $u(t) \in \mathbf{R}^{m}$ is the system control input, and $y(t) \in \mathbf{R}^{r}$ is the system measured output, $f(t) \in \mathbf{R}^{m}$ is the actuator fault, $\rho(x(t), t) = [\rho_1(x_1(t), t), \ldots, \rho_n(x_n(t), t)]^{T}$ is the nonlinear function, $A \in \mathbf{R}^{n\times n}, B \in \mathbf{R}^{n\times m}, C \in \mathbf{R}^{r\times n}, B_f \in \mathbf{R}^{n\times m}, F \in \mathbf{R}^{n\times n}$ are the system parameter matrices with appropriate dimensions.

Assumption 1 (See [32, 33]). It is assumed that the nonlinear function $\rho(x(t), t)$ is continuous and bounded, and satisfies Lipschitz conditions. Therefore, the following condition is satisfied

$$\left\|\rho(x_1(t), t) - \rho(x_2(t), t)\right\| \le \delta\left\|x_1(t) - x_2(t)\right\|, \tag{2}$$

where δ is the Lipschitz constant.

Assumption 2. Assume that the derivative of the fault is norm-bounded, i.e. $\|\dot{f}(t)\| \le f_{\Delta}$, where f_{Δ} is a constant.

3. Design of Weighted Average Event-Triggered Fault-Tolerant Control

The proposed weighted average event-triggered FTC scheme is shown in Figure 1. In order to save the network communication resources in nonlinear NCSs, a WAETM is designed to reduce the measured output data from $y(t)$ to $y(t_k h)$. The zero-order holder ZOH guarantees the continuity of the successfully triggered data packet $\tilde{y}(t)$ within the holding time-interval. The state-fault observer is designed to obtain the real-time system state estimation $\hat{x}(t)$ and fault estimation $\hat{f}(t)$. Finally, the fault-tolerant controller $u(t)$ is designed based on the system state estimation and fault estimation to compensate and reduce the influence caused by the fault and nonlinear factors.

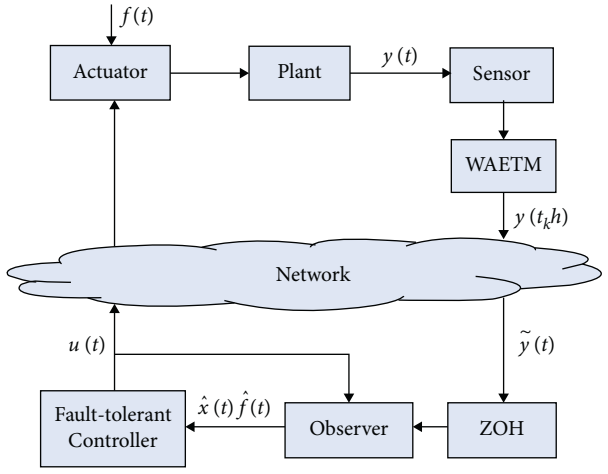

Figure 1: Weighted average event-triggered FTC scheme.

3.1. WAETM. Event-triggered mechanism is an effective way to alleviate the communication congestion and save the network communication resources. However, the conventional event-triggered mechanism depends on the difference between the values of the latest released data packet and the current sampling data packet. The conventional event-triggered mechanism is [21].

$$t_{k+1}h = t_k h + \min_{l\in\mathbb{N}^+}\left\{lh \middle| e_c^T(t)\Omega e_c^T(t) > \sigma y^T(t_k h + lh)\Omega y(t_k h + lh)\right\}, \tag{3}$$

where $t_k h$ represents the release instant, t_k is a positive integer, and h is the sampling period. l denotes the interval time between the latest triggered instant and the next triggered instant, σ is a constant, Ω is the constant weighted matrix, and $e_c(t) = y(t_k h) - y(t_k h + lh)$.

In order to further decrease the triggered data error and save the network communication resources, the WAETM is designed as follows:

$$\Psi = \left\{l \middle| e^T(t)\Omega e(t) - \sigma\overline{y}^T(t_k h)\Omega\overline{y}(t_k h) + \phi\sigma\left[\overline{y}^T(t_k h)\Omega e(t) + e^T(t)\Omega\overline{y}^T(t_k h)\right] \le 0\right\}, \tag{4}$$

where Ψ denotes a set of events satisfying the event trigger condition, $\overline{y}(t_k h) = [t_k h y(t_k h) + (t_k h + lh)y(t_k h + lh)]/(2t_k h + lh)$ denotes the weighted average value between the latest released data packet and the current sampling data packet, $e(t) = y(t_k h) - \overline{y}(t_k h)$ denotes the difference between the latest released data packet and the weighted average data packet, and ϕ is a constant.

Remark 1. Compared with the conventional event-triggered mechanism (2), the proposed WAETM (3) can decrease the triggered data error $e(t)$, avoiding unexpected triggered events. Meanwhile, the item $\phi\sigma[\overline{y}^T(t_k h)\Omega e(t) + e^T(t)\Omega\overline{y}^T(t_k h)]$ in the WAETM (3) contains a triggered data packet $y(t_k h)$. Therefore, the controller can obtain data packets from the network even when the system is subjected to others noises or disturbances. In fact, the WAETM in (3) can be converted into the conventional event-triggered mechanism in [21] when $\phi = 0$.

The release instant of WAETM is denoted as $t_{k+1}h = t_k h + (l_M + 1)h$, where $l_M = \max\{l|l \in \Psi\}$. When the data packets are successfully transmitted to the observer, the system measured output can be written as follows:

$$\widetilde{y}(t) = y(t_k h), \quad t \in [t_k h + \tau_k, t_{k+1}h + \tau_{k+1}), \tag{5}$$

where $\widetilde{y}(t)$ denotes the data successfully transmitted at the triggered instant and τ_k is the time delay.

Considering that the data packets transmitted by the WAETM are subjected to time delay $\tau_k = j_k - t_k h$, where j_k represents the instant when the data packets arrive at the ZOH. The ZOH deals with the data packets out-of-sequence and guarantees the continuity of control input within the holding time-interval. The subintervals are defined as follows:

$$I = \begin{cases} I_1 = [j_k, j_k + h), \\ I_2 = [j_k + h, j_k + 2h), \\ \vdots \\ I_{\overline{n}_k} = [j_k + (\overline{n}_k - 1)h, j_{k+1}), \end{cases} \tag{6}$$

where $\overline{n}_k = \min\{l|j_k + (l-1)h \ge j_{k+1}\}$, and the time delay function can be written as follows:

$$\tau(t) = \begin{cases} t - t_k h, & t \in I_1, \\ t - (t_k + 1)h, & t \in I_2, \\ \vdots \\ t - [t_k + (j_k - 1)]h, & t \in I_{\overline{n}_k}, \end{cases} \tag{7}$$

where $0 \le \tau(t) \le \tau_M$, $\dot{\tau}(t) \le \tau_\Delta$, τ_M is the maximum value of the $\tau(t)$, and τ_Δ is a constant. Then the error function of ZOH can be expressed as follows:

$$e_y(t) = \begin{cases} y(t_k h) - y(t_k h), & t \in I_1, \\ y(t_k h) - y((t_k + 1)h), & t \in I_2, \\ \vdots \\ y(t_k h) - y(t_k h + (\overline{n}_k - 1)h)), & t \in I_{\overline{n}_k}, \end{cases} \tag{8}$$

which implies that

$$\widetilde{y}(t) = e_y(t) + y(t - \tau(t)), \quad t \in [j_k, j_{k+1}]. \tag{9}$$

3.2. State-Fault Observer. According to the data packets $\widetilde{y}(t)$ successfully transmitted by the WAETM, the state-fault observer is designed as follows:

$$\begin{cases} \dot{\widehat{x}}(t) = A\widehat{x}(t) + Bu(t) + B_f\widehat{f}(t) + F\rho(\widehat{x}(t),t) + L(\widetilde{y}(t) - \widehat{y}(t-\tau(t))), \\ \dot{\widehat{f}}(t) = G\widehat{f}(t) + H(\widetilde{y}(t) - \widehat{y}(t-\tau(t))), \\ \widehat{y}(t) = C\widehat{x}(t), \end{cases} \tag{10}$$

where $\widehat{x}(t) \in \mathbf{R}^n$, $\widehat{y}(t) \in \mathbf{R}^r$, $\widehat{f}(t) \in \mathbf{R}^m$, $\rho(\widehat{x}(t),t) = [\rho_1(\widehat{x}_1(t),t),\ldots,\rho_n(\widehat{x}_n(t),t)]^T$ are the system state estimation vector, system measured output estimation, fault estimation signal, and nonlinear function estimation, respectively. L and H are observer gain matrices to be designed later.

The estimation error of system state is defined as $e_x(t) = x(t) - \widehat{x}(t)$, the estimation error of fault is defined as $e_f = f(t) - \widehat{f}(t)$, and the estimation error of nonlinear function is defined as $g(e_x(t)) = \rho(x(t)) - \rho(\widehat{x}(t))$. Then, the estimation error of system state and fault can be respectively rewritten as follows:

$$\begin{aligned} \dot{e}_x(t) &= Ae_x(t) + Fg(e_x(x)) + B_f e_f(t) - Le_y(t) \\ &\quad - LCe_x(t-\tau(t)), \\ \dot{e}_f(t) &= (1-G)f(t) + Ge_f(t) - He_y(t) \\ &\quad - HCe_x(t-\tau(t)). \end{aligned} \tag{11}$$

Define $\xi(t) = [e_x(t)e_f(t)]^T$, then the observation error dynamic system can be given as follows:

$$\dot{\xi}(t) = \overline{A}\xi(t) + \overline{B}\xi(t-\tau(t)) + \overline{L}e_y(t) + \overline{D}f(t) + \overline{F}g(e_x(t)), \tag{12}$$

where $\overline{A} = \begin{bmatrix} A & B_f \\ 0 & G \end{bmatrix}$, $\overline{B} = \begin{bmatrix} -LC & 0 \\ -HC & 0 \end{bmatrix}$, $\overline{L} = \begin{bmatrix} -L \\ -H \end{bmatrix}$, $\overline{D} = \begin{bmatrix} 0 \\ 1-G \end{bmatrix}$, $\overline{F} = \begin{bmatrix} F \\ 0 \end{bmatrix}$.

Up to now, we need some lemmas and definitions before proceeding the stability of observation error dynamic.

Lemma 1 (See [34]). For any positive definite constant matrix $Y \in \mathbf{R}^{n\times n}$, scalar $\alpha > 0$, and vector function $\dot{x}$: $[-\alpha, 0] \longrightarrow \mathbf{R}^n$, the following integration is defined:

$$-\alpha\int_{t-\alpha}^{t} \dot{x}^T(\theta)Y\dot{x}(\theta)d\theta \le \begin{bmatrix} x(t) \\ x(t-\alpha) \end{bmatrix}^T \begin{bmatrix} -Y & Y \\ * & -Y \end{bmatrix} \begin{bmatrix} x(t) \\ x(t-\alpha) \end{bmatrix}. \tag{13}$$

Definition 1 (See [35]). System (12) satisfies the H_∞ performance under initial condition, and the following performance index holds for all nonzero $f(t) \in L_2[0,\infty)$.

$$\int_0^\infty \xi^T(s)\xi(s)ds \le \lambda_1 \int_0^\infty f^T(s)f(s)ds\ , \lambda_1 > 0. \tag{14}$$

Theorem 1. *For given positive scalars h, τ_M, ϕ, σ, λ_1 and υ, there exists symmetric positive definite matrices $P > 0$, $R_1 > 0$, $R_2 > 0$, $R_3 > 0$, $G > 0$, $Q > 0$, and appropriate matrices M and Z such that the following condition holds.*

$$\Xi = \begin{bmatrix} \Xi_{11} & \Xi_{12} & \Xi_{13} & Q & M^T\overline{F} & Z & M^T\overline{D} \\ * & \Xi_{22} & M^T\overline{B} & 0 & M^T\overline{F} & Z & M^T\overline{D} \\ * & * & \Xi_{33} & 0 & 0 & \Xi_{36} & 0 \\ * & * & * & \Xi_{44} & 0 & 0 & 0 \\ * & * & * & * & -\upsilon I & 0 & 0 \\ * & * & * & * & * & -\Omega & 0 \\ * & * & * & * & * & * & -\lambda_1 I \end{bmatrix} < 0, \tag{15}$$

where $\Xi_{11} = R_1 + R_2 - \pi^2/4G - Q + M^T\overline{A}$, $\Xi_{12} = 2P - M^T + \overline{A}^T M^T$,

$$\begin{aligned} \Xi_{13} &= \frac{\pi^2}{4}G + \frac{\pi^2}{4}G^T + M^T\overline{B}, \\ \Xi_{22} &= \tau_M^2 G + \tau_M^2 Q, \\ \Xi_{33} &= \sigma C^T\Omega C + (1-\tau)R_2 - (1-\tau)R_1 - \frac{\pi^2}{4}G, \\ \Xi_{36} &= \phi\sigma\left(C^T\Omega + \Omega C\right), \\ \Xi_{44} &= -R_2 - R_3 - Q, \end{aligned} \tag{16}$$

then the observation error dynamic system (12) with the WAETM (4) is asymptotically stable. In addition, the state-fault observer gain matrices can be obtained by $\overline{L} = M^{-T}Z$.

Proof. Choose a Lyapunov–Krasovskii function as follows:

$$V_1(t) = V_{11}(t) + V_{12}(t) + V_{13}(t), \tag{17}$$

where

$$V_{11}(t) = \xi^T(t)P\xi(t) + \int_{t-\tau(t)}^{t} \xi^T(\theta)R_1\xi(\theta)\mathrm{d}\theta + \int_{t-\tau_M}^{t-\tau(t)} \xi^T(t)R_2\xi(t) + \int_{t-\tau_M}^{t} \xi^T(\theta)R_3\xi(\theta)\mathrm{d}\theta,$$

$$V_{12}(t) = \tau_M^2 \int_{i_k h}^{t} \dot{\xi}^T(\theta)G\dot{\xi}(\theta)\mathrm{d}\theta - \frac{\pi^2}{4}\int_{i_k h}^{t} [\xi(\theta) - \xi(i_k h)]^T G[\xi(\theta) - \xi(i_k h)]\mathrm{d}\theta, \tag{18}$$

$$V_{13}(t) = \tau_M \int_{t-\tau_M}^{t}\int_{r}^{t} \dot{\xi}^T(\theta)Q\dot{\xi}(\theta)\mathrm{d}\theta\mathrm{d}r.$$

The derivative of (17) is obtained as follows:

$$\begin{aligned}
\dot{V}_{11}(t) &= 2\xi^T(t)P\dot{\xi}(t) + \xi^T(t)R_1\xi(t) - (1-\tau)\xi^T(t-\tau(t))R_1\xi(t-\tau(t)) + (1-\tau)\xi^T(t-\tau(t)) \\
&\quad R_2\xi(t-\tau(t)) - \xi^T(t-\tau_M)R_2\xi(t-\tau_M) + \xi^T(t)R_3\xi(t) - \xi^T(t-\tau_M)R_3\xi(t-\tau_M), \\
\dot{V}_{12}(t) &= \tau_M^2\dot{\xi}^T(t)G\dot{\xi}(t) - \frac{\pi^2}{4}[\xi(t) - \xi(t-\tau(t))]^T G[\xi(t) - \xi(t-\tau(t))], \\
\dot{V}_{13}(t) &= \tau_M^2\dot{\xi}^T(t)Q\dot{\xi}(t) - \tau_M\int_{t-\tau_M}^{t} \dot{\xi}^T(\theta)Q\dot{\xi}(\theta)\mathrm{d}\theta.
\end{aligned} \tag{19}$$

According to Lemma 1, we can obtain the following equation:

$$-\tau_M\int_{t-\tau_M}^{t} \dot{\xi}^T(\theta)Q\dot{\xi}(\theta)\mathrm{d}\theta \le \begin{bmatrix} \xi(t) \\ \xi(t-\tau_M) \end{bmatrix}^T \begin{bmatrix} -Q & Q \\ * & -Q \end{bmatrix} \begin{bmatrix} \xi(t) \\ \xi(t-\tau_M) \end{bmatrix}. \tag{20}$$

Therefore, from (19) we can get the following equation:

$$\begin{aligned}
\dot{V}_1(t) &\le 2\xi^T(t)P\dot{\xi}(t) + \xi^T(t)\left[R_1 + R_3 - \frac{\pi^2}{4}G - Q\right]\xi(t) - \xi^T(t-\tau(t))\left[(1-\tau)R_2 - (1-\tau)R_1 - \frac{\pi^2}{4}G\right] \\
&\quad \cdot \xi(t-\tau(t)) + \xi^T(t-\tau_M)[-R_2 - R_3 - Q]\xi(t-\tau_M) + \dot{\xi}^T(t) \\
&\quad \cdot \left[\tau_M^2 G + \tau_M^2 Q\right]\dot{\xi}(t) + \xi^T(t)\left[\frac{\pi^2}{4}G + \frac{\pi^2}{4}G^T\right]\xi(t-\tau(t)) + \xi^T(t)Q\xi(t-\tau_M).
\end{aligned} \tag{21}$$

In addition, the WAETM (3) is equivalent to the following equation:

$$\begin{aligned}
e_y^T(t)\Omega e_y(t) &\le \sigma y^T(t-\tau(t))\Omega y(t-\tau(t)) + \phi\sigma\left[y^T(t-\tau(t))\Omega e_y(t) + e_y^T(t)\Omega y(t-\tau(t))\right] \\
&= \sigma\xi^T(t-\tau(t))C^T\Omega C\xi(t-\tau(t)) + \phi\sigma\left[\xi^T\left(t-\tau(t)C^T\Omega e_y(t) + e_y^T(t)\Omega C\xi(t-\tau(t)\right)\right].
\end{aligned} \tag{22}$$

It is worth noting that for any matrix M with appropriate dimensions, we have the following equation:

$$\left[\xi^T(t)M^T + \dot{\xi}^T(t)M^T\right]\left[-\dot{\xi}(t) + \overline{A}\xi(t) + \overline{B}\xi(t-\tau(t)) + \overline{L}e_y(t) + \overline{D}f(t) + \overline{F}g(e_x(t))\right] = 0. \tag{23}$$

According to Assumption 1, the nonlinear function $\rho(x(t),t)$ satisfies the Lipschitz condition, and for any positive number υ we have the following equation:

$$\upsilon\xi^T(t)\delta^2\xi(t) - \upsilon g^T(e_x(t))g(e_x(t)) \geq 0. \tag{24}$$

Define a new function as follows:

$$J_1(t) = \dot{V}_1(t) + \xi^T(t)\xi(t) - \lambda_1 f^T(t)f(t). \tag{25}$$

Integrating both sides of (25) under the zero initial condition gives us the following equation:

$$\int_0^t J_1(s)\mathrm{d}s = V_1(t) + \int_0^t \xi^T(s)\xi(s)\mathrm{d}s - \lambda_1\int_0^t f^T(s)f(s)\mathrm{d}s, \tag{26}$$

where $V_1(t) > 0$. Then according to Definition 1, we can obtain the following equation:

$$\int_0^t \xi^T(s)\xi(s)\mathrm{d}s \leq \lambda_1\int_0^t f^T(s)f(s)\mathrm{d}s. \tag{27}$$

Define a variable as $\varpi_1(t) = [\xi^T(t)\dot{\xi}^T(t)\xi^T(t-\tau(t))\ \xi^T(t-\tau_M)g^T(e(x))e_y^T(t)f^T(t)]$. Then according to (21) and (25) and (27), we can get the following equation:

$$\begin{aligned} J_1(t) &= \dot{V}_1(t) + \xi^T(t)\xi(t) - \lambda_1 f^T(t)f(t) \\ &\leq \varpi_1^T(t)\Xi\varpi_1(t). \end{aligned} \tag{28}$$

According to (15) and (28), $J_1(t) < 0$ when $\Xi < 0$. When $f(t) = 0$, $\dot{V}_1(t) < 0$. Therefore, the observation error dynamic system (12) is asymptotically stable with WAETM (3). The proof of Theorem 1 is completed. □

3.3. Fault-Tolerant Controller. With the system state estimation, fault estimation, and nonlinear function estimation obtained by the sate-fault observer, the fault-tolerant controller can be designed as follows:

$$u(t) = K\hat{x}(t) - B^{\dagger}B_f\hat{f}(t) - B^*\rho(\hat{x}(t)), \tag{29}$$

where K is the controller gain. The fault-tolerant controller consists of three terms. The first term $K\hat{x}(t)$ is a state feedback control, the second term $-B^{\dagger}B_f\hat{f}(t)$ is used to compensate the influence of faults, and the third term $-B^*\rho(\hat{x}(t))$ is used to reduce the influence of nonlinear factors.

Combining the fault-tolerant controller (28) and the state-fault observer (10), we can obtain the following equation:

$$\begin{aligned} \dot{\hat{x}}(t) &= A\hat{x}(t) + BK\hat{x}(t) - BB^{+}B_f\hat{f}(t) - BB^*\rho(\hat{x}(t)) + B_f\hat{f}(t) + F\rho(\hat{x}(t)) + L(\tilde{y}(t) - \hat{y}(t-\tau(t))) \\ &= (A+BK)\hat{x}(t) + (F - BB^*)\rho(\hat{x}(t)) + Le_y(t) + LCe_x(t-\tau(t)). \end{aligned} \tag{30}$$

According to (10) and (30), the overall closed-loop system can be written as follows:

$$\dot{\varepsilon}(t) = \widetilde{A}\varepsilon(t) + \widetilde{B}\varepsilon(t-\tau(t)) + \widetilde{L}e_y(t) + B_f e_f(t) + \widetilde{F}\varphi(\varepsilon(t)), \tag{31}$$

where $\varepsilon(t) = [\hat{x}^T(t)e_x^T(t)]^T$, $\varphi(\varepsilon(t)) = [\rho^T(\hat{x}(t))g(e_x^T(t))]^T$, and

$$\begin{aligned} \widetilde{A} &= \begin{bmatrix} A+BK & 0 \\ 0 & A \end{bmatrix}, \\ \widetilde{B} &= \begin{bmatrix} 0 & LC \\ 0 & -LC \end{bmatrix}, \\ \widetilde{L} &= \begin{bmatrix} L \\ -L \end{bmatrix}, \\ \widetilde{F} &= \begin{bmatrix} F - BB^* & 0 \\ F & 0 \end{bmatrix}. \end{aligned} \tag{32}$$

There needs a lemma before the subsequent discussion.

Lemma 2 (See [36]). For a fixed constant matrix Q with full column rank, the unknown matrix Y can be calculated by the following equality for any real matrix X, Y and N with appropriate dimensions:

$$Y = \left(Q^TXQ\right)^{-1}Q^TQN, \tag{33}$$

when the following condition satisfies the following equation:

$$XQY = QN. \tag{34}$$

Theorem 2. *For given positive scalars h, τ_M, ϕ, σ, λ_2 and μ, there exist symmetric positive definite matrices $P_1 > 0$, $S_1 > 0$, $S_2 > 0$, $S_3 > 0$, $H > 0$, $W > 0$. Then, suppose there exists matrix Λ, event-triggered weighted matrix $\Omega > 0$, and matrices M_1 and Θ with appropriate dimensions such that the following condition holds:*

$$\Pi = \begin{bmatrix} \prod_{11} & \prod_{12} & \prod_{13} & W & M_1^T\tilde{F} & M_1^T\tilde{L} & M_1^T B_f \\ * & \prod_{22} & M_1^T\tilde{B} & 0 & M_1^T\tilde{F} & M_1^T\tilde{L} & M_1^T B_f \\ * & * & \prod_{33} & 0 & 0 & \prod_{36} & 0 \\ * & * & * & \prod_{44} & 0 & 0 & 0 \\ * & * & * & * & -\mu I & 0 & 0 \\ * & * & * & * & * & -\Omega & 0 \\ * & * & * & * & * & * & -\lambda_2 I \end{bmatrix} < 0, \quad (35)$$

where $\prod_{11} = S_1 + S_2 - \pi^2/4H - W + M_1^T\tilde{A}$, $\prod_{12} = 2P_1 - M_1^T + \tilde{A}^T M_1^T$,

$$\begin{aligned} \prod_{13} &= \frac{\pi^2}{4}H + \frac{\pi^2}{4}H^T + M_1^T\tilde{B}, \\ \prod_{22} &= \tau_M^2 H + \tau_M^2 W, \\ \prod_{33} &= \sigma C^T \Omega C + (1-\tau)S_2 - (1-\tau)S_1 - \frac{\pi^2}{4}, \\ \prod_{36} &= \varphi\sigma\left(C^T\Omega + \Omega C\right), \\ \prod_{44} &= -S_2 - S_3 - W, \end{aligned} \quad (36)$$

then, the overall closed-loop system (31) is asymptotically stable under the WAETM with the controller gain designed as $K = (B^T\Theta B)^{-1}B^T B\Lambda$.

Proof. According to Lemma 2, if condition $\Theta BK = B\Lambda$ is satisfied, one can obtain that

$$K = \left(B^T\Theta B\right)^{-1}B^T B\Lambda, \quad (37)$$

whereafter, choose a Lyapunov-Krasovskii function as follows:

$$V_2(t) = V_{21}(t) + V_{22}(t) + V_{23}(t), \quad (38)$$

where

$$\begin{aligned} V_{21}(t) &= \varepsilon^T(t)P_1\varepsilon(t) + \int_{t-\tau(t)}^{t}\varepsilon^T(\theta)S_1\varepsilon(\theta)d\theta \\ &\quad + \int_{t-\tau_M}^{t-\tau(t)}\varepsilon^T(t)S_2\varepsilon(t) + \int_{t-\tau_M}^{t}\varepsilon^T(\theta)S_3\varepsilon(\theta)d\theta, \\ V_{22}(t) &= \tau_M^2\int_{i_k h}^{t}\dot{\varepsilon}^T(\theta)H\dot{\varepsilon}(\theta)d\theta - \frac{\pi^2}{4}\int_{i_k h}^{t}\left[\varepsilon(\theta) - \varepsilon(i_k h)\right]^T \\ &\quad \cdot H\left[\varepsilon(\theta) - \varepsilon(i_k h)\right]d\theta, \\ V_{23}(t) &= \tau_M\int_{t-\tau_M}^{t}\int_{r}^{t}\dot{\varepsilon}^T(\theta)W\dot{\varepsilon}(\theta)d\theta\, dr, \end{aligned} \quad (39)$$

and the derivative of (39) is obtained as follows:

$$\begin{aligned} \dot{V}_{21}(t) &= 2\varepsilon^T(t)P_1\dot{\varepsilon}(t) + \varepsilon^T(t)S_1\varepsilon(t) \\ &\quad - (1-\tau)\varepsilon^T(t-\tau(t))S_2\varepsilon(t-\tau(t)) + (1-\tau)\varepsilon^T(t-\tau(t))S_2\varepsilon(t-\tau(t)) \\ &\quad - \varepsilon^T(t-\tau_M)S_2\varepsilon(t-\tau_M) + \\ &\quad \varepsilon^T(t)S_3\varepsilon(t) - \varepsilon^T(t-\tau_M)S_3\varepsilon(t-\tau_M), \\ \dot{V}_{22}(t) &= \tau_M^2\dot{\varepsilon}^T(t)H\dot{\varepsilon}(t) - \frac{\pi^2}{4}[\varepsilon(t) - \varepsilon(t-\tau(t))]^T H[\varepsilon(t) - \varepsilon(t-\tau(t))], \\ \dot{V}_{23}(t) &= \tau_M^2\dot{\varepsilon}^T(t)W\dot{\varepsilon}(t) - \tau_M\int_{t-\tau_M}^{t}\dot{\varepsilon}^T(\theta)W\dot{\varepsilon}(\theta)\mathrm{d}\theta. \end{aligned} \quad (40)$$

According to Lemma 1, we can obtain the following equation:

$$-\tau_M\int_{t-\tau_M}^{t}\dot{\varepsilon}^T(\theta)W\dot{\varepsilon}(\theta)\mathrm{d}\theta \le \begin{bmatrix} \varepsilon(t) \\ \varepsilon(t-\tau_M) \end{bmatrix}^T \begin{bmatrix} -W & W \\ * & -W \end{bmatrix} \begin{bmatrix} \varepsilon(t) \\ \varepsilon(t-\tau_M) \end{bmatrix}. \quad (41)$$

Then, from (40) we can get the following equation:

$$\begin{aligned}\dot{V}_2(t) \le{}& 2\varepsilon^T(t)P_1\dot{\varepsilon}(t) + \varepsilon^T(t)\left[S_1 + S_3 - \frac{\pi^2}{4}H - W\right]\\ &\cdot \varepsilon(t) - \varepsilon^T(t-\tau(t))\left[(1-\tau)S_2 - (1-\tau)S_1 - \frac{\pi^2}{4}H\right]\\ &\cdot \varepsilon(t-\tau(t)) + \varepsilon^T(t-\tau_M)[-S_2 - S_3 - W]\varepsilon(t-\tau_M)\\ &+ \dot{\varepsilon}^T(t)\left[\tau_M^2 H + \tau_M^2 W\right]\dot{\varepsilon}(t) + \varepsilon^T(t)\left[\frac{\pi^2}{4}H + \frac{\pi^2}{4}H^T\right]\varepsilon(t-\tau(t)) + \varepsilon^T(t)W\varepsilon(t-\tau_M).\end{aligned} \tag{42}$$

Again, the WAETM (4) is equivalent to the following equation:

$$\begin{aligned}e_y^T(t)\Omega e_y(t) &\le \sigma y^T(t-\tau(t))\Omega y(t-\tau(t)) + \phi\sigma\left[y^T(t-\tau(t))\Omega e_y(t) + e_y^T(t)\Omega y(t-\tau(t))\right]\\ &= \xi^T(t-\tau(t))C^T\Omega C\xi(t-\tau(t)) + \phi\sigma\left[\xi^T(t-\tau(t)C^T\Omega e_y(t) + e_y^T(t)\Omega C\xi(t-\tau(t))\right].\end{aligned} \tag{43}$$

It is worth noting that for any matrix M_1 with appropriate dimension, we have the following equation:

$$\left[\varepsilon^T(t)M_1^T + \dot{\varepsilon}^T(t)M_1^T\right]\left[-\dot{\varepsilon}(t) + \widetilde{A}\varepsilon(t) + \widetilde{B}\varepsilon(t-\tau(t)) + \widetilde{L}e_y(t) + B_f e_f(t) + \widetilde{F}\varphi(\varepsilon(t))\right] = 0. \tag{44}$$

According to Assumption 1, the nonlinear function $\rho(x(t),t)$ satisfies the Lipschitz condition, and for any positive number μ we have the following equation:

$$\mu\varepsilon^T(t)\delta^2\varepsilon(t) - \mu\varphi^T(\varepsilon(t))\varphi(\varepsilon(t)) \ge 0. \tag{45}$$

Define a new variable as $\varpi_2(t) = [\varepsilon^T(t)\dot{\varepsilon}^T(t)\varepsilon^T(t-\tau(t))\ \varepsilon^T(t-\tau_M)\varphi^T(\varepsilon(x))e_y^T(t)e_f^T(t)]$. Then according to (42) and (45), we can get the following equation:

$$J_2(t) = \dot{V}_2(t) + \varepsilon^T(t)\varepsilon(t) - \lambda_2 e_f^T(t)e_f(t). \tag{46}$$

Similar to the proof of Theorem 1, we can obtain the following equation:

$$J_2(t) \le \varpi_2^T(t)\prod\varpi_2(t). \tag{47}$$

According to (47), for any small scalar $\beta > 0$ under the initial condition, the following inequality holds:

$$J_2(t) \le -\beta\|\varepsilon(t)\|^2. \tag{48}$$

According to (35) and (47), it is obvious that $J_2(t) < 0$when $\prod < 0$. Also, (48) indicates $\lim_{t\longrightarrow\infty}\|\varepsilon(t)\|^2 = 0$ and hence the closed-loop system (31) is asymptotically stable with WAETM (4). The proof of Theorem 2 is completed. □

4. Results

In this section, the networked motor control system shown in Figure 2 is adopted to verify the effectiveness of the proposed weighted average event-triggered FTC scheme. The mathematical model of the brushless direct current motor is

$$\begin{aligned}A &= \begin{bmatrix} 0 & 1.000 \\ -5.867 & -3.038 \end{bmatrix},\\ B &= \begin{bmatrix} 0.340 \\ 4.868 \end{bmatrix},\\ C &= [\,1\ \ 0\,],\\ F &= \begin{bmatrix} -0.818 & -1.65 \\ -0.2 & -0.02 \end{bmatrix},\\ B_f &= \begin{bmatrix} -4.811 \\ -25.852 \end{bmatrix}.\end{aligned} \tag{49}$$

The control input of the motor is the voltage value. The system measured output of the motor is the speed (r/min). The reference input function is set as $y_r(t) = 400\sin(t) + 1200$, and the nonlinear function is $\rho(x(t),t) = [40\ \sin(x(t))0]^T$. The delay is

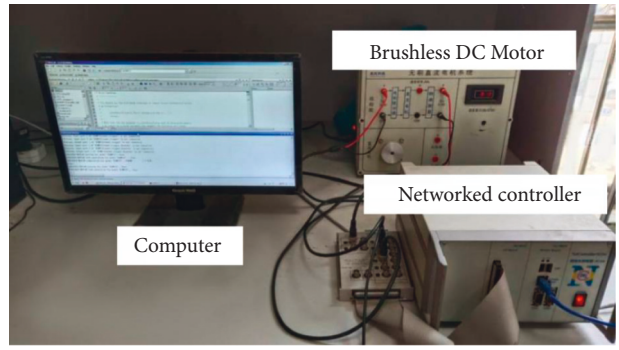

Figure 2: Brushless direct current networked motor control system.

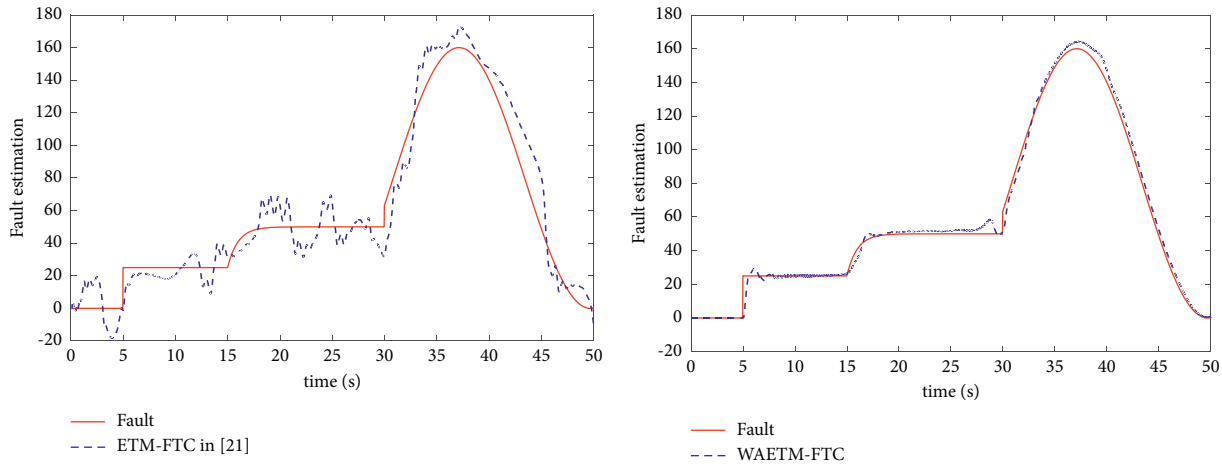

Figure 3: Fault estimation (a) ETM-FTC in [21]; (b) WAETM-FTC.

$\tau(t) = 0.2\sin(\pi t)$, and hence $\tau_M = 0.2$, $\tau_\Delta = 0.2$. In addition, parameters in the event-triggered mechanism are set as $\sigma = 0.0015$, and $\phi = 0.12$. The sampling time is $h = 0.02s$. The event-triggered weighted matrix here is set as $\Omega = I$.

According to Theorem 1 and Theorem 2, the gains of the state-fault observer and the fault-tolerant controller can be obtained as follows:

$$\begin{aligned} L &= \begin{bmatrix} 49.522 \\ -26.896 \end{bmatrix}, \\ H &= -10.982, \\ K &= \begin{bmatrix} -2.5 & -0.264 \end{bmatrix}. \end{aligned} \tag{50}$$

Other parameters of the state-fault observer and the fault-tolerant controller are

$$\begin{aligned} G &= 0.2, \\ B^{\dagger} &= \begin{bmatrix} 0.014 & 0.204 \end{bmatrix}, \\ B^{*} &= \begin{bmatrix} -0.271 & -0.232 \end{bmatrix}. \end{aligned} \tag{51}$$

Besides, the actuator fault signal is considered as follows:

$$f(t) = \begin{cases} 25, & 5 \le t < 15, \\ 50 - 25e^{(-t+15)}, & 15 \le t < 30, \\ 80 + 80\cos(0.1(t-30)), & 30 \le t < 50, \\ 0, & \text{otherwise}. \end{cases} \tag{52}$$

The scheme proposed in this paper (denoted by WAETM-FTC) is compared with the scheme in [21] (denoted by ETM-FTC). In [21], an FTC scheme was proposed, however, the conventional event-triggered mechanism was utilized and the influence of the nonlinear factors in NCSs were not considered.

Figures 3 and 4 show the fault estimation and fault estimation error, respectively. Compared with the ETM-FTC in [21], when WAETM-FTC is employed it is obvious that the fault can be estimated much better in the networked motor control system.

As shown in Figure 5, when WAETM-FTC is employed the nonlinear function can also be effectively estimated. In contrast, the ETM-FTC in [21] does not consider nonlinear factors and thus the nonlinear function estimation is not shown here.

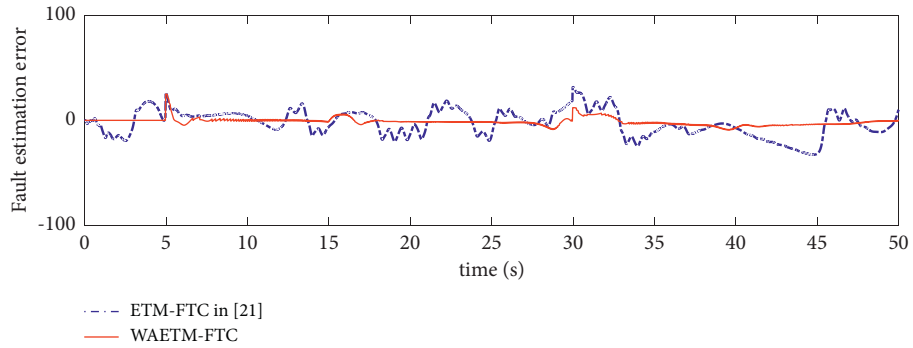

Figure 4: Fault estimation error.

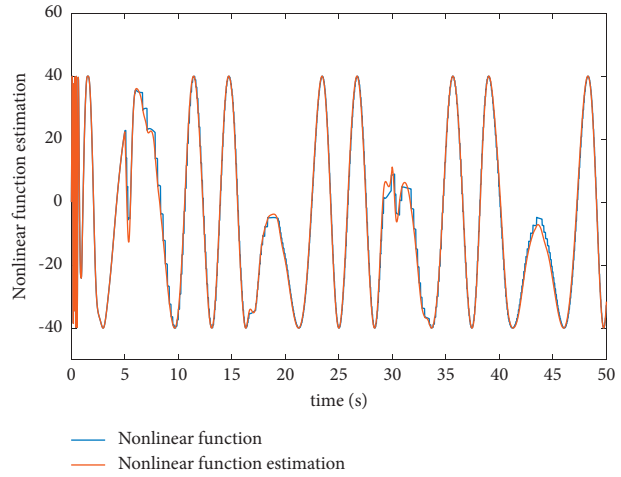

Figure 5: Nonlinear function estimation.

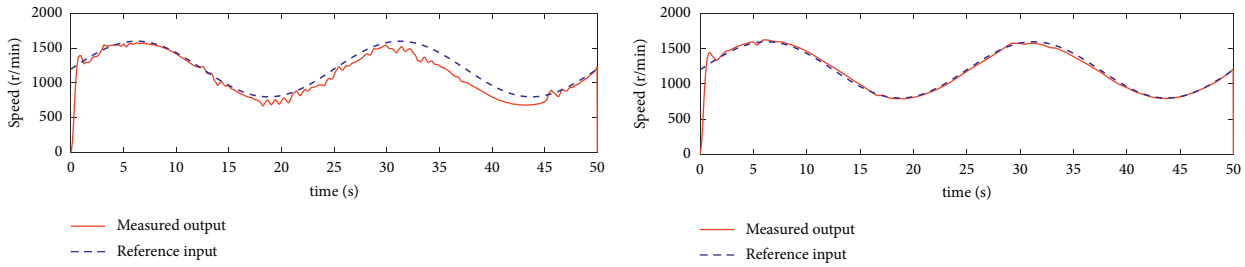

Figure 6: Measured output and reference input (a) ETM-FTC in [21]; (b) WAETM-FTC.

Figure 6(a) shows the measured output (speed) with the ETM-FTC in [21]. During 0-5second, although there is no fault in the system, the measured output can not track the reference input well because there are still nonlinear factors in the system. After 5 seconds, the fault occurs and the system measured output suffers from both fault and nonlinear factors. Therefore, the error between the measured output and the reference input becomes even larger as shown in Figure 7. Figure 6(b) shows the measured output (speed) with the WAETM-FTC scheme. During 0–5 seconds when the fault does not occur while there are nonlinear factors, the measured output can track the reference input. After 5 seconds, even though there are both fault and nonlinear factors in the system, the measured output can still track the reference input well. Therefore, the error between the measured output and the reference input can converge in Figure 7.

The release intervals are shown in Figure 8, when the ETM-FTC in [21] is adopted, most of the release intervals are the same with the sampling time of 0.02 seconds, which may lead to the communication congestion. In contrast, when WAETM-FTC is adopted, it is clearly that most of the release intervals are larger than 0.02 seconds, which indicates that the unnecessary transmitted data packets are reduced.

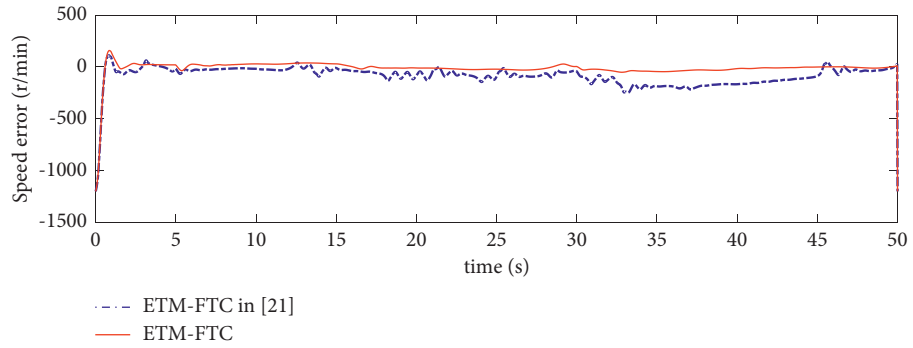

Figure 7: Measured output error.

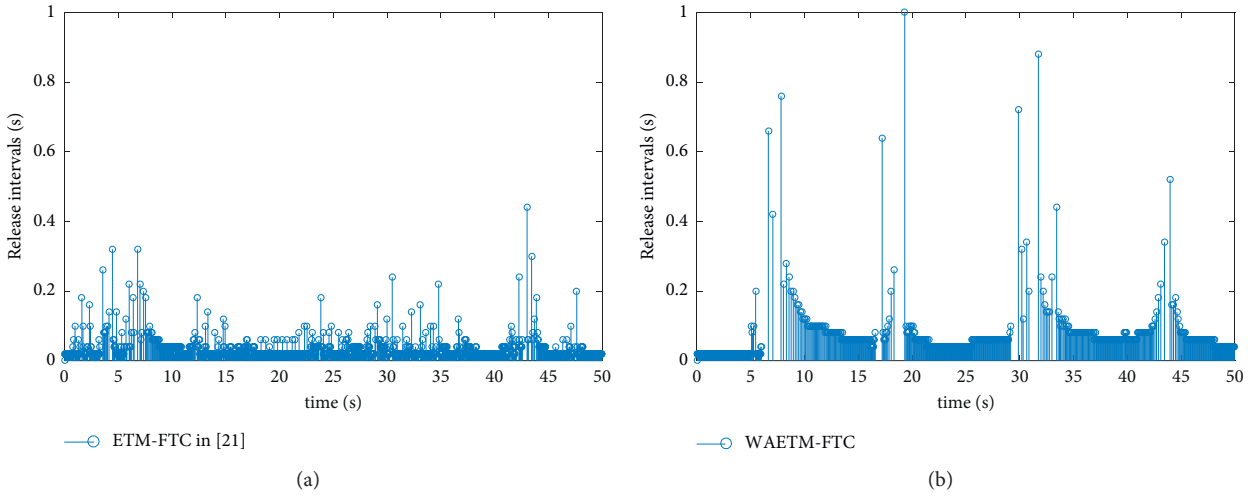

Figure 8: Release intervals (a) ETM-FTC in [21]; (b) WAETM-FTC.

Moreover, the triggered times are 1688 in Figure 8(a), and the triggered times are 837 in Figure 8(b), which indicates that the proposed WAETM can decrease the triggered data packets by 34.04%. Therefore, the communication congestion is effectively alleviated.

5. Conclusions

In this paper, a weighted average event-triggered fault-tolerant control scheme is proposed for nonlinear NCSs with the communication congestion and actuator fault. The weighted average event-triggered mechanism, which adopts the weighted average of data packets, is to alleviate the communication congestion and save the network communication resources. The state-fault observer based on the weighted average event-triggered mechanism is to estimate the system state and fault. With the system state estimation and fault estimation, the fault-tolerant control law is obtained. The proposed weighted average event-triggered fault-tolerant control scheme can effectively save the network communication resources in nonlinear NCSs, while compensating the influence of the fault and reducing the influence of nonlinear factors. Adaptive event-triggered based fault-tolerant control for nonlinear networked control systems will be investigated in our future work.

Data Availability

The data that support our manuscript conclusions are some open access articles that have been properly cited, and the readers can easily obtain these articles to verify the conclusions.

Conflicts of Interest

The authors declare that they have no known competing financial interests or personal relationships that could have appeared to influence the work reported in this paper.

Acknowledgments

This paper was supported by the National Natural Science Foundation of China under Grant no. 61973257.

References

[1] X. M. Zhang, Q. L. Han, and X. Yu, "Survey on recent advances in networked control systems," *IEEE Transactions on Industrial Informatics*, vol. 12, no. 5, pp. 1740–1752, 2016.

[2] X. M. Zhang, Q. L. Han, X. Ge et al., "Networked control systems: a survey of trends and techniques," *IEEE/CAA Journal of Automatica Sinica*, vol. 7, no. 1, pp. 1–17, 2019.

[3] J. Alcaina, A. Cuenca, J. Salt, V. Casanova, and R. Pizá, "Delay-independent dual-rate PID controller for a packet-based networked control system," *Information Sciences*, vol. 484, pp. 27–43, 2019.

[4] N. Zhao, P. Shi, and W. Xing, "Dynamic event-triggered approach for networked control systems under denial of service attacks," *International Journal of Robust and Nonlinear Control*, vol. 31, no. 5, pp. 1774–1795, 2021.

[5] Z. H. Pang, C. G. Xia, W. F. Zhai, G. P. Liu, and Q. L. Han, "Networked active fault-tolerant predictive control for systems with random communication constraints and actuator/sensor faults," *IEEE Transactions on Circuits and Systems II-Express Briefs*, vol. 69, no. 4, pp. 2166–2170, 2022.

[6] T. Li, W. A. Zhang, and L. Yu, "Improved switched system approach to networked control systems with time-varying delays," *IEEE Transactions on Control Systems Technology*, vol. 27, no. 6, pp. 2711–2717, 2019.

[7] Y. Ma, J. Guo, Y. Wang, and A. Chakrabarty, "Optimal dynamic transmission scheduling for wireless networked control systems," *IEEE Transactions on Control Systems Technology*, pp. 1–17, 2022.

[8] H. Zhang, J. Liu, and S. Xu, "H-Infinity load frequency control of networked power systems via an event-triggered scheme," *IEEE Transactions on Industrial Electronics*, vol. 67, no. 8, pp. 7104–7113, 2020.

[9] M. Bahraini, M. Zanon, A. Colombo, and P. Falcone, "Optimal control design for perturbed constrained networked control systems," *IEEE Control Systems Letters*, vol. 5, no. 2, pp. 553–558, 2021.

[10] J. Song and Y. Niu, "Dynamic Event-triggered sliding mode control: dealing with slow sampling singularly perturbed systems," *IEEE Transactions on Circuits and Systems II-Express Briefs*, vol. 67, no. 6, pp. 1079–1083, 2020.

[11] D. Yue, E. Tian, and Q. L. Han, "A delay system method for designing event-triggered controllers of networked control systems," *IEEE Transactions on Automatic Control*, vol. 58, no. 2, pp. 475–481, 2013.

[12] C. Peng and F. Li, "A survey on recent advances in event-triggered communication and control," *Information Sciences*, vol. 475, pp. 113–125, 2018.

[13] J. Song, Y. Niu, and J. Xu, "An event-triggered approach to sliding mode control of Markovian jump Lur'e systems under hidden mode detections," *IEEE Transactions on Systems Man and Cybernetics-Systems*, vol. 50, no. 4, pp. 1514–1525, 2020.

[14] J. Wu and C. Peng, "Observer-based adaptive event-triggered PID control for networked systems under aperiodic DoS attacks," *International Journal of Robust and Nonlinear Control*, vol. 32, no. 5, pp. 2536–2550, 2022.

[15] C. Peng, D. Yue, and M. R. Fei, "A higher energy efficient sampling scheme for networked control systems over IEEE 802.15.4 wireless networks," *IEEE Transactions on Industrial Informatics*, vol. 12, no. 5, pp. 1766–1774, 2016.

[16] C. Albea and A. Seuret, "Time-triggered and event-triggered control of switched affine systems via a hybrid dynamical approach," *Nonlinear Analysis-Hybrid Systems*, vol. 41, Article ID 101039, 2021.

[17] T. Li, X. Tang, J. Ge, and S. Fei, "Event-based fault-tolerant control for networked control systems applied to aircraft engine system," *Information Sciences*, vol. 512, pp. 1063–1077, 2020.

[18] J. Wang, F. Fang, X. Yi, and Y. Liu, "Dynamic event-triggered fault estimation and sliding mode fault-tolerant control for networked control systems with sensor faults," *Applied Mathematics and Computation*, vol. 389, Article ID 125558, 2021.

[19] H. Li, J. Pan, X. Zhang, and J. Yu, "Integral-based event-triggered fault estimation and impulsive fault-tolerant control for networked control systems applied to underwater vehicles," *Neurocomputing*, vol. 442, pp. 36–47, 2021.

[20] Z. Gu, P. Shi, D. Yue, S. Yan, and X. Xie, "Fault estimation and fault-tolerant control for networked systems based on an adaptive memory-based event-triggered mechanism," *IEEE Transactions on Network Science and Engineering*, vol. 8, no. 4, pp. 3233–3241, 2021.

[21] X. Wang, Z. Fei, Z. Wang, and X. Liu, "Event-triggered fault estimation and fault-tolerant control for networked control systems," *Journal of the Franklin Institute*, vol. 356, no. 8, pp. 4420–4441, 2019.

[22] R. F. Araujo, L. A. B. Torres, and R. M. Palhares, "Distributed control of networked nonlinear systems via interconnected takagi-sugeno fuzzy systems with nonlinear consequent," *IEEE Transactions on Systems, Man, and Cybernetics: Systems*, vol. 51, no. 8, pp. 4858–4867, 2021.

[23] M. T. Angulo, A. Aparicio, and C. H. Moog, "Structural accessibility and structural observability of nonlinear networked systems," *IEEE Transactions on Network Science and Engineering*, vol. 7, no. 3, pp. 1656–1666, 2020.

[24] Y. A. Liu, S. Tang, Y. Liu, Q. Kong, and J. Wang, "Extended dissipative sliding mode control for nonlinear networked control systems via event-triggered mechanism with random uncertain measurement," *Applied Mathematics and Computation*, vol. 396, Article ID 125901, 2021.

[25] T. Wu, X. Huang, X. Chen, and J. Wang, "Sampled-data H∞ exponential synchronization for delayed semi-Markov jump CDNs: a looped-functional approach," *Applied Mathematics and Computation*, vol. 377, Article ID 125156, 2020.

[26] J. Wang, Y. Wang, H. Yan, J. Cao, and H. Shen, "Hybrid event-based leader-following consensus of nonlinear multi-agent systems with semi-markov jump parameters," *IEEE Systems Journal*, vol. 16, no. 1, pp. 397–408, 2022.

[27] M. Sathishkumar and Y. C. Liu, "Resilient Event-triggered fault-tolerant control for networked control systems with randomly occurring nonlinearities and DoS attacks," *International Journal of Systems Science*, vol. 51, no. 14, pp. 2712–2732, 2020.

[28] J. Li, Z. Yang, X. Mu, and X. Wu, "Passivity-based event-triggered fault tolerant control for nonlinear networked control system with actuator failures and DoS jamming attacks," *Journal of the Franklin Institute*, vol. 357, no. 14, pp. 9288–9307, 2020.

[29] F. Jani, F. Hashemzadeh, M. Baradarannia, and H. Kharrati, "Robust finite-time contractive fault tolerant control of uncertain nonlinear network-based systems with adaptive event-triggered communication scheme," *Iranian Journal of Science and Technology-Transactions of Electrical Engineering*, vol. 46, no. 1, pp. 141–155, 2021.

[30] Q. Y. Fan and G. H. Yang, "Event-based fuzzy adaptive fault-tolerant control for a class of nonlinear systems," *IEEE Transactions on Fuzzy Systems*, vol. 26, no. 5, pp. 2686–2698, 2018.

[31] W. Wu and Y. Zhang, "Event-triggered fault-tolerant control and scheduling codesign for nonlinear networked control systems with medium-access constraint and packet disordering," *International Journal of Robust and Nonlinear Control*, vol. 28, no. 4, pp. 1182–1198, 2018.

[32] M. Mahmoud, A. Memon, and P. Shi, "Observer-based fault-tolerant control for a class of nonlinear networked control

systems," *International Journal of Control*, vol. 87, no. 8, pp. 1707–1715, 2014.

[33] F. Rahimi and H. Rezaei, "A distributed fault estimation approach for a class of continuous-time nonlinear networked systems subject to communication delays," *IEEE Control Systems Letters*, vol. 6, pp. 295–300, 2022.

[34] Q. L. Han, "Absolute stability of time-delay systems with sector-bounded nonlinearity," *Automatica*, vol. 41, no. 12, pp. 2171–2176, 2005.

[35] S. Yan, M. Shen, S. K. Nguang, and G. Zhang, "Event-triggered $H_{\infty }$ control of networked control systems with distributed transmission delay," *IEEE Transactions on Automatic Control*, vol. 65, no. 10, pp. 4295–4301, 2020.

[36] H. Yan, H. Zhang, X. Zhan, Y. Wang, S. Chen, and F. Yang, "Event-triggered sliding mode control of switched neural networks with mode-dependent average dwell time," *IEEE Transactions on Systems Man and Cybernetics-Systems*, vol. 51, no. 2, pp. 1233–1243, 2021.

Hindawi
Mathematical Problems in Engineering
Volume 2022, Article ID 4730870, 9 pages
https://doi.org/10.1155/2022/4730870

Research Article

Load Frequency Control for Interconnected Multi-area Power Systems with the Semi-Markov Jumping Parameter and Actuator Failure

Yanjun Jiang,[1] Jinfeng Wang ,[1] Zeyang Bai,[2] Zhengmou Ren,[1] Xiaochen Sun,[1] and Guangliang Yu[1]

[1]*State Grid Shaanxi Electric Power Economic Technology Research Institute, Xi'an, Shaanxi 710065, China*
[2]*State Grid Shaanxi Electric Power Company Limited, Xi'an, Shaanxi 710048, China*

Correspondence should be addressed to Jinfeng Wang; dk.618@stu.xjtu.edu.cn

Received 18 May 2022; Revised 8 June 2022; Accepted 14 June 2022; Published 1 July 2022

Academic Editor: Yong Chen

In this study, we study the load frequency control (LFC) problem for interconnected multiarea power systems (IMAPSs) with quantization and actuator failure. To effectively reduce the amount of data in the channel, input signals will be quantized before being transmitted from a controller to a system through the digital communication channel. To reveal the asynchronous phenomenon between the original plant and LFC with actuator failure, a hidden semi-Markov model is formulated. In addition, the stability of the jump system under network attack is discussed. On the basis of the Lyapunov theory, sufficient conditions are derived to ensure the stochastic stability of IMAPSs. Finally, the validity of the theoretical results is tested via a simulation example.

1. Introduction

The power system is a complex nonlinear system, which has developed into a multiregional interconnected power system (PS) since the Industrial Revolution. To deal with the low-frequency little oscillations of interconnected PSs, the LFC was proposed in [1], which has been effectively applied to PSs [2–4]. According to the LFC technique, the frequency can be adjusted at a desired level, which guarantees the stability of entire PSs. Over the past few decades, researchers have proposed a number of techniques concerning with LFC, such as use of the integral control law [5], PI case [6], and PID case [7]. These approaches have been verified to improve the control performance of interconnected PSs [8, 9].

In practical applications, the dynamic systems may undergo sudden changes in their parameters or structures due to component failures, sudden environmental changes, etc. In this case, Markov chains are widely adopted to model the variations in PS states. In [10], the Markov chain was employed to describe the random mutations of the discrete-time PS. In [11], the uncertain Markov chain was applied for the decentralized control of the PS. However, in most existing literature concerning Markov PSs, the residence time of Markov processes obeys a memory-free random distribution, in which the probability of the transition rate is time-independent. As signified in [12–14], compared with the conventional Markov chain, the semi-Markov chain is more general in approximating practical dynamics owing to its time-varying transition rate. Consequently, it is meaningful to study the LFC problem for PSs with semi-Markov jumping parameters, the so-called semi-Markov PSs. To the best of our knowledge, quite a few theoretical results have been applied to semi-Markov PSs due to their inherent difficulty, and this motivates this article.

In reality, the signal is communicated through a limited bandwidth network [13, 15, 16]. Note that massive signals are transmitted via the limited network, which may lead to channel congestion, thus reducing the system performance. To overcome this shortcoming, we quantify the control inputs, in which quantization stands for the process of mapping the continuous values of a signal to a limited

number of discrete values [17, 18]. By means of quantization, the amount of data in the channel and load of the channel can be effectively reduced. The quantizers can be roughly categorized into linear quantizers [19], and logarithm quantizers [20, 21]. The problem of stabilizing a continuous-time switched system affected by the time-varying delay and data quantization has been addressed in [22]. In the quantitative input multiarea, however, results of the power system are very few; in order to fill the gap, this article takes into account the interconnected more regional power system with quantitative input, and the quantification method is used as the basis of the design, making the obtained quantitative instruments with the crudest density and further reducing the burden of transmission. We would like to mention that, in practice, capturing system information is a tricky task. Therefore, the asynchrony between the system mode and the controller mode cannot be omitted. Nevertheless, the asynchronous control of the semi-Markov IMAPS has not been researched thoroughly, which partially motivates the current work.

Motivated by the above considerations, this work considers the LFC problem of the IMAPS subject to quantization input. Different from the existing homogeneous Markov IMAPS, the semi-Markov chain is employed to describe the dynamic behavior of the IMAPS. Aiming to describe the asynchronous phenomenon between the original plant and LFC, the hidden semi-Markov model is formulated. By resorting to the Lyapunov theory, sufficient conditions are derived to ensure the stochastic stability of the resulting dynamic. In the end, one numerical example is inferred to show the correctness of the proposed method. The general structure is rendered as follows: the second section describes the asynchronous LFC of the semi-Markov PS with quantization form. In section 3, sufficient conditions of random stability are given. A numerical example is given in section 4.

Notations: diag$\{*\}$ means a block-diagonal matrix; $He\{R\} = R + R^{\top}$; $P > 0$ means P is positive definite; Pr$\{*\}$ implies occurrence probability; $\varepsilon\{*\}$ indicates the mathematical expectation; $\|*\|$ signifies the Euclidean vector norm. $\mathfrak{I}$ signifies the identity matrix; $A^{\top}$ and A^{-1} stand for the transpose and inverse matrix, respectively.

2. Problem Formulations

2.1. System Model. In this study, the dynamic model of the multiarea LFC is described as follows:

$$\begin{cases} \dot{x}(t) = A(r(t))x(t) + H(r(t))\Delta P_L(t) + B(r(t))u(t), \\ y(t) = C(r(t))x(t), \end{cases} \tag{1}$$

where $x_i(t) \in \mathbb{R}^5$, $y_i(t) \in \mathbb{R}^2$, $u_i(t) \in \mathbb{R}$, and $\Delta P_L^i(t) \in \mathscr{L}_2[0, \infty)$ represent the state, the output, the control input, and the disturbance, respectively, and

$$y_i(t) = \left[\mathrm{ACE}_i \quad \int_0^t \mathrm{ACE}_i(s)\mathrm{d}s \right]^{\top},$$

$$y(t) = \left[y_1(t) y_2(t) \cdots y_N(t) \right]^{\top},$$

$$u(t) = \left[u_1(1) u_2(t) \cdots u_N(t) \right]^{\top},$$

$$\Delta P_L(t) = \left[\Delta P_L^1(t) \Delta P_L^2(t) \cdots \Delta P_L^N(t) \right]^{\top},$$

$$x_i(t) = \left[\Delta f_i(t), \Delta P_m^i(t), \Delta Y_i(t), \Delta P_{tie}^i(t), \int_0^t ACE_i(s)\mathrm{d}s \right] \top,$$

$$x(t) = \left[x_1(t) x_2(t) \cdots x_N(t) \right]^{\top},$$

$$B_i(r(t)) = \left[0 \;\; 0 \;\; \frac{1}{T_g(i)(r(t))} \;\; 0 \;\; 0 \right]^{\top},$$

$$B(r(t)) = \mathrm{diag}\{B_1(r(t)) B_2(r(t)) \cdots B_N(r(t))\},$$

$$H_i(r(t)) = \left[-\frac{1}{M_i(r(t))} \;\; 0 \;\; 0 \;\; 0 \;\; 0 \right]^{\top},$$

$$H(r(t)) = \mathrm{diag}\{H_1(r(t)) H_2(r(t)) \cdots H_N(r(t))\}$$

$$C_i(r(t)) = \begin{pmatrix} \beta_i(r(t)) & 0 & 0 & 1 & 0 \\ 0 & 0 & 0 & 0 & 1 \end{pmatrix},$$

$$C(r(t)) = \mathrm{diag}\{C_1(r(t)) C_2(r(t)) \cdots C_N(r(t))\},$$

$$A_{ii}(r(t)) = \begin{pmatrix} -\frac{D_i(r(t))}{M_i(r(t))} & \frac{1}{D_i(r(t))} & 0 & -\frac{1}{D_i(r(t))} & 0 \\ 0 & -\frac{1}{T_t^i(r(t))} & \frac{1}{T_t^i(r(t))} & 0 & 0 \\ -\frac{1}{R_i(r(t))T_g^i(r(t))} & 0 & -\frac{1}{T_g^i(r(t))} & 0 & 0 \\ \sum_{j=1, j\neq i}^{N} 2\pi T_{ij}(r(t)) & 0 & 0 & 0 & 0 \\ \beta_i(r(t)) & 0 & 1 & 0 & 0 \end{pmatrix}. \tag{2}$$

$A_{ij} = [a_{ls}]_{l,s=1}^{5}$ with $a_{51} = -2\pi T_{ij}$, $a_{ls} = 0$, and $A = [A_{ij}]_{j,i=1}^{N}$. Each ACE signal is described as a linear combination of the tie-line power exchange and frequency deviation, i.e., $\mathrm{ACE}_i = \beta_i(r(t))\Delta f_i(t) + P_{\mathrm{tie}}^i(t)$, where $\Delta P_{\mathrm{tie}}^i$ refers to the net exchange of the tie-line power. The nomenclature of other parameters is shown in Table 1.

In view of the uncertain fault time of the power system, the semi-Markov process $\{r(t)\}_{t\geq 0} \in \mathcal{S} = \{1, 2, \ldots, S\}$ is adopted. For all $k \in \mathbb{N}$,

$$\begin{aligned} &R_k \text{ the Markov chain} \\ &T_k \text{the sojourn time, i.e., } T_k = t_k - t_{k-1} \\ &G_p \text{ the probability distribution function} \\ &\chi_p \text{ the Markov chain.} \end{aligned} \tag{3}$$

Then, $\{(R_k, r_k)\}$ is said to be a renewal process if $r(t) = R_N(t)$ where $N(t) = \sup\{k\colon t \geq t_k\}$ with

$$\Pr\{R_{k+1} = q | R_k = p\} = \begin{cases} \Pi_{pq}, & p \neq q, \\ 0, & p = q. \end{cases} \tag{4}$$

Meanwhile, the probability distribution function G_p can be described as follow:

$$G_p(h) = \Pr\{T_{k+1} < h | r(t_k) = p\}. \tag{5}$$

According to the aforementioned observation, we have

$$\begin{aligned} \Pr\{r(t+\delta) = q | r(t) = p\} &= \begin{cases} \Pr\{T_{k+1} \leq h + \delta, R_{k+1} = q | T_{k+1} > h, R_k = p\}, & p \neq q, \\ \Pr\{T_{k+1} > h + \delta, R_{k+1} = q | T_{k+1} > h, R_k = p\}, & p = q. \end{cases} \\ &= \begin{cases} \pi_{pq}(h)\delta + o(\delta), & p \neq q, \\ 1 + \pi_{pq}(h)\delta + o(\delta), & p = q. \end{cases} \end{aligned} \tag{6}$$

Hence, by simple calculation, the transition rate matrix can be defined by $\Psi(h) = [\pi_{pq}^h]_{S\times S}$, where

$$\begin{aligned} \pi_{pq}(h) &= \lim_{\delta \longrightarrow 0} \frac{\Pr\{r(t+\delta) = q | r(t) = p\}}{\delta} \\ &= \Pi_{pq} \frac{\chi_p(h)}{1 - G_p(h)}, \quad p \neq q, \end{aligned} \tag{7}$$

and $\pi_{pp}(h) = -\sum_{q=1, q\neq p}^{S} \pi_{pq}(h) < 0$.

2.2. Asynchronous Control Input with Quantized. As exhibited in Figure 1, the control input $u(t)$ is required to be quantized before sending it to the power system. Inspired by this fact, the logarithmic quantizer can be described as follows:

$$\mathfrak{q}(u(t)) = [\mathfrak{q}_1(u_1(t))\mathfrak{q}_2(u_2(t)) \cdots \mathfrak{q}_\iota(u_\iota(t))], \tag{8}$$

where the wth subquantizer $\mathfrak{q}_w(\cdot)$ satisfying $\mathfrak{q}_w(u_w(t)) = -\mathfrak{q}_w(-u_w(t))$, $w = 1, 2, \ldots, \iota$. The set of the logarithmic quantization level can be described as

$$\begin{aligned} \mathbb{U}_w = \{ &\pm \theta_n^w \colon \pm \theta_n^w = \rangle_w^n \theta_0^w, \\ &n = \pm 1 \pm 2, \cdots\} \cup \{\pm \theta_0^w\} \cup \{0\}, \end{aligned} \tag{9}$$

where $0 < \varrho_w^n < 1$ and $\theta_0^w > 0$ on behalf of the quantizer density and the initial quantization, respectively .And $\lambda_\omega = 1 - \varrho_w / 1 + \varrho_w$. Then, we define the subquantizer $\mathfrak{q}_\omega(u_\omega(t))$ as

Table 1: The physical meaning of parameters.

Parameters	Nomenclature
$\Delta f_i(t)$	Frequency deviation
$\Delta P_m^i(t)$	Mechanical power output increment
$\Delta Y_i(t)$	Valve position of turbine
$D_i(r(t))$	Mode-dependent damping coefficient
$T_t^i(r(t))$	Turbine time constant
$T_g^i(r(t))$	Governor time constant
$\beta_i(r(t))$	Frequency bias
$T_{ij}(r(t))$	Coefficient between the i-th and j-th area

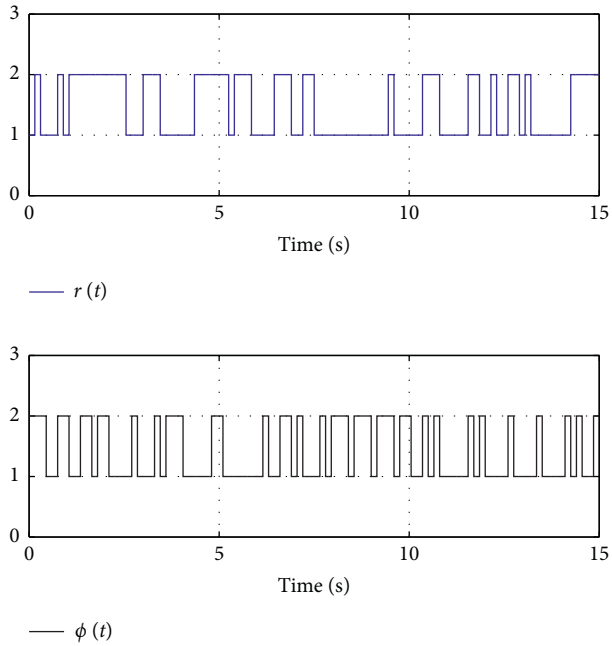

Figure 1: The evolution of modes $r(t)$ and $\varphi(t)$.

$$\mathfrak{q}_\omega(u_\omega(t)) = \begin{cases} \theta_n^\omega, & \text{if} \quad \dfrac{\theta_n^\omega}{1+\lambda_\omega} < u_\omega(t) < \dfrac{\theta_n^\omega}{1-\lambda_\omega}, \\ 0, & \text{if} \quad u_\omega(t) = 0, \\ -\mathfrak{q}_\omega(-u_\omega(t)), & \text{if} \quad u_\omega(t) < 0. \end{cases} \tag{10}$$

Then, we have that

$$\mathfrak{q}(u(t)) = u(t), \tag{11}$$

where $\Lambda = \text{diag}\{\Lambda_1, \Lambda_2, \ldots, \Lambda_\iota\}$, $\Lambda_w^\top \Lambda_w \le \mathfrak{F}$.

In this work, the i-th control area of an asynchronous PI controller is given by

$$\begin{aligned} u_i(t, \varphi(t)) &= K_{P\varphi(t)}^i ACE_i(t) + K_{I\varphi(t)}^i \int_0^t \text{ACE}_i(s)\text{d}s \\ &= K_{\varphi(t)}^i y_i(t), \end{aligned} \tag{12}$$

where $K_{P\varphi(t)}^i$, and $K_{I\varphi(t)}^i$ are the i -th proportional and integral gains, respectively, and $K_{\varphi(t)}^i = [K_{P\varphi(t)}^i \, K_{I\varphi(t)}^i]$. The variable $\varphi(t)$ that refers to the Markov chain belongs to the space $\mathscr{M} = \{1, 2, \ldots, M\}$, whose conditional probability matrix is inferred $\Gamma = [\rho_{pm}]_{S\times M}$ with

$$\Pr\{\varphi(t) = m | r(t) = p\} = \rho_{pm}, \tag{13}$$

with $\sum_{m\in\mathscr{M}} \rho_{pm} = 1$. According to equations (11) and (12), the control signal $u_i(t, \varphi(t))$ can be devised as follows:

$$u_i(t, \varphi(t)) = a_i(t)\left(\mathfrak{F}_i + \Lambda_i\right) K_{\varphi(t)}^i y_i(t), \tag{14}$$

where $a_i(t) \in \{0, 1\}$, and $\varepsilon\{a_i(t)\} = \overline{a}_i$.

2.3. Model Transformation. Let $r(t) = p$ and $\varphi(t) = m$, substituting equations (14) into (1), the closed-loop IMAPS is formulated as follows:

$$\begin{cases} \dot{x}_i(t) = A_p^{ii}x_i(t) + \sum_{j=1,j\neq i}^{N} A_p^{ij}x_j(t) + \overline{a}_i B_p^i(\mathfrak{F}_i + \Lambda_i)K_{pm}^i C_p^i x_i(t) + H_p^i \Delta P_L^i(t), \\ y_i(t) = C_p^i x_i(t). \end{cases} \tag{15}$$

For analysis convenience, based on the compatible matrix $\widehat{B}_p^i$, we can obtain a full rank matrix $\overline{B}_p^i = [B_p^i \ \widehat{B}_p^i]$. We define $\mathfrak{X}_i(t) = (\overline{B}_p^i)^{-1}x_i(t)$, we have that

$$\begin{cases} \dot{\mathfrak{X}}_i(t) = \overline{A}_p^{ii}\mathfrak{X}_i(t) + \sum_{j=1,j\neq i}^{N} \overline{A}_p^{ij}\mathfrak{X}_j(t) + \overline{a}_i(\mathfrak{F}_i + \Lambda_i)\overline{K}_m^i C_p^i \mathfrak{X}_i(t) + \overline{H}_p^i \Delta P_L^i(t), \\ y_i(t) = \overline{C}_p^i \mathfrak{X}_i(t), \end{cases} \tag{16}$$

where $\overline{A}_p^{ij} = (\overline{B}_p^i)^{-1}A_p^{ij}\overline{B}_p^i$, $\overline{K}_m = [(K_m^i)^\top \quad 0]\top$, $\overline{C}_p^i = C_p^i\overline{B}_p^i$, and $\overline{H}_p^i = (\overline{B}_p^i)^{-1}H_p^i$. It is worth noting that linear transformation $\overline{B}_p^i$ is invertible. Thus, the overall IMAPS can be inferred as

$$\begin{cases} \dot{\mathfrak{X}}(t) = \overline{A}_p\mathfrak{X}(t) + \overline{a}(\mathfrak{F} + \Lambda)\overline{K}_m\overline{C}_p\mathfrak{X}(t) + \overline{H}_p\Delta P_L(t), \\ y(t) = \overline{C}_p\mathfrak{X}(t), \overline{C}_p\mathfrak{X}(t), \end{cases} \tag{17}$$

where $\overline{a} = \mathrm{diag}_N\{\overline{a}_i\}$, $\mathfrak{F} + \Lambda = \mathrm{diag}_N\{(\mathfrak{F}_i + \Lambda_i)\}$, $\overline{C}_p = \mathrm{diag}_N\{\overline{C}_p^i\}$, $\overline{H}_p^i = \mathrm{diag}_N\{\overline{H}_p^i\}$, and

$$\overline{A}_p = \begin{bmatrix} \overline{A}_p^{11} & \overline{A}_p^{12} & \cdots & \overline{A}_p^{1N} \\ \overline{A}_p^{21} & \overline{A}_p^{22} & \cdots & \overline{A}_p^{2N} \\ \vdots & \vdots & \ddots & \vdots \\ \overline{A}_p^{N1} & \overline{A}_p^{N2} & \cdots & \overline{A}_p^{NN} \end{bmatrix}. \tag{18}$$

Definition 1. ([23]) The interconnected power system with $\Delta P_L(t) = 0$ is called stochastic stability if the following equation holds:

$$\varepsilon\left\{\int_0^\infty \|\mathfrak{X}(t)\|^2 \mathrm{d}t | r(t_0), \varphi(t_0)\right\} < \infty. \tag{19}$$

Under the zero initial condition, the system with $\Delta P_L(t) \in \mathscr{L}_2[0,\infty)$ and $\gamma > 0$, the H_∞ performance index is satisfied:

$$\varepsilon\left\{\int_0^\infty y^T(t)y(t) - \gamma^2 P_L^T(t)P_L(t)\right\} < 0. \tag{20}$$

Lemma 1. *([21]) For the given matrix Ω_1 and matrices Ω_2 and Ω_3 with appropriate dimensions, if inequality $\Omega_1 + He\{\Omega_2\Lambda\Omega_3\} < 0$ holds for all $\|\Lambda\| \le \mathfrak{F}$, for any scalar s_1, such that $\Omega_1 + s_1\Omega_3^\top\Omega_3 + s_1^{-1}\Omega_2^\top\Omega_2 < 0$.*

3. Main Results

Theorem 1. *For given scalars $\gamma > 0$ and $\eta > 0$ and the matrix M_p, the IMAPS is stochastic stability with preset performance, such that*

$$\overline{\Xi}_{pm} = \begin{bmatrix} \Xi_{pm}^{11} + \overline{C}_p^\top\overline{C}_p & * & * \\ \Xi_{pm}^{21} & -He\{\eta M^\top\} & * \\ \overline{H}_p^\top M^\top & \eta\overline{H}_p^\top M^\top & -\gamma^2 \end{bmatrix} < 0, \tag{21}$$

where

$$\begin{aligned} \Xi_{pm}^{11} &= \sum_{q=1}^{S}\overline{\Pi}P_q + \sum_{m=1}^{M}\rho_{pm}He\left\{M^\top\left(\overline{A}_p + \overline{a}(\mathfrak{F} + \Lambda)\overline{K}_m\overline{C}_p\right)\right\}, \\ \Xi_{pm}^{21} &= -M + P_p^\top + \sum_{m=1}^{M}\rho_{pm}\eta M^\top\left(\overline{A}_p + \overline{a}(\mathfrak{F} + \Lambda)\overline{K}_m\overline{C}_p\right), \\ \overline{\Pi}_{pq} &= \varepsilon\{\pi_{pq}(h)\} = \int_0^\infty \pi_{pq}(h)\chi_p(h)\mathrm{d}h. \end{aligned} \tag{22}$$

Proof. Establish the semi-Markov-based Lyapunov function as follows:

$$V(\mathfrak{X}(T), r(t), \varphi(t)) = \mathfrak{X}^\top(t)P_{r(t)}\mathfrak{X}(t). \tag{23}$$

It follows that

$$\varepsilon\{\mathscr{L}V(\mathfrak{X}(t),r(t),\varphi(t))\} = \lim_{\delta\longrightarrow 0} \frac{1}{\delta}\left\{\varepsilon\left\{\sum_{q\neq p}\pi_{pq}(h)\delta\mathfrak{X}^{\top}(t+\delta)P_q\mathfrak{X}(t+\delta)+\left(1+\pi_{pp}(h)\delta\right)\mathfrak{X}^{\top}(t+\delta)P_p\mathfrak{X}(t+\delta)\right\}+\mathfrak{X}^{\top}(t)P_p\mathfrak{X}(t)\right] = \mathfrak{X}^{\top}(t)\left(\sum_{q=1}^{S}\overline{\Pi}_{pq}P_q\right)\mathfrak{X}(t)+He\left\{\dot{\mathfrak{X}}^{\top}(t)P_p\mathfrak{X}^{\top}(t)\right\}. \tag{24}$$

On the basis of equation (17), for any proper matrix M, such that

$$0 = 2\left[\mathfrak{X}^{\top}(t)M^{\top}+\eta\dot{\mathfrak{X}}(t)M^{\top}\right]\times\left[-\dot{\mathfrak{X}}(t)+\overline{A}_p\mathfrak{X}(t)+\overline{a}(\mathfrak{F}+\Lambda)\overline{K}_m\overline{C}_p\mathfrak{X}(t)+\overline{H}_p\Delta P_L(t)\right]. \tag{25}$$

It follows from equations (24) and (25) that

$$\begin{aligned}&\varepsilon\{\mathscr{L}V(\mathfrak{X}(t),r(t),\varphi(t))\}\\&\quad=\mathfrak{X}^{\top}(t)\left(\sum_{q=1}^{S}\overline{\Pi}_{pq}P_q\right)\mathfrak{X}(t)+He\left\{\dot{\mathfrak{X}}^{\top}(t)P_p\mathfrak{X}^{\top}(t)\right\}\\&\qquad+2\left[\mathfrak{X}^{\top}(t)M^{\top}+\eta\dot{\mathfrak{X}}(t)M^{\top}\right]\times\left[-\dot{\mathfrak{X}}(t)+\overline{A}_p\mathfrak{X}(t)+\overline{a}(\mathfrak{F}+\Lambda)\overline{K}_m\overline{C}_p\mathfrak{X}(t)+\overline{H}_p\Delta P_L(t)\right]\\&\quad=\zeta^{\top}(t)\Xi_{pm}\zeta(t),\end{aligned} \tag{26}$$

where $\zeta^{\top}(t)=[\xi^{\top}(t)\quad \Delta P^{\top}(t)]$, $\xi^{\top}(t)=[\mathfrak{X}^{\top}(t)\quad \dot{\mathfrak{X}}^{\top}(t)]$ $\overline{\Pi}_{pq}=\varepsilon\{\pi_{pq}(h)\}=\int_0^{\infty}\pi_{pq}(h)\chi_p(h)dh$ and

$$\Xi_{pm}=\begin{bmatrix}\Xi_{pm}^{11} & * & *\\ \Xi_{pm}^{21} & -He\{\eta M^{\top}\} & *\\ \overline{H}_p^{\top}M^{\top} & \eta\overline{H}_p^{\top}M^{\top} & 0\end{bmatrix}. \tag{27}$$

In case of $\Delta P_L(t)=0$, we have $\varepsilon\{\mathscr{L}V(\mathfrak{X}(t),r(t),\varphi(t))\}\le\xi^{\top}(t)\Xi_{pm}^{1}\xi^{\top}(t)$, by equation (21), we have $\Xi_{pm}^{1}<0$, when $\Xi_{pm}^{1}=\begin{bmatrix}\Xi_{pm}^{11} & *\\ \Xi_{pm}^{21} & -He\{\eta M^{\top}\}\end{bmatrix}$, $\Xi_{pm}^{11}=\sum_{q=1}^{S}\overline{\Pi}P_q+\sum_{m=1}^{M}\rho_{pm}He\{M^{\top}(\overline{A}_p+\overline{a}(\mathfrak{F}+\Lambda)\overline{K}_m\overline{C}_p)\}$, $\Xi_{pm}^{21}=-M+P_p^{\top}+\sum_{m=1}^{M}\rho_{pm}\eta M^{\top}(\overline{A}_p+\overline{a}(\mathfrak{F}+\Lambda)\overline{K}_m\overline{C}_p)$. Subsequently, we have

$$\begin{aligned}&\varepsilon\{\mathscr{L}V(\mathfrak{X}(t),r(t),\varphi(t))\}\\&\quad\le-\lambda\varepsilon\left\{\|\mathfrak{X}(t)\|^2\mid\mathfrak{X}(t_0),r(t_0),\varphi(t_0)\right\},\end{aligned} \tag{28}$$

where $\lambda=\lambda_{\min}(-\Xi_{pm}^{1})$, we can further have

$$\begin{aligned}&\varepsilon\left\{\int_0^{\infty}\|\mathfrak{X}(t)\|^2|\mathfrak{X}(t_0),r(t_0),\varphi(t_0)\right\}\\&\quad\le\frac{1}{\lambda}V(\mathfrak{X}(t_0),r(t_0),\varphi(t_0))<\infty.\end{aligned} \tag{29}$$

Furthermore, for $\Delta P_L(t)\neq 0$, according to equation (24), it yields

$$\mathscr{L}V+y^{\top}(t)y(t)-\gamma^2\Delta P_L^{\top}(t)\Delta P_L(t)\le\zeta^{\top}(t)\overline{\Xi}_{pm}\zeta(t). \tag{30}$$

Note that $\overline{\Xi}_{pm}<0$, from which one can obtain

$$\int_0^{\infty}\left(\mathscr{L}V+z^{\top}(t)z(t)-\gamma^2\Delta P_L^{\top}(t)\Delta P_L(t)\right)dt<0, \tag{31}$$

which indicates

$$\int_0^{\infty}\left(z^{\top}(t)z(t)-\gamma^2\Delta P_L^{\top}(t)\Delta P_L(t)\right)dt<0, \tag{32}$$

this completes the proof. □

Theorem 2. *For given scalars $\gamma>0$, $\eta>0$, and $s_1>0$, system equation (13) is stochastic stability with the preset H_∞ performance index γ, if there exist matrices M and $\overline{K}_m$, such that*

$$\begin{bmatrix} \overline{\Xi}_{pm}^{11} & * & * & * & * & * & * \\ \overline{\Xi}_{pm}^{21} & -He\{\eta M^{\top}\} & * & * & * & * & * \\ \overline{H}_p^{\top} M^{\top} & \eta \overline{H}_p^{\top} M^{\top} & -\gamma^2 \mathfrak{I} & * & * & * & * \\ \overline{C}_p & 0 & 0 & -\mathfrak{I} & * & * & * \\ \theta_p^{\top} & 0 & 0 & 0 & \theta_p^{11} & * & * \\ \left(\theta_p^{111}\right)^{\top} & \eta\left(\theta_p^{111}\right)^{\top} & 0 & 0 & 0 & -He\{\widehat{a}\overline{s}_1\} & * \\ M^{\top} & \eta M^{\top} & 0 & 0 & 0 & 0 & -He\{\widehat{a}s_1\} \end{bmatrix} < 0, \tag{33}$$

where $\overline{s}_1 = s_1^{-1}$, $\widehat{a} = \eta \overline{a}^{-1}$

$$\begin{aligned} \overline{\Xi}_{pm}^{11} &= \overline{\Pi}_{pp} P_p + He\left\{M^{\top} \overline{A}_p\right\} + \sum_{m=1}^{M} \rho_{pm} He\left\{\overline{a} Y \mathscr{K}_m \overline{C}_p\right\}, \\ \overline{\Xi}_{pm}^{21} &= -M + P_p^{\top} + \sum_{m=1}^{M} \rho_{pm} \overline{a} \eta Y \mathscr{K}_m \overline{C}_p \\ \theta_p^{11} &= -\mathrm{diag}\left\{P_1 P_2 \cdots P_{p-1} P_{p+1} \cdots P_S\right\}, \\ \theta_p^{111} &= \left[\sqrt{\rho_{p1}} \overline{C}^{\top} \overline{K}_1^{\top} \sqrt{\rho_{p2}} \overline{C}^{\top} \overline{K}_2^{\top} \cdots \sqrt{\rho_{pM}} \overline{C}^{\top} \overline{K}_M^{\top}\right] \\ \theta_p &= \left[\sqrt{\overline{\Pi}_{p1}} P_1 \sqrt{\overline{\Pi}_{p2}} P_2 \cdots \sqrt{\overline{\Pi}_{p(p-1)}} P_{p-1} \sqrt{\overline{\Pi}_{p(p+1)}} P_{p+1} \cdots \sqrt{\overline{\Pi}_{pS}} P_S\right], \\ Y &= \mathrm{diag}\{Y_1, Y_2, \ldots, Y_N\}, \quad Y_i = \mathrm{diag}\left\{\mathfrak{I}_p, 0\right\}. \end{aligned} \tag{34}$$

Furthermore, controller gain matrices are given by $\overline{K}_m = (M^{\top})^{-1} Y \mathscr{K}_m$.

Proof. Let $Y\mathscr{K}_m = M^{\top}\overline{K}_m$, with the purpose of structure of the matrix $\overline{K}_m$. In detail,

$$\overline{K}_m^i = \left(M_i^{\top}\right)^{-1} Y_i \mathscr{K}_m^i == \begin{bmatrix} M_{1i}^{-1} & 0 \\ 0 & M_{2i}^{-1} \end{bmatrix} \begin{bmatrix} \mathfrak{I}_p & 0 \\ 0 & 0 \end{bmatrix} \mathscr{K}_m^i. \tag{35}$$

According to Lemma 1 and by using the Schur complement in equation (21)(10) the proof is completed. □

4. Numerical Example

In this section, to show the effectiveness of the attached methodology, a numerical example of the 3-area interconnected semi-Markov switching power system is presented. Suppose that the coefficients are selected $T_{12}(r(t)) = 0.2$, $T_{13}(r(t)) = 0.25$, and $T_{23}(r(t)) = 0.12$, $r(t) = 1, 2$. Furthermore, for any $i = 1, 2, 3$, set

$$\widehat{B}_p^i = \begin{bmatrix} 0.001 & 0 & 0 & 0 \\ 0 & 0.001 & 0 & 0 \\ 0 & 0 & 0.001 & 0 \\ 0 & 0 & 0.001 & 0.001 \end{bmatrix}. \tag{36}$$

Let $\overline{a}_i = 0.5$, $\gamma = 7$, $\eta = 0.2$, and $s_1 = 0.4$. Other nominal parameters are listed in Table 2 [3, 24].

Specifically, the transition rate function can be written $\pi_{pq} = \Pi_{pq}(h) k/\epsilon^k h^{k-1}$, and the Weibull distribution density function is given by $\chi_p(h) = k/\epsilon(h/\epsilon)^{k-1} \exp(-(h/\epsilon)^k)$, where k and ϵ indicate the parameters of the shape and scale, respectively. Noting that when $p = 1$, we choose $\epsilon = 1$ and $k = 3$. Otherwise, for $p = 2$, we set $\epsilon = 1$ and $k = 4$. Accordingly, the transition rate matrix can be expressed as

$$\pi_{pq}(h) = \begin{bmatrix} -3h^2 & 3h^2 \\ 4h^3 & -4h^3 \end{bmatrix}. \tag{37}$$

Thus, we have

$$\begin{aligned} \overline{\Pi}_{pq} &= \varepsilon\{\pi(h)\} \\ &= \begin{bmatrix} -2.7082 & 2.7082 \\ 3.6763 & -3.6763 \end{bmatrix}. \end{aligned} \tag{38}$$

In order to better describe the asynchronous phenomenon, the condition probability matrix is set as follows $\Gamma = [0.6\ \ 0.4;\ 0.5\ \ 0.5]$. According to Theorem 2, the asynchronous controller gains can be easily devised. We select the initial state $x_{10} = [0.048\ -0.04\ 0.065\ 0.024\ -0.55]^{\top}$, $x_{20} = [0.045\ -0.09\ 0.015\ 0.022\ -0.46]^{\top}$, $x_{30} = [0.07\ -0.05\ 0.07\ -0.08\ -1.1]^{\top}$, and the load disturbance $\Delta P_L^i = 0.005 \quad \sin(k)$, $(i = 1, 2, 3)$. Added by the

Table 2: Parameters of the IMAPS.

	Mode	$M_i(r(t))$	$D_i(r(t))$	$T_t^i(r(t))$	$T_g^i(r(t))$	$\beta_i(r(t))$	$R_i(r(t))$
Area 1	$r=1$	10	1	0.3	0.1	21	0.05
	$r=2$	10	1.1	0.35	0.15	20.5	0.05
Area 2	$r=1$	12	1	0.4	0.17	21.5	0.05
	$r=2$	10	1.5	0.4	0.1	18	0.05
Area 3	$r=1$	12	1.8	0.35	0.12	21.8	0.05
	$r=2$	12.5	1.25	0.15	0.15	23	0.05

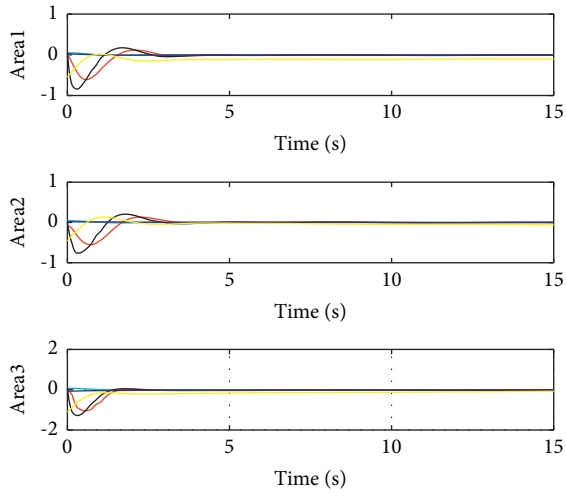

Figure 2: The state trajectories $x_i(t)$ $(i=1,2,3)$.

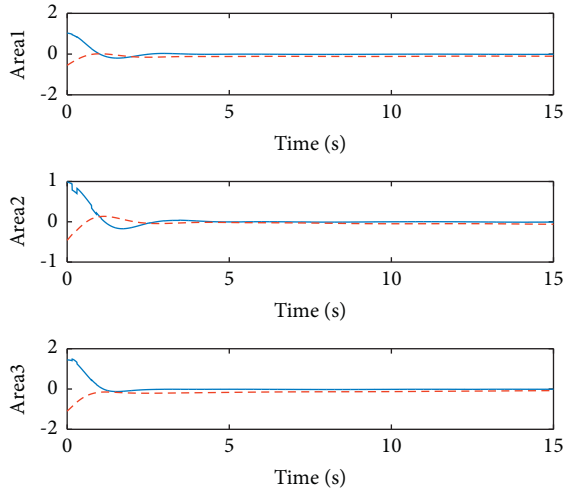

Figure 3: The measured output $y_i(t)$ $(i=1,2,3)$.

above-derived gains, the mode evolution of $r(t)$ and $\varphi(t)$ is shown in Figure 1. The trajectories of the state are plotted in Figure 2. Figure 3 thatdepict the state trajectories and the measured output. These simulation results verify the effectiveness of the proposed method.

5. Conclusions

In this study, the problem of the asynchronous load frequency control problem for semi-Markov interconnected multi-area power systems with the quantization effect has been addressed. In this case, the system under consideration is modeled as the semi-Markov jump system. The merit of this work is to tackle the asynchronous phenomenon between the control and semi-Markov interconnected multi-area power systems. By designing an asynchronous controller with quantized form, the quantized closed-loop system has stochastic stability under the specified performance. At last, the effectiveness of the developed method has been tested by the simulation result.

Data Availability

The data used to support the findings of this study are included in the article.

Conflicts of Interest

The authors declare that they have no conflicts of interest.

References

[1] O. I. Elgerd and C. E. Fosha, "Optimum megawatt-frequency control of multiarea electric energy systems," *IEEE Transactions on Power Apparatus and Systems*, no. 4, pp. 556–563, 1970.

[2] M. Toulabi, M. Shiroei, and A. Ranjbar, "Robust analysis and design of power system load frequency control using the kharitonov's theorem," *International Journal of Electrical Power & Energy Systems*, vol. 55, pp. 51–58, 2014.

[3] H. Zhang, J. Liu, and S. Xu, "Load frequency control of networked power systems via an event-triggered scheme," *IEEE Transactions on Industrial Electronics*, vol. 67, no. 8, pp. 7104–7113, 2019.

[4] H. K. Shaker, H. El Zoghby, M. E. Bahgat, and A. Abdel-Ghany, "Advanced control techniques for an interconnected multi area power system for load frequency control," in *Proceedings of the 2019 21st International Middle East Power Systems Conference (MEPCON)*, pp. 710–715, IEEE, Cario, Egypt, December 2019.

[5] B. Paramasivam and I. Chidambaram, "Design of load-frequency controller using artificial bee colony algorithm for an interconnected power system coordinated with upfc and rfb," *International Journal of computer applications*, vol. 36, no. 5, pp. 1–12, 2011.

[6] Y. Arya, "Automatic generation control of two-area electrical power systems via optimal fuzzy classical controller," *Journal of the Franklin Institute*, vol. 355, no. 5, pp. 2662–2688, 2018.

[7] R. Shankar, A. Kumar, U. Raj, and K. Chatterjee, "Fruit fly algorithm-based automatic generation control of multiarea interconnected power system with facts and ac/dc links in deregulated power environment," *International Transactions*

on Electrical Energy Systems, vol. 29, no. 1, Article ID e2690, 2019.

[8] C. Peng, J. Zhang, and H. Yan, "Adaptive event-triggering H_∞ load frequency control for network-based power systems," *IEEE Transactions on Industrial Electronics*, vol. 65, no. 2, pp. 1685–1694, 2017.

[9] X. Zhao, S. Zou, and Z. Ma, "Decentralized resilient H_∞ load frequency control for cyber-physical power systems under dos attacks," *IEEE/CAA Journal of Automatica Sinica*, vol. 8, no. 11, pp. 1737–1751, 2021.

[10] S. Kuppusamy, Y. H. Joo, and H. S. Kim, "Asynchronous control for discrete-time hidden Markov jump power systems," *IEEE Transactions on Cybernetics*, pp. 1–6, 2021, in press.

[11] V. Ugrinovskii and H. R. Pota, "Decentralized control of power systems via robust control of uncertain Markov jump parameter systems," *International Journal of Control*, vol. 78, no. 9, pp. 662–677, 2005.

[12] M. Perman, A. Senegacnik, and M. Tuma, "Semi-markov models with an application to power-plant reliability analysis," *IEEE Transactions on Reliability*, vol. 46, no. 4, pp. 526–532, 1997.

[13] J. Cheng, L. Xie, J. H. Park, and H. Yan, "Protocol-based output-feedback control for semi-markov jump systems," *IEEE Transactions on Automatic Control*, p. 1, 2022, in press.

[14] L. Xie, J. Cheng, H. Wang, J. Wang, M. Hu, and Z. Zhou, "Memory-based event-triggered asynchronous control for semi-markov switching systems," *Applied Mathematics and Computation*, vol. 415, Article ID 126694, 2022.

[15] J. Cheng, L. Liang, J. H. Park, H. Yan, and K. Li, "A dynamic event-triggered approach to state estimation for switched memristive neural networks with nonhomogeneous sojourn probabilities," *IEEE Transactions on Circuits and Systems I: Regular Papers*, vol. 68, no. 12, pp. 4924–4934, 2021.

[16] J. Cheng, J. H. Park, Z.-G. Wu, and H. Yan, "Ultimate boundedness control for networked singularly perturbed systems with deception attacks: a Markovian communication protocol approach," *IEEE Transactions on Network Science and Engineering*, vol. 9, no. 2, pp. 445–456, 2022.

[17] J. Wang, Z. Xi, and L. Sun, "Dynamic logarithmic vector quantizer design for stochastic continuous time linear systems with state feedback control," *IEEE Access*, vol. 8, pp. 46440–46447, 2020.

[18] J. Cheng, Y. Wang, J. H. Park, J. Cao, and K. Shi, "Static output feedback quantized control for fuzzy Markovian switching singularly perturbed systems with deception attacks," *IEEE Transactions on Fuzzy Systems*, vol. 30, no. 4, pp. 1036–1047, 2022.

[19] H. Saito, I. Umoto, A. Sasou, S. Nakamura, Y. Horio, and T. Kubota, "Subadaptive piecewise linear quantization for speech signal (64 kbit/s) compression," *IEEE Transactions on Speech and Audio Processing*, vol. 4, no. 5, pp. 379–382, 1996.

[20] M. Zhang, P. Shi, L. Ma, J. Cai, and H. Su, "Quantized feedback control of fuzzy Markov jump systems," *IEEE Transactions on Cybernetics*, vol. 49, no. 9, pp. 3375–3384, 2019.

[21] J. Cheng, Y. Wu, Z.-G. Wu, and H. Yan, "Nonstationary filtering for fuzzy Markov switching affine systems with quantization effects and deception attacks," *IEEE Transactions on Systems, Man, and Cybernetics: Systems*, pp. 1–10. in press, 2022.

[22] J. Yan, Y. Xia, X. Wang, and L. Li, "Quantized stabilization of continuous-time switched systems with delay and disturbance," *IEEE Transactions on Systems, Man, and Cybernetics: Systems*, vol. 52, no. 7, pp. 4530–4543, 2022.

[23] J. Cheng, Y. Wu, H. Yan, Z. G. Wu, and K. Shi, "Protocol-based filtering for fuzzy Markov affine systems with switching chain," *Automatica*, vol. 141, p. 110321, 2022.

[24] A. Kazemy and M. Hajatipour, "Event-triggered load frequency control of Markovian jump interconnected power systems under denial-of-service attacks," *International Journal of Electrical Power & Energy Systems*, vol. 133, Article ID 107250, 2021.